Characterization of TRPV4-mediated channelopathies and effect of TRPV4 in mitochondrial function and regulation

By
Rashmita Das
LIFE11201504004
National Institute of Science Education and Research, Bhubaneswar

A thesis submitted to the

Board of Studies in Life Sciences

In partial fulfillment of requirements

for the Degree of

DOCTOR OF PHILOSOPHY

of

HOMI BHABHA NATIONAL INSTITUTE

December, 2021

Homi Bhabha National Institute

Recommendations of the Viva Voce Committee

As members of the Viva Voce Committee, we certify that we have read the dissertation prepared by Rashmita Das entitled "Characterization of TRPV4-mediated channelopathies and effect of TRPV4 in mitochondrial function and regulation" and recommend that it may be accepted as fulfilling the thesis requirement for the award of Degree of Doctor of Philosophy.

	Date
Chairman – Dr Shikha Varma	27.5.22
Guide / Convener – Dr Chandan Goswami	29/05/2022
Examiner - Prof. Dr. Ferdinand Hucho	26/05/2022
Member 1- Dr. Tirumala Kumar Chowdary	27.05.22
Member 2- Dr. Praful Singru	27/05/2022
Member 3- Dr. Nagendra Sharma	27-05-22
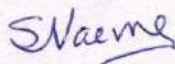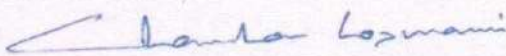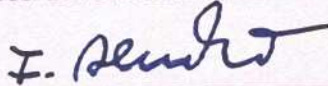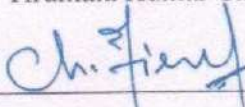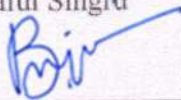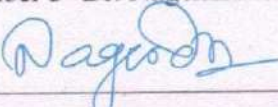
Final approval and acceptance of this thesis is contingent upon the candidate's submission of the final copies of the thesis to HBNI.

I/We hereby certify that I/we have read this thesis prepared under my/our direction and recommend that it may be accepted as fulfilling the thesis requirement.

Date: 27/05/2022

Place: NISER, Jatni
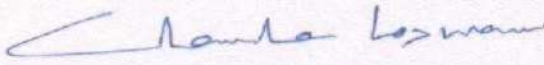
Dr. Chandan Goswami

(Thesis Supervisor)

STATEMENT BY AUTHOR

This dissertation has been submitted in partial fulfillment of requirements for an advanced degree at Homi Bhabha National Institute (HBNI) and is deposited in the library to be made available to borrowers under the rules of the HBNI.

Brief quotations from this dissertation are allowable without special permission, provided that accurate acknowledgment of the source is made. Requests for permission for extended quotation from or reproduction of this manuscript in whole or in part may be granted by the Competent Authority of HBNI when in his or her judgment the proposed use of the material is in the interests of scholarship. In all other instances, however, permission must be obtained from the author.

Rashmita Das

DECLARATION

I, hereby declare that the investigation presented in the thesis has been carried out by me. The work is original and has not been submitted earlier as a whole or in part for a degree/diploma at this or any other Institution / University.

Rashmita Das

List of Publications arising from the thesis

1. **Das R**, Kumar A., Dalai, R., Goswami C. Cytochrome-C interacts with the pathogenic mutational hotspot region of TRPV4 and forms complexes that differ in mutation and metal ion-sensitive manner. *BBRC*. 2022; 611: 172-178.

2. **Das R**, Goswami C. TRPV4 expresses in bone cell lineages and TRPV4-R616Q mutant causing Brachyolmia in human reveals "loss-of-interaction" with cholesterol. *BBRC*. 2019 Oct 1;517(4):566-574.

3. **Das R**., Mohanta S., Dubey, N.K., Chandan Goswami. Human skeletal dysplasia causing L596P-mutant alters the conserved amino acid pattern at the Lipid-water-interface of TRPV4 (*Under revision*)

Other Publications

1. Acharya, T.K., Kumar, S., Tiwari, N., Ghosh, A., Tiwari, A., Pal, S., Majhi, R.K., Kumar, A., **Das, R**., Singh, A., Maji, P.K., Chattopadhyay, N., Goswami, L. & Goswami, C. TRPM8 channel inhibitor-encapsulated hydrogel as a tunable surface for bone tissue engineering. *Sci Rep* **11,** 3730 (2021).

Conference, Symposium and workshop attended

* Attended 4 days **Proteomics Workshop** at ILS Bhubaneswar from 15th to 18th March 2016.

* Participated in "**Advanced Microscopy and Imaging Techniques**" held at NISER, Bhubaneswar from 4th-6th August 2016

* Participated in "**2nd meeting of Indian Immunological Society Odisha Chapter**" held in NISER, Bhubaneswar on 6th January 2017

* Presented poster entitled "Importance of membrane components in the regulation of TRPV4 channel: Implication in health and diseases". Rashmita Das[1] and Chandan Goswami[2] in "**International Conference on Microscope and 18th annual meeting of Electron Microscope Society of India 2018**" organised by IOP, Bhubaneswar from 18th-20th July 2018.

* Presented poster entitled "Thermo-gated ion channel TRPV4 and its mutants causing skeletal dysplasia in human reveals altered interaction pattern with cholesterol as revealed by high-end imaging". Rashmita Das[1] and Chandan Goswami[2] in "**EMBO | EMBL Symposium: Seeing is Believing -Imaging the Molecular Processes of Life**" from 09 -12 October 2019, EMBL Heidelberg, Germany.

[1]-Presenting author   [2]-Corresponding author

Rashmita Das

Dedicated to…

All those who listened to me in my

tough times.

ACKNOWLEDGEMENTS

SCIENTIFIC CONTRIBUTIONS

Content

Summary

Transient Receptor Potential (TRP) protein superfamily are ca^{2+} permeable non-selective cation channels that are activated by a plethora of physical and chemical stimuli such as temperature, osmolarity, pressure, lipid metabolites, capsaicin, isothiocyanates, camphor, cannabinoids, etc. The basic monomeric structure of the protein comprises an intracellular N- and C-terminus, 6-transmembrane regions interconnected by loops, and a "pore-region" located between the 5th and 6th transmembrane segment. Four such monomers make a tetrameric structure that forms the functional pore capable of conducting ions through it (Nilius & Owsianik, 2011; Zheng, J., 2013). Apart from sensory perception, TRP channels are involved in many other functions including Ca^{2+}- and Mg^{2+}-homeostasis, cell adhesion, control of development and differentiation, multiplication, cell death, and lysosomal function etc. (Minke, B., 2010). Because the TRP channels are involved in so many physiological processes, TRP family proteins are involved in several human diseases (Verma et al., 2010). These channels are important for Ca^{2+}-entry in cells as well as in different subcellular compartments (Zhang et al., 2018).

The focus of this thesis is TRPV4 ion channel which is the fourth member of the TRPV subfamily. It is a calcium-permeable non-selective cation channel detectable in the brain, kidneys, liver, lungs, hearts, dorsal root, and trigeminal sensory ganglia, and many other tissues and cells (Heller & O'Neil, 2006). So far more than 50 naturally occurring point-mutations of TRPV4 have been identified in humans causing diseases ranging from dwarfism to embryonic death. Most of these mutations are either "gain-of-function" or "loss-of-function" in nature, and the exact molecular and cellular mechanisms behind such channelopathies are unknown.

TRPV4 is known to be regulated by several physical or chemical stimuli such as temperature, pH, voltage, osmolality, or even by different lipids present in the membranous environment. Such lipid molecules often modulate precise localization of TRPV4 in submembranous

compartments such as lipid rafts, caveolae, and filopodial tips and thereby the functions of these specialized subcellular structures (Caires et al., 2017; White et al., 2016). Previous reports suggest that TRPV4 interacts with cholesterol and other steroids and such interactions may be relevant for channel gating (Das & Goswami, 2019; Kumari et al., 2015).

However, the exact mechanisms by which cholesterol and steroids regulate the gating of TRP channels are poorly understood. This thesis work deals with the molecular and cellular characterization of TRPV4-mediated channelopathies and the effect of TRPV4 in mitochondrial metabolism. In this work, the molecular evolution of TRPV4 and the impact of cholesterol interaction were studied using both *in silico* and experimental approaches. The localization of the channels and several pathogenic mutants in lipid rafts and cholesterol-binding motifs were investigated. The importance of TRPV4 during vertebrate evolution, its expression in bone cell lineages, its role in steroidogenesis, and co-localization with mitochondrial protein cytochrome c (Cyt C) were characterized in detail.

Key findings from this work:

1) There is a specific signature of amino acids that is evident in the lipid-water interface (LWI) of TRPV4. During vertebrate evolution, certain amino acids have been completely excluded from the LWI regions. In the same context, some residues are either positively selected, or negatively selected, or remain at a constant frequency in specific LWI regions. Most notably, the total frequency of positively charged, negatively charged, hydrophobic and hydrophilic residues and their respective ratio in the LWI regions remain constant, especially in the inner LWI region throughout the vertebrate evolution. Our observation fits well with the "positive inside" as well as "negative inside depletion/outside enrichment" theories proposed before. Our analysis points to a "specific pattern" that remains conserved in the LWI regions during vertebrate evolution. Accordingly, different point-mutations located in the LWI regions may

or may not alter this specific pattern and therefore may cause changes in the cell behaviour leading to certain pathophysiologies.

2) TRPV4-L596P mutation lies in one of the LWI regions of TRPV4. Cells expressing this mutation have properties that suggest that the membrane mobility of the mutant protein differs from the Wt and the mutation may have more open probabilities, especially in the optimum or sub-optimum levels of agonists. Therefore, it is most likely that TRPV4-L596P has more spontaneous opening in physiological conditions and thus causes altered cellular behaviour.

3) TRPV4 fragment containing a cholesterol-binding motif interacts with cholesterol forming a high-molecular-weight complex in the gel pockets of SDS-PAGE. Utilizing various methodologies, we exhibit that cholesterol interaction is diminished if not abrogated if there should arise an occurrence of TRPV4-R616Q mutant. Membrane mobility of TRPV4-R616Q is lower than TRPV4-Wt, particularly in cholesterol-depleted conditions. All these factors strongly recommend different aspects of cholesterol-mediated regulation of TRPV4. Taken together, information recommends that TRPV4 interacts with cholesterol, and such interaction is strong enough and has an evolutionary origin.

4) The metal and temperature dependency of steroid biosynthesis and the tight linkage of TRPV4 with MVK and GLTP genes suggest possible crosstalk between TRPV4 and steroid biosynthesis. To analyze such correlation, the role of TRPV4 in steroidogenesis was studied. TRPV4 channel was found to regulate several factors needed for steroidogenesis like mitochondrial metal entry, temperature, steroidogenic protein expression, and ER-mitochondria contact establishment. This analysis would therefore help establish the involvement of TRPV4 in steroid function.

5) Cholesterol is known to play a supporting role in Cyt C mediated toroidal lipid pore formation in the mitochondria during apoptosis. Our previous study advocates TRPV4 as a

mitochondrial protein and the biochemical interaction of TRPV4 with cholesterol suggests a possible TRPV4 and Cyt C interaction during apoptosis. The differential interaction of TRPV4 and Cyt C in presence of different metals as well as the differential interaction pattern of TRPV4 MTS mutants with Cyt C as observed in our studies opens a new dimension into TRPV4 research in the field of channelopathies and also in Cyt C release.

List of Figures

List of Tables

ABBREVIATIONS

4α-PDD	4α-phorbol 12,13-didecanoate
ANKRD13A	Ankyrin repeat domain 13A
APS	Ammonium persulfate
ARD	Ankyrin-like Repeat Domain
ARDS	Acute respiratory distress syndrome
ATL	Ascending thin limb of the loop of Henle
ATP	Adenosine triphosphate
BCYM3	Brachyolmia Type 3
BLAST	Basic Local Alignment Search Tool
BSA	Bovine Serum Albumin
CaM	Calmodulin
CARC	Inverted CRAC
Cav1	Caveolin1
CBB	Coomassie Brilliant Blue-stained
CCD	Cortical collecting duct
CCM	Cholesterol-consensus-motif
CMT2C	Charcot-Marie-Tooth Neuropathy, Type 2C
CNT	Connecting tubule
CRAC	Cholesterol Recognition/ interaction Amino acid Consensus
cryo-EM	Cryogenic electron microscopy
CTX-B	Cholera Toxin B
CYP11A1	cytochrome P450 family 11 subfamily A member 1
CYP11B1	cytochrome P450 family 11 subfamily B member 1
CYP11B2	cytochrome P450 family 11 subfamily B member 2
CYP17A1	cytochrome P450 family 17 subfamily A member 1
Cyt C	cytochrome c
DAPI	4′,6-diamidino-2-phenylindole
DCT	Distal convoluted tubule
DHEA-S	Dehydroepiandrosterone sulfate
DHT	Dihydrotestosterone
DIC	Differential interference contrast
DkTx	Double knot toxin
DMEM	Dulbecco's modified Eagle's medium
DMSO	Dimethyl Sulfoxide
dNTP's	Deoxynucleoside triphosphate
DRG	Dorsal Root Ganglia
DTL	Descending thin limb of the loop of Henle
E. coli.	*Escherichia coli*
EDTA	Ethylenediaminetetraacetic acid

E-GFP	Enhanced Green Fluorescence protein
EGTA	Ethylene glycol-bis(β-aminoethyl ether)-N,N,N′,N′-tetraacetic acid
ELISA	Enzyme Linked Immunosorbent Assay
ER	Endoplasmic Reticulum
EtBr	Ethidium Bromide
FACS	Fluorescence-activated cell sorting
FAK	Focal Adhesion Kinase
FASTA	Fast-all/ FastA
FDAB	Digital Arthropathy-Brachydactyly, Familial
FRAP	Fluorescence recovery after photobleaching
GCLJ	Central Giant cell lesions of the jaw
GFP	Green Fluorescent Protein
GIT2	G-protein-coupled receptor kinase interacting ArfGAP 2
GLTP	Glycolipid transfer protein
GST	Glutathione-S-Transferase
HaCaT	Cultured Human Keratinocyte
HADDOCK	High Ambiguity Driven protein-protein DOCKing
HMN8	Neuronopathy, Distal Hereditary Motor, Type VIII
HMSN2C	Hereditary motor and sensory neuropathy, type IIC
hPSC-CMs	Human pluripotent stem cell-derived cardiomyocytes
HRP	Horseradish peroxidase
HSD 3β1	3β-hydroxysteroid dehydrogenase
HSP	Heat shock protein
IAEC	Institute Animal Ethics Committee
IgG	Immunoglobulin G
IMCD	Inner medullary collecting duct
IPTG	Isopropyl thio galactoside
IR	Infrared
ITS	Insulin, human transferrin, and selenous acid
KCTD10	Potassium channel tetramerization domain containing 10
LB	Lysogeny broth
LWI	Lipid-Water-Interface
MAM	Mitochondria-associated membranes
MD	Macula densa
MFI	Mean fluorescence intensity
Mfn	Mitofusin
MMAB	Methylmalonic aciduria (cobalamin deficiency) cblB type
MSC	Mesenchymal Stem Cell
MSC	Mesenchymal Stem Cells
MTS	Mitochondrial Target Sequence
MTY	Mito Thermo Yellow
MUSCLE	MUltiple Sequence Comparison by Log- Expectation

MVK	Mevalonate Kinase
MYA	Million Years Ago
NAN	Nanchung
NCBI	National Center for Biotechnology Information
NEB	New England Biolabs
NIR	Near-infrared
NMR	Nuclear Magnetic Resonance
OD	Optical Density
OMCD	Outer medullary collecting duct
OSM 9	OSMotic avoidance abnormal family member 9
PBD	Phosphoinositide binding domain
PBS	Phosphate-buffered saline
PBST	PBS supplemented with 0.1% Tween-20
PCR	Polymerase Chain Reaction
PDB	Protein Data Bank
PDB	Protein Data Bank
PFA	Paraformaldehyde
PKD	Polycystic Kidney Disease
PLC	Phospholipase C
PMNs	Polymorphonuclear neutrophil granulocytes
PMSF	Phenylmethylsulfonyl fluoride
PRD	Proline-rich domain
PUFA	Polyunsaturated fatty acids
PVDF	Polyvinylidene fluoride
RbCl	Rubidium Chloride
RDA	Rhodamine B-[(2,2'-bipyridine-4-yl)-aminocarbonyl]benzyl ester
RE	Recycling endosomes
RFP	Red Fluorescent Protein
RGB	Red Green Blue
RN1734	2,4-Dichloro-N-isopropyl-N-(2-isopropylaminoethyl)benzenesulfonamide
ROI	Region-of-interest
ROS	Reactive Oxygen Species
RPM	Rotation Per Minute
RPMI	Roswell Park Memorial Institute
RT	Room Temperature
SDS-PAGE	Sodium dodecyl sulfate-polyacrylamide gel electrophoresis
SED	Spondyloepiphyseal Dysplasia
SEDM-PM2	Spondylo-epimetaphyseal dysplasia Maro- teaux—pseudo-Morquio type 2
SMDK	Spondylometaphyseal Dysplasia, Kozlowski Type
SPSMA	Scapuloperoneal spinal muscular atrophy

TAE   Tris base, acetic acid and EDTA
TCHP   Trichoplein, keratin filament binding
TEMED   Tetramethylethylenediamine
TG   Trigeminal ganglia
TGN   Trans-Golgi network
TM   Transmembrane
UBE3B   Ubiquitin protein ligase E3B
UV   Ultra Violet
VGIC   Voltage-Gated Ion Channel
YASARA   Yet Another Scientific Artificial Reality Application
β-MCD   Methyl β-Cyclodextrin
Δ^9-THC Δ^9-tetrahydrocannabinol

Chapter 1

Introduction

1.1. General introduction to TRP channels

1.1.1 Brief introduction to ion channels

The lipid bilayer of cells is greatly impermeable to charged atoms, regardless of how little: the charge and high level of hydration of such particles keep them from entering through the hydrocarbon phase of the lipid bilayer (Figure 1). Two significant classes of transport proteins present on the lipid layer that help their transport inside the cells are carrier proteins and channel proteins. Transport through channel proteins is much faster than carrier proteins as channel proteins form aqueous pores through which solutes such as inorganic ions can cross the membrane easily (Alberts et al., 2002).
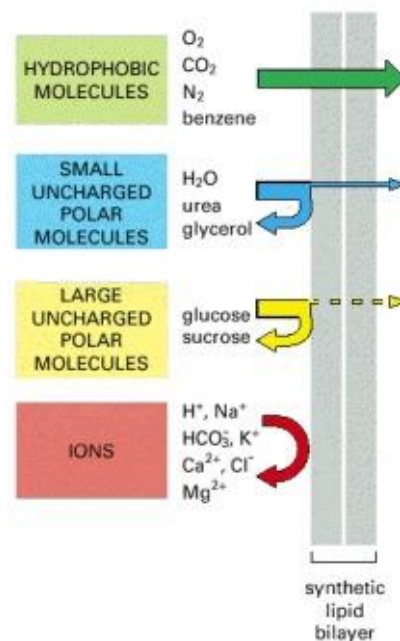
Figure 1: A protein-free lipid bilayer is excessively impermeable to ions. Schematic diagram demonstrating the relative permeability to different classes of molecules by a synthetically prepared lipid bilayer (Alberts et al., 2002).

Channel proteins, specifically Ca^{2+}-permeable channels are of prime significance for the survival of almost all cells. Ca^{2+} is an important second messenger in addition to its role as a charge carrier. Three primary classes of Ca^{2+}-penetrable channels are present in cells; they are voltage-

3

gated, ligand-gated, and TRP channels (Minke & Parnas, 2006). The focus of this thesis is on TRP

channels which is a group of ion channels that are located in many different types of tissues and

cells and are involved in various types of cellular functions.

1.1.2. Discovery of TRP channels

Cosens and Manning in 1969 identified a *Drosophila melanogaster* mutant that behaved

as though blind under bright light illumination. "We are working with a mutant strain of *D.*

melanogaster which, though behaving phototactically positive in a T-maze under low ambient

light, is visually impaired and behaves as though blind in a simple optomotor apparatus" (Cosens

& Manning, 1969). They mapped this mutation to the third chromosome of the *Drosophila*

genome. They also measured the electrical response of the entire eye, to light (ERG). They

described the ERG phenotype of this mutant as follows: "The light response decays to baseline in

10 to 15 sec. At this point, the mutant eye is apparently blind, for it will not respond to second test

light, and mutant flies exposed to continual bright light ceased to make any phototactic choice in

the T-maze but recover their responsiveness only after a time in low ambient light". Minke et al.,

in 1975 designated the mutant 'Transient Receptor Potential' or in short 'trp' because of the

transient response to sustained intense lights (Minke et al., 1975). Later on, TRP was adapted as

the name of the entire TRP superfamily by an international committee (Montell et al., 2002). Minke

et al. explained the mutant phenotype by demonstrating that the original Cosens-Manning trp

mutant (now designated trp^{CM}) was a *developmental temperature-sensitive mutant*, showing faster

decay to baseline and slower dark recovery kinetics when raised at room temperature (24°C)

relative to 19°C. The trp mutant becomes more similar to wild type when raised at 19°C ~ instead

of ~24°C (Minke B., 1983). The conclusion made from all these early studies was that the trp

phenotype arises from a reduction in excitation efficiency (i.e., that intense light becomes

4

equivalent to dim light) during constant illumination, due to an unknown defect at an intermediate stage of the phototransduction cascade (Minke B., 1977; Minke B., 1982). It is to be noted that the phototransduction in *Drosophila* is mediated by a G-protein coupled phospholipase C (PLC) cascade leading to activation of two classes of Ca^{2+}-permeable cation channels, TRP and TRPL— the prototypical members of the transient receptor potential (TRP) superfamily of cation channels.

1.1.3. Classification of TRP channel superfamily

All TRP channels are cation-selective, with some being highly selective for Ca^{2+} or Mg^{2+}. Distantly related to voltage-gated K^+, $Na^{+,}$ and Ca^{2+}-superfamilies, the TRP superfamily is composed of 9 animal subfamilies divided into two groups, Group 1 and Group 2 based on sequence and topological differences (Figure 2 & 3).

Group 1: TRPs-TRPA (ankyrin), TRPC (canonical), TRPM (melastatin), TRPN (nompC, or no mechanoreceptor potential C), TRPS (soromelastatin), TRPV (vanilloid), and TRPVL (vanilloid-like)

Group 2: TRPs- TRPP (polycystin), TRPML (mucolipin) and possibly TRPY/TRPF(fungus-specific TRP channels) (Montell C., 2005; Himmel & Cox, 2020).
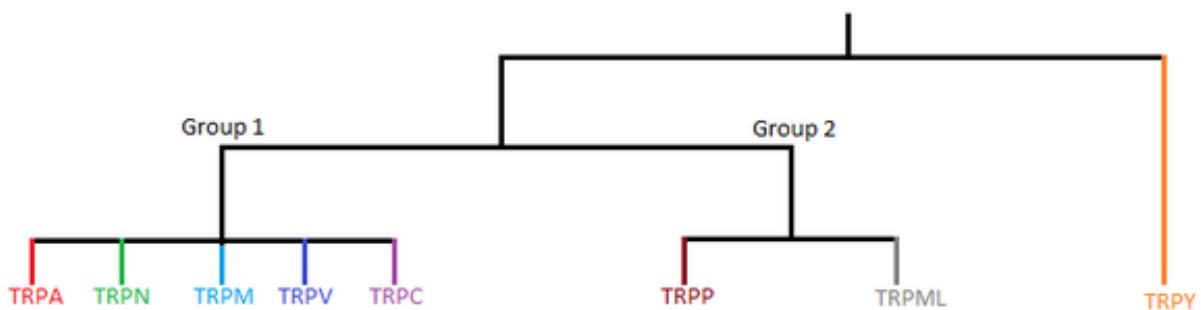
Figure 2: TRP channel subfamily members in their respective groups. The TRP superfamily is classically divided into 7 subfamilies majorly split into two groups. Group 1 members include TRPA, TRPN, TRPM, TRPV and TRPC while Group 2 members include TRPP and TRPML. A distantly related group TRPY also occurs in yeast (http://pfam.xfam.org/family/pf06011)

TRP ion channels were initially found in *Drosophila* and have since been comprehensively examined in animals. Out of six kingdoms of life, TRP channels are found only in two kingdoms i.e., Animals and fungi. With the recent advancement in genomic data, these channels are now discovered in other species like choanoflagellates and algae (Himmel & Cox, 2020). TRPY1 which is a Ca^{2+}-permeable TRP channel is found in the vacuolar membrane in *Saccharomyces cerevisiae* (Lange et al., 2016). At least eight TRP channel genes are found in fresh water, green alga *Chlamydomonas reinhardtii* (Wada et al., 2020). Despite several attempts, no study to date has identified a single TRP encoding gene in land plants, suggesting a probable loss of TRP genes during its divergence from chlorophyte algae (Nilius & Owsianik, 2011).
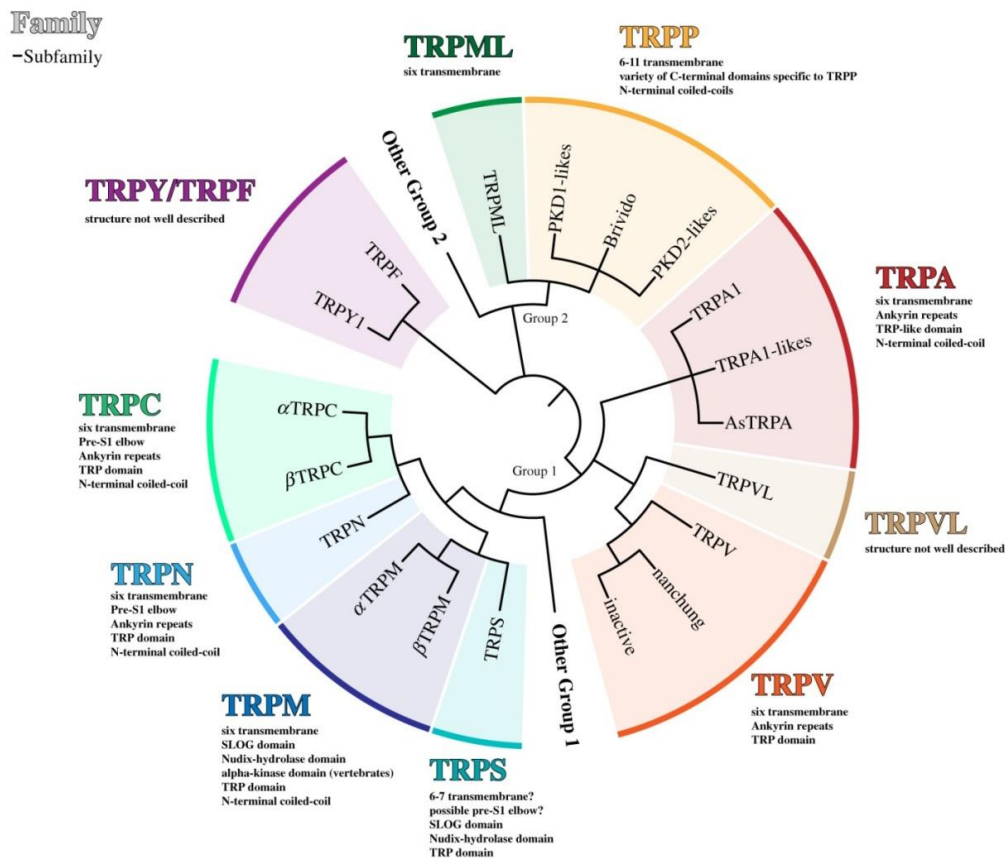
Figure 3. **Current view of the relationship between TRP families (bold large) and subfamilies (at tree tips)** The last two decades, research has brought about a restructure of the TRP superfamily from its original conception. Current research opinion suggests nine TRP sub families namely TRPP, TRPML, TRPA, TRPV, TRPVL, TRPC, TRPN , TRPM and TRPS (Himmel & Cox, 2020).

1.1.4. Molecular evolution of TRP channels

In the last twenty years, an extensive study on TRP channels has provided large genomic and transcriptomic data which have helped to identify their existence in genomes of a variety of creatures. Modern comprehensive phylogenetic analyses have additionally helped to restructure the superfamily from its original conception.

As TRP channels are described in a variety of eukaryotic channels and there is no evidence of these channels in Archaea or Bacteria, TRP channels most likely formed early in eukaryote evolution. TRP channels are also linked to the survival of living forms. Species existence is linked to the detection of predator cues by the preys who respond by changing their physiological behaviour. For example, a predator-prey relationship study between *Pristionchus pacificus* and *Caenorhabditis elegans* respectively, showed that the sulfolipids secreted by the predator are detected by *C. elegans* sensory neurons that in turn utilize cyclic nucleotide-gated (CNG) and TRP channel to produce fast avoidance (Liu et al., 2018).

TRP channels also shield skin cells from ecological stress like infrared (IR) or near-infrared (NIR) radiation by regulating the production of heat shock protein (Hsp). After IR or NIR exposure, via TRP channel, Ca^{2+}-level gets elevated inside the cells. The elevated levels of Ca^{2+} thereby increase ROS and ATP production inside mitochondria that in turn incite the production of chaperones and thus protect the human skin from high temperature (Hsu & Yoshioka, 2015). The role of TRP channels in the skin is therefore pivotal for accomplishing the interior temperature equilibrium and thermal homeostasis.

Similarly, the involvement of TRP channels in the detection of a plethora of essential stimuli like toxins, temperature, and their role in temperature-dependant sex determination in some

reptiles have placed them in a privileged position in terms of essential ingredients required for life to take form (Yatsu et al,2015; Vennekens et al, 2008).

Various literature recommends that the phylogenetic tree root of the TRP channels is between Group 1 and Group 2 and the split pre-dates the bikont–unikont split (Palovcak et al., 2015; Peng et al., 2015).

Many of the group 1 members possibly pre-date the emergence of animals, as choanoflagellate (unicellular flagellates closely related to animals) have at least TRPM, TRPC, and TRPA. Members of this group also pre-date the Cnidaria–Bilateria split that happened earlier than 750 million years ago (Peng et al., 2015).

In Group 2, evidence supports an early split between TRPML and TRPP, as at least animals, amoebozoans and alveolates express both the channels (Himmel & Cox, 2020). TRPY and TRPF which are fungus-specific TRP channels may have diversified specifically in fungi and are likely to be a sister group to TRPP, which also has proven functional members in yeast (Figure 3).

1.1.5. General architecture of TRP channels

The structure of ion channels provides important information about their functions and activation mechanisms. All TRP channel subunits have six putative transmembrane segments and a pore-forming loop between the last two transmembrane segments. A functional channel is formed by four TRP channel subunits. The amino (N) and carboxyl (C) termini are located intracellularly and the cytoplasmic region contains several domains and motifs required for channel function (Figure 4). The ion-selectivity filter of TRP channel resembles the ion selectivity filter of potassium channels and can be identified from the linear sequence. In most TRPV ion

channels, the ion selectivity sequence is TIGXGD, where X can be an M or L (Zheng, J., 2013). Several members of the TRP super family contain an N-terminal ankyrin-like repeat domain (ARD) and several other domains/motifs like TRP-box domain, a coiled-coil domain, enzymatic domain, ER retention-signaling domain, Ca^{2+}-binding motif (EF-hand), etc. in the C-terminus (Méndez-Reséndiz et al., 2020; Zheng J., 2013).

3D structure prediction for membrane proteins remains a classic setback for protein structural biologists due to their partial hydrophobic surfaces, flexibility, and lack of functional integrity. With the recent advancement in technologies like single-particle cryo-EM, novel detergents, and nano-disc technologies, new membrane protein structures are being solved in high resolution rapidly (Carpenter et al., 2008; Cao E., 2020).
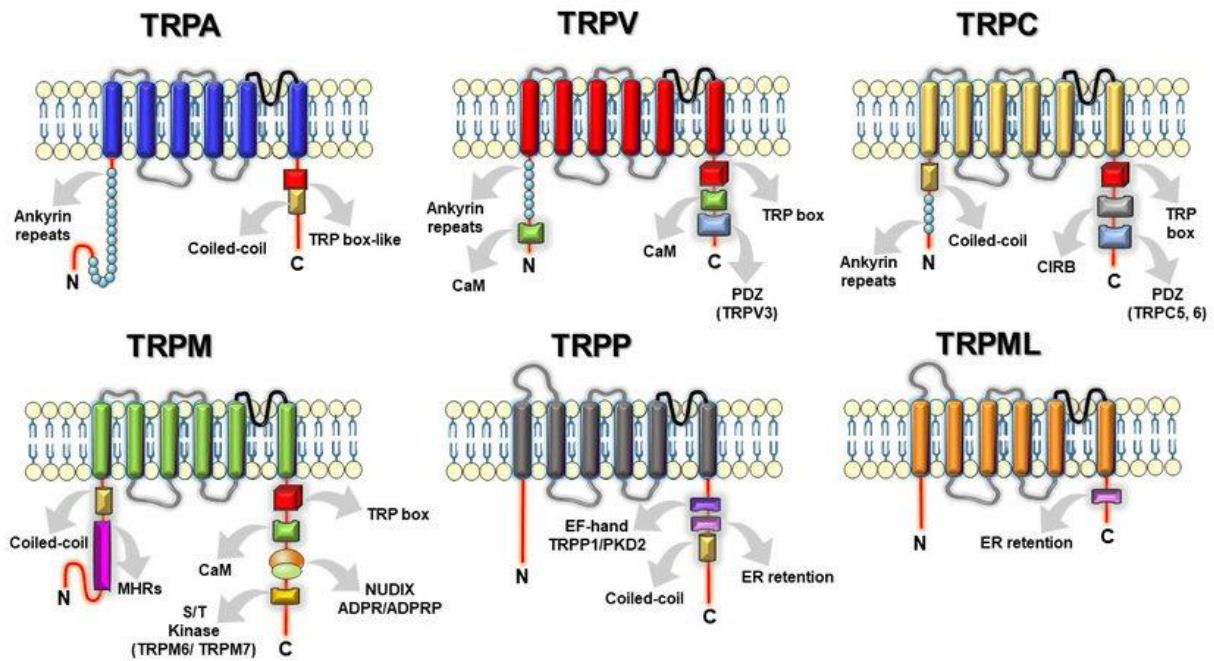
Figure 4: **Structural domains and motifs in the N- and C-terminus of TRP channel subfamilies** (Méndez-Reséndiz et al., 2020).

So far, 3D structures for some of the full-length TRP channels as well as some domains have been solved by Electron microscopy, X-Ray crystallography or NMR and all these structures are available in Protein Data Bank. For examples, domains like ARD, EF-hand, coiled-coil, PKD, α-kinase, C-terminus + CaM are accessible in PDB. Full-length 3D structures of TRP proteins like TRPV1, TRPV4, TRPA1, TRPM2, TRPC3, TRPV2, TRPV6, and TRPML1 are also available which helps reveal the mechanism of action of these channels (Figure 5) (Hellmich & Gaudet, 2014; Singh et al., 2018; Chen et al., 2017).

The focus of this thesis is TRPV4, a member that belongs to the TRPV subfamily. The TRPV subfamily has six members, TRPV1-6, that can be further divided into two groups, TRPV1-4, and TRPV5/TRPV6. The TRPV1-4 members are weakly Ca^{2+}-selective and can be "heat-activated" whereas TRPV5/TRPV6 are highly Ca^{2+}-selective but are not heat-activated channels.
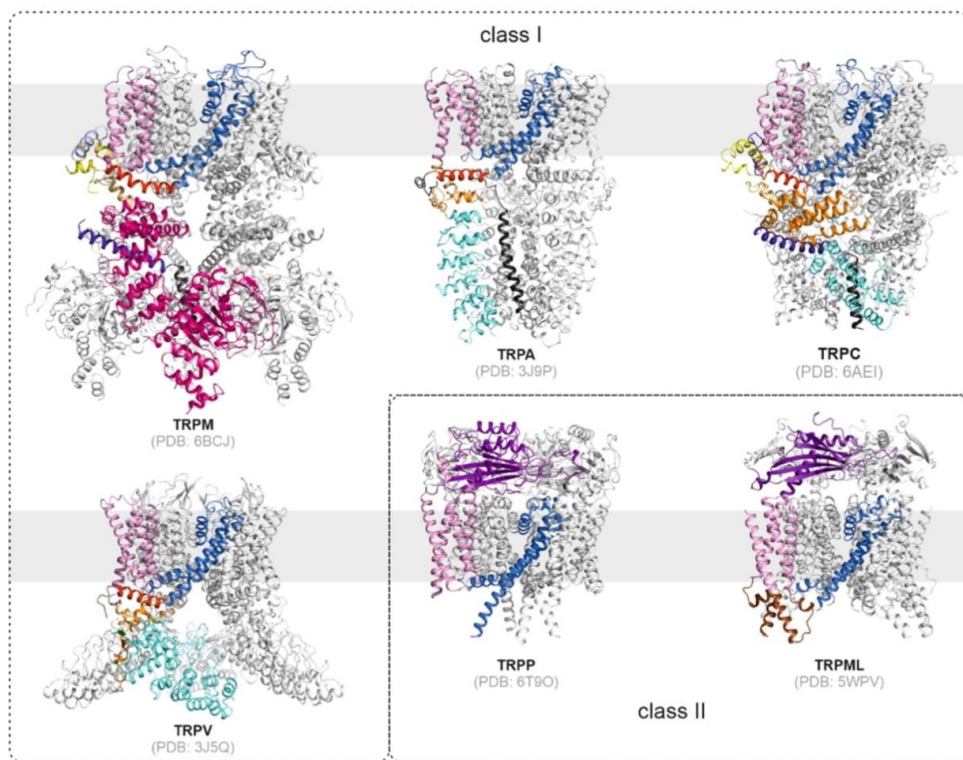
Figure 5: 3D structure of TRP channels. Three-dimensional high-resolution structures of representative channels of Class I and Class II TRP channels from six subfamilies are shown. TRPM4, TRPA1, TRPC5, TRPV1, TRPP2, and TRPML1 structures with respective PDB IDs are specified below each structure (Goretzki et al., 2021).

TRPV proteins function as tetramers and subunits of this subfamily contain an N-terminal ARD with six ankyrin repeats, a ~150 residue long C-terminus that helps to interact with other proteins and ligands, a TRP-box domain, and several other domains required for channel function (Hellmich & Gaudet, 2014; Zheng J., 2013). TRP channels assemble mostly into homo, but also as heterotetramer in certain combinations. Many reports suggest co-assembly of different TRPs that form functional channels, like TRPM6/TRPM7, TRPV5/TRPV6, TRPC1/TRPC3, TRPC1/TRPC4, TRPC1/TRPC5, TRPC3/TRPC4, TRPC4/TRPC5 (Figure 6) (Zheng J., 2013).
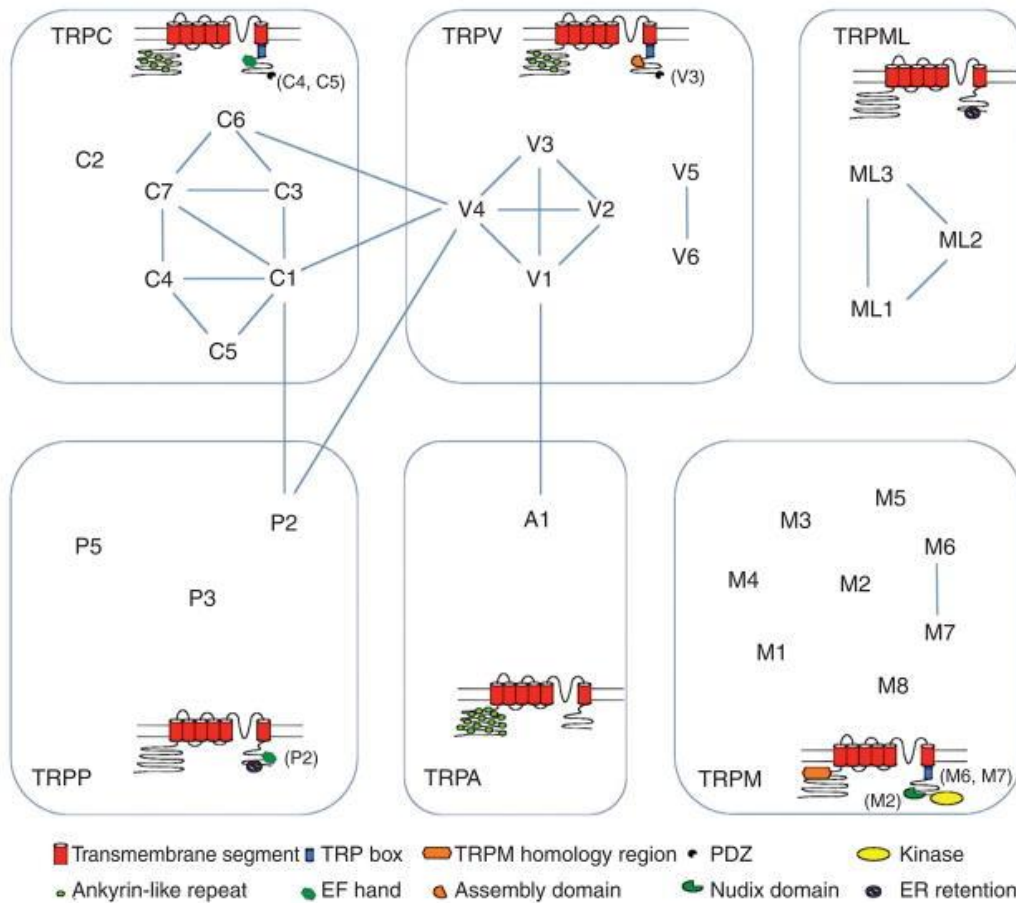
Figure 6: TRP channel subunits and their co-assembly partners. TRP channels known to co-assemble together are indicated by line. The domains found in TRP channels are colour-coded and specified below the main image (Zheng J., 2013). .

1.1.6. Tissue-specific distribution of different TRP channels

TRP channels are widely expressed in various tissue types. The expression of these proteins can be identified by immunohistochemistry and their functional expression can be verified by patch clamping, Ca^{2+}-imaging, mRNA, and protein expression studies. Mutations in these TRP channels give rise to several disorders in the specific organ where the protein is expressed (Figure 7). Some of the TRP channels are universally expressed and some of them are restricted to specific tissue. The tissue distribution of TRPV4 protein is explained in the later stage of the thesis. Major tissue distributions for TRPV channel are listed (Table 1). A comprehensive interpretation of the distribution of each TRP channel is beyond the scope of this study. The updated tissue-wise expression of individual TRP channels can be accessed on the protein atlas website (https://www.proteinatlas.org/ENSG00000111199-TRPV4/tissue).
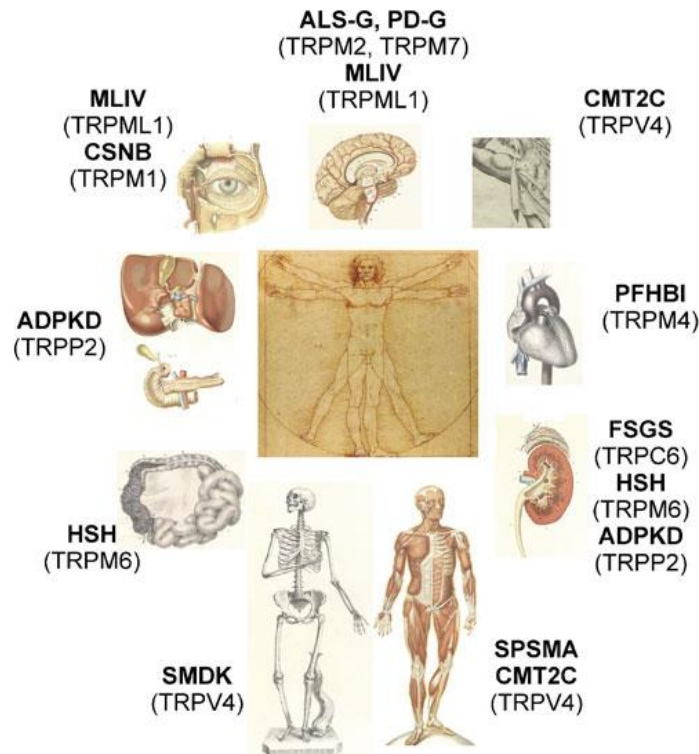
Figure 7: Major target organs in the body where TRP channel-related channelopathy are observed. The major organs of the human bodies are diagrammatically represented. The major diseases observed in them due to mutation in TRP channels are shown in bold letters (Nilius & Owsianik, 2010).

Table 1

Gene name	Chromosomal localization	Selectivity PCa:PNa	Modulation of activity	Highest expression
TRPV1	17p13.3	3.8 (heat), 9.6 (vanilloids)	Heat (43°C), vanilloids, anandamide, camphor, piperine (black pepper), allicin (garlic), ethanol, nicotine, proinflammatory cytokines, protons, PIP_2, phosphorylation exocytosis	TG, DRG, neurons, urinary bladder, testis
TRPV2	17p11.2	3	Heat (52°C), osmotic cell swelling, exocytosis	DRG, spinal cord, brain, spleen, intestine
TRPV3	17p13.3	2.6	Warm (33–39°C); PUFAs; menthol; compounds from oregano, cloves, and thymes	TG, DRG, spinal cord, brain, keratinocytes, tongue
TRPV4	12q24.1	6	Warm (27–34°C), osmotic cell swelling, 5′6′-EET, exocytosis	DRG, kidney, lung, spleen, testis, heart, keratinocytes, heart, liver, endothelia
TRPV5	7q35	>100	Low intracellular Ca^{2+}, hyperpolarization, exocytosis	Kidney, intestine, pancreas, placenta
TRPV6	7q33–q34	>100	Store depletion, exocytosis	Small intestine, pancreas, placenta

Table 1: Major tissue expression of TRPV ion channel. TRPV1-6 ion channels showing the highest expression in various tissues are listed. Other details like chromosomal location, selectivity of Ca^{2+} over Na^+, and modulation of activity are also specified. DRG: dorsal root ganglia, TG: trigeminal ganglia (Venkatachalam & Montell, 2007).

1.2 Activation mechanisms of TRP channels

1.2.1 Voltage

Many members of TRP channels are voltage-sensitive although the voltage sensitivity is very low in comparison to the classic voltage-gated Na^+, K^+, and Ca^{2+} channels. The S4 transmembrane domain is involved in voltage-sensing like most voltage-gated channels (Voets et al., 2007). Although the voltage sensitivity falls in the non-physiological range, a coupling between voltage-gating and other gating processes shifts the voltage range at which the channel is reactive. For example, if the temperature is increased from 17°C to 42°C for TRPV1, the activation curve is shifted leftward by nearly 200 mV, likewise, a leftward shift of ∼170 mV for TRPM8 is induced on 37°C to 15°C cooling (Voets et al., 2004). A similar kind of phenomenon is observed in other channels like TRPM4 and TRPM5. The basis for this coupling between voltage-dependant and temperature-dependant gating is right now under debate. Reports suggest either shared machinery or an allosteric modulation is involved in this gating process (Zheng J., 2013).

1.2.2 Temperature

Several TRP channels are temperature sensitive. Some members like TRPA1, TRPV1, TRPV4, TRPV2, TRPV3, TRPM2, TRPM4, TRPM5 are sensitive to hot temperature while channels like TRPM8, TRPC5, and TRPA1 (though controversial in nature) are cold-sensitive. TRPV1 gets activated when the temperature rises to 40°C, TRPV2 activates at 50°C while TRPV3 and TRPV4 get activated near 30°C. The cold-sensitive TRPM8 channel activates near 20°C, TRPC5 is highly sensitive to cold in the temperature range 37-25°C (Zimmermann et al., 2011; Numata et al., 2011). A broadly utilized portrayal of temperature sensitivity is the Q_{10} value, which measures the fold change in the rate of activation or deactivation upon a 10°C expansion in

14

temperature. Ion channels having a Q_{10} value $\geq$2-5 are considered to be thermally gated. Thermo TRPs which are very reliant upon temperature, show Q_{10} value >20 (Lamas et al., 2019). Expression of thermo-sensitive TRP channels brings high-temperature sensitivity into host cells that do not otherwise show high-temperature affectability (Feng Q., 2014; Patapoutian et al., 2003).

1.2.3. Mechanical force

Mechanotransduction couple's ion influx with mechanical stimulation required for the correct regulation of biological processes. Mechanical stimuli in the form of cell swelling or shrinkage due to change in osmolarity, direct pressure on cell or fluid flow in blood vessels may indirectly affect the TRP channel by intracellular signaling molecules. TRPV4 ion channel is a major osmosensor that is expressed in kidney, liver, heart, lung, inner-ear hair cells, and other cell types. In addition to TRPV4, TRPM7, TRPV2, TRPM4, TRPM7, TRPC1, TRPC6 are also activated by membrane tension (Strotmann et al., 2000; Wu et al., 2007). Other important non-TRP channels which are mechanically activated are MscL, Piezo1, and TREK-2 (Ridone et al., 2019). It is noteworthy to mention that the work on mechanosensitive Piezo channels begged the Nobel prize in medicine 2021 (https://www.nobelprize.org/prizes/medicine/2021/press-release/).

1.2.4. pH

Among all TRPs, activation by acidification was first studied for TRPV1. Several TRP channels thereafter were discovered in the TRPV, TRPM, TRPC, TRPML, TRPA, and TRPP subfamilies that are sensitive to pH changes. Not only acidification but also alkalization affects TRP channels like TRPA1, TRPP3, and TRPM7 (Numata et al., 2011). Residues critical for

regulations of pH are often located in the pore region of the channel. pH may affect the channel function by either potentiation, activation, or suppression (Zheng J., 2013)

1.2.5. Endogenous activators

1.2.5.1. Lipid metabolites

Lipid metabolites are endogenous activators of TRP channels. They may behave as potent agonists or antagonists (Figure 8). As TRP channels are membrane proteins, lipids may modulate their location and function either by directly interacting with them or by indirectly modulating the Physico-chemical properties of the cell membrane.
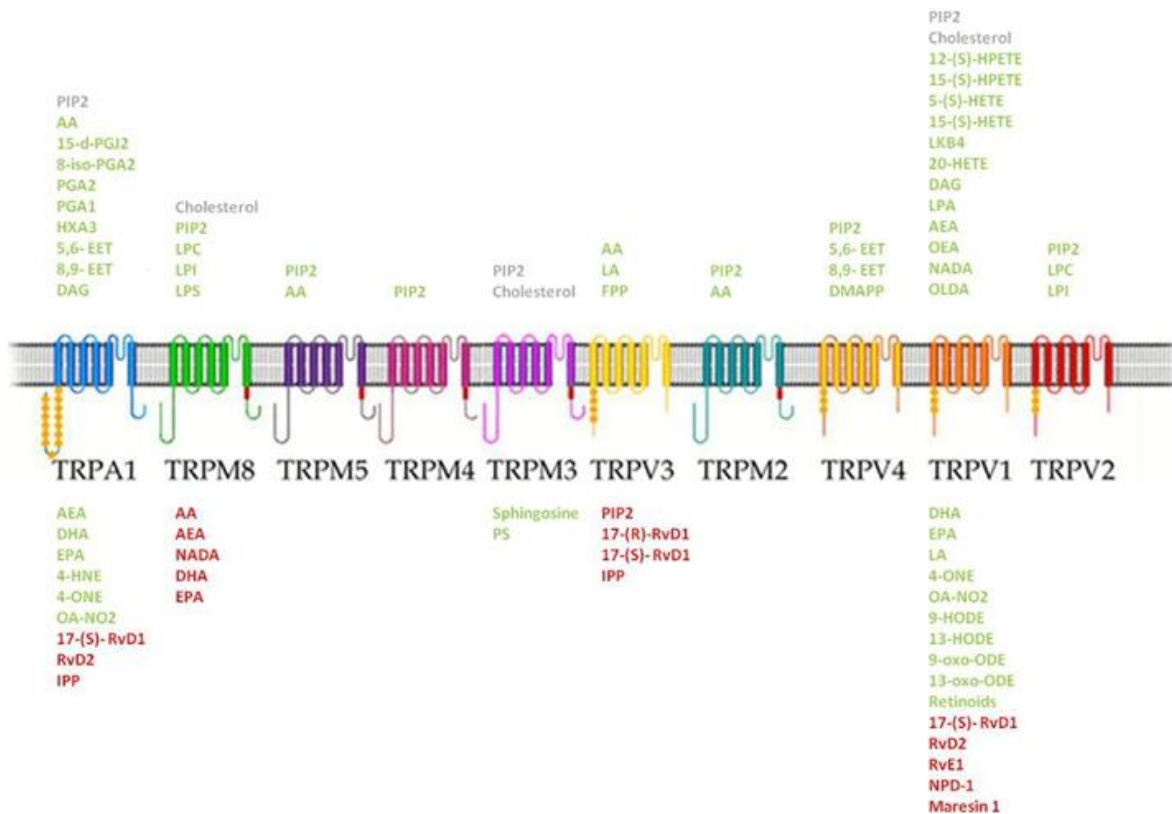
Figure 8. Different lipid modulators of TRP channels (Ciardo & Ferrer-Montiel, 2017).

More than 50 endogenous lipids have been recognized as TRP channel modulators including metabolites of phospholipase C (PLC) and A_2 (PLA$_2$), omega-3 (ω-3) and omega-6 (ω-6) polyunsaturated fatty acids (PUFAs), metabolites of cyclooxygenase, lipoxygenase, and cytochrome-P450 pathways, oxidized lipids, phospholipids, lysophospholipids, sphingolipids, cholesterol and related steroids, and mevalonate pathway metabolites (Ciardo & Ferrer-Montiel, 2017; Taberner et al., 2015).

1.2.5.2. Ca^{2+} and Ca^{2+}-binding proteins

As most TRP channels are permeable to Ca^{2+}, their activation serves as an important Ca^{2+}-entry pathway inside the cell. Ca^{2+} is an important second messenger in various signal transduction pathways. Many TRP ion channels are major downstream targets of Ca^{2+}-signaling. In TRPV5 and TRPV6, Ca^{2+}-entry rapidly triggers the inactivation of these channels that prevents excessive Ca^{2+}-influx, giving rise to a feedback mechanism (Nilius et al., 2002). A Ca^{2+}-dependent activation is also observed in TRPM3, where Ca^{2+}-influx is enhanced by activating the Gq-coupled muscarinic receptor or by depleting the intracellular calcium stores (Lee et al., 2003). Ca^{2+}-induced potentiation and inactivation have also been well-studied in TRPA1, TRPV4, TRPV2, TRPV3, TRPM4, TRPM2, TRPM3, TRPP2 , TRPM5 and, TRPM8 (Hasan & Zhang, 2018).

The Ca^{2+}-binding protein Calmodulin (CaM) is known to regulate a large number of TRP channels. TRPV1, TRPV3, TRPC2, and TRPC4α channels are reported to contain CaM-binding sites (Zheng J., 2013) . Reports suggest the interaction between CaM and TRPV3 is needed for TRPV3 potentiation (Xiao et al., 2008). TRPV1 desensitization upon repetitive application of capsaicin is linked to Ca^{2+}-induced activation of apo-CaM (Rosenbaum et al., 2004). Similarly, CaM activation causes inactivation of TRPC1 and TRPV6 and Ca^{2+}-dependent potentiation of TRPV3, TRPV4, and TRPV5 (Zheng J., 2013).

1.2.6. Exogenous activator

1.2.6.1. 4αPDD

The synthetic agonist 4α-phorbol 12,13-didecanoate (4α-PDD) has been distinguished as a TRPV4-particular activator. It activates TRPV4 by directly binding to its TM3 and TM4 regions. Y556 is the essential amino acid present in the TM3 region needed for 4αPDD mediated channel gating (Figure 9). This residue is analogous to the tyrosine residue in TRPV1 needed for capsaicin binding (Everaerts et al., 2010). Additionally, two other important residues for phorbol binding in the TM4 are Leu584 and Trp586, mutations of which cause a reduction of the sensitivity of the channel to 4αPDD (White et al., 2016).

1.2.6.2 Monoterpenes

Monoterpenes like menthol, eucalyptol, and camphor modulate various TRP channels including TRPM8 which is a "cold" receptor that gets activated by plant-derived natural cooling compounds like menthol and eucalyptol. Channels like TRPV1, TRPV3, TRPA1 are also modulated by these compounds (McKemy et al., 2002; Vogt-Eisele et al., 2007; Xu et al., 2005).
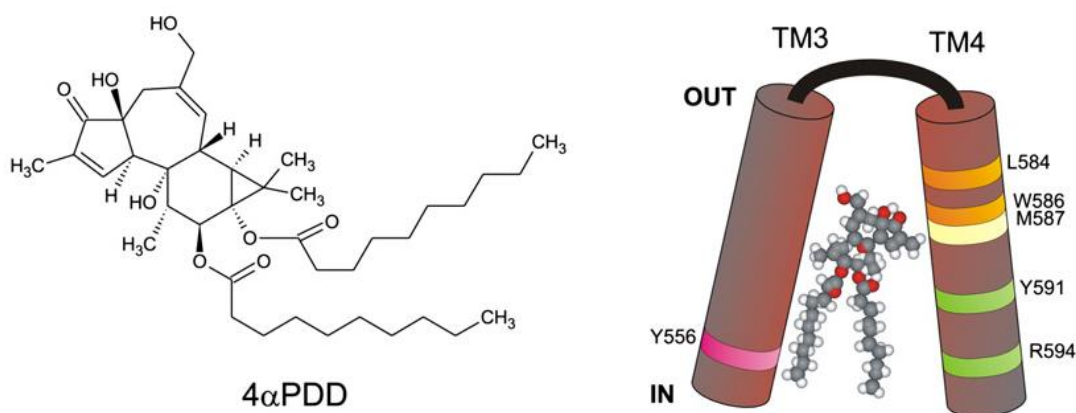
Figure 9: Binding of 4αPDD to TRPV4, a potent agonist: The molecular structure of the synthetic agonist 4α-phorbol 12,13-didecanoate and its putative binding pocket present between TM3-TM4 of TRPV4. Residues involved in 4αPDD-mediated channel gating are indicated in different colours (Everaerts et al., 2010).

1.2.6.3. Toxins

There are few reports that suggest that different toxins act on diverse TRP channels, though the majority of the work has been conducted on TRPV1. A few insect poisons have been distinguished that influence TRP channels (Figure 10). TRPV1 gets activated by the venom of a tarantula that contains vanillotoxin peptides and gets blocked by the venom of funnel web spider that contains acyl polyamine toxins (Vennekens et al., 2008). Pressure-induced activation of TRPC6 gets inhibited by GsMTx peptide from the tarantula venom (Spassova et al., 2006). Soricidin, isolated from the salivary glands of *Blarina brevicauda* represses Ca^{2+}-uptake through the TRPV6 ion channel (Bowen et al., 2013).
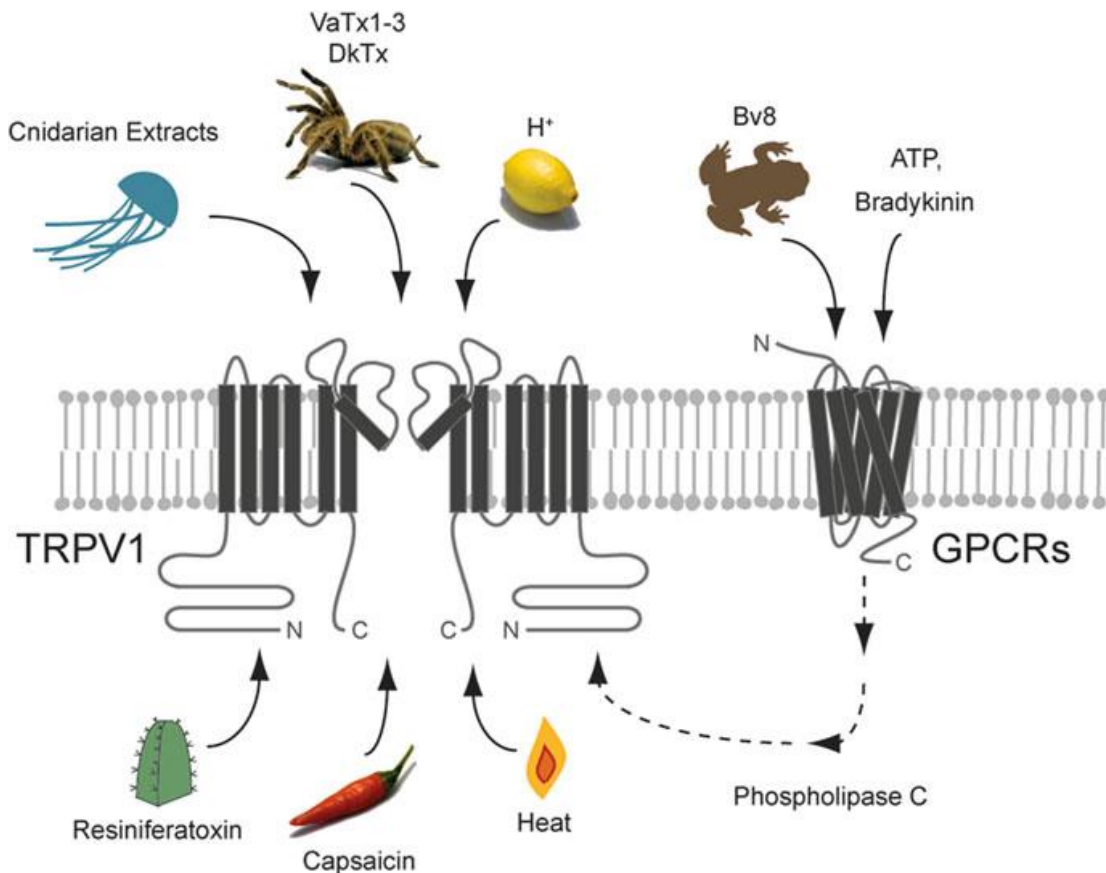
Figure 10: Toxins targeting TRPV1 ion channels. TRPV1 gets activated by tarantula toxins, cnideria extracts, and several plant irritants. Toxins like Bv8 from frog skin sensitize TRPV1 through direct activation of GPCRs. TRPV1 also gets sensitized by phospoholipase C activation triggered by bradykinin or ATP that are delivered downstream from venom lipases, proteases, and kallikreins (Siemens & Hanack, 2014).

Pain and swelling produced by honey bee string are caused by a toxic compound Melittin that targets TRPC channels (Siemens & Hanack, 2014). Another toxin that targets TRPV1 is the venom of Chinese red-headed centipede (*Scolopendra subspinipes mutilans)* that contain RhTx peptide toxin (Yang et al., 2015). "Double knot toxin" (DkTx) isolated from *Ornithoctonus huwena* binds to the outer pore region of TRPV1 and makes the channel constitutively open. Bv8, a protein toxin from the skin secretions of the yellow-bellied frog (*Bombina variagata)* causes PKR-mediated hyperalgesia that is to a great extent reliant upon TRPV1 (Siemens & Hanack, 2014).

1.2.6.4. Capsaicin

The exclusive activation of TRPV1 by Capsaicin makes it the most studied member of the TRP family. The revelation of TRPV1 was driven by the quest for "the capsaicin receptor" whose presence had been known for quite a long time. This search ultimately led the discoverer to fetch the Nobel Prize in medicine recently (https://www.nobelprize.org/prizes/medicine/2021/press-release/). The binding site of capsaicin is located in the S2-S4 region of TRPV1. This binding induces protein conformational changes that in turn open the ion permeation pore (Jordt & Julius, 2002).

1.3. Steroids as TRP channel modulators

TRP channels have been examined for the signaling mediated by a variety of steroids and might be a significant target for the long-term as well as fast non-genomic actions of different steroids (Kumar et al., 2015). Recent research suggests that the expression profile of TRP channels are affected by steroids, for example, dihydrotestosterone (DHT) manages the transcription of TRPM8 in human prostate cells, 17β-estradiol regulates TRPV5 and TRPV6 levels in rats, estrogen induce expression of TRPV1 and so on (Bidaux et al., 2005; Abel et al., 2003; Yan et al., 2007). The expression of several TRP channels has been identified in various steroid-sensitive tissues and cells like neurons, bones, immune cells, pancreatic cells, sperm cells, etc. Not only long-term effects but also non-genomic fast response of steroids is thought to be regulated by TRP channels. Various steroids might possibly initiate complex conformational changes prompting bidirectional changes, for example, channel opening or closing and can also make permanent conformational changes in the ion channels prompting either constitutively "on" or constitutively "off" (Figure 11) (Kumar et al., 2015).

Other modulators

In addition to the above regulators, TRP channels are also modulated by various other factors like anoxia and hypoxia, UV light, NAD^+, and its metabolites, nucleotide phosphates, several endogenous inorganic ions like Mg^{2+}, Zn^{2+}, phosphates such as pyrophosphate and pyrotriphosphate, polyvalent inorganic cations like La^{3+} and Gd^{3+} and many others (Zheng J., 2013; Zhu MX., 2011). In many cases heavy metals are known to block the TRP channels effectively.
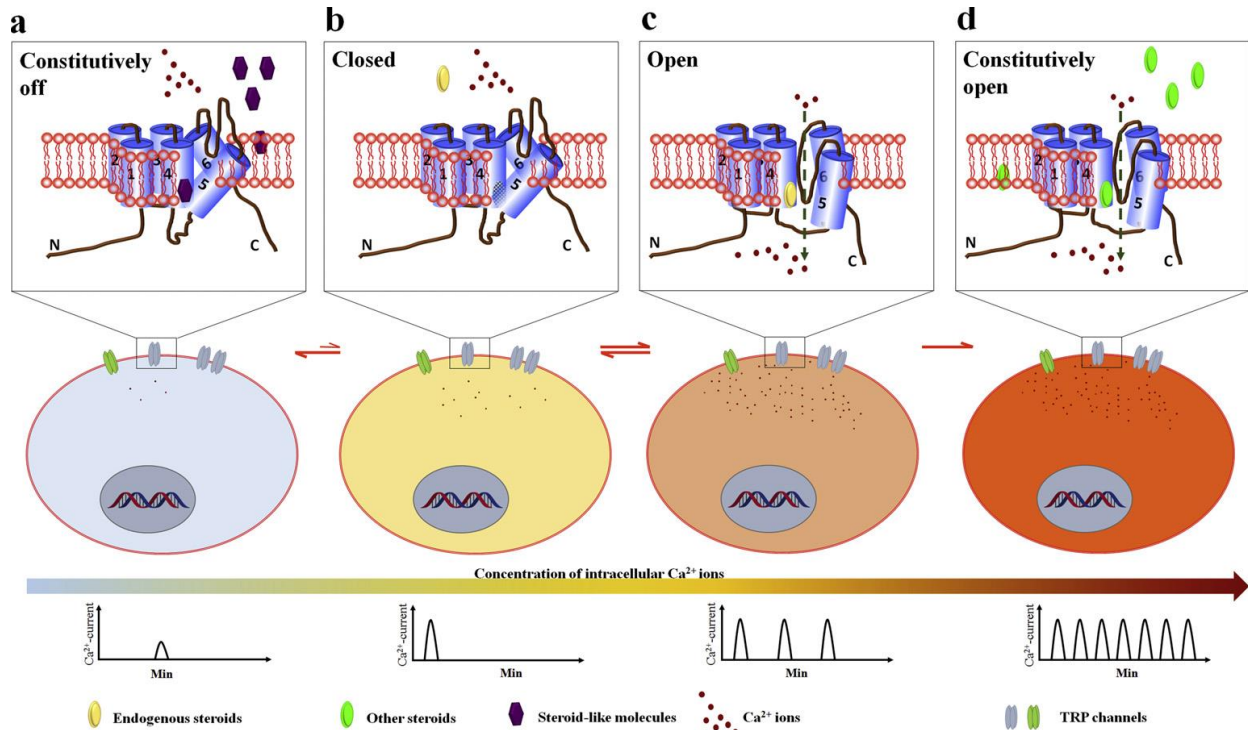
Figure 11: Non-genomic activity of various steroids and steroid-like molecules on TRP channels. Steroid binding regulates the ''on-and-off'' conformation form of TRP channels and thereby controls the Ca^{2+} ion concentration inside the cell (b & c). Excess steroid activity might prompt irreversible changes in the protein conformation prompting constitutive "on" (d) or "off" (a) mode of the channel resulting in irregular Ca^{2+}-dynamics and homeostasis inside the cells. Under these situations, anticipated Ca^{2+}-currents inside the cells are described at the base (Kumar et al., 2015).

1.4   Metal permeability of TRP channels

The pore that is formed by S5 and S6 helices forms an opening that traverses the lipid bilayer and passes ions and other hydrophilic atoms through it, which are otherwise impermeable through the lipid bilayer. A selectivity filter checks what sort of particles is permitted through the pore. Though the involvement of TRP channels in the transport of Ca^{2+} and Na^+ is well documented, recent studies have discovered their involvement in the transport of other biologically important metal ions like zinc, magnesium, manganese, cobalt, and many others (Table 2) (Bouron et al., 2014). These trace metal ions can activate or inhibit these channels. The hydrophobicity and the diameter of the ion permeation pathway are important factors while considering the ability of these ions to permeate.
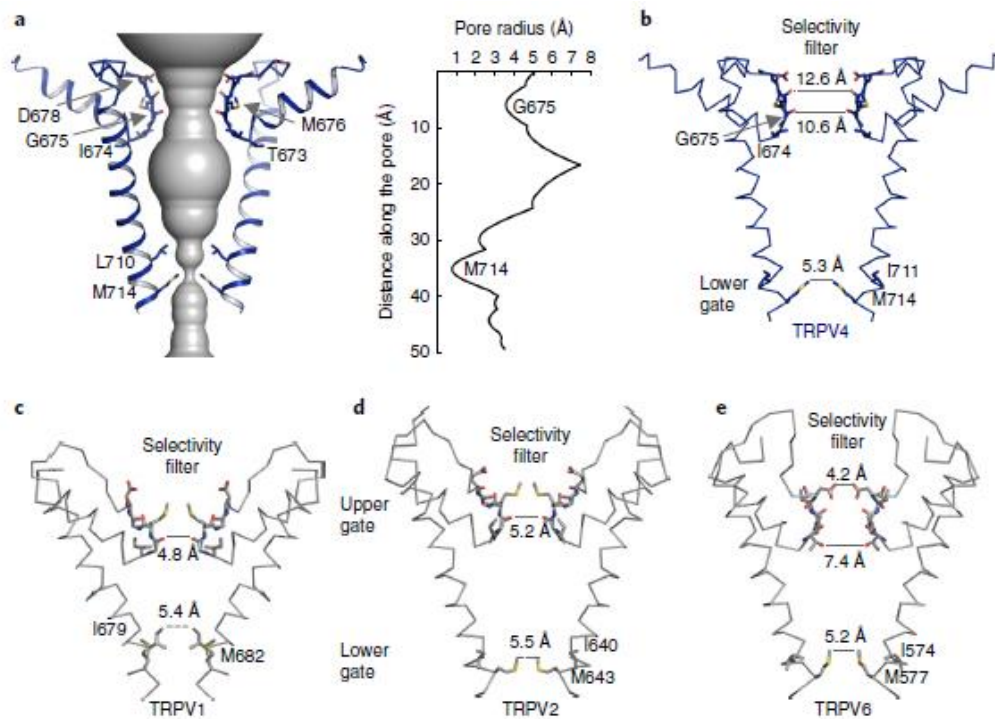
Figure 12: Ion permeation pathway of TRP channel. a. Single constriction formed by M714 residues defines the intracellular gate in S6. The pore radius along the permeation pathway is shown at the right. **b.** Details of the TRPV4 pore. Comparison with other TRPV pore structures shown in c–e reveals a closed lower gate and the absence of an upper gate in TRPV4. **c–e.** The pore structures of TRPV1 (PDB 3J5P) (c), TRPV2 (PDB 5AN8) (d), and TRPV6 (PDB 5IWK) (e) show two constrictions: an upper gate in the selectivity filter and a lower gate in S6 (Deng et al., 2018).

Unfortunately, due to less availability of crystal data for open state of TRP channels, it is uncertain to specify the "pore radius" for all the TRP channels. Some of the TRP channels like zebrafish TRPM2 represent an open state with a 4.4 Å radius (Huang et al., 2018). For TRPV1 and TRPV2, the narrowest point defining the selectivity filter is made by glycine residues (4.8 Å in TRPV1 and 5.2 Å in TRPV2). However, the selectivity filter is remarkably wide in case of TRPV4. The narrowest point in the TRPV4 upper gate position, made by glycine 675 carbonyl oxygen atoms, has a diameter of 10.6 Å. This distance is greater than the corresponding distance in the activated and open TRPV1 structure (7.6 Å) and is big enough to conduct even hydrated ions like Na^+, K^+, and Ca^{2+}, which have diameters falling in the range of 6–10 Å (Figure 12) (Deng et al., 2018).

Table 2

Channel	Permeable metal ions and rank order of inward current amplitudes	Rank order of relative permeability ratios
TRPA1	Ca^{2+}, Mg^{2+}, Ba^{2+}, Zn^{2+}, Cd^{2+}, Co^{2+}	n.d.
TRPC3	Ca^{2+}, Ba^{2+}, Mn^{2+}	n.d.
TRPC4/5	Ca^{2+}, Mn^{2+}	n.d.
TRPC6	Ca^{2+}, Ba^{2+}, Mn^{2+}, Zn^{2+}, Fe^{2+}/Fe^{3+}	n.d.
TRPC7	Ca^{2+}, Ba^{2+}, Mn^{2+}	n.d.
TRPM1	$Ca^{2+} > Ba^{2+} > Mg^{2+} > Ni^{2+}$	$Ba^{2+} > Ca^{2+} > Mg^{2+} > Ni^{2+}$
TRPM2	Ca^{2+}, Mg^{2+}, Ba^{2+}, Mn^{2+}	$Ca^{2+} \approx Mg^{2+} \approx Ba^{2+}$
TRPM3α2	$Ca^{2+} > Zn^{2+} > Mg^{2+} > Ni^{2+}$	$Ni^{2+} > Mg^{2+} > Zn^{2+} \approx Ca^{2+} > Ba^{2+}$
TRPM6	$Ba^{2+} > Ni^{2+} > Mg^{2+} > Ca^{2+}$ $Ba^{2+} > Ni^{2+} > Mg^{2+} > Zn^{2+} \sim Ca^{2+}$ $Zn^{2+} > Ba^{2+} > Mg^{2+} \sim Ca^{2+} > Sr^{2+} > Cd^{2+} > Ni^{2+}$	$Ni^{2+} > Mg^{2+} > Ca^{2+} > Mg^{2+}$
TRPM7	$Zn^{2+} \sim Ni^{2+} >> Ba^{2+} > Co^{2+} > Mg^{2+} \geq Mn^{2+} \geq Sr^{2+} \geq Cd^{2+} \geq Ca^{2+}$ $Ba^{2+} > Ni^{2+} > Zn^{2+} > Mg^{2+} > Ca^{2+}$ $Ni^{2+} > Ba^{2+} \approx Mg^{2+} \approx Zn^{2+} \approx Sr^{2+} > Cd^{2+}$	$Ni^{2+} \approx Co^{2+} \approx Ca^{2+} > Mn^{2+} > Sr^{2+} > Ba^{2+} \approx Mg^{2+}$ $Ca^{2+} \approx Mg^{2+} > Ba^{2+}$

TRPM8	Ca^{2+}, Mg^{2+}, Ba^{2+}, Mn^{2+}	$Ba^{2+} > Ca^{2+} > Mg^{2+}$
	$Ca^{2+} > Sr^{2+} = Ba^{2+} > Mn^{2+}$ (in LNCaP cells)	
dTRPM	$Zn^{2+} > Co^{2+} \approx Mn^{2+} > Ni^{2+} \approx Ca^{2+} > Ba^{2+}$	n.d.
GON-2	Ca^{2+}, Mg^{2+}	n.d.
GTL-1	Ca^{2+}, Mg^{2+}	n.d.
TRPML1	Fe^{2+}, Zn^{2+}, Mn^{2+}, Ca^{2+}, Mg^{2+}, Ni^{2+}, Co^{2+}, Cd^{2+}	n.d.
TRPML2	Fe^{2+}	n.d.
TRPML3	Ca^{2+}, Sr^{2+}, Ba^{2+}, Mg^{2+}	$Ca^{2+} > Sr^{2+} > Ba^{2+}$
TRPP2	Ca^{2+}, Mg^{2+}, Ba^{2+}	n.d.
TRPP3	Ca^{2+}, Ba^{2+}, $Sr^{2+} > Mg^{2+}$	n.d.
	Ca^{2+}, Ba^{2+}, Mg^{2+}, Mn^{2+}	
TRPP3 + PKD1L1	Ca^{2+}, Ba^{2+}	$Ca^{2+} \approx Ba^{2+}$
TRPP3 + PKD1L3	Ca^{2+}, Mg^{2+}	n.d.
TRPV1	Ca^{2+}, Mg^{2+}, Co^{2+}	$Ca^{2+} > Mg^{2+}$
TRPV2	Ca^{2+}, Mg^{2+}	$Ca^{2+} > Mg^{2+}$
TRPV3	Ca^{2+}, Sr^{2+}	
TRPV4	Ca^{2+}, Mg^{2+}, Sr^{2+}, Mn^{2+}	$Ca^{2+} \approx Sr^{2+} > Ba^{2+}$
TRPV5	$Ca^{2+} > Ba^{2+} > Sr^{2+} > Mn^{2+}$	$Ca^{2+} > Mn^{2+} > Ba^{2+} \approx Sr^{2+}$
	Zn^{2+}, Cd^{2+}	
TRPV6	$Ca^{2+} > Sr^{2+} > Ba^{2+} > Mn^{2+}$	$Ca^{2+} > Sr^{2+} > Ba^{2+} > Mn^{2+}$
	$Zn^{2+} > Cd^{2+} > Ca^{2+}$; La^{3+}, Gd^{3+}	

Table 2: Rank orders of inward current amplitudes and relative permeability ratios of TRP channels to metal ions in comparison to other divalent cations (Bouron et al., 2014).

1.5. Sub-cellular distribution of different TRP channels

Organellar TRPs involve the most un-comprehended bunch amongst TRP channels. TRP channels found in intracellular organelles are believed to be targeted for plasma membrane that go through various biosynthetic or secretory pathways en-route to their destination (Dong et al., 2010). Recent development in research methodologies like organellar calcium imaging and organellar electrophysiology have offered proof for the meanings of organellar TRPs. The most important TRP member of the intracellular organelle are TRPML's which are effectively localized in intracellular endosomes and lysosomes. The activity of TRPML1 has been recorded by direct patch-clamp of enlarged lysosomes isolated from vacuolin-treated cells (Dong et al., 2008). Several other TRP channels are also predicted to be found in intracellular organelles, a list of which is provided (Table 3).

Table 3

Channels	Organelle	Reference(s)
TRPA1	Endolysosomes, Secretory granules,	Shang et al., 2016 Zhang et al., 2018
TRPV1	ER and Golgi compartments Cytosolic vesicles, Mitochondria	Turner et al., 2003; Morenilla-Palao et al., 2004 Hurt et al., 2016; Miyake et al., 2015
TRPV2	Early Endosomes	Saito et al., 2007
TRPV3	Lysosomes	Yadav & Goswami, 2017
TRPV4	Mitochondria	Kumar et al., 2018
TRPV5	Recycling endosomes (RE) secretory vesicles	van de Graaf et al., 2006 Zhang et al., 2018
TRPV6	Recycling endosomes (RE), secretory vesicles	van de Graaf et al., 2006; Zhang et al., 2018

TRPP1	endoplasmic reticulum	Geng et al., 2008; Koulen et al., 2002
TRPC3	Intracellular vesicles, Mitochondria, TGN (trans-Golgi network), and the Golgi stack	Singh et al., 2004; Feng et al., 2013; Lavender et al., 2008
TRPC4	secretory vesicles	Zhang et al., 2018
TRPC5	Intracellular vesicles	Bezzerides et al., 2004
TRPC7	TGN (trans-Golgi network) and the Golgi stack	Lavender et al., 2008
TRPM1	Melanosomes	Zhang et al., 2018
TRPM2	Lysosomes, late endosome, and lysosome	Lange et al., 2009; Zhang et al., 2018
TRPM7	synaptic vesicles	Brauchi et al., 2008; Krapivinsky et al., 2006
TRPM8	ER	Thebault et al., 2005
TRPY1	yeast vacuole	Denis & Cyert, 2002; Palmer et al., 2001; Zhou et al., 2003
TRPML1	Late endosome and Lysosome, tubulovesicles.	Dong et al., 2009; Zhang et al., 2018
TRPML2	Recycling endosomes, Late endosome, and Lysosome	Zhang et al., 2018
TRPML3	Early endosomes, Late endosome, and Lysosome	Zhang et al., 2018

Table 3: Organellar TRP channels.

1.6 Specific introduction to TRPV4

1.6.1. Overall architecture and different domain organization of TRPV4

The tetrameric structure of TRPV4 is like that of most TRPV channels, such as TRPV1, TRPV2, and TRPV6, comprising six transmembrane domains from segments 1-6. The first four segments, S1-4 are analogous to the voltage-sensing domain of Voltage-Gated Ion Channel (VGIC). A pore is formed by S5-6 from all four monomers and four S1-4 domains surround the ion permeation pathway.

Both the N-terminal and C-terminal face the cytoplasm and contain different functional domains and motifs. A proline-rich domain (PRD) follows an N-terminal ARD consisting of 6 ankyrin repeats. A TRP-box, a MAP7-binding domain and a CaM-binding site is present in the C-terminus (Nilius & Voets, 2013) (Figure 13).
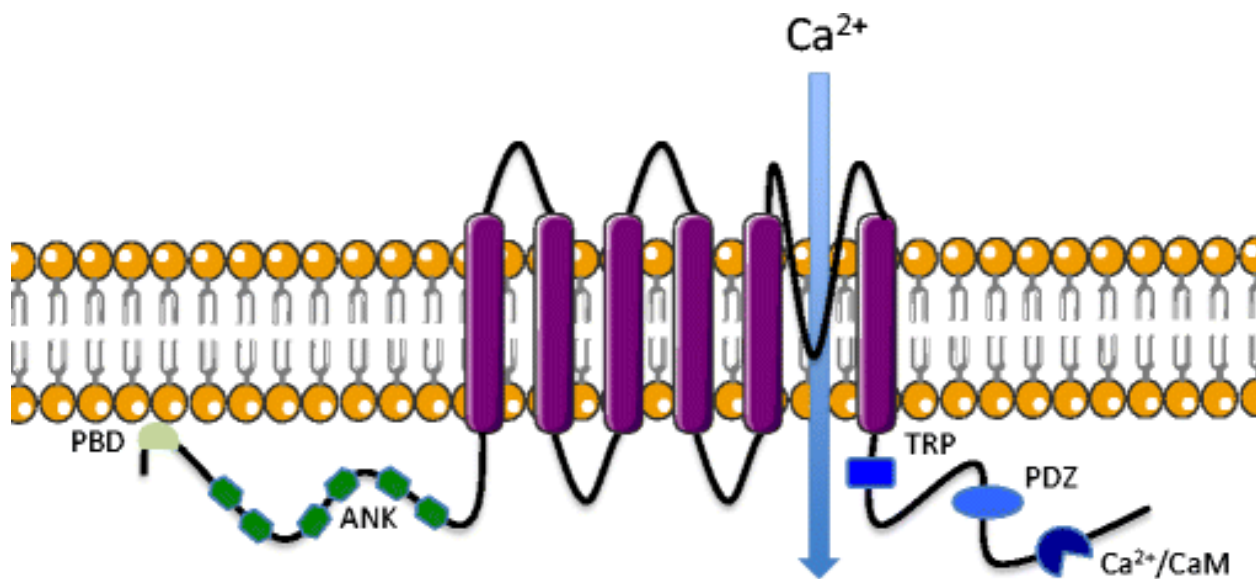
Figure 13: Overall architecture of TRPV4 ion channel. The TRPV4 ion channels contain total six transmembrane domains, a phosphoinositide binding domain (PBD), and several ankyrin repeats (ANK) in the N-terminal, a TRP-box, a PDZ-domain, and a Ca^{2+}–calmodulin-binding region (Ca^{2+}/CaM) at the C-terminus (Goldenberg et al., 2014).

1.6.2. Structure of TRPV4 channel

Recently a 3.8-Å resolution TRPV4 cryo-EM structure from *Xenopus tropicalis* revealed the overall architecture of the channel in great detail (Deng et al., 2018). The structure used for the crystal study was made by removing some portions of N- and C-terminal sections and generating a shortened construct containing amino acid 133–797. For better X-ray diffraction, a site for glycosylation was eliminated by adding the point mutation N647Q. The subsequent TRPV4 construct (133–797 N647Q) permitted near-atomic resolution cryo-EM structure determination. TRPV4 follows the same tetrameric architecture as its close homolog TRPV1, TRPV2, and TRPV6. The first four helices constitute a structural unit, the S1–S4 domain, analogous to the voltage-sensor domain in VGICs. Four S1–S4 domains surround the central ion-conduction pore formed by S5 and S6 and the intervening pore-loops from four identical subunits. The S4–S5 linker, adopts an ordered loop structure, unlike TRPV1 and TRPV2 where an α-helix structure is formed by the S4–S5 linker. In VGICs, the S4–S5 linker usually forms an α-helical segment functioning as a "mechanical lever" to couple voltage-sensor activation and pore opening, and the absence of this α-helical coupler results in different gating behaviour for TRPV4.

A single constriction in the lower gate was observed inside the ion permeation pathway of TRPV4. A narrowest point is formed by side chains of M714, measuring 5.3 Å in diameter which is adequate to prevent ion passage, thus indicating that the structure signifies a closed conformation of the channel. In addition to the lower gate, other TRP channels like TRPV1 and TRPV2 have the second constriction in the selectivity filter, the so-called "upper gate", nearby the extracellular side suggesting a dual gating mechanism (Figure 14).
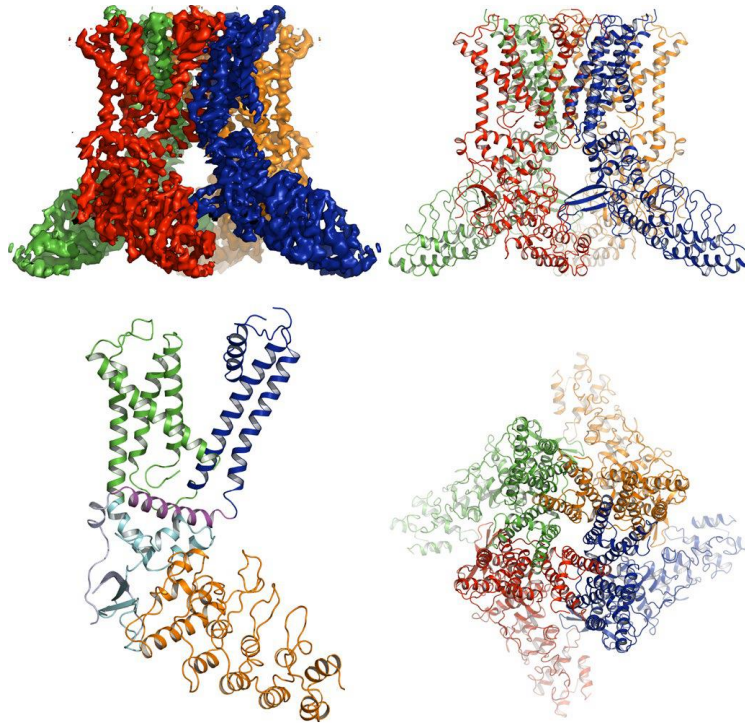
Figure 14: Cryo-EM structure of TRPV4. The monomers of the tetrameric TRPV4 are shown in a different colour. Lateral and orthogonal views are shown. A monomeric structure with different coloured domains is also shown (Deng et al., 2018).

1.6.3. Activation of TRPV4

TRPV4 ion channels are activated by an array of stimuli such as cell swelling, heat, 4 alpha-phorbol esters (4αPDD), endocannabinoids, arachidonic acid, low pH, citrate, etc. which can induce Ca^{2+}-entry inside cells. Epoxyeicosatrienoic acid metabolites (50,60 -EET) directly activate TRPV4 via the EET-binding pocket on the S2-S3 linker. Phorbol esters like 4αPDD, 4αPDH, phorbol 12-myristate 13-acetate, synthetic lipid-like GSK1016790A activate the TRPV4 channel and induce membrane currents (Toft-Bertelsen & Macaulay, 2021). The potent compound in cannabis Δ^9-tetrahydrocannabinol (Δ^9-THC) acts on TRPV4 in addition to other TRP channels. Most abundant endocannabinoids, AEA and 2-AG acts on TRPV4 and activate it. Certain *N*-acyl amides also act as TRPV4 modulators (Muller et al., 2019). The expression of TRPV4 channels in various tissue types including brain, kidney, eyes, skin, pancreas, lungs, urinary systems, hair, and

many other cell types suggests its role in important physiological functions. Their abnormal expression is closely linked to the development of many diseases including gastric, lung, and colorectal cancer (Nilius & Voets, 2013; Falcón et al., 2019; Lawhorn et al., 2020; Nilius & Owsianik, 2011; Watanabe et al., 2002).

1.6.4   Expression of TRPV4 in different tissue and cells

1.6.4.1 Respiratory airways

TRPV4 is believed to be involved in various respiratory diseases. They are expressed in many tissues including pulmonary fibroblasts, lung endothelium, alveolar macrophages, bronchial epithelium, and alveolar epithelium (Pairet et al., 2018). In the lung endothelium, it facilitates vasodilation and endothelial permeability. TRPV4 has been involved in the pathogenesis of asthma, Cystic fibrosis, and Acute respiratory distress syndrome (ARDS) (Scheraga et al., 2017). The role of TRPV4 in treating lung edema has been studied by various research groups recently, where treating with TRPV4 inhibitors helped to inhibit lung edema and acute lung injury. The role of TRPV4 as a therapeutic option in COVID-19 patients was also suggested by researchers, though not successful in the clinical trial till now (Rajan et al., 2021).

1.6.4.2 Skin

TRPV4 channels are found in various skin cells like keratinocytes, mast cells, and macrophages. In human epidermal keratinocytes, it strengthens the tight-junction barrier by co-expressing with junctional proteins like β-catenin and E-cadherin (Akazawa et al., 2013; Suzuki et al., 2003). Recent studies have identified the role of TRPV4 in chronic and acute itch (pruritus) which comes under a pathophysiological condition that triggers the desire to scratch the skin

(Zhang et al., 2021). In the mouse psoriasis model, the role of TRPV4 is also established by various research groups (Sakai et al., 2016; Yan et al., 2021).

1.6.4.3 Vasculature

Recent studies have uncovered the role of TRPV4 in blood vessel function. Shear stress resulting due to blood flow, changes in blood viscosity, and vessel diameter basically follow up on endothelial cells. The endothelial cells respond by segregating TRPV4 from β-catenin, thus destabilizing the junction complex and by Ca^{2+}-influx via shear stress-dependent Ca^{2+} channels like TRPV4 and thereby maintaining normal blood pressure (Baratchi et al., 2017). The role of TRPV4 has been revealed in vasodilation, vasoconstriction, vascular permeability, vascular remodeling, and also is in vascular damage (Liu et al., 2021). Its association with cardiovascular homeostasis and blood pressure control may turn TRPV4 into a remedial objective in hypertension treatment (Earley et al., 2009; Randhawa & Jaggi, 2015).

1.6.4.4 Kidney

TRPV4 is highly significant for kidney function, as it directs the equilibrium of water in cells. It express at high level in the kidney and react to hypotonicity (Liedtke et al., 2000). The expression of the protein is missing in the early part of the kidney tubule but appears in the distal convoluted tubule and further all through the kidney (Figure 15). The expression of these channels in the nephron suggests its function in osmotic stimuli detection and that it might control blood pressure within the sight of expanded salt intake (Gao et al., 2009). Such functions can be linked with a variety of physiological states and pathophysiological conditions.
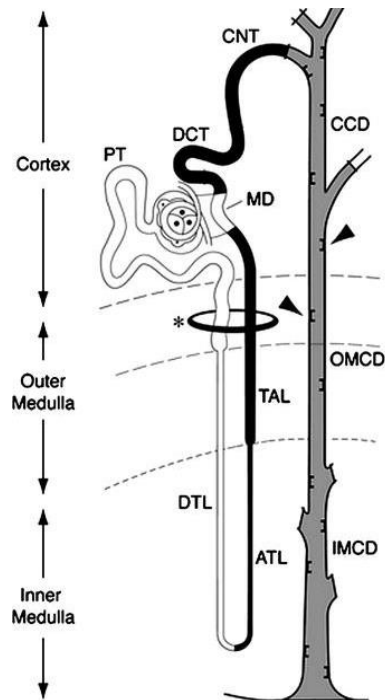
Figure 15: TRPV4 in the mammalian kidney. The kidney consists of an outer cortex and medulla. PT- proximal tubule, DTL-descending thin limb of the loop of Henle, ATL-ascending thin limb of the loop of Henle, MD-macula densa, DCT- distal convoluted tubule, CNT-connecting tubule, CCD-cortical collecting duct, OMCD-outer medullary collecting duct, IMCD-inner medullary collecting duct. Dark color- Abundant TRPV4 expression, Grey- Moderate, White-TRPV4 expression absent (Cohen DM., 2005).

In addition to the above-mentioned tissues, TRPV4 is widely expressed in various other tissues like the adrenal gland, cerebral cortex, placenta, ovary, colon, heart muscle, stomach, appendix, and many others (Figure 16).
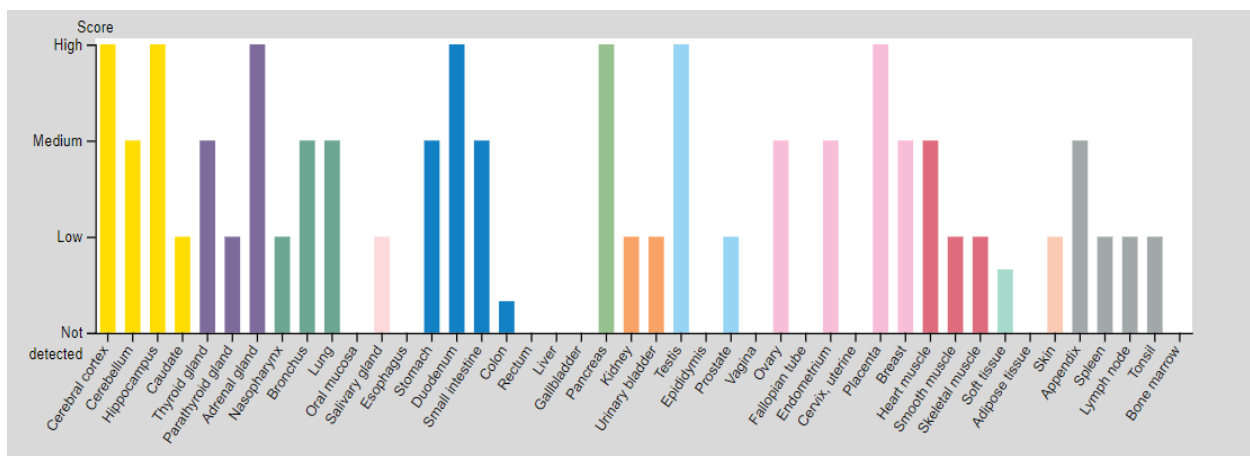
Figure 16: Protein expression overview of TRPV4 in various organs.
(https://www.proteinatlas.org/ENSG00000111199-TRPV4/tissue).

1.6.4.5 Bone

Bone depends on an adequate supply of calcium to keep up with its structural and mechanical properties. Ca^{2+}-signaling is conceivably associated with osteoblast differentiation, osteoclastogenesis, and chondrocyte differentiation required for bone homeostasis (Figure 17). TRPV4-mediated intracellular Ca^{2+}-signaling is suggested to play a significant role in those processes (Masuyama et al., 2008; Muramatsu et al., 2007; Suzuki et al., 2013). Mutation in TRPV4 leads to a wide range of bone-related disorders known as skeletal dysplasias, which further suggest the importance of TRPV4 in the bone cell functions (McCray et al., 2020).
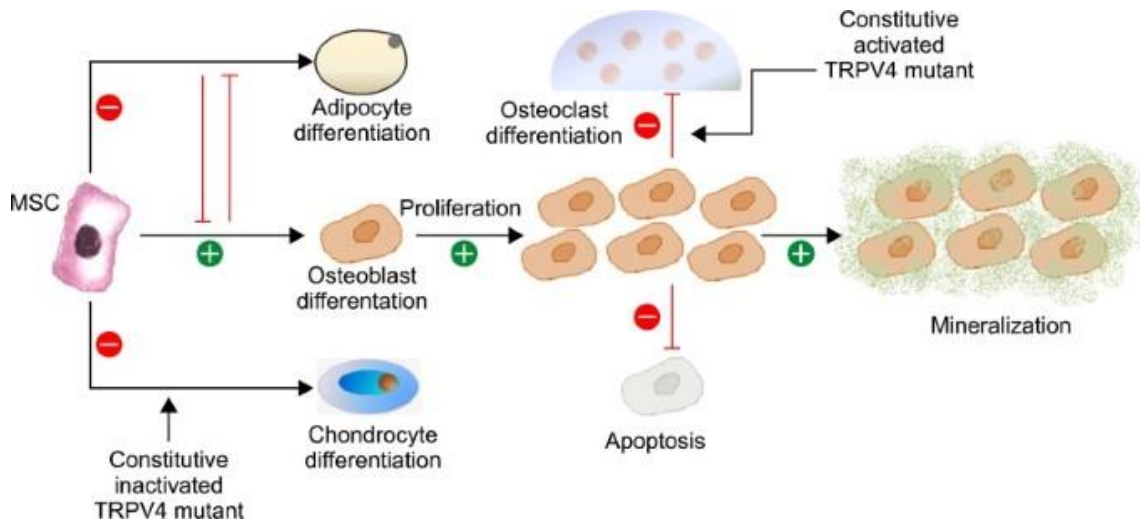
Figure 17: TRPV4 mediated osteogenesis regulation. TRPV4 promotes osteoblast differentiation, proliferation, and mineralization. It represses alternate MSC differentiation into chondrocytes or adipocytes (Kang et al., 2012).

1.6.4.6 Sperm

TRPV4 protein is expressed in all vertebrate sperm cells ranging from fishes to mammals (Figure 18). In fishes, amphibians, reptiles, birds, and mammals including humans, TRPV4 was
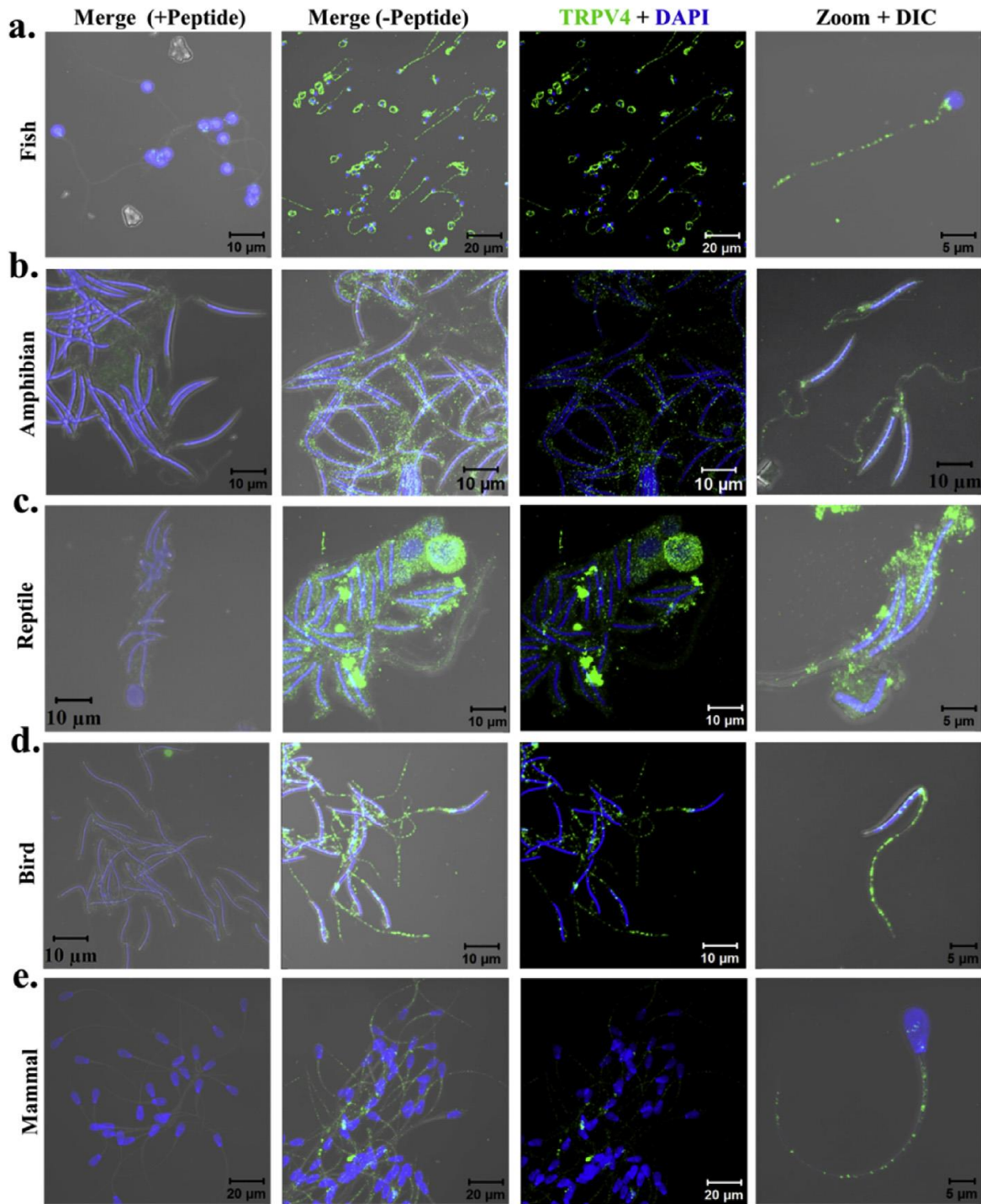
Figure 18: TRPV4 is expressed in vertebrate sperm. Immunofluorescence images depict the presence of TRPV4 (green) protein in **a.** fish (rohu), **b.** amphibian (common toad), **c.** reptile (house lizard), **d**. bird (duck) and **e.** mammals (bovine). The specificity of the primary antibody was confirmed by using a specific blocking peptide. DAPI (Blue) locates in the head of the sperm (Kumar et al., 2016a).

found to be expressed suggesting its role in sensing temperature, osmolarity, and different other chemicals (Kumar et al., 2016a). The DSper channel (Depolarizing Channel) of Sperm which conducts Na^+ ions was found out to be a TRPV4 ion channel based on pharmacological matching (Mundt et al., 2018). TRPV4 channel was also found to be involved in thermotaxis in mice that were suggested using TRPV4 knock out mice model by sperm motility test (Hamano et al., 2016).

1.6.4.7 Immune cells

Recent TRP research has begun to underline their role in immune and inflammatory cells. TRP channels are expressed in various types of immune cells like monocytes/macrophages, lymphocytes, dendritic cells, polymorphonuclear neutrophil granulocytes (PMNs), and mast cells (Partida-Sanchez et al., 2021). TRPV4 ion channels are expressed in T-cells, mast cells, macrophages, leukocytes, neutrophils and monocytes (Parenti et al., 2016; Majhi et al., 2015; Michalick & Kuebler, 2020). Mechanosensation through TRPV4 is likely to activate the innate immune system. At the site of inflammation, TRPV4 activation regulates the delivery of the circulating immune cells. It releases pro- and anti-inflammatory cytokines upon activation and impacts the host defence and thus has emerged as a major regulator of the inflammatory response (Michalick & Kuebler, 2020).

1.6.4.8 Cardiac cells

Ca^{2+} is an important factor for cardiac function. It is the link between the electrical signals that pass through the heart and the contraction of the myocytes to propel blood (Fearnley et al., 2011). Several members of TRP channels like TRPC, TRPV, TRPM, TRPP, TRPA are expressed in various cardiac cells. TRPV4 is required for the differentiation of cardiac fibroblasts into myofibroblasts. In human pluripotent stem cell-derived cardiomyocytes (hPSC-CMs), activation

of TRPV4 by specific agonists leads to Ca^{2+}-influx (Freichel et al., 2017). In human c-kit[+] cardiac stem cells, TRPV4 functional expression is also observed where it helps in cell proliferation and migration (Che et al., 2016).

1.7. Proteins interacting with TRPV4

TRPV4 channel interacts with several other proteins. Some of them change the localization of TRPV4 like PACSIN 3, OS-9, and AIP4, some are cytoskeletal proteins that interact with TRPV4 like tubulin, actin, and neurofilament proteins. Some modulates TRPV4 signaling like β-arrestin and some are ion channel proteins like TRPP2, TRPC1, etc. that interact with TRPV4 (White et al., 2016). Some of the interacting partners are specified below (Figure 19). The work portrayed by Kumar et al. builds up an actual connection of TRPV4 with various mitochondrial proteins, namely with Mfn1, Mfn2, Hsp60, and Cyt C (Kumar et al., 2018, Kumar et al., 2016b). These associations are to a great extent characteristic of the significance of TRPV4 in mitochondrial fission, fusion, and other functions. Of all the interacting partners identified, Cyt C interaction was studied in extensive detail in this thesis work.

Figure 19: TRPV4 interacting proteins. Proteins recognized as interacting with TRPV4. So far, 38 interacting partners have been distinguished for TRPV4. However, this is a partial interaction data set and few other proven interacting proteins are not shown here (White et al., 2016).

1.8 TRPV4 channels and disease

The diseases caused by TRPV4 mutations are inherited in an autosomal dominant manner (McCray et al., 2020). This means that the gene of interest is located on one of the non-sex chromosomes and if any of the parents harbour the abnormal gene, it gets transferred to offspring. TRPV4 diseases are majorly classified into two types, either neuromuscular disorders or skeletal dysplasias (Table 4,5 & 6) (Figure 20). Overlap between the previous two symptoms has also been reported.

Table 4

Autosomal Dominant TRPV4 Disorders	
Neuromuscular disorders	Hereditary motor and sensory neuropathy, type IIC (HMSN2C)
	Scapuloperoneal Spinal Muscular Atrophy (SPSMA)
	Neuronopathy, Distal Hereditary Motor, Type VIII (HMN8)
Skeletal dysplasias	Digital Arthropathy-Brachydactyly, Familial (FDAB)
	Brachyolmia Type 3; BCYM3 (BO3)
	Spondylometaphyseal Dysplasia, Kozlowski Type (SMDK)
	Spondyloepiphyseal Dysplasia, Maroteaux Type (SEDM)
	Parastremmatic Dwarfism (PD)
	Metatropic dysplasia (MD)

Table 4: Autosomal dominant TRPV4 mutations (McCray et al., 2020)**.**

1.8.1 Neuromuscular disorders

1.8.1.1 Hereditary motor and sensory neuropathy, type IIC (HMSN2C) (MIM 606071)

Alternative names [HMSN IIC, Charcot-Marie-Tooth Neuropathy, Type 2C (CMT2C)].

It is an autosomal dominant peripheral neuropathy. The disease phenotype resembles with CDSMA (congenital distal spinal muscular atrophy) and SPSMA (scapuloperoneal spinal muscular atrophy) (Auer-Grumbach et al., 2010). The onset of phenotype is birth-adulthood and

its seriousness is variable from patient to patient. The disease is associated with laryngeal dysfunction, loss of sensorineural hearing, respiratory dysfunction, and joint contractures.

1.8.1.2 Scapuloperoneal Spinal Muscular Atrophy (SPSMA) (MIM 181405)

*Alternative titles; symbols (*Amyotrophy, Neurogenic Scapuloperoneal, New England Type)

Clinical features of this disease include laryngeal dysfunction and sensorineural hearing loss similar to CMT2C, rare cases of sensory deficits and kyphoscoliosis, weakness of muscles and atrophy in the shoulder, neck flexor weakness, etc. In some serious cases, the absence of muscle and weakness are evident from birth itself (Delong & Siddique, 1992). The age of onset is birth-adulthood.

1.8.1.3 Neuronopathy, Distal Hereditary Motor, Type VIII; HMN8

Alternative titles; symbols (Neuropathy, Distal Hereditary Motor, type VIII; DHMN8, Spinal Muscular Atrophy, Distal, Congenital Nonprogressive Spinal Muscular Atrophy)

It is an autosomal dominant disease, symptoms of which include proximal and distal muscle weakness, atrophy of distal leg muscles, and clubfoot. Extensive fatty atrophy in the thigh and calf muscles with preservation of the biceps femoris in the lateral thighs and the medial gastrocnemius in the posteromedial calves. Additional features included scoliosis, pes cavus, vocal cord paresis, scapular winging, and increased serum creatine kinase. Phenotypes overlap with HMSN2C and SPSMA. The age of onset is prenatal (Astrea et al., 2012; Echaniz-Laguna et al., 2014).

1.8.2 Skeletal dysplasias

1.8.2.1 Digital Arthropathy-Brachydactyly, Familial (FDAB) (MIM 606835)

The transmission pattern of FDAB (MIM 606835) is autosomal dominant. Patients with this disease appear normal at birth, with no evidence of developmental skeletal dysplasia. During the

first decade of their life, relative shortening of the middle and distal phalanges and swelling and decreased range of motion of the interphalangeal joints become apparent. Later, the other joints of the hands and feet become affected by deforming and painful osteoarthritis (Lamandé et al., 2011).

1.8.2.2 Brachyolmia Type 3; BCYM3

Brachyolmia comes from the Greek for 'short trunk'. Brachyolmias are a heterogeneous group of skeletal dysplasias that affect primarily the spine. Four types of Brachyolmias are found in nature, among which only Type 3 Brachyolmia (BCYM3; 113500) is caused by a mutation in the TRPV4 gene (OMIM 605427). It is inherited in an autosomal dominant form and characterized with severe kyphoscoliosis and flattened irregular cervical vertebrae. The other three types of Brachyolmia are inherited in an autosomal recessive fashion and do not involve TRPV4.

1.8.2.3 Spondylometaphyseal Dysplasia, Kozlowski Type; SMDK

SMDs are a group of short-stature disorders illustrated by irregularities in the vertebrae and the metaphyses of the tubular bones. SMD Kozlowski (SMDK) is characterized by substantial scoliosis and minor metaphyseal abnormalities in the pelvis. The vertebrae display platyspondyly and over-faced pedicles (Krakow et al., 2009). Inheritance of SMDK is demonstrated to be autosomal dominant (Dai et al., 2010; Krakow et al., 2009).

1.8.2.4 Spondyloepiphyseal Dysplasia, Maroteaux Type

Alternative titles; *symbols* SED, Maroteaux Type Pseudo-Morquio Syndrome, Type 2.

The disease is categorized by short-trunk dwarfism and brachydactyly. While the height of the patient at birth is normal, in early childhood short stature is observed with poor growth and a short trunk. Other features like osteoporosis, kyphoscoliosis and genu valgum, etc. are also observed.

1.8.2.5 Parastremmatic Dwarfism (MIM 168400)

Parastremmatic dwarfism was named Parastremmatic from the Greek term "twisted". It is the rarest autosomal dominant skeletal dysplasia of TRPV4. Clinical features include deformities of the legs with severe genu valgum, bowing of the long bones, twisted thighs, short trunks, kyphoscoliosis, multiple contractures of major joints, etc. that gets worsen through time.

1.8.2.6 Metatropic dysplasia (MD) (MIM 156530)

Metatropic dysplasia term is derived from the Greek term metatropos, meaning "changing patterns", as an inversion of body proportion among birth and adolescence is seen. The disease could be lethal in the prenatal or perinatal period. Often patients have shortened limbs, narrow chest in the new born period that evolves into severe kyphoscoliosis, frequently compromising lung function (Krakow et al., 2009).

Table 5

Findings	Phenotype					
	Mild	**Intermediate**			**Severe**	
	FDAB	**BO3**	**SMDK**	**SEDM**	**PD**	**MD**
Hands/ Feet	Normal at birth; progressive swelling & arthropathy	Clinodactyly	Brachydactyly; hypoplastic carpal bones w/severe delay in ossification	Brachydactyly	Joint contractures	Brachydactyly w/delayed carpal ossification
Spine	Normal	± scoliosis, kyphosis; mild platyspondyly	Platyspondyly; overfaced pedicles		Significant kyphoscoliosis; overfaced pedicles	Platyspondyly; overfaced pedicles
Long bones	NA	Minimal metaphyseal changes; short femoral neck w/irregular proximal femoral metaphyses	± mild metaphyseal changes; genu varum	Mild-to-moderate metaphyseal changes; genu varum	Severe metaphyseal changes w/severe limb deformity; joint contractures; other	Dumbbell-shaped long bones w/epiphyseal dysplasia & prominent joints; progressive joint contractures; other
Pelvis	Normal	NA	Square, short, flared iliac	Champagne-glass	Halberd-shaped pelvis; supra-acetabular notches	

			wings; flat, irregular acetabulae; coxa vara; ± supra-acetabular notches	configuration of pelvic inlet		
Other	Average height; early-childhood onset	Mild short stature; limbs unaffected; good physical function	Short-trunk short-stature dwarfism; broad chest; early-childhood onset w/waddling gait	Short-trunk short-stature dwarfism	Significant short-trunk short-stature dwarfism	May be lethal prenatally or perinatally; at birth, short-limb short-stature dwarfism

Table 5: Characteristic features of autosomal dominant *TRPV4* Skeletal Dysplasias (McCray et al., 2020).
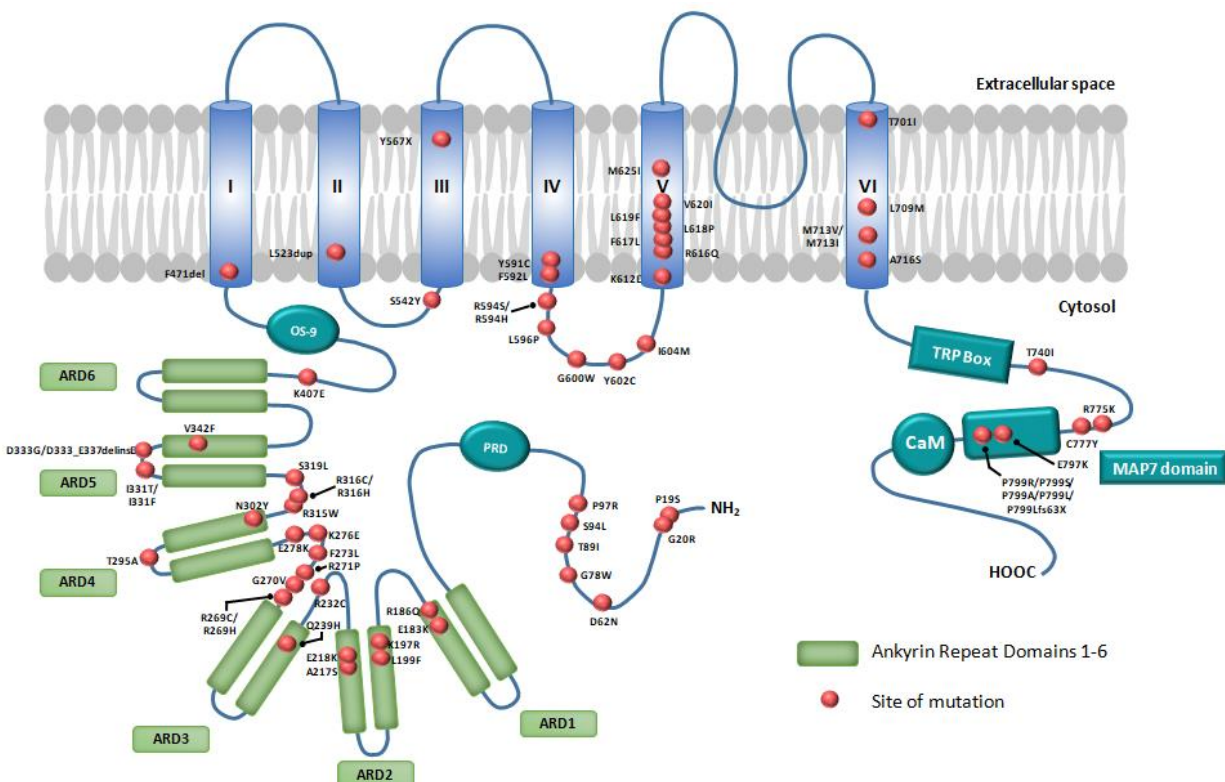
Figure 20: TRPV4 mutation and hotspots. The TRPV4 protein in human is found to comprise approx. 60 different mutations (red dots) spread over several domains in N- and C-terminal as well as in the transmembrane region (Image courtesy: Ranabir Chakraborty).

Table 6

Sl no	Mutation	Residue	Disease	Effects on ion conductivity	Reference(s)
1	--	P19S	Hyponatremia (reduced response to hypotonic stress)	Loss of channel function	Tian et al., 2009
2	58G>A	G20R	Distal hereditary motor neuropathy (dHMN)		Fawcett et al., 2012
3	184G > A (exon 2)	D62N	Phenotype is compatible with CMT type 2C and presented with intra-cytoplasmic basophilic inclusions besides the neurogenic changes.		Evangelista et al., 2015
4	- -	G78W	Dual phenotype of metatropic dysplasia and fetal akinesia		Unger et al., 2011
5	C366 >T (Exon 2)	T89I	Neonatal lethal metatrophic dysplasia	Elevated basal Ca^{2+}	Camacho et al., 2010
6	281C>T	S94L	Congenital spinal muscular atrophy and arthrogryposis (CSMAA)	Increase in the channel activity	Velilla et al., 2019
7	290C > G (Exon 2)	P97R	Distal muscular atrophy (dSMA) and vocal cord paralysis	Loss-of-function	Fiorillo et al., 2012
8	547G>A (exon 3)	E183K	SEDM-PM2		Nishimura et al., 2010
9	557G>A	R186Q	Charcot–Marie–Tooth disease type 2C	Slight increase in Ca^{2+} levels	Landouré et al., 2012
10	A590 >G	K197R	Metatropic dysplasia		Camacho et al., 2010
11	597G>C (exon 4)	L199F	Metatropic dysplasia		Dai et al., 2010
12	649G > T	A217S	SMDK and a neurological phenotype compatible with scapulo-humeral spinal muscular atrophy		Cho et al., 2012
13	652G>A	E218K	CMT2 with Complex neurological syndrome with demyelinating neuropathy		Fawcett et al., 2012
14	694C > T (Exon 4)	R232C	HMN with vocal fold paralysis, SPSMA, HMSN2		Zimoń et al., 2010
15	717G>C (Exon 5)	Q239H	Metatropicdysplaisa		Andreucci et al., 2011

16	805C > T (exon 5)	R269C	HSMN type IIC, with SPSMA and also with distal congenital non progressive SMA.		Evangelista et al., 2015
17	G806A (exon 5)	R269H	SMA, CMT2C, SPSMA	gain-of-function	Deng et al., 2010
18	c.809G>T (exon 5)	G270V	Familial digital arthropathy-brachydactyly (FDAB)	Reduced response to agonist	Lamandé et al., 2011
19	c.812G>C (exon 5)	R271P	Familial digital arthropathy-brachydactyly (FDAB)	Reduced response to agonist	Lamandé et al., 2011
20	c.819C>G (exon 5)	F273L	Familial digital arthropathy-brachydactyly (FDAB)	Reduced response to agonist	Lamandé et al., 2011
21	- -	K276E	Dual phenotype of metatropic dysplasia and fetal akinesia		Unger et al., 2011
22	832G>A (exon 5)	E278K	SMDK		Dai et al., 2010
23	883A>G (Exon 6)	T295A	Metatropic dysplasia		Dai et al., 2010
24	904A>T	N302Y	Charcot–Marie–Tooth disease type 2C (CMT2C)		Fawcett et al., 2012
25	943 C>T (Exon 6)	R315W	CMT2C		Chen et al., 2010
26	C946T (exon 6)	R316C	HMSN2C	gain-of-function	Deng et al., 2010
27	G947>A (exon 6)	R316H	Charcot–Marie–Tooth disease type 2C	increased intracellular Ca^{2+}	Klein et al., 2011
28	c.956C>T	S319L	Isolated scapular winging		Brown & Nguyen, 2017
29	A991 >T (Exon 6)	I331F	Severe Metatropic dysplasia	constitutive open channels	Camacho et al., 2010
30	992T>C (Exon 6)	I331T	Metatropic dysplasia		Dai et al., 2010
31	cA992→G (Exon 6)	D333G	SMDK	Increased Ca^{2+}-influx	Krakow et al., 2009
32	1024G>T (Exon 6)	V342F	Metatropic dysplasia		Dai et al., 2010
33	1219A>G (Exon 7)	K407E	Metatropic dysplasia (MD)		Andreucci et al., 2011
34	1412_1414del (Exon 8) 471	F471del	Metatropic dysplasia (MD)		Camacho et al., 2010; Dai et al., 2010
35	1566_68dup; p.L523dup (Exon 9)	L523dup	SMDK		Andreucci et al., 2011
36	1625C>A (Exon 10)	S542Y	CMT2C		Chen et al., 2010

37	1701C>A	Y567X	Charcot–Marie–Tooth disease type 2C		Fawcett et al., 2012
38	1772A>G (Exon 11)	Y591C	Brachyolmia, SMDK		Andreucci et al., 2011
39	1780C>A (Exon 11)	R594S	Metatropic dysplasia (MD)		Andreucci et al., 2011
40	1774T>C (Exon 11)	F592L	Metatropic dysplasia		Dai et al., 2010
41	1781G>A (Exon 11)	R594H	SMDK, Parastremmatic dysplasia	Increased Ca^{2+}-influx	Nishimura et al., 2010
42	c.1787T>C (Exon 11)	L596P	SMDK		Dai et al., 2010
43	1798G>T (Exon 11)	G600W	SMDK		Dai et al., 2010
44	c.1805A>G (Exon 11)	Y602C	SEDM-PM2		Nishimura et al., 2010
45	C1812 >G (Exon 11)	I604M	Metatropic dysplasia		Camacho et al., 2010
46	1834A>G (Exon 12)	K612E	Metatropic dysplasia	_	Narayanan et al, 2016
47	1847G>A (Exon 12)	R616Q	Brachyolmia	Increased Ca^{2+}-influx	Rock et al., 2008
48	C1851 >A (exon 12)	F617L	Metatropic dysplasia		Camacho et al., 2010
49	T1853 >C (Exon 12)	L618P	Metatropic dysplasia		Camacho et al., 2010
50	1855C > T	L619F	Metatropic dysplasia (accelerated chondrogenic differentiation of dental pulp stem cells)	enhanced intracellular Ca^{2+}-level	Nonaka et al., 2019
51	1858G>A (Exon 12)	V620I	Brachyolmia	Increased Ca^{2+}-influx	Rock et al., 2008
52	1875G>A (Exon 12)	M625I	SMDK		Dai et al., 2010
53	2102C>T	T701I	Charcot–Marie–Tooth disease type 2C		Fawcett et al., 2012
54	2125C>A (Exon 13)	L709M	SMDK/BO		Dai et al., 2010
55	- -	M713V/I	Central Giant cell lesions of the jaw (GCLJ)	Increased channel activity	Gomes et al., 2018

56	c.G2146→T (Exon 13)	A716S	SMDK	Same as WT	Krakow et al., 2009
57	- -	T740I	Dual phenotype of metatropic dysplasia and fetal akinesia		Unger et al., 2011
58	2324G>A (Exon 14)	R775K	Metatropic dysplasia		Dai et al., 2010
59	2330G>A (Exon 14)	C777Y	SMDK		Dai et al., 2010
60	c.2389G>A (Exon 15)	E797K	Spondylo-epimetaphyseal dysplasia Maro- teaux—pseudo-Morquio type 2 (SEDM-PM2), SMDK and Metatropic dysplasia		Nishimura et al., 2010; Camacho et al., 2010; Dai et al., 2010
61	2396C>G (Exon 15)	P799R	Metatropic dysplasia		Dai et al., 2010
62	2395C>T (Exon 15)	P799S	Metatropic dysplasia		Dai et al., 2010
63	2395C>G (Exon 15)	P799A	Metatropic dysplasia		Dai et al., 2010
64	C2396 >T (Exon 15)	P799L	Metatropic dysplasia, SEDM-PM2	constitutive open channels	Camacho et al., 2010; Nishimura et al., 2010; Dai et al., 2010
65	999_1010del (Exon 6)	D333_E3 37delinsE	Mild Metatropic Dysplasia		Camacho et al., 2010
66	2396_2412del17	Pro799Lfs 63X	SEDM-PM2		Nishimura et al., 2010

Table 6: Mutation list of TRPV4 protein

1.9 Specific objectives of this study

The focus of this thesis is the molecular and functional characterization of TRPV4 ion channel which is the fourth member of the TRPV subfamily. It is a Ca^{2+}-permeable non-selective cation channel detectable in brain, kidneys, liver, lungs, hearts, dorsal root and trigeminal sensory ganglia and in many other tissues and cells (Heller & O'Neil, 2006). TRPV4 represents an important ancient TRP channel that is very much conserved in all vertebrates. So far more than 50 naturally occurring point mutations of TRPV4 have been identified in humans causing diseases ranging from dwarfism to embryonic death. The variable phenotypes (with different levels of penetration) with pathophysiological abnormalities due to these mutations are commonly termed as "channelopathies" (McCray et al., 2020). Most of these are either "gain-of-function" or "loss-of-function" in nature, and the exact mechanisms behind such channelopathies are unknown.

Recent studies have described lipids as central modulators of sensory TRP channels. There has long been an interest to understand how these integral membrane proteins interact with lipids in their surroundings. Lipids and lipid-like molecules can directly activate some thermosensitive channels or regulate their activities. TRP channels are located in special membrane microdomains that are rich in cholesterol, some of whose functions are affected by the cholesterol content of the membrane (Gutorov et al., 2019; Ciardo & Ferrer-Montiel, 2017; Taberner et al., 2015). In the last few years, the interaction of different cytoskeletal components (such as tubulin/actin) and membrane components (such as cholesterol) with TRP channel members have been described (Gutorov et al., 2019; Liu et al., 2006; Morales-Lázaro and Rosenbaum, 2017). Until now, in excess of 50 different types of lipids that can control TRP channel functions have been described (Cao et al., 2013; Morenilla-Palao et al., 2009; Lukacs et al., 2013; Yoo et al., 2014). This lipid-

based modulatory impact is an alternative and promising way to study TRP channel dysfunction/s relevant in diseases (Ciardo & Ferrer-Montiel, 2017)

TRPV4 is known to be regulated by several physical or chemical stimuli such as temperature, pH, voltage, osmolality or even by different lipids present in the membranous environment. Such lipid molecules often modulate precise localization of TRPV4 in submembranous compartments such as lipid rafts, caveolae, and filopodial tips and thereby the functions of these specialized subcellular structures (Caires et al., 2017; White et al., 2016). Previous reports suggest that TRPV4 interacts with cholesterol, other steroids and such interactions may be relevant for channel gating (Das & Goswami, 2019; Kumari et al., 2015). However, the exact mechanism/s by which cholesterol and steroids regulate the gating of TRPs are poorly understood. This thesis work deals with the molecular and cellular characterization of TRPV4-mediated channelopathies and the effect of TRPV4 in mitochondrial metabolism. In this work, the molecular evolution of TRPV4 and the impact of cholesterol interaction were studied using both *in silico* and experimental approaches. The localization of the TRPV4 in lipid rafts in different cellular context has been characterized. Also, few pathogenic mutants (which are located in the cholesterol-binding motifs) were investigated. The importance of TRPV4 during vertebrate evolution, its expression in bone cell lineages, its role in steroidogenesis, and functional relationship with Cyt C was characterized.

<u>Aims of the present study:</u>

* Molecular evolution of TRPV4 during vertebrate radiation.

* Characterization TRPV4-L596P mutation causing SMDK.

* Characterization TRPV4-R616Q mutation causing Brachyolmia.

* Steroidogenesis as a function of mitochondrial metabolism and the role of TRPV4 in it.

* Characterization of TRPV4 interaction with mitochondrial protein Cyt C.

Chapter 2

Results

2.1 Molecular evolution of TRPV4 during vertebrate radiation

Previous studies have demonstrated that TRPV4 is a highly conserved protein and has evolved ~450 Million years (MY) ago, when vertebrate evolution started (Kumari et al., 2015). By synteny analysis it is revealed that TRPV4 gene is flanked by two genes involved in cholesterol biosynthesis pathway i.e., MVK and GLTP. The orientation and location of these genes are conserved for 450 MY and in all vertebrates (corresponding to human 12q24.1 chromosome location). This suggests a possible functional regulation of TRPV4 by metabolites of the cholesterol biosynthesis pathway. Proteins that interact with cholesterol often possess certain cholesterol-recognition motifs known as CRAC, CARC or CCM. We analyzed CRAC, CARC and unique sphingolipid-binding motif/s present in the full-length TRPV4. Conservation analysis of these cholesterol-binding motifs were performed.

Subsequently, amino acids of TRPV4 that are present in the Lipid-Water-Interface (LWI) were analyzed. LWI-residues are defined as 5 amino acids long sequence on either side of transmembrane (TM) helices which are critical for ion channel functions as they remain functional in a unique physico-chemical microenvironment. Total 60 amino acids representing 12 LWI stretches from 6 TM regions were considered. We have analyzed the conservation of LWI motifs. At least two naturally occurring and pathogenic mutants, namely, R594H and L596P are located in this LWI regions. We analyzed the molecular exclusion, retention or selection of amino acids in LWI regions. The percentage of occurrence for all the amino acids and their conservation throughout the vertebrate evolution were also analyzed.

2.1.1. Phylogenetic analysis of TRPV4

TRPV4 protein is evolved during the progress of Silurian from Devonian period (ca 450 MYA). The TRPV4 protein shares less sequence homology and identity with the invertebrate homologues OSM 9 and NAN of *C. elegans* and *Drosophila* respectively. The vertebrate protein sequences are very well conserved in TRPV4. Total 74 TRPV4 protein sequences from vertebrate and invertebrates were used for phylogenetic analysis. Total 47 mammals, 8 reptiles, 4 birds, 4 amphibians, 9 fishes and 2 invertebrate protein sequences were considered for this analysis. All the different classes formed separate monophyletic clusters and the invertebrates diverged first in the cluster (Figure 21). Overall, TRPV4 represent a well conserved protein within all vertebrates.

2.1.2   Homology modeling of hTRPV4

The 3D structure of human TRPV4 protein and the mutant R616Q-TRPV4 was predicted by YASARA's homology modeling. The target sequence contained 871 residues and 606 of 871 target residues (69.6%) were aligned to template residues (608 of 871, 69.8% in case of R616Q). Among these aligned residues, the sequence identity was 87.1% (87.3% for R616Q) and the sequence similarity was 94.7% for Wt (94.9% for R616Q). The side-chains were built, optimized and fine-tuned and newly modelled parts were subjected to a combined steepest descent and simulated annealing minimization . The overall quality (determined by Z-score -0.793 for Wt and -0.785 for R616Q) of the model fell in the 'good' category. The derived structure is represented below (Figure 22). The R616Q-TRPV4 structure and other parameter details are specified in the annexure (Annexure 1).

Mammals

				0.0000	Wolf
			0.0000	0.0000	Dingo dog
		0.0017	0.0000	0.0000	Dog
	0.0000		0.0066		Red fox
0.0057			0.0117		seal
		0.0032	0.0050		monk seal
0.0049		0.1067		Mountain lion
	0.0169	0.0016	cheetah
0.0034		0.0017	0.0000	cat
	0.0586	horse
0.0019	0.0407	bat mammals
	0.0104	Chinese rufous horseshoe bat
0.0034	0.0090	Pig
0.0045	0.0053	0.0320	common vampire bat
	0.0017	Pacific white-sided dolphin
0.0100	0.0017	Narrow-ridged finless porpoise
	0.0050	sperm whale
0.0035	0.0060	goat
	0.0021	water buffalo
0.0132	0.0000	Bos taurus
0.0025	0.0000	humped cattle
0.0021	0.0033	Northern greater galago
0.0254	pygmy chimpanzee

Northern greater galago
pygmy chimpanzee
Common chimpanzee
HUMAN
Gorilla gorilla gorilla
Sumatran orangutan
Black snub-nosed monkey
Old World monkey
pig-tailed macaque monkey
North American beaver
common degu
Damaraland mole
Guinea pig
squirrel
Thirteen-lined ground squirrel
Spalax
prairie vole-rodent
golden hamster rodent
RAT
Brown rat
MOUSE
Ryukyu mouse rodent
Gairdners shrewmouse
Rabbit
nine-banded armadillo
Ugandan red colobus monkey

Reptiles

American alligator
Chinese alligator
painted turtle
common box turtle-reptile
Japanese striped snake
Japanese grass lizard
eastern brown snake
Tiger snakes

Birds

golden-collared manakin
Chicken
emu
Chilean tinamou

Amphibians

Japanese tree frog
Tibetan frog
Western clawed frog
African clawed frog

Fishes

iridescent shark
blind cave fish
Zebra fish
Japanese rice fish
zebra mbuna
Tilapia burtoni
killfish
clown fish
spiny chromis damselfish

Invertebrates

D. melanogaster
Caenorhabditis elegans

54

Figure 21: Phylogenetic tree and molecular evolution of TRPV4. Maximum likelihood tree illustrates phylogenetic tree of TRPV4 sequences collected from invertebrates to vertebrates. TRPV4 had evolved around 450 MYA and traces back to the evolution of vertebrates and functional TRPV4 homologues are present in invertebrates as well.
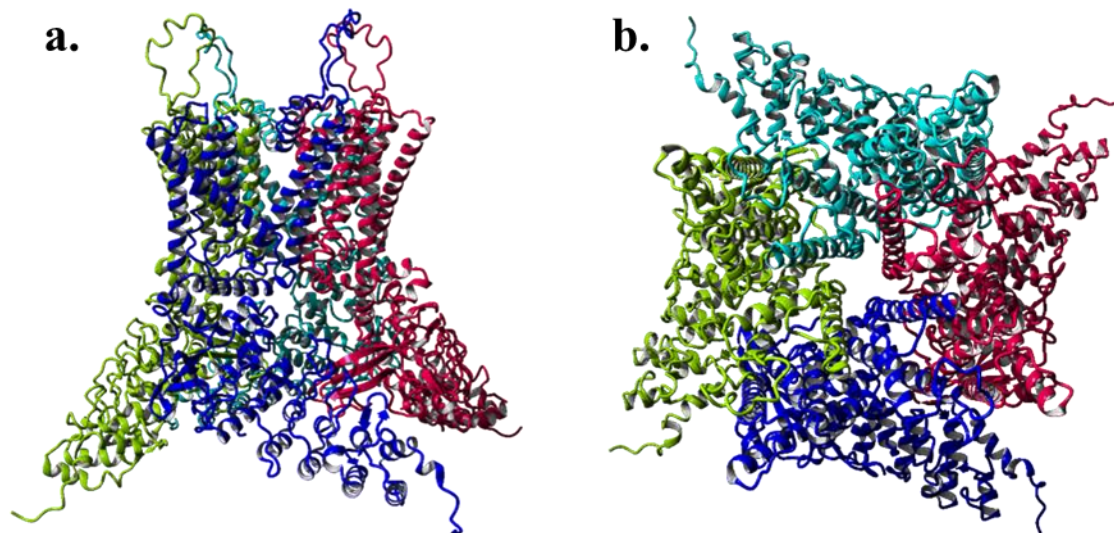
Figure 22: **Three-dimensional model of the hTRPV4.** Homology modeling derived 3D structure of hTRPV4 using 6BBJ as a template. a) side view b) Top view. Four individual subunits are colored in different shades.

2.1.3   Conservation of different structural domains of TRPV4

To test the conservation of TRPV4 throughout the vertebrate evolution, we have analyzed the sequences from various vertebrates and utilized statistics to evaluate it. We have also analyzed at the conservation of different domains and motifs (as per the literatures and databases) (Table 7). Some of the regions are well conserved, some are semi conserved and some are less conserved. Regions like TM4, Loop 4, TM5 and TRP-box are conserved to the maximum, whereas PRD, Loop 3 and Loop 6 etc. are diverged (Figure 23). These conserved regions [such as TM4-Loop 4-TM5 and Ankyrin Repeat Domains (ARD)] are those where large number of mutations are found in human population that causes several channeopathies (Figure 20).

Domains	Amino acids
ANK-1	157-187
ANK-2	193-223
ANK-3	237-266
ANK-4	284-313
ANK-5	320-250
ANK-6	369-398
CaM-binding region	812-831
Loop1	491-507
Loop2	535-547
Loop3	569-572
Loop4	594-608
Loop5	637-665
Loop6	686-693
MAP7-binding region	789-809
Pore Loop	666-685
PRD	132-144
TM1	470-490
TM2	508-534
TM3	548-568
TM4	573-593
TM5	609-636
TM6	694-722
TRP-BOX	732-737

Table 7: Different domains and motifs of TRPV4 used for conservation analyses (White et al., 2016; Kumari et al., 2015).
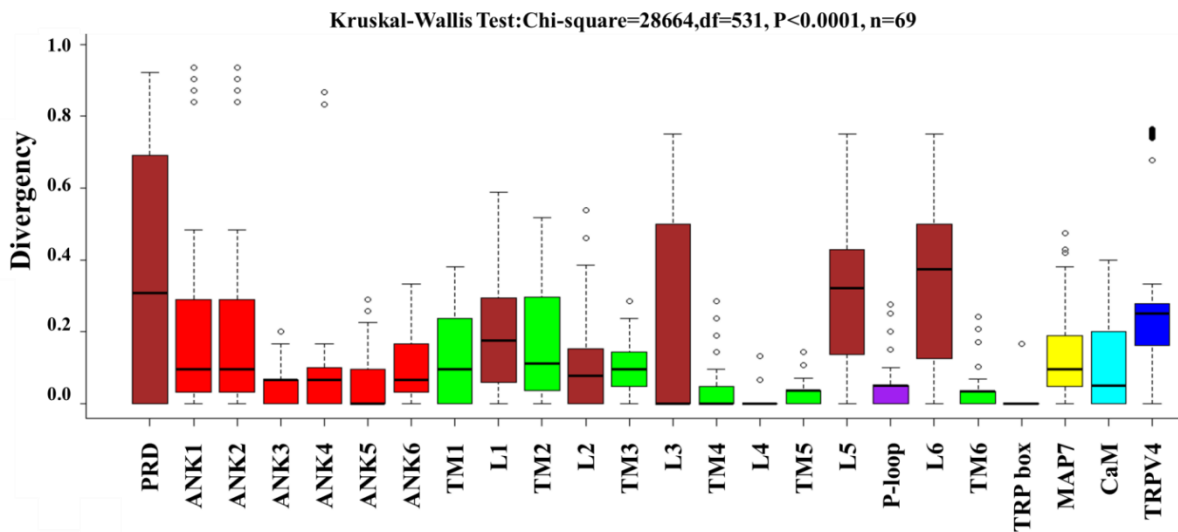
Figure 23: Conserved domains and motifs of TRPV4. The lower value in Y-axis indicates higher conservation and higher value indicate less conservation. Various regions of TRPV4 are shown by various shadings. Total 69 vertebrate sequences were used for this analysis.

2.1.4   TRPV4 sequence contains many conserved CARC- and CRAC-motifs

Cholesterol-binding CRAC, CARC, CCM-motifs and sphingolipid-binding motif/s present in hTRPV4 were analyzed. We found total 6 CRAC and 18 CARC motifs and 1 unique sphingolipid-binding motif present in the entire protein sequence (Figure 24a). No CCM motif was observed in hTRPV4. Conservation analysis of all these motifs indicate that these motifs are either highly conserved or semi conserved in all vertebrates (Figure 24b).

In this thesis work, we have selected two mutations R616Q and L596P lying on selected CARC and CRAC motif respectively. The CARC motif consisting of amino acid 612-623 has two overlapping CARC-motifs and at least four disease causing mutations (R616Q/ F617L/ L618P/ V620I) located in this region (Verma et al., 2010). R616Q is a "gain-of-function" mutation that cause autosomal dominant Brachyolmia (Rock et al., 2008). Notably, this mutation is located in CARC motif and this specific Arginine residue is found to be very well conserved both in vertebrate as well as invertebrate species. Never-the-less, other critical amino acids that define the CARC-motif are absent in invertebrate sequences. The CRAC-motif (consisting amino acid 596-608) is highly conserved and contains an SMDK-causing mutation, i.e., L596P. The detail characterization of these two mutants is done in later part of the thesis.

2.1.5   Determination of the Lipid-Water Interface (LWI) amino acids of TRPV4

The LWI region signifies a unique physico-chemical microenvironment in a membrane-bound system where the concentration of free water is minimum (but not absent totally). The residues present in LWI are mostly unstructured and form several non-covalent contacts through their side chains with specific components present in the lipid bilayer (Hübner & Blume, 1998; Killian & Von Heijne, 2000).
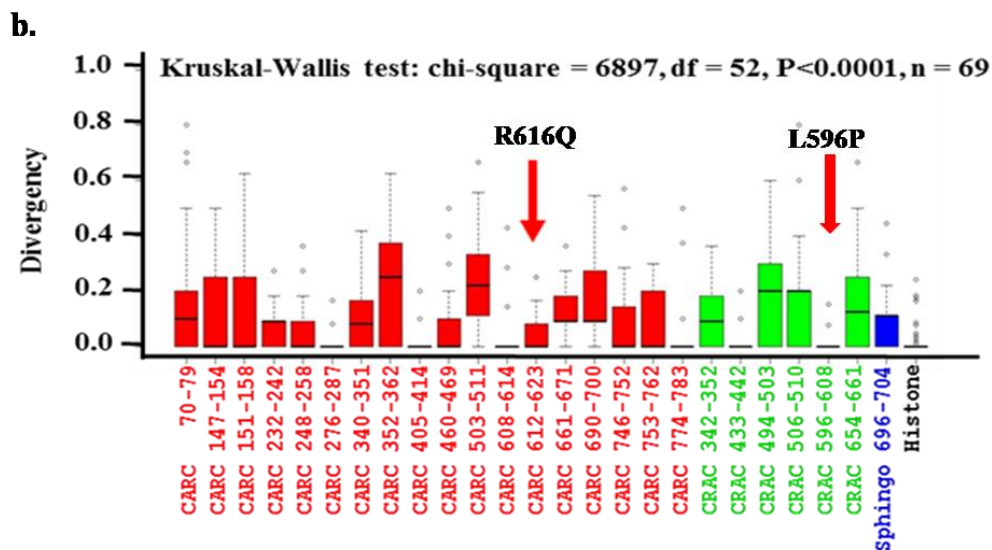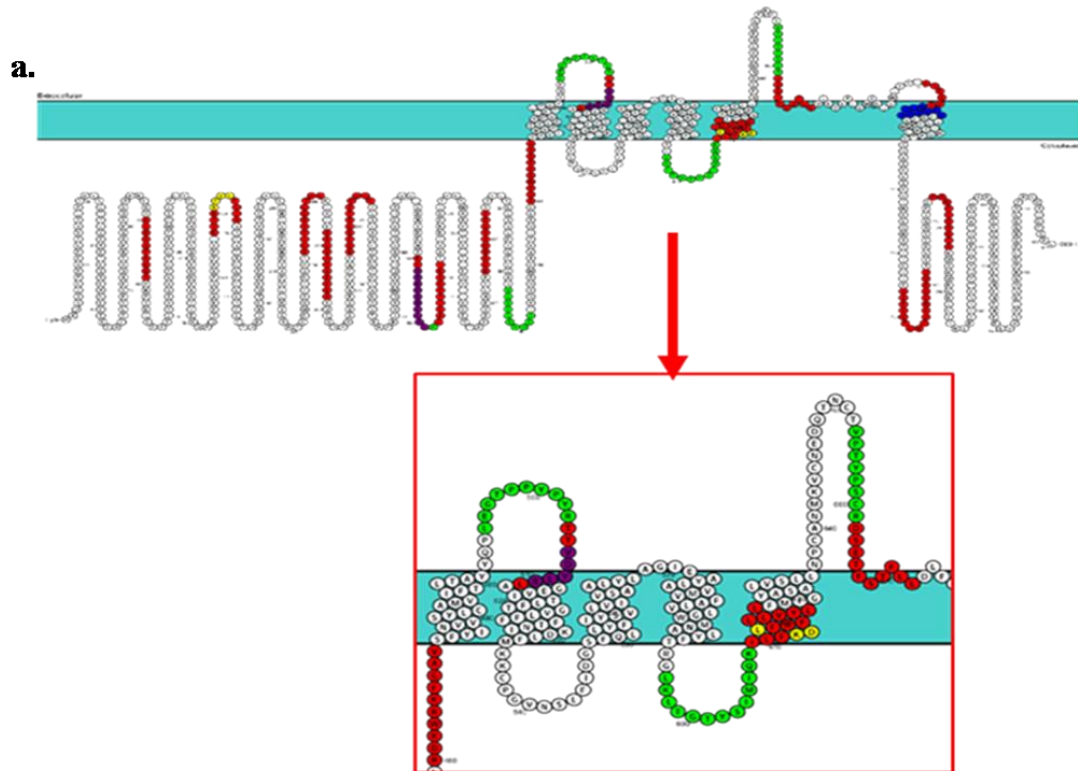
Figure 24: Conserved cholesterol-binding motifs of TRPV4. The TRPV4 protein containing several CARC- and CRAC-motifs are plotted in protter webserver (**a**). The conservation of total 25 motifs were analyzed (**b**). The lower value in Y axis indicate higher conservation and higher value indicate less conservation. Various regions of TRPV4 are shown by various shadings. All values are significant (p < 0.0001, Kruskal–Wallis test).

LWI-residues are defined as the 5 amino acids stretch (Typically ~6-10 Å long) on both sides of the N-terminal and C-terminal ends of each TM helices. These TM regions are based on Uniprot-derived topology and plotted in Protter. Total 60 amino acids constituting 12 LWI stretches from 6 TM regions were considered (Figure 25).
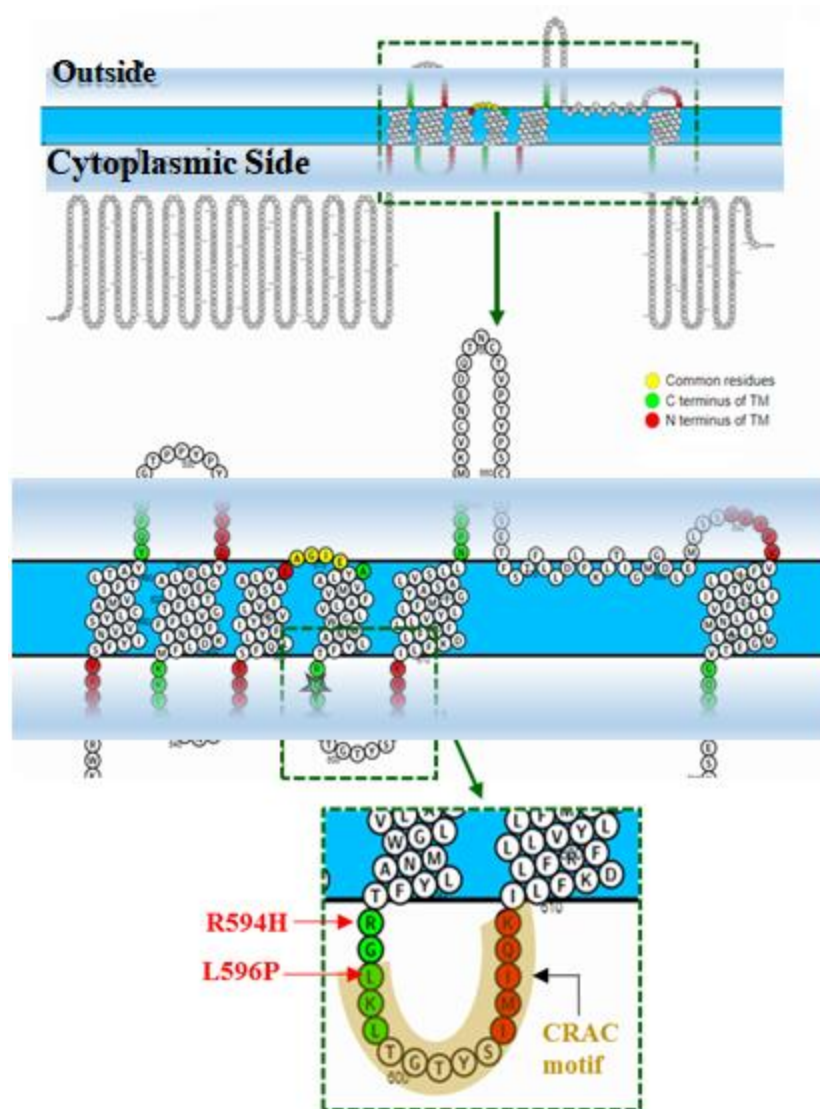
Figure 25: There is total 12 lipid-water-interface region present in TRPV4 protein. Schematic representation of total 12 lipid-water-interface regions present in full-length TRPV4 is shown. The N-terminal and C-terminal LWI regions are colored in red and green respectively. Two mutations (marked with arrows), namely R594H and L596P are specifically located at the C-terminal LWI of TM4. An overlapping CRAC-motif is also indicated by filled color. The outer LWI region flanking TM3 and TM4 has few overlapping residues.

2.1.6 Amino acids present in the Lipid-Water-Interface are highly conserved

To analyze the conservation of different residues present at the LWI, we calculated the 5 amino acid stretches flanking the TM regions. We noted that almost all these stretches are well conserved (Figure 26). Among all, the C-terminal portion of the TM2 (termed as TM2C), C-terminal portion of the TM4 (termed as TM4C) and N-terminal portion of the TM5 (termed as TM5N) and C-terminal portion of the TM6 (termed as TM6C) are highly conserved stretches. All inside LWI stretches are more conserved than all outside LWI stretches suggesting that overall selection pressure is high in the inner LWI region than the outer LWI region (Figure 26a). The N-terminal portion of the TM2 (termed as TM2N), the C-terminal portion of the TM3 (termed as TM3C) and the N-terminal portion of the TM4 (termed as TM4N) are divergent to some extent. The seqlogo analysis suggests that certain amino acids present in these LWI regions are more conserved than other amino acids (Figure 26b). Especially the amino acids that demark the LWI boundary to the membrane are most conserved, at least for TM1-TM4. The amino acid demarking the outer pore-loop seems to be the most diverged among others. Notably, the TM4-Loop-TM5 region has few cholesterol-binding motifs and some of these motifs also overlap with these LWI regions. At least two naturally occurring and pathogenic mutants, namely, R594H and L596P are located in the LWI regions. Further analysis indicates that this stretch as well as critical amino acids that mark the signature of CRAC-motif are highly conserved in the vertebrates, but not so much in invertebrates (Annexure 2).
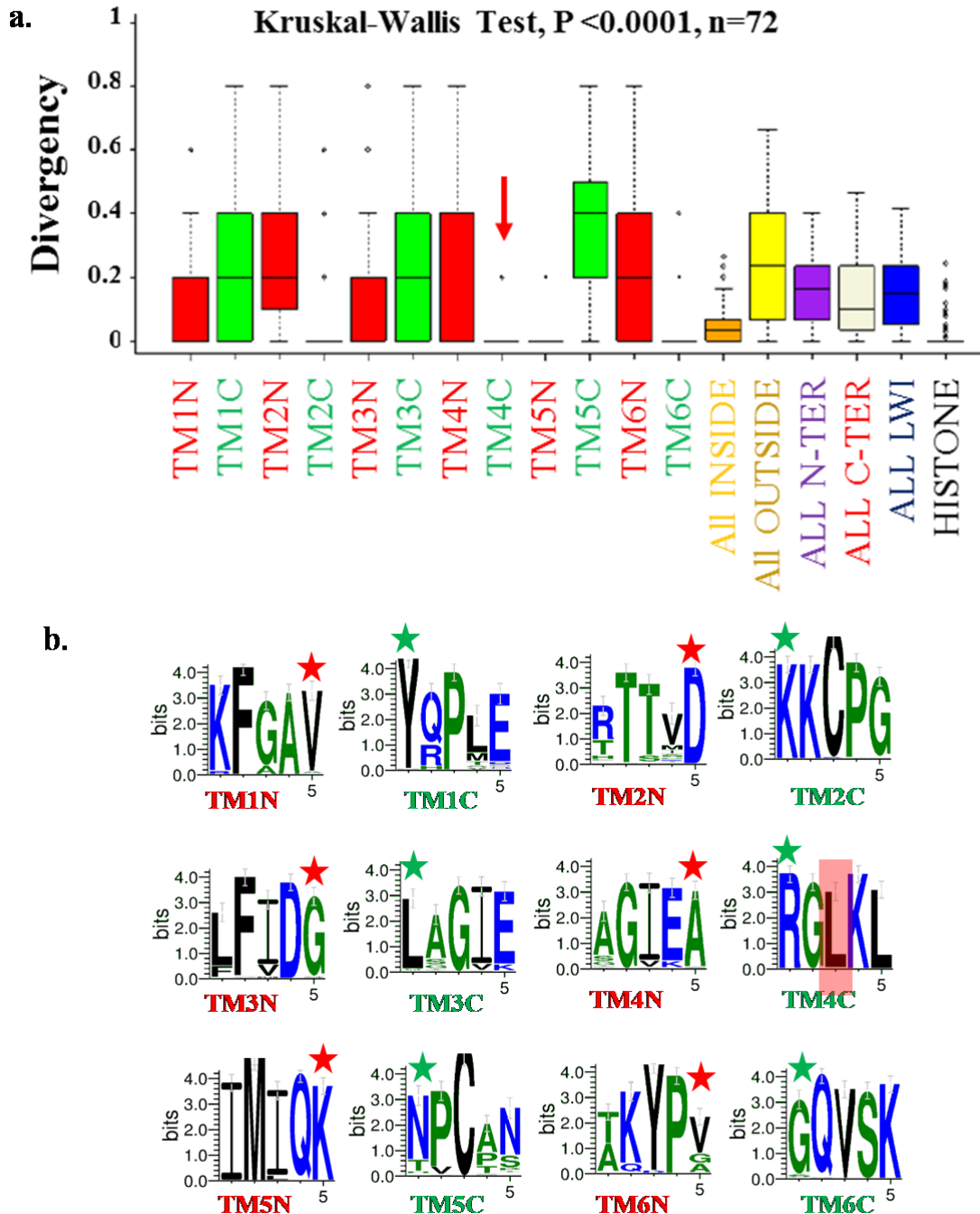
Figure 26: Amino acids present in the Lipid-Water-Interface region of TRPV4 are conserved throughout the vertebrate evolution. a. Conservation analysis of all 12 individual LWI regions of TRPV4 from 72 vertebrate sequences are depicted as box-plots. Histone H4 was used as control. The lower and higher values indicate more and less conservation respectively. All values are significant (p < 0.0001, Kruskal-Wallis test). The C-terminal region of LWI of TM4 (indicated by red arrow) remains highly conserved (a). The consensus sequence of 12 LWI regions of TRPV4 used in this study are shown **b**. The asterisks (*) indicate the amino acids that are at the juxtaposition to the lipid bilayer. The L596 residue is marked in red and a mutation (L596P) in this position prevents bone development as observed in human Kozlowski-type spondylometaphyseal dysplasia.

2.1.7. Molecular exclusion, retention or selection of amino acids in the LWI regions throughout vertebrate evolution

Next, we analyzed the molecular exclusion, retention or selection of amino acids in LWI regions. Changes in the percentage values of individual amino acids provide important information about the functional requirement of such residues for TRPV4 function and the microenvironment in which such amino acids become critical. We found that percentage of occurrence for most of the amino acids, are either highly conserved or conserved with minor variations throughout the vertebrate evolution (Figure 27).

Exclusion of residues:

Amino acids that are excluded in a certain region/s of TRPV4 throughout the vertebrates are indicative of their no importance and/or misfit in such microenvironments. Exclusion also suggests that such residues are mostly non-suitable for TRPV4 function/s in all vertebrates. For example, we noted that Trp residue is totally absent in the any LWI regions of TRPV4. His residue is mostly excluded in the total as well as in outer LWI region and absolutely excluded in the inner LWI region. Similarly, Glu, Asn, Thr, and Tyr residues are absolutely excluded in the inner LWI regions. This data strongly suggests that Glu, Asn, Thr, and Tyr residues at the inner LWI region are misfit for TRPV4 functions. In a similar manner, Phe residue is totally excluded in the outer LWI regions in most species. Therefore, the data suggests that any substitution mutation leading to presence of these excluded residue/s in the LW1 is most-likely to induce higher-level of detrimental effect.

Positive selection of residues:

We noted that certain amino acids are positively selected in the LWI regions during vertebrate evolution and therefore the frequency of such amino acids increased gradually during

the course of evolution. This "positive selection" is evident as per the natural frequency of amino acids described before (Dyer, KF., 1971; King & Jukes, 1969). Such pattern indicates the importance of such residues not only for the TRPV4 functions, but also for the fitness of such residues in the microenvironments where TRPV4 become functional. For example, frequencies of Glu in the outer LWI region and Gly in the inner LWI region are increased gradually from lower vertebrates and finally stabilized at higher frequencies in higher vertebrates. These residues are present at much higher frequencies than the natural abundance of such residues suggesting true enrichment of these residues in these respective LWI regions.

Negative selection of residues:

We noted that the frequencies of certain amino acids are negatively selected in the LWI regions during vertebrate evolution and therefore the frequency of such amino acids decreased (but may not be excluded completely) gradually during the course of evolution. During the course of vertebrate evolution, such amino acids are most-likely to be replaced by amino acids that are positively selected. For example, Ser in the total LWI is negatively selected. Asp and Ser in the outer LWI region, and Ala in inner LWI region are also negatively selected. Notably, these residues are present at much lower frequencies than the natural abundance of such residues suggesting true negative selection of these residues in these respective LWI regions.

Retention of critical amino acids:

There are certain amino acids for which the frequency of occurrence remains constant throughout the vertebrate evolution. Such aspects indicate that no change, i.e., neither increase nor decrease in frequency of these residues were tolerated in the LWI regions of TRPV4 during vertebrate evolution. In other words, such amino acids are example of critical amino acids present in LWI regions and are essential for TRPV4 functions. For example, Cys and Tyr residues remain

AA	Total LWI	Outer LWI	Inner LWI	pKa value (Side chain)	Hydrophobicity (Kyte-Doolite)	Snorkeling ability	Snorkeling extent	Snorkeling score
Glu (2.23)				4.25	-3.5	Yes	♠♠	-0.79
Asp (3.02)				3.65	-3.5	Yes	♠♠	-0.81
Gln (3.67)					-3.5	Yes	♠♠	-0.62
Lys (3.77)				10.53	-3.9	Yes	♠♠♠	-0.97
Pro (3.8)					-1.6	No	#	
Arg (3.91)				12.48	-4.5	Yes	♠♠♠	-1.3
Asn (3.83)					-3.5	Yes	♠♠	-0.64
His (4.08)				6.00	-3.2	No	♠	-0.01
Ala (4.08)	****	****		1.8	No	#		
Thr (4.11)	ns	ns		-0.7	Yes	♠♠♠	-0.93	

ΔG values of side chain at Lipid-Water-Interface (membrane to water)

64

AA	Total LWI	Outer LWI	Inner LWI	pKa value (Side chain)	Hydrophobicity (Kyte-Doolite)	Snorkeling ability	Snorkeling extent	Snorkeling score
Ser (4.12)			ns		-0.8	Yes	♠	-0.33
Val (4.18)	ns	*			4.2	No	♠	-0.03
Gly (4.24)	****	****			-0.4	No	#	
Met (4.48)	ns	*			1.9	Yes	♠♠	-0.6
Cys (4.49)				8.18	2.5	Yes	♠♠	-0.66
Ile (4.52)	**	***			4.5	Yes	♠♠♠	-1.58
Leu (4.81)		ns			3.8	Yes	♠	-0.27
Tyr (5.19)				10.07	-1.3	Yes	♠♠♠	1.07
Phe (5.38)					2.8	Yes	♠♠	0.56
Trp (6.1)					-0.9	Yes	♠	0.1

ΔG values of side chain at Lipid-Water-Interface (membrane to water)

65

Figure 27: Frequency of amino acid distribution in Lipid-Water-Interface (LWI) region of TRPV4 in all vertebrates. The amino acid frequency distribution for LWI region of TRPV4 in different species across vertebrate class mammals (**M**), birds (**B**), reptiles (**R**), amphibians (**A**) and fishes (**F**) are shown in red, green, brown, blue and violet colored dots respectively. The amino acid distributions are determined for total (left most column) as well as for outer (middle column) and inner (right most column) LWI separately. For certain amino acids the frequency remains constant throughout evolution (marked by a light blue thick arrow) whereas for some amino acids the frequency declines during vertebrate evolution (marked in red solid background) or increases (marked in green solid background) and finally gets stabilized in the most evolved class i.e.in mammals. The natural frequency of amino acids observed in nature is marked with a dotted blue line in each graph. Higher and lower values compared to the dotted line indicates "enrichment" and "reduction/exclusion" of amino acids respectively. The pKa values of the side chains, hydrophobicity (According to the Kyte-Doolite scale), Snorkeling extent is classified as per their values (♠ = 0.01 to 0.33, ♠♠ = 0.33 to 0.9, ♠♠♠ = ≥ 0.91) and respective snorkeling values are indicated in the right side. For some amino acids an increase (Green circle) or decrease (Red circle) in frequency distribution can be seen during the transition in body temperature (i.e., evolution of birds from reptiles). The statistical significance values are as follows: ns = non-significant, * = <0.05, ** = <0.005, *** = <0.0005, **** = <0.0001 respectively.

constant in the outer LWI region during vertebrate evolution. Also, Asp, Gln, Lys, Pro, Arg, Met, Cys residues are highly conserved in the inner LWI region. Also, Val and Ser residues are mostly conserved (with some minor variation) in the inner LWI region. Lys, Cys, Tyr residues remain with a constant frequency in total LWI regions. Glu residue also remain mostly at constant frequency in all vertebrates other than fishes. Among all these Glu, Cys and Tyr at the total LWI, Cys residue at outer LWI region, Arg, Val, Cys at the inner LWI region occurs with frequencies that matches well with the natural occurrence of these residues. This in general suggests for fine tuning of functional positioning of these residues in respective LWI of TRPV4 during vertebrate evolution.

2.1.8 Analysis of frequency of amino acids due to change in body temperature

We analyzed the changes in the frequency of amino acids in all cold-blooded with respect to all warm-blooded vertebrates (Figure 28). Considering both outer and inner LWI region, total 12 different amino acids (Glu, Asp, Pro, Arg, Asn, Thr, Ser, Val, Gly, Met, Leu and Phe) are significantly different in cold-blooded and warm-blooded animals. Similarly, in the outer LWI region only, 10 amino acids (Glu, Asp, Pro, Asn, Ala, Thr, Ser, Val, Met and Leu) are significantly

AA	Total LWI	Outer LWI	Inner LWI	pKa value (Side chain)	Hydrophobicity (Kyte-Doolite)	Snorkeling ability	Snorkeling extent	Snorkeling score
Glu (2.23)	****	****	ns	4.25	-3.5	Yes	♠♠	-0.79
Asp (3.02)	****	***	ns	3.65	-3.5	Yes	♠♠	-0.81
Gln (3.67)	ns	ns	ns		-3.5	Yes	♠♠	-0.62
Lys (3.77)	ns	ns	ns	10.53	-3.9	Yes	♠♠♠	-0.97
Pro (3.8)	***	****	ns		-1.6	No	#	
Arg (3.91)	*	ns	**	12.48	-4.5	Yes	♠♠♠	-1.3
Asn (3.83)	****	****	ns		-3.5	Yes	♠♠	-0.64
His (4.08)	ns	ns	ns	6.00	-3.2	No	♠	-0.01
Ala (4.08)	ns	**	****		1.8	No	#	
Thr (4.11)	**	**	ns		-0.7	Yes	♠♠♠	-0.93

ΔG values of side chain at Lipid-Water-Interface (membrane to water)

67

AA	Total LWI	Outer LWI	Inner LWI	pKa value (Side chain)	Hydrophobicity (Kyte-Doolite)	Snorkeling ability	Snorkeling extent	Snorkeling score
Ser (4.12)	****	****	***	-0.8	Yes	♠	-0.33
Val (4.18)	**	**	ns	4.2	No	♠	-0.03
Gly (4.24)	*	ns	****	-0.4	No	#	
Met (4.48)	**	*	**	1.9	Yes	♠♠	-0.6
Cys (4.49)	ns	ns	ns	8.18	2.5	Yes	♠♠	-0.66
Ile (4.52)	ns	ns	ns	4.5	Yes	♠♠♠	-1.58
Leu (4.81)	****	****	ns	3.8	Yes	♠	-0.27
Tyr (5.19)	ns	ns	ns	10.07	-1.3	Yes	♠♠♠	1.07
Phe (5.38)	*	ns	*	2.8	Yes	♠♠	0.56
Trp (6.1)	ns	ns	ns	-0.9	Yes	♠	0.1

ΔG values of side chain at Lipid-Water-Interface (membrane to water)

68

Figure 28: Frequency of amino acid distribution in lipid-water-interface region of TRPV4 in cold-blooded and warm-blooded vertebrates. The amino acid frequency distribution for lipid-water-interface region of TRPV4 in different species across vertebrates representing warm-blooded (mammals and birds) (Warm), and cold-blooded (reptiles, amphibians and fishes) (Cold) animals are shown in red and blue coloured dots respectively. The amino acid distributions are determined for total (left most column) as well as for outer (middle column) and inner (right most column) LWI separately. The natural frequency of amino acids observed in nature is marked with a dotted blue line in each graph. Higher and lower values compared to the dotted line indicates "enrichment" and "reduction/exclusion" of amino acids respectively. The pKa values of the side chains, hydrophobicity (According to the Kyte-Doolite scale), Snorkeling extent is classified as per their values (♠ = 0.01 to 0.33, ♠♠ = 0.33 to 0.9, ♠♠♠ = ≥ 0.91) and respective snorkeling values are indicated in the right side. The statistical significance values are as follows: ns = non-significant, * = <0.05, ** = <0.005, *** = <0.0005, **** = <0.0001 respectively.

different among cold-blooded and warm-blooded animals. In the inner LWI region only, at least 14 amino acids have no significant changes. In inner LWI region, only Arg, Ala, Ser, Gly, Met, Phe are significantly changed between cold-blooded and warm-blooded animals. Though these changes in amino acid frequencies in "cold-blooded" and "warm-blooded animals" are indicative, there are several amino acids for which the percentage occurrence in LWI regions remain random and no straight forward trend can be derived. Therefore, we analyzed the same in a more specific manner and looked for residues that reveal a sudden change between reptiles to avian species (Figure 29). Such changes are most likely to adjust the change in increased body temperature that happened during the evolution of birds from reptiles. Amino acid frequencies for Ala, Thr, Ile, as well as Leu decreased in the outer LWI region during the transition from reptiles to avian. In contrast, frequencies of Val, Gly and Met increases in the outer LWI region during this transition. Accordingly, frequencies of Val, Gly, Met have increased from reptiles to birds in total LWI region. In contrast, decrease in percentage value is observed for Ala, Thr and Ile in total LWI. No drastic change is observed in the inner LWI regions during the transition from reptiles to birds. The data suggests that the inner LWI residues are mostly conserved and thus not involved in the regulation of temperature-dependent spontaneous activation of TRPV4.
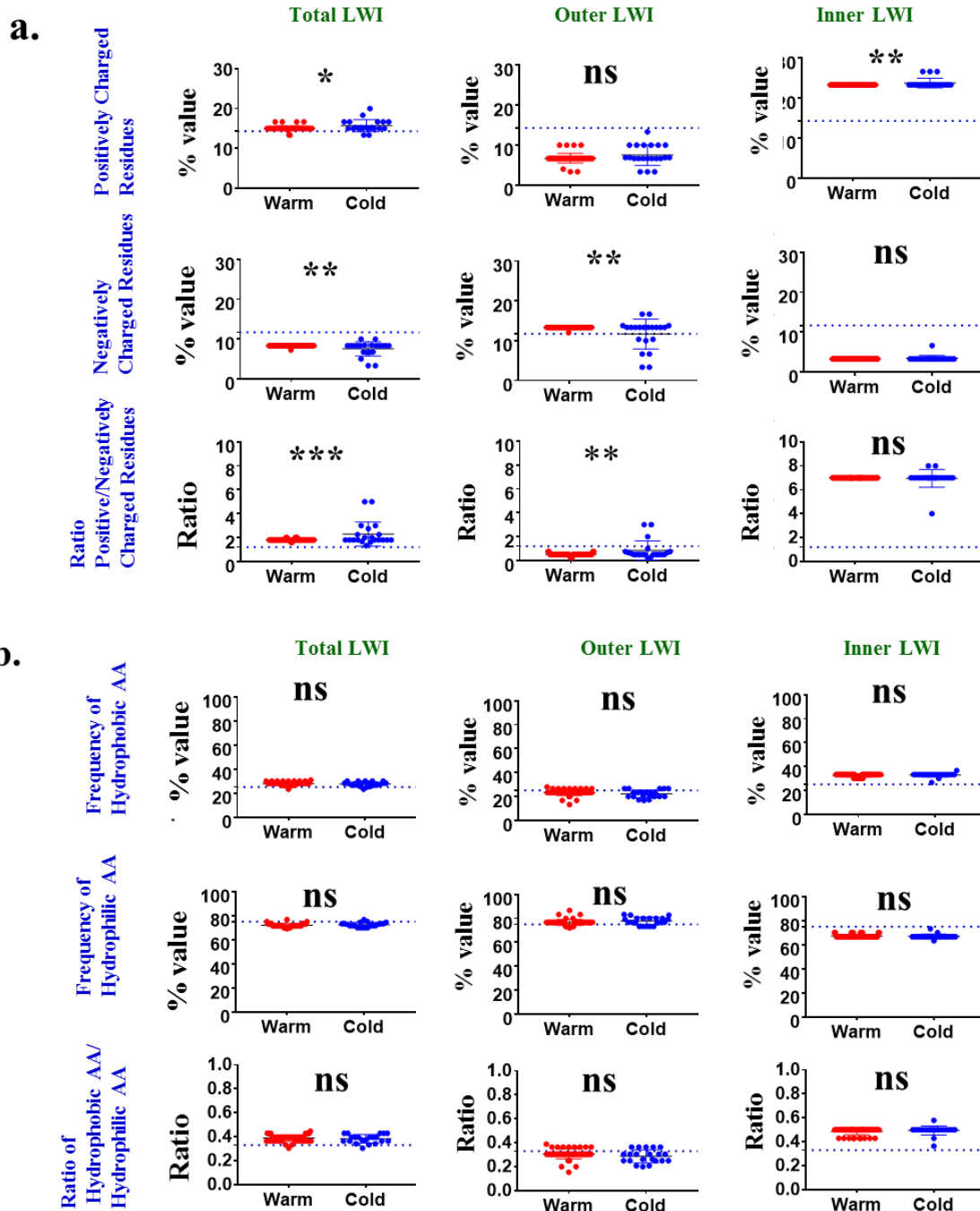
Figure 29: Specific changes in the amino acid frequency in LWI region are most likely due to changes in the body temperature. a. Total frequency of the positively charged residues as well as negatively charged residues present in all the LWI regions, or in inner LWI or in outer LWI are plotted. The statistical significance values are as follows: ns = non-significant, * = <0.05, ** = <0.005, *** = <0.001 respectively. **b.** The total frequency of hydrophobic, hydrophilic amino acids and their respective ratio remain non-significantly different (ns) among cold-blooded and warm-blooded animals. This suggests that the total hydrophobicity, hydrophilicity and their respective ratio are unlikely to play a role in temperature-gating of TRPV4.

The frequency of total positively charged residues is different in the inner LWI as well as in the total LWI region but remain non-significant in outer LWI region. In contrast, the total frequency of negatively charged residues are different in the outer LWI as well as in the total LWI region but remain non-significant in inner LWI region. Accordingly, the ratio of positively-charged residue to negatively charged residues remain different in total as well as in outer LWI regions, but not in inner LWI region (Figure 29a). These minute differences in the positively charged and negatively charged residues may contribute in the spontaneous channel opening in different body temperatures, thus in thermo-gating behavior of TRPV4.

In contrast, there is no significant change in the frequency of hydrophobic and hydrophilic amino acids at the inner, outer or even total LWI regions. The ratio of hydrophobic and hydrophilic residues remains unchanged in cold-blooded and warm-blooded animals, in inner, outer as well as in total LWI regions (Figure 29b). This also suggest that total hydrophobicity, total hydrophilicity and their ratio seems to be same for both cold-blooded as well as warm-blooded animals, thus critical for overall channel gating *per se*, but may not be critical for thermo-gating.

2.1.9. Identification of a conserved pattern through-out the vertebrate evolution: Conserved ratio of positive-negative and hydrophobic-hydrophilic residues in the LWI regions of TRPV4

We analyzed the total percentage of positive as well as total negative charged residues as well as their relative ratio in the inner, outer LWI regions as well as for total LWI region. We observed that the total positive charge, total negative charge and their ratio are well conserved throughout the vertebrate evolution in the inner LWI regions of TRPV4 (Figure 30a). These values are also conserved (other than in fishes), for both outer as well as for total LWI region.

We further analyzed the total hydrophobic as well as total hydrophilic residues as well as their ratio in these LWI regions. We observed that throughout the vertebrate evolution, total percentage of hydrophobic residues and hydrophilic residues, as well as their relative ratio remain well conserved in the LWI regions of TRPV4 (Figure 30b). These results strongly suggest that in case of TRPV4, there is a "conserved pattern" of amino acids in the LWI region that remain conserved throughout the vertebrate evolution and thus remain crucial for TRPV4 channel function.

As individual amino acids differ in the absolute hydrophobicity scale, we explored if there is any correlation between the percentages of amino acids with the absolute hydrophobicity or hydrophilicity values. The data suggest that there is a good correlation between the percentages of residues with the absolute values (Figure 31). A refined analysis suggests that the frequencies of amino acids (for hydrophobic as well as hydrophobic) residues correlate well with the absolute hydrophobicity (Annexure 3). Thus, "frequency" of amino acids can be considered as readout of "absolute hydrophobicity or hydrophilicity" as such.
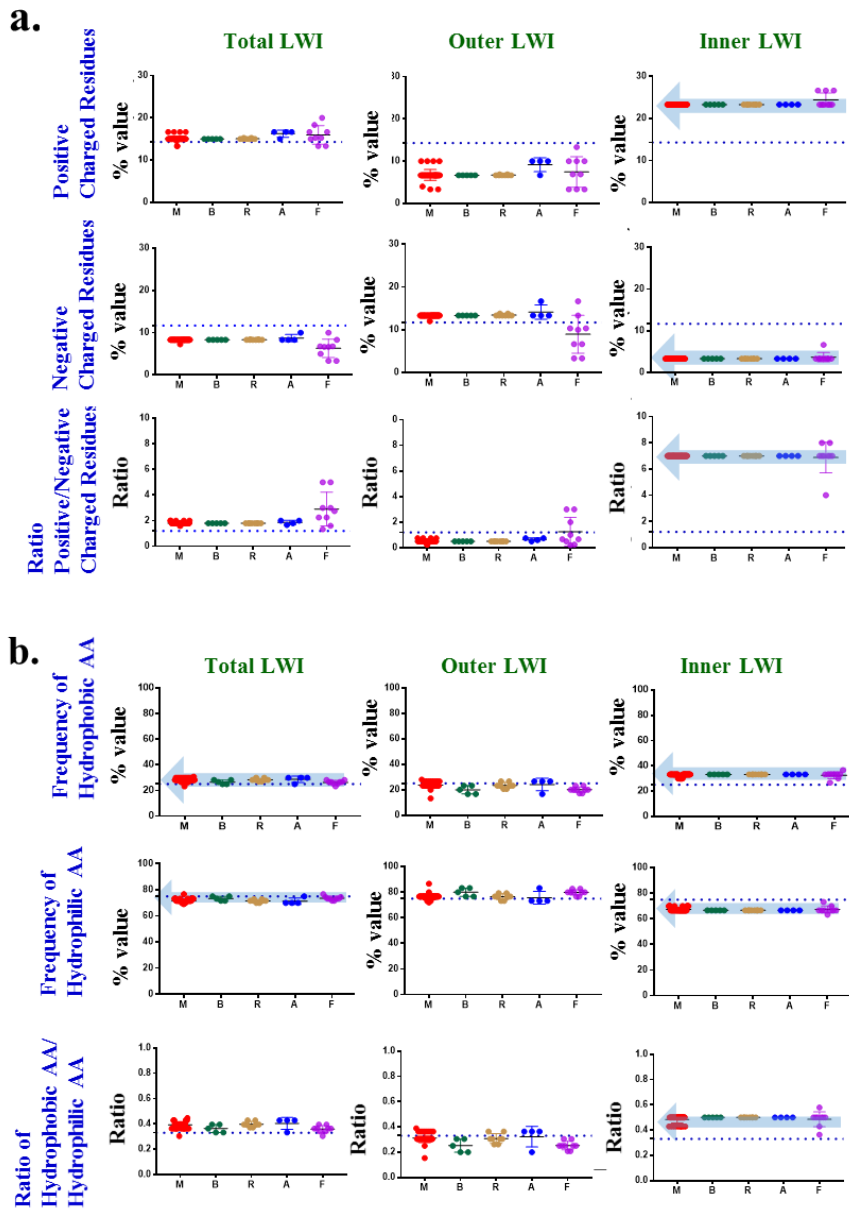
Figure 30: Conservation of amino acid patterns in the lipid-water-interface regions of TRPV4. a-b. Ratio of acidic/basic (**a**) and hydrophobic/hydrophilic (**b**) amino acids in inner, outer and total LWI regions of TRPV4 are shown. The total frequencies of all acidic, basic, hydrophobic and hydrophilic amino acids as well as specific ratios remain conserved in LWI region of TRPV4 throughout the vertebrate evolution. The frequency of acidic, basic amino acids along with their ratio is plotted for different classes, i.e. for Mammals (M), Birds (B), Reptiles (R), Amphibians (A) and Fishes (F) are shown in red, green, yellow, blue and violet respectively.

2.1.10. L596P mutation differs from other TRPV4 mutations present in LWI region

We analyzed different naturally occurring mutants, especially if these mutants alter the positive-negative ratio, and/or correlation of absolute hydrophobicity with the percentage of occurrence. There are two naturally occurring mutation namely R594H and L596P, both located in TM4C region (Figure 31). The analysis suggests that the L596P is not changing the ratio between positive-negative charged residues, but actually shifting the absolute hydrophobicity and hydrophilicity drastically from rest of the vertebrate sequences. In contrast, R594H mutation does not shift absolute hydrophobicity and hydrophilicity values. Values for R594H coincide well with the other vertebrate sequences. This analysis suggests that L596P mutation is capable of altering the LWI behavior.
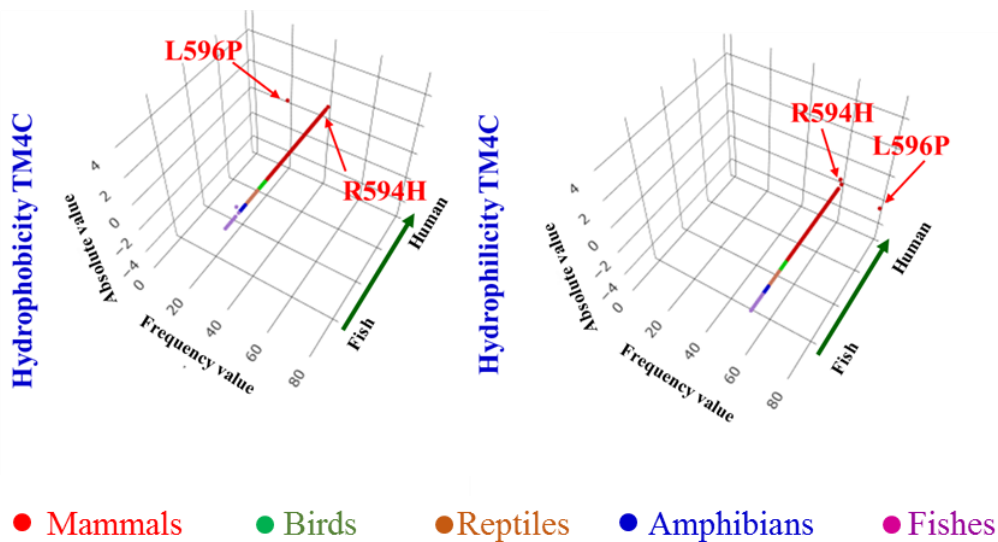
Figure 31: L596P mutation differs from other LWI mutations present in TRPV4. Comparison of total hydrophilic or hydrophobic values of all amino acids present in the lipid-water-interface of C-terminus of Transmembrane region 4 with the frequency of occurrence of amino acids in LWI region of TRPV4 across vertebrate evolution. The absolute values of amino acids present in the LWI are plotted in the Y-axis and the frequency of occurrence of amino acid is plotted in the X-axis. Values for different species from (Fish to human) are plotted in Z-axis. The absolute hydrophobicity or hydrophilicity values correlate well with the frequency-of-occurrence of these amino acids. Values for different species (total n = 72) belongs to different classes, i.e. Mammals (M) (total 46 sp), Birds (B)(total 5 sp), Reptiles (R)(total 8 sp), Amphibians (A)(total 4 sp) and Fishes (F)(total 9 sp) are shown in Red, green, yellow, blue and violet respectively. Graphs are also drawn for two naturally occurring mutations found in the TM4C LWI region having L596P and R594H. The L596P mutation significantly shifts the values while R594H mutation clusters well with the values that are conserved in all vertebrates.

Therefore, TRPV4-L596P offers as a good candidate to study the impact of mutations at the LWI region and molecular as well as cellular basis of channelopathy-induced by point mutation.

2.1.11. Conservation analysis of TRPV4 and its nearby genes

The syntenic analysis revealed several genes which lie in the nearby location of TRPV4 as previously observed in our lab (Kumari et al., 2015) (Figure 32a).
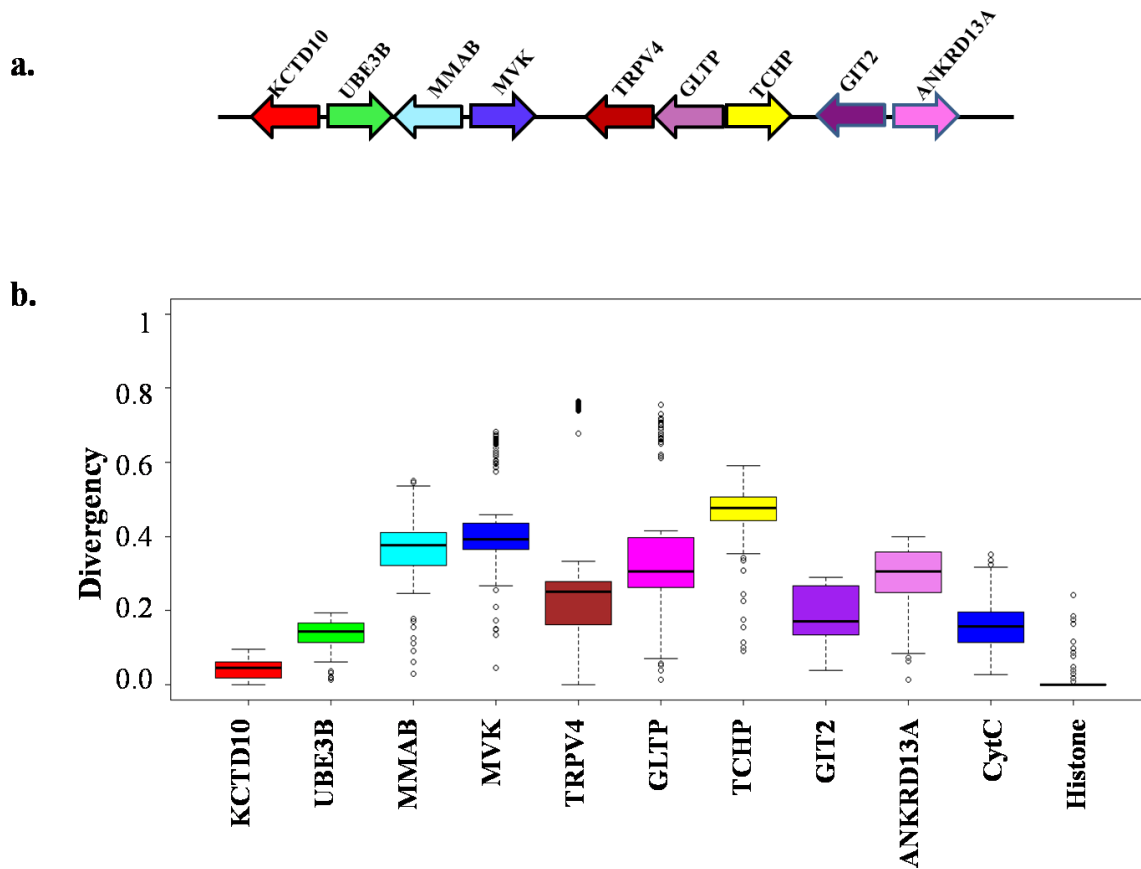
Figure 32: The TRPV4 and the nearby gene cassette is semi conserved. Four genes from either side of TRPV4 derived from synteny analysis (**a**.) adapted from (Kumari et al., 2015) were subjected to conservation analysis. Conservation analyses of the protein sequences are depicted in box-plots are assigned different colours. Histone H4 and Cyt C were used as control. The lower and higher values indicate more and less conservation respectively (**b**). All values are significant (p < 0.0001, Kruskal-Wallis test, Total numbers of sequences used for each protein ≥14).

We performed conservation analysis of 4 genes to the left and 4 genes to the right of TRPV4. The genes were mevalonate kinase (MVK), methylmalonic aciduria (cobalamin deficiency) cblB type (MMAB), ubiquitin protein ligase E3B (UBE3B) and potassium channel tetramerization domain containing 10 (KCTD10) to the left of TRPV4 and glycolipid transfer protein (GLTP), trichoplein, keratin filament binding (TCHP), G-protein-coupled receptor kinase interacting ArfGAP 2(GIT2) and ankyrin repeat domain 13A (ANKRD13A) to the right of TRPV4. Cyt C (a semi-conserved protein) and Histone (a highly conserved protein) were taken as control. The two adjacent genes on either side of TRPV4 are less conserved than TRPV4 suggesting that the TRPV4 has gone through more selection pressure than its immediate neighbor genes (Figure 32b).

2.2. Characterization TRPV4-L596P mutation causing SMDK

Like many other ion channels, TRPV4 also interact with cholesterol and availability of cholesterol modulates TRPV4 functions such as its presence in lipid rafts and its membrane mobility (Das & Goswami, 2019; Kumari et al., 2015). Therefore, the specific microenvironment as well as the structure-function relationship of TRPV4 is influenced by cholesterol. Such aspects also impose a fine selection pressure on TRPV4, at least to the specific amino acids that are crucial for structure-function relationship of TRPV4. In this work, we analyzed the TRPV4 sequences from multiple vertebrate sequences and explored if there is a specific pattern of amino acids formed at the LWI region of TRPV4 which remain conserved throughout the vertebrate evolution. We analyzed one naturally occurring mutation causing channelopathy, namely L596P that lie in the LWI region. We characterized if this mutation can induce altered cellular functions. Caveolin seem to have a profound role in the regulation of TRPV4 function (Daneva et al., 2020). To characterize if TRPV4-Wt and TRPV4-L596P are able to form complex with Caveolin1, we performed colocalization analysis of the Wt and mutant protein with Caveolin1. FRAP analysis was also done to study their mobility pattern in control and cholesterol-reduced condition. We also have analyzed if this mutation affects the parameters that are equivalent to channel opening. For this live cell Ca^{2+}-imaging in different doses of agonists was performed.

2.2.1 L596P mutation alters cellular morphology

We tested the effect of over expression of TRPV4-Wt-GFP and TRPV4-L596P-GFP on the morphology of the Saos-2 cells and localization of these two forms of TRPV4 channel. We found that cells expressing TRPV4-Wt-GFP are mostly normal in morphology. However, cells expressing TRPV4-L596P-GFP have often irregular morphology and often show presence of several filopodia-like structures (Figure 33a & Annexure 4). Presence of TRPV4-L596P-GFP in such filopodia-like structure is visible. When expressed together with Caveolin1, TRPV4-Wt show certain degree of colocalization in the cell body. However, under the same conditions, TRPV4-L596P containing filopodia-like structures are mainly devoid of Caveolin1 (Figure 33a).

2.2.2 Localization of TRPV4-L596P in the filopodia-like structures can be limited by the presence of TRPV4-Wt

In heterogeneous condition (considering that some patient has one copy of TRPV4 as wild type and another one in mutant form) both forms of TRPV4 might be expressing in the same cell. Therefore, we tested if the localization of TRPV4-Wt and TRPV4-L596P can differ in cells that express both. For that purpose, we over expressed TRPV4-Wt and TRPV4-L596P as mCherry- and GFP-tagged protein or *vice versa* and performed live cell imaging experiments. Both TRPV4-Wt and TRPV4-L596P show colocalization with each other in cell bodies (Figure 33b-c). However, we could not find any filopodia-like structure or presence of TRPV4-L596P in the filopodia-like structures in these cases. These results suggest that presence of TRPV4-Wt limits TRPV4-L596P-mediated filopodia-like structure formation or even localization of TRPV4-L596P there. This can be due to the complex Ca^{2+}-signaling that differs from Wt to L596P.
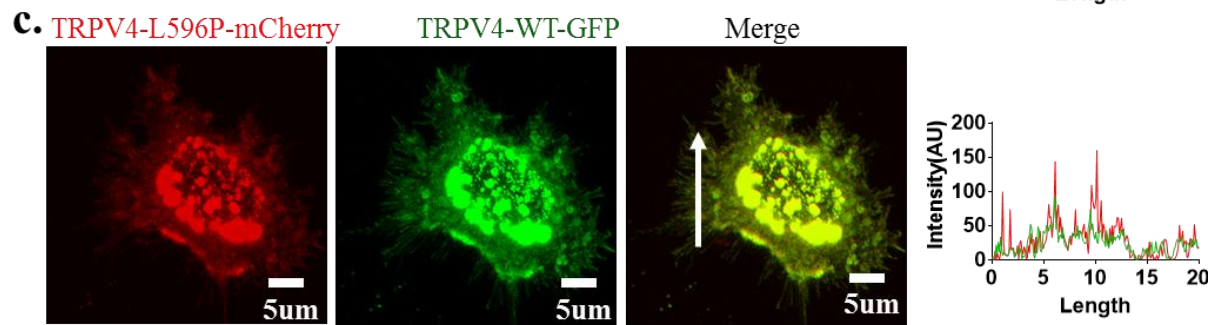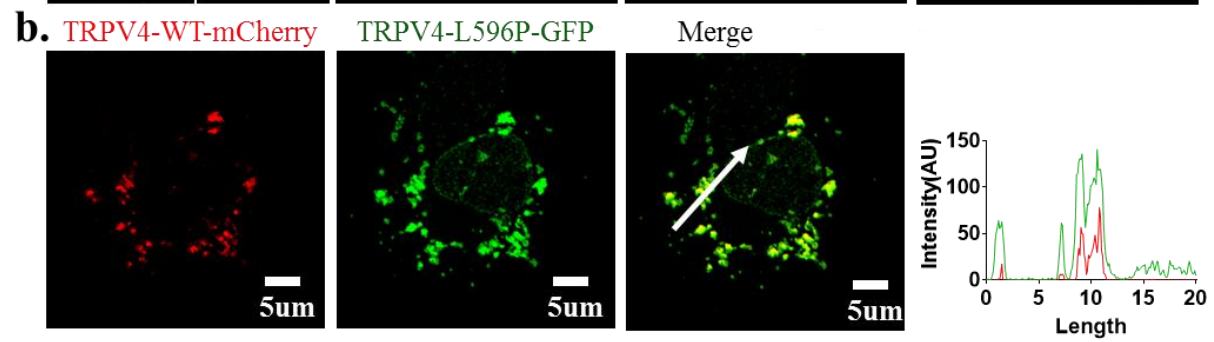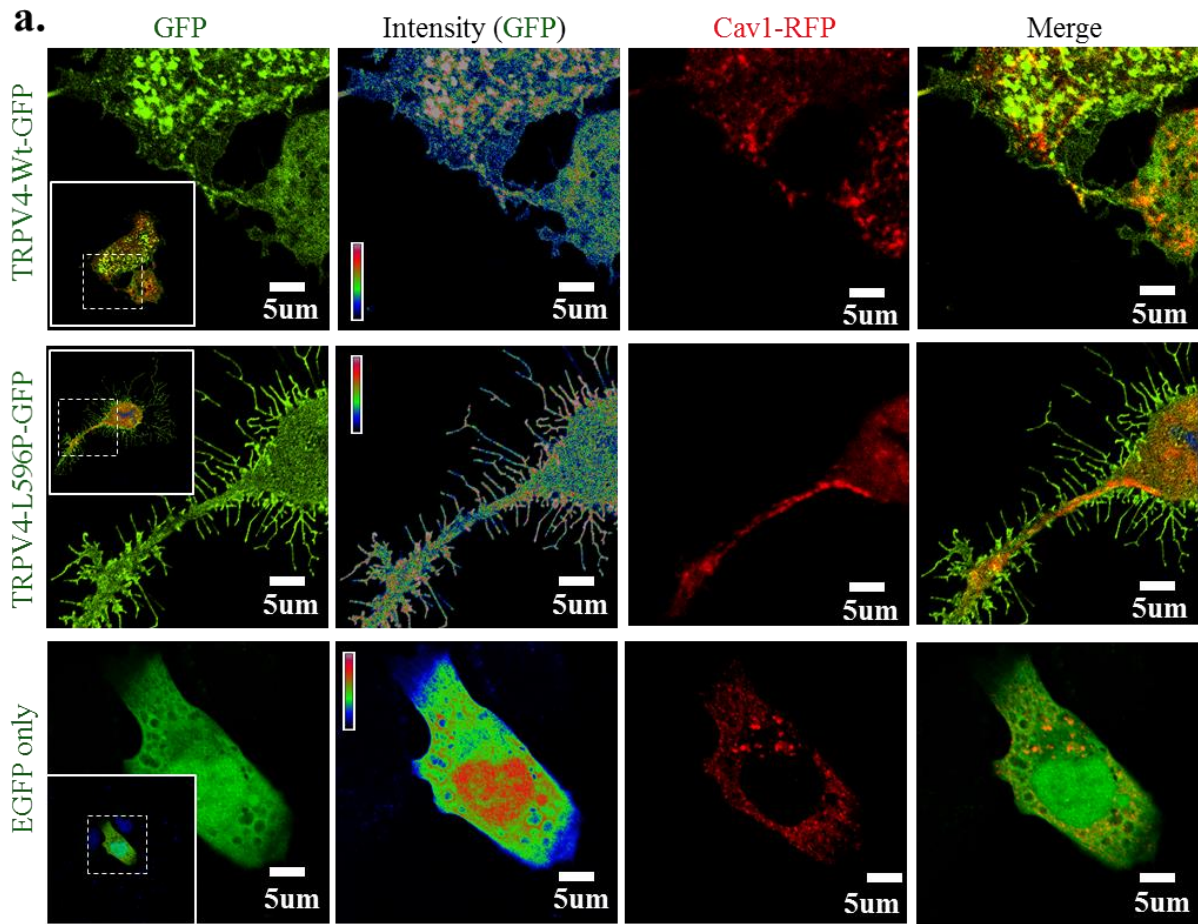
Figure 33: Localization of TRPV4-Wt and TRPV4-L596P mutant in osteogenic cells. a. Shown are the confocal images of Saos-2 cells expressing either TRPV4-Wt-GFP or TRPV4-L596P-GFP or only GFP (green) along with Caveolin1-RFP (red). TRPV4-Wt-GFP but not TRPV4-L596P-GFP show better co-localization with Caveolin1 RFP. In contrast, expression of TRPV4-L596P-GFP often results in the development of enhanced filopodia-like structures where TRPV4-L596P-GFP but not the Caveolin1-RFP is enriched. Fluorescence intensity from GFP in all cases is represented in pseudo rainbow color (red and blue represents highest and lowest intensity respectively). Scale bar 5µm. **b-c.** Analysis of relative distribution and membrane localization of TRPV4 in heterozygous conditions expressing both TRPV4-Wt and TRPV4-L596P in the same cell. TRPV4-Wt-GFP and TRPV4-L596P-mCherry (b) or TRPV4-Wt-mCherry and TRPV4-L596P-GFP (c) were co-expressed in Saos-2 cells and confocal images were acquired. Both TRPV4-Wt-GFP and TRPV4-L596P-mCherry (or TRPV4-L596P-GFP and TRPV4-Wt-mCherry as depicted in **c**) are observed to co-localize extensively and the enhanced localization of TRPV4-L596P-mCherry in the cell membrane and filopodia-like structures are limited by the presence of TRPV4-Wt-GFP. Scale bar 5um. Intensity profile of TRPV4-Wt and TRPV4-L596P across a fixed length is shown in right side.

2.2.3. TRPV4-L596P mutant but not the TRPV4-Wt has less membrane mobility in response to cholesterol reduction

We measured the membrane mobility of TRPV4-Wt and TRPV4-L596P in control and cholesterol-reduced condition (cells treated with β-MCD). In Saos-2 cells, membrane mobility of TRPV4-Wt remain comparable in both control and cholesterol-reduced conditions, suggesting that even reduced level of cholesterol is sufficient to maintain the normal membrane mobility of TRPV4-Wt (Figure 34a). However, TRPV4-L596P mutant show comparable membrane mobility with TRPV4-Wt in control condition, but not in cholesterol-reduced condition. In cholesterol-reduced condition, TRPV4-L596P mutant show approximately 13% less movement (in approximately 3 min), suggesting that cholesterol reduction affects the membrane mobility of this mutant (Figure 34b).

2.2.4. Both TRPV4-Wt and L596P mutant sequester and restrict fast membrane mobility of Cav1

TRPV4 is known to interact with Cav1 (Li et al., 2018). Therefore, we tested if and how TRPV1-Wt and TRPV4-L596P regulate Cav1. For that purpose, we first expressed Cav1-RFP and tested the membrane distribution as well as membrane mobility of the same in Saos-2 cells. Cav1-

RFP show high membrane mobility in Saos-2 cells, both in control condition as well as in cholesterol-reduced conditions (Figure 34c). Due to the high mobility, on an average Cav1-RFP fluorescence intensity that can be bleached is only 64% and remaining 36% fluorescence intensity is retained after bleaching. This analysis suggests that ~2/3rd fraction of Cav1-RFP is mobile and ~1/3rd fraction is immobile. The mobility of Cav1-RFP in these two conditions remain mostly comparable (Figure 34c). However, when expressed along with TRPV4-Wt-GFP or TRPV4-L596P, the membrane mobility of Cav1-RFP is significantly reduced suggesting that ~2/3rd fraction of total Cav1-RFP is restricted by the presence of TRPV4-Wt-GFP or TRPV4-L596P-GFP (Figure 34d-e). In such conditions, more than 95% fluorescence intensity of the Cav1 can be bleached efficiently in the same manner. This in general suggests that TRPV4-Wt-GFP and Cav1-RFP complex as well as TRPV4-L596P-GFP and Cav1-RFP complex are not mobile, at least in control condition. This accords well with the previous report that suggests that TRPV4 forms complex with Caveolin1 and other ion channels (Li et al., 2018).

2.2.5. In cholesterol-reduced condition, Wt is more restricted and L596P fails to restrict fast membrane mobility of Cav1

We noted that in cholesterol-reduced condition, there is an approximately 10% increment (in approximately 3 min) in the membrane mobility of Cav1-RFP in case of cells expressing TRPV4-L596P-GFP but not in cells expressing TRPV4-Wt-GFP (Figure 34d-e). In the same experimental settings and on cholesterol reduction (using β-MCD), the mobility of TRPV4-WT-GFP decreased while the TRPV4-L596P-GFP mobility got increased when compared to the control condition. This in general suggests that in case of cholesterol-limited conditions, a fraction of TRPV4-L596P-GFP pool fails to get restricted in the cholesterol-enriched membrane fraction

whereas majority of TRPV4-WT-GFP is possibly restricted in the cholesterol-enriched membrane fraction.

To analyze if Cav1-RFP recovers independently or as a complex with TRPV4-Wt-GFP or TRPV4-L596P-GFP, we calculated the differences in the recovery percentage between two different fluorophores (i.e., Cav-RFP and TRPV4-Wt-GFP or TRPV4-L596P-GFP) at the end of the experiment. These differences in the end point values (approximately 3 min after photo-bleaching) of two fluorophores in the same ROI also suggest that TRPV4-Wt-GFP and TRPV4-L596P-GFP recovers separately or as a complex with Cav1-RFP (values remain non-significant, data not shown). The $t_{1/2}$ calculations suggest that majority of TRPV4-Wt-GFP or TRPV4-L596P-RFP forms complex with Cav-RFP, both in cholesterol-enriched membrane fraction as well as outside of that specific membrane domain (Figure 34f).
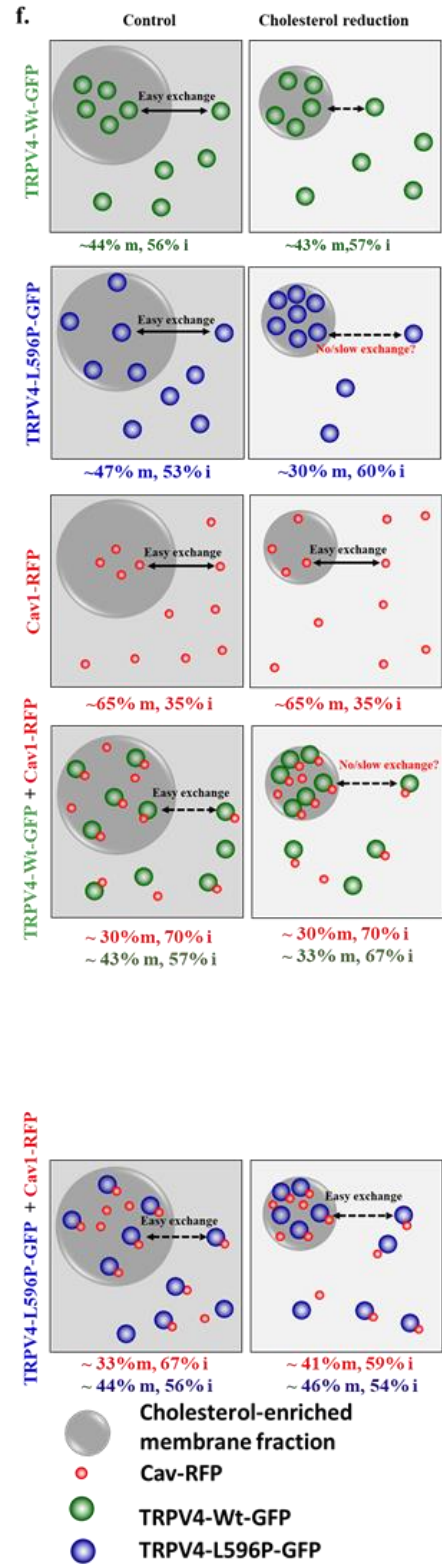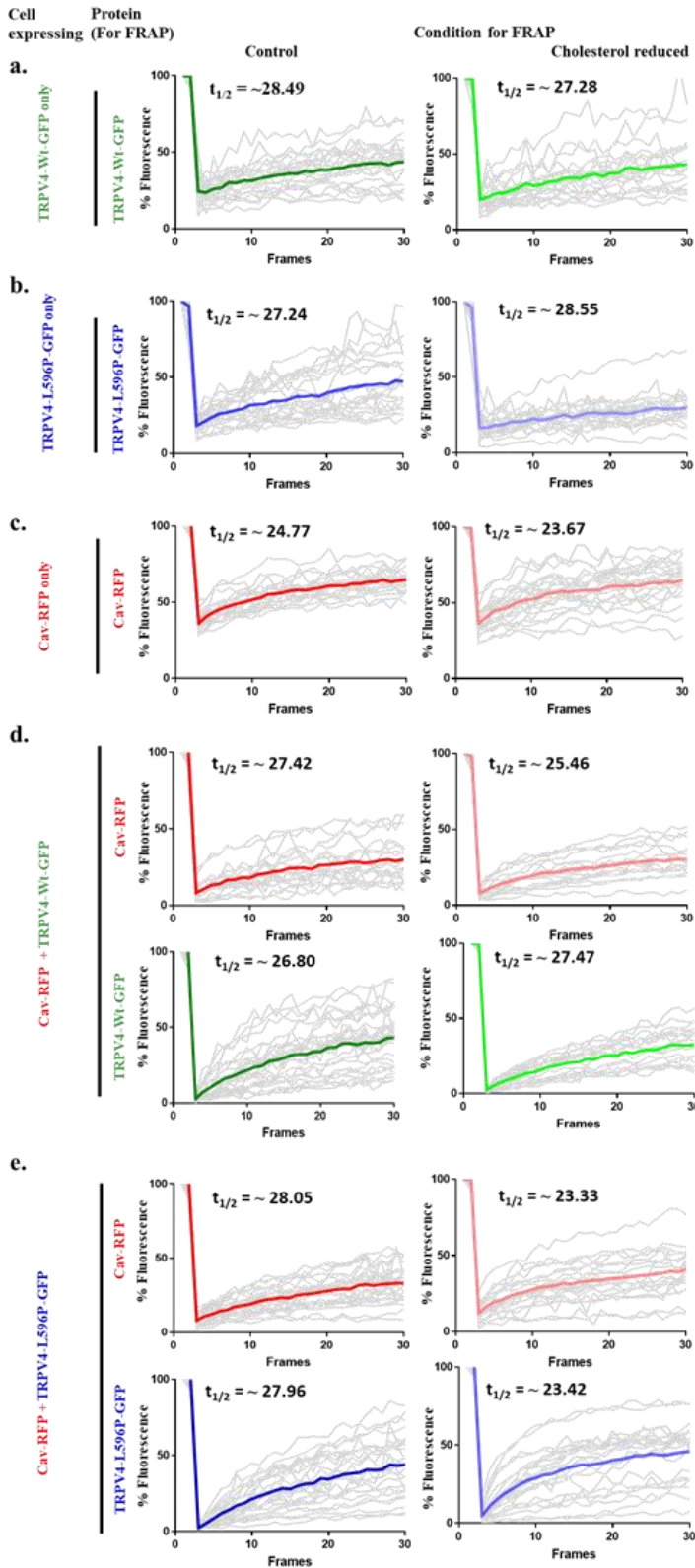
Figure 34: TRPV4-Wt and TRPV4-L596P differs subtly in their membrane mobility. a-b. Fluorescence recovery after photobleaching (FRAP) experiment is done for TRPV4-Wt-GFP (a) and TRPV4-V4-L596P-GFP (b) in control and in cholesterol-reduced conditions. Mobility pattern for TRPV4-Wt and TRPV4-L596P does not differ much in control condition but differ significantly in cholesterol-reduced condition. In cholesterol reduced condition, TRPV4-L596P mutant moves slower compared to TRPV4-Wt. **c.** Caveolin1 movement remain unchanged in control and cholesterol reduced conditions. Compared to TRPV4, Caveolin1 moves fast, both in control and cholesterol-reduced conditions. **d-e.** Movement of Caveolin1 is reduced significantly in presence of either TRPV4-Wt (d) or TRPV4-L596P (e), both in control and cholesterol-reduced conditions. In presence of Caveolin1, TRPV4-Wt moves much slower than TRPV4-L596P. In left side the recovery pattern in control and cholesterol-reduced conditions are shown for different fluorophores. **f.** The distribution of TRPV4-Wt, TRPV4-L596P or Caveolin1 in lipid raft and non-raft membrane is shown schematically. Both TRPV4-Wt and TRPV4-L596P seem to form complex with Cav1, both in cholesterol-enriched membrane fraction and outside of this fraction. However, the dynamics as well as easy-exchange of free TRPV4-Wt, TRPV4-L596P, Cav1 or TRPV4-Wt+Cav1 complex or TRPV4-L596P+Cav1 complex between different membrane microdomains are not same in control and cholesterol-reduced conditions. TRPV4-Wt + Cav1 complex is better restricted in the cholesterol-enriched membrane microdomain than TRPV4-L596P + Cav1 complex, especially in cholesterol-reduced condition. The mobile and immobile fractions are noted below the FRAP model in percentage values termed as 'm' for mobile fraction and 'i' for immobile fraction.

2.2.6. TRPV4-L596P has more channel opening properties than of TRPV4-Wt

We analyzed the Ca^{2+}-dynamics in Saos-2 cells expressing TRPV4-Wt-GFP and TRPV4-L596P-GFP. For that purpose, the cells were co-expressed with Ca^{2+}-sensor GCaMP6f protein along with either TRPV4-Wt-mCherry or TRPV4-L596P-mCherry or only with mCherry and activated by 4αPDD (1 µM), an agonist specific for TRPV4 (Figure 35a-e). We noted that cells expressing TRPV4-L596P-mCherry show relatively faster response than TRPV4-Wt against 4αPDD. When compared at the basal levels, for multiple cells, no significant fluorescence differences were noticed between Wt or mutant expressing cells (Annexure 6). In the cells expressing TRPV4-L596P, the Ca^{2+}-spikes appear earlier (time taken to reach maximum after adding agonist) (Figure 35f), stays for longer duration (time taken to reach half maximum from highest values) (Figure 35g), and stay at higher values (fluorescence intensity at the last frame of the experiment) (Figure 35h) as compared to the cells expressing TRPV4-Wt. As a result, cells expressing TRPV4-L596P seem to have more Ca^{2+}-influx (area under the curve) as compared to the cells expressing TRPV4-Wt (Figure 35i). However, these differences between TRPV4-L596P and TRPV4-Wt appears non-significant when activated with higher doses of agonist (4αPDD, 10

μM) (Annexure 7). These possibly suggest that under the low intensity of stimulus, TRPV4-L596P mutant has more opening properties than the TRPV4-Wt. Apart from the quantitative differences in the whole cell; there are specific qualitative differences at the specific subcellular regions. For example, we noted that in case of TRPV4-L596P-mCherry expressing cells, the Ca^{2+}-levels are much higher at the cell periphery and at the tip of the filopodia-like projections and this higher level of Ca^{2+}-sustains for longer duration in such specific areas than that of cells expressing TRPV4-Wt-mCherry (Figure 36).
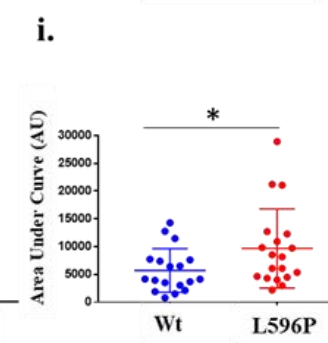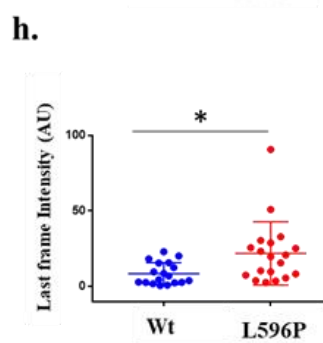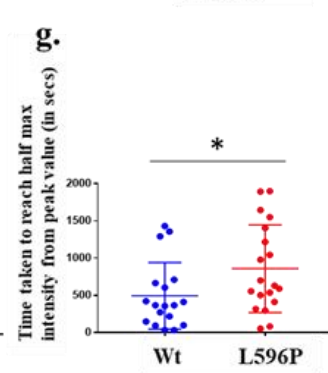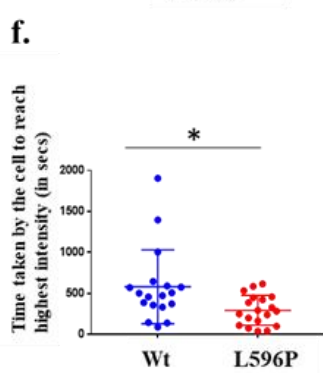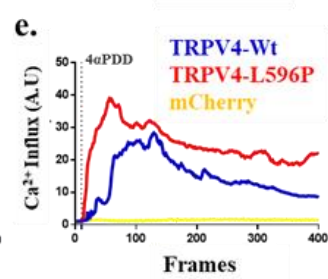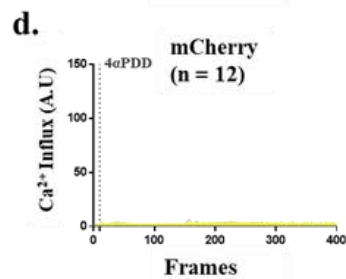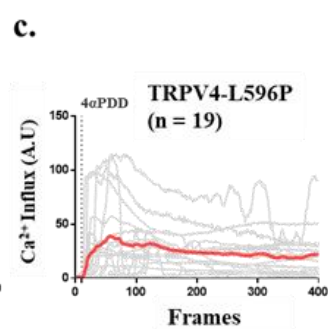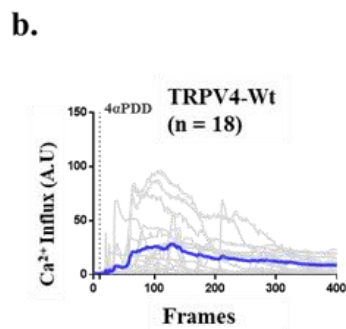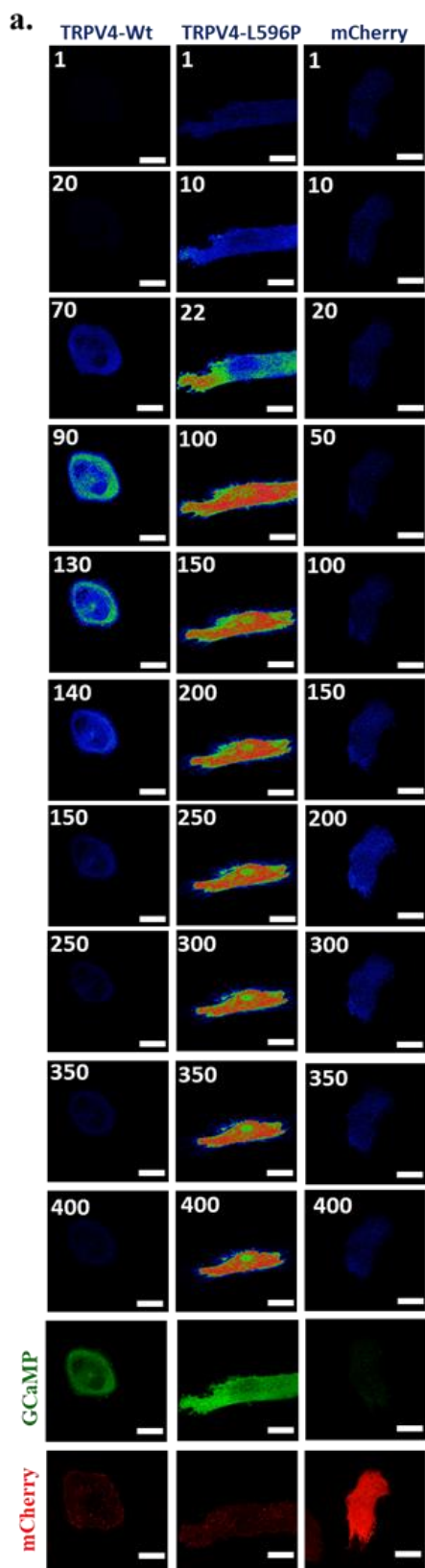
Figure 35: TRPV4-L596P mutant has more open properties than TRPV4-Wt. a. Shown are the time-series fluorescence of Ca^{2+}-sensor protein (GCaMP6f) expressed in the Saos-2 cells in response to TRPV4 activation. The Saos-2 cells were doubly transfected with plasmids coding for either of TRPV4-Wt-mCherry, TRPV4-L596P-mCherry, or only pmCherryC1 (red color) along with the Ca^{2+}-sensor GCaMP6f (green). In all cases, cells were stimulated with 4αPDD (1 μM) added at 10th frame. In TRPV4-L596P mutant expressing cells, Ca^{2+}-influx which not only appears earlier but also often sustained for longer duration. The changes in fluorescence intensity of pGP-CMV-GCaMP6f before and after agonist stimulation has been depicted in RGB pseudo color. Scale bar is 50 μm. For details see supplementary movies (M1-M3). **b-e.** Shown are the changes in the Ca^{2+}-levels of cells expressing either TRPV4-Wt-mCherry (n =18) (b), TRPV4-L596P-mCherry (n =19) (**c**), or only pmCherryC1 (n =12) (d). The time point at which 4αPDD is added is shown as dotted line. The initial value recorded at the 1st-frame is considered as 1 and the intensities for all the frames were subsequently calculated relative to the 1st-frame. Values from individual cells and average value from all the cells are as thin and thick lines. The comparison of average Ca^{2+}-influx is shown (e). **f-i.** Time taken to reach the point of highest fluorescence intensity after stimulation (f) and time taken to fall fluorescence intensity half maximum from highest value (g) for each individual cell have been calculated. The relative fluorescence intensities at the end of the experiment (h), areas under the curve as a parameter for total Ca^{2+}-influx (i) were calculated. All these values show significant differences (* = $P<0.05$) between Wt and L596P mutant.
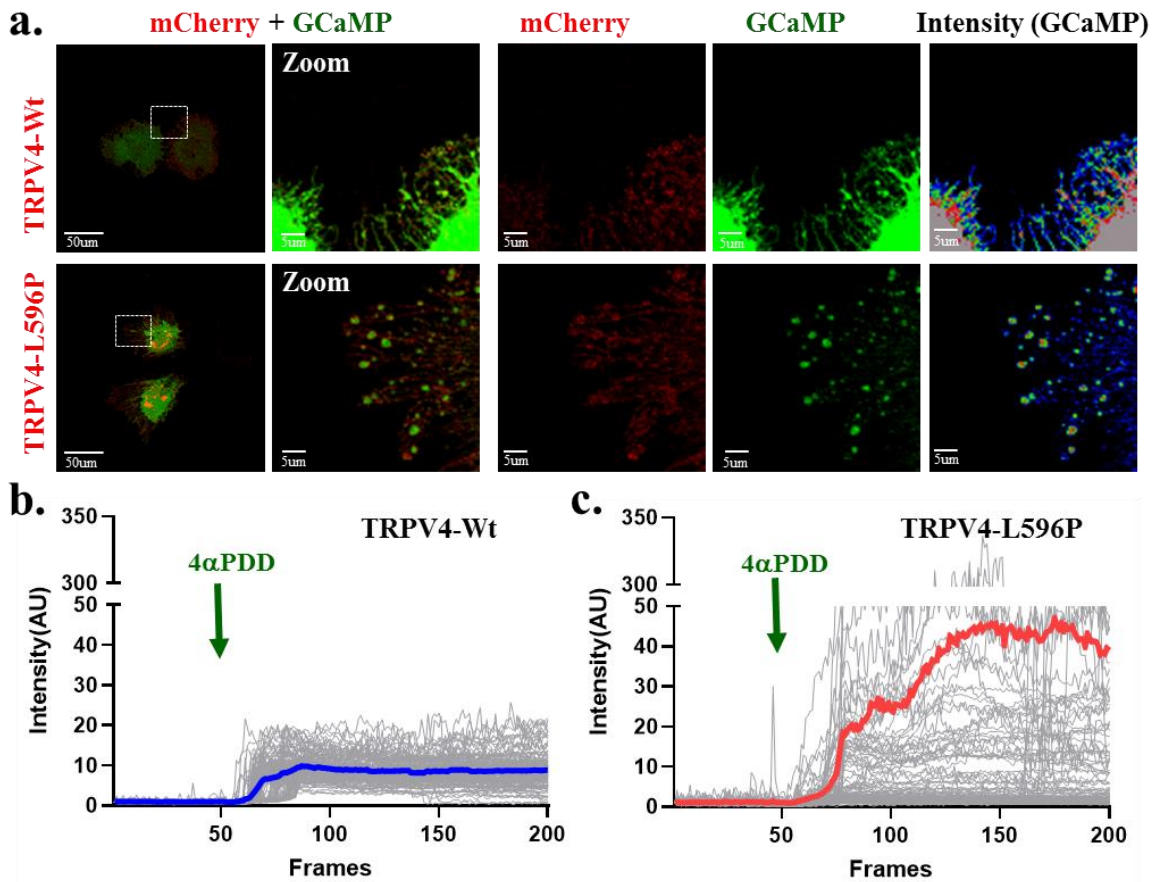
Figure 36: TRPV4-L596P expressing cells have higher Ca^{2+} at the filopodial tips compared to the TRPV4-Wt after activation. a. Shown are the confocal images of Saos-2 cells expressing TRPV4-Wt-mCherry or TRPV4-L596P-mCherrry (red) along with GCaMP6f (green). The enlarged portion of a cell is shown and the fluorescence intensity of theGCaMP6f is shown in pseudo color. **b-c.** Shown are the changes in the Ca^{2+}-levels in filopodial tips of cells expressing TRPV4-Wt-mCherry or TRPV4-L596P-mCherrry. TRPV4 activator, namely 4αPDD has been added in the 50th frame. TRPV4-L596P mutant expressing cells retain much higher Ca^{2+} in the filopodial tips.
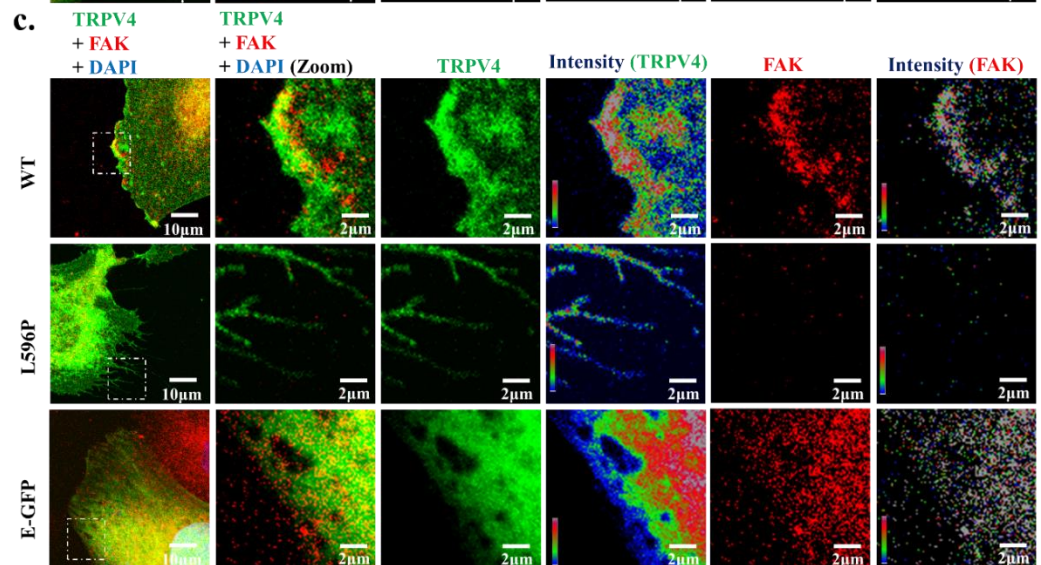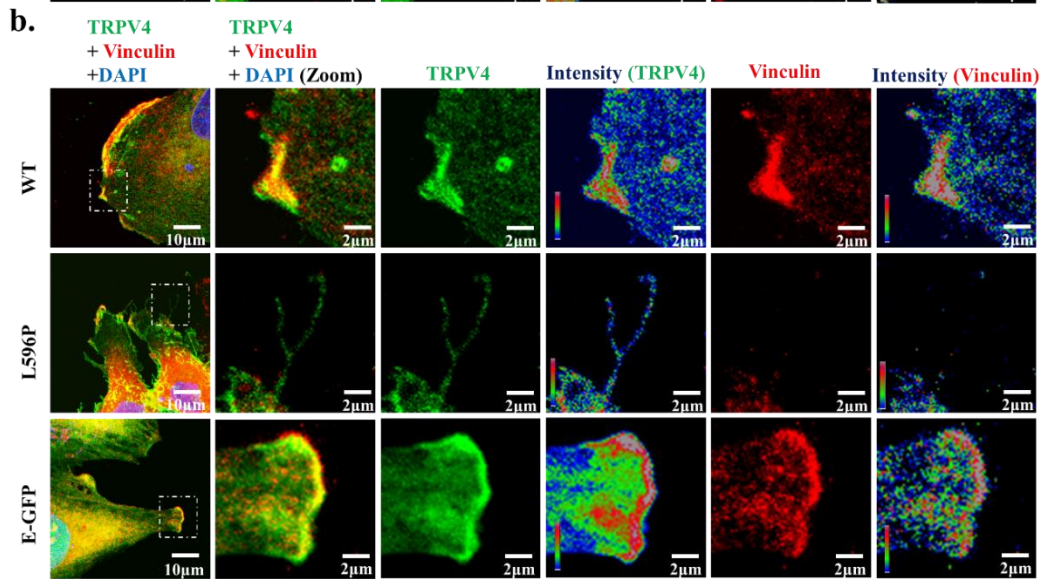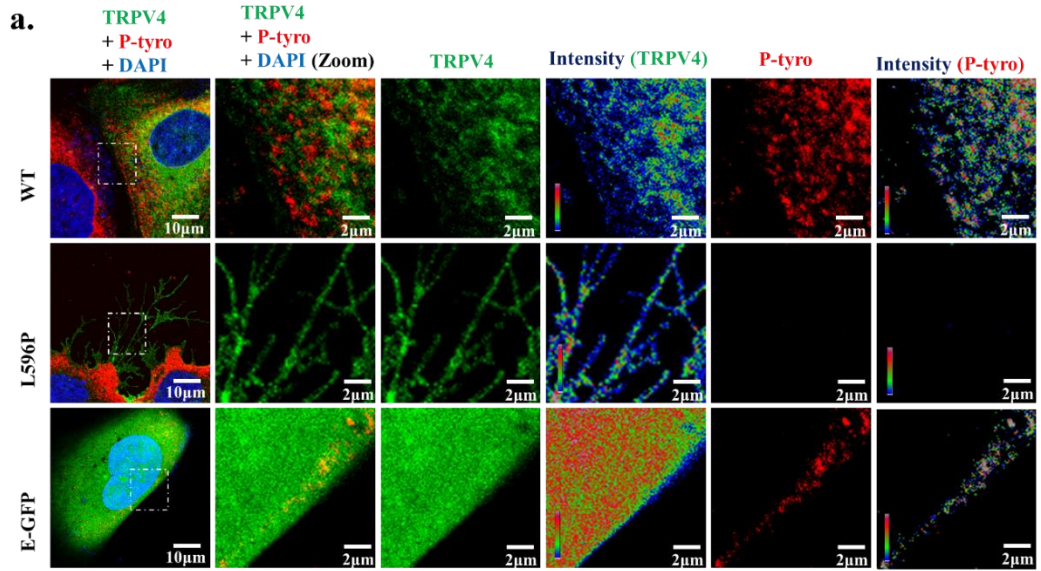
Figure 37: Phospho-Tyrosine, Vinculin and FAK are present in the periphery of cells expressing of TRPV4-Wt but not TRPV4-L596P mutant. Shown are the confocal images of Saos-2 cells expressing either TRPV4-Wt-GFP, TRPV4-L596P-GFP or only E-GFP (green) stained with Phospho-tyrosine (red) (**a**), Vinculin (**b**) or FAK (**c**) (red). The enlarged area of the peripheral region of cell with either lamellipodia or filopodia-like structure is shown in right side. The fluorescence intensity of GFP or the respective marker protein is shown in intensity scale. The L596P mutant expressing cells have filopodia-like structures where these markers are not present.

2.2.7. Lamellipodia of TRPV4-Wt GFP expressing cells but not filopodia-like structures of TRPV4-L596P-GFP expressing cells contains phospho-Tyrosine, Vinculin and FAK

Next, we tested the presence of specific markers in the membrane periphery (lamellipodia) or filopodia-like structures of SaOS cells expressing TRPV4-Wt-GFP, or TRPV4-L596P-GFP of only E-GFP. We could detect phospho-Tyrosine, Vinculin and FAK in the lamellipodia of cells expressing TRPV4-Wt-GFP, or only E-GFP. On the other hand, we could not detect these markers in the filopodia-like structures of SaOS cells expressing TRPV4-L596P-GFP (Figure 37). Additionally, the amount of filamentous actin (as seen by Phalloidin staining) is low there or missing in many of such structures. That is why we have termed them "Filopodia-like" structures. The images depicting the phalloidin levels in the filopodia-like regions are shown (Annexure 5).

Taken together, the results suggest that TRPV4 has evolved with a specific pattern of amino acids at the LWI regions during vertebrate evolution. Such pattern formation is likely to be guided by the several membrane properties and membrane composition; such as by cholesterol. Changes in such pattern due to the point mutations results in altered channel functions, localization and regulation that correlates well with the development of pathophysiological situations observed in bone cell.

2.3 Characterization TRPV4-R616Q mutation causing Bracholymia

About 60 naturally occurring mutations affect the TRPV4 ion channel functions and this cause various bone and neuromuscular diseases (Table 6). R616Q causes brachyolmia in human population that primarily affects the spine. R616Q mutation is previously reported to act as a "gain-of-function" mutant that keeps TRPV4 "constitutively open" in physiological temperature (Rock et al., 2008). How R616Q change modifies the channel-gating conduct isn't clear. Previously we have reported that TRPV4-Wt interacts with cholesterol and such associations might be significant for channel gating (Kumari et al., 2015). In this work we addressed if and how cholesterol can control TRPV4 utilizing *in silico*, biochemical and cell biological methodologies.

We have accessed the physical interaction of cholesterol with TRPV4 and the R616Q mutant protein. Their localization in the lipid raft and their membrane mobility was observed. Taken together, this information would help to provide information about evolutionary origin of TRPV4 in the context of cholesterol interaction and the regulatory role of cholesterol on TRPV4 in the lipid bilayer.

2.3.1. TRPV4 expresses endogenously in Mesenchymal Stem Cells (MSC) and its localization in lipid raft depends on temperature

The endogenous localization of TRPV4 and its localization pattern in accordance to lipid raft was studied at varying temperature. At 37°C, we noted that TRPV4 co-localizes with Caveolin-1 (Figure 38). However, after cholesterol reduction by β-MCD, or by Pravastatin only (12 hour) Caveolin-1 as well as TRPV4 revealed altered distribution, membrane clustering and much lesser colocalization. The results were different when cells were grown at 27°C and stained for lipid rafts. Less co-localization was seen in case of the lower temperature.
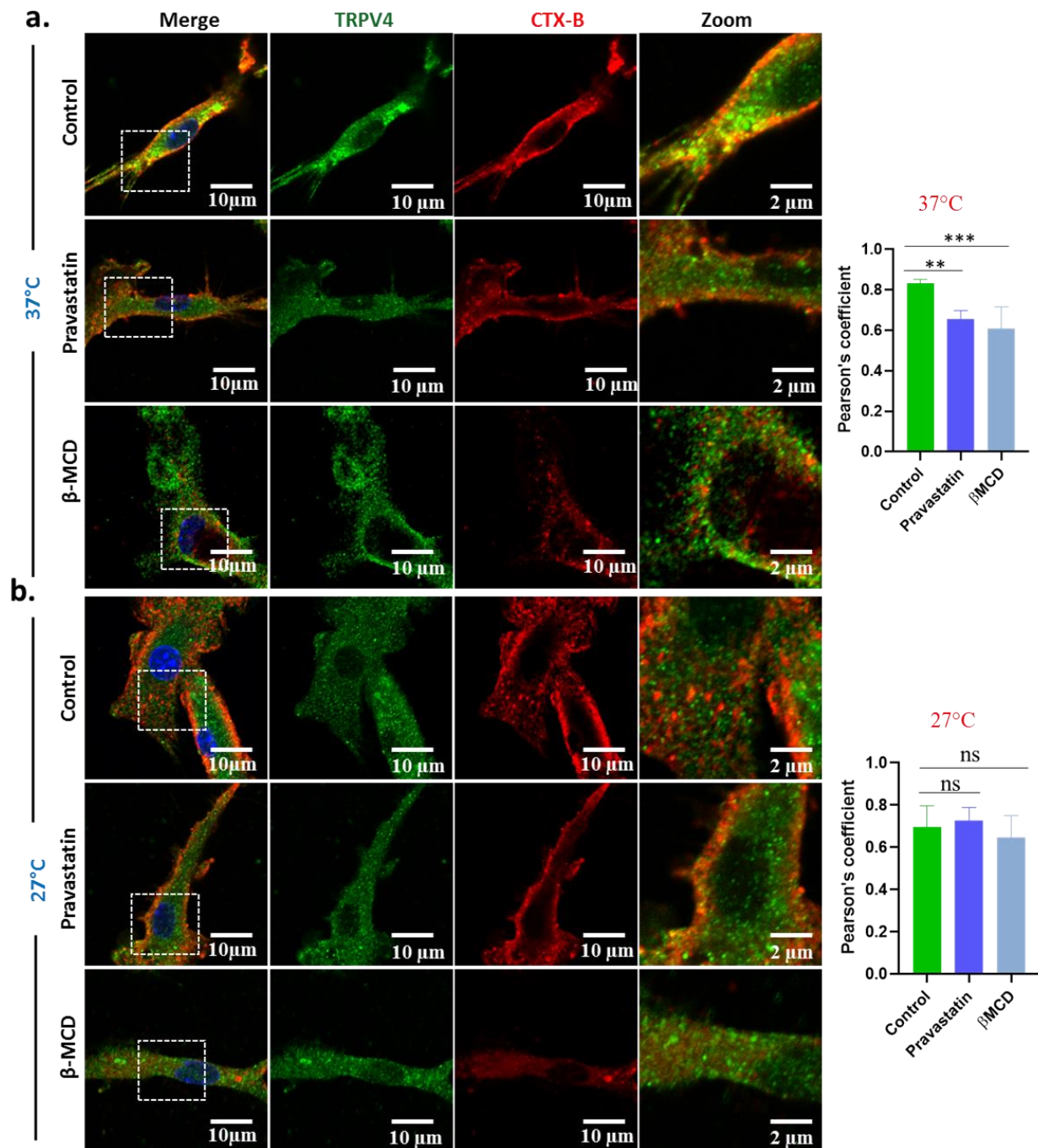
Figure 38. TRPV4 is endogenously expressed in Mesenchymal stem cells and its localization in lipid raft is dependent on the temperature and/or amount of membrane cholesterol. Shown are the confocal images of MSCs immunostained for endogenous TRPV4 (green) and Cholera Toxin B (Red). Reduction of membrane cholesterol by βMCD or Pravastatin results in reduction in colocalization. The cells were grown at two different temperatures, 37°C (**a**) or 27°C (**b**) for 3 hours before fixation. At 37°C cells have greater colocalization between Caveolin (stained indirectly with Cholera toxin B) and TRPV4. Pearson's colocalization coefficient calculated for endogenous TRPV4 (green) and Cholera Toxin B (Red) is shown in the right side.

2.3.2 TRPV4-Wt but not TRPV4-R616Q mutant shows interaction with cholesterol *in-silico*

In silico homology modeling was done to characterize the cholesterol-binding pockets. On obtaining the structural data, further tests were done using YASARA docking module and several binding modes were found. Further filtration was done to discard all improper poses and modes of cholesterol interaction with the TRPV4. We noted that cholesterol binds to the TRPV4-Wt at CARC motif previously identified by us mostly by hydrophobic interactions. However, cholesterol doesn't bind to the TRPV4-R616Q in the same mode and poses (Figure 39). This observation allowed us to test further if cholesterol interacts differentially with TRPV4-Wt and R616Q in experimental conditions.
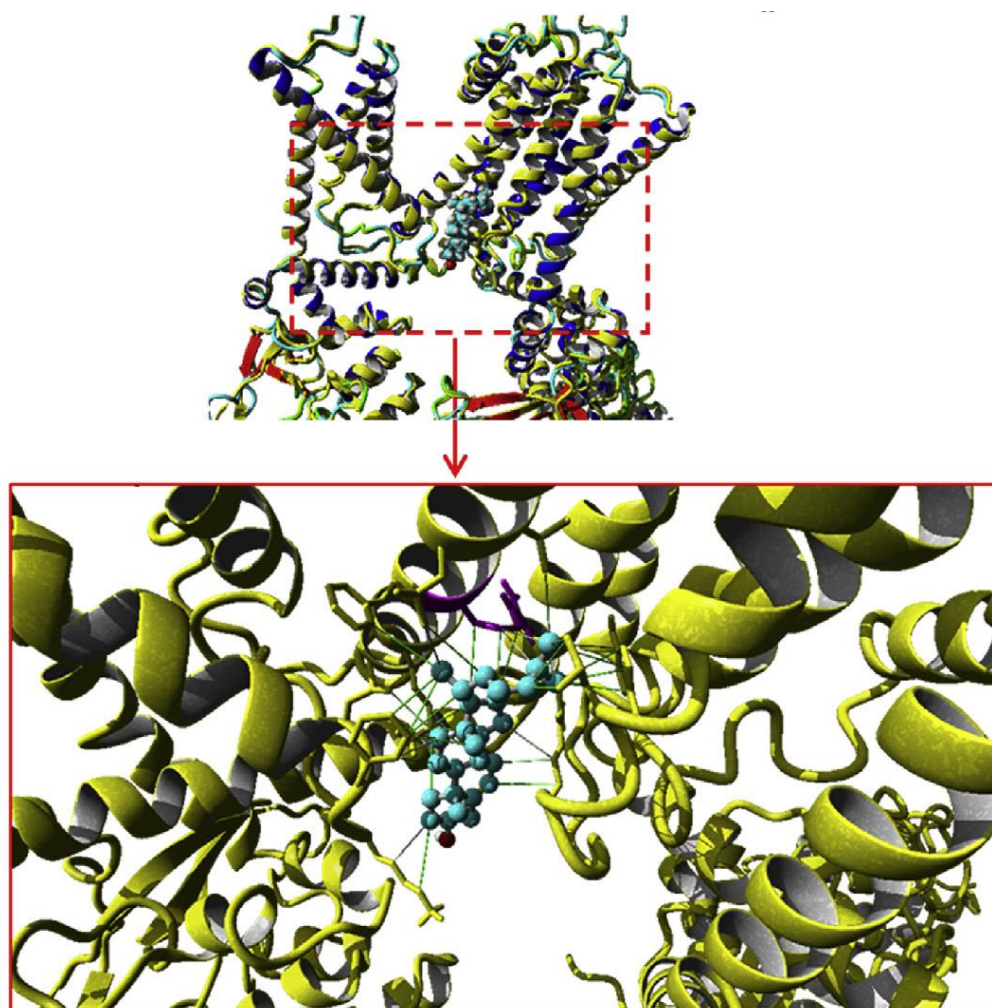
Figure 39: Interaction of cholesterol with TRPV4-WT but not TRPV4-R616Q mutant. hTRPV4-Wt structure is (indicated in yellow ribbon) superimposed with the hTRPV4-R616Q mutant structure (indicated in blue ribbon). Docking of cholesterol with hTRPV4-WT shows interaction (binding affinity -7.76 kCal/Mol) while the hTRPV4-R616Q mutant does not show any interaction within the defined-binding pocket.

2.3.3. TRPV4-WT but not its mutant R616Q localizes in membrane microdomains

To confirm localization of TRPV4 in lipid rafts by another independent method, we did double transfection of hTRPV4-GFP and Caveolin at 37°C in two different cell lines, i.e., Saos-2 and F11 cell line. We observed colocalization of hTRPV4-GFP with Caveolin-RFP in both the cell lines (Figure 40). However, no colocalization was seen even when the cells were double transfected with hTRPV4-R616Q-GFP mutant and Caveolin-RFP.
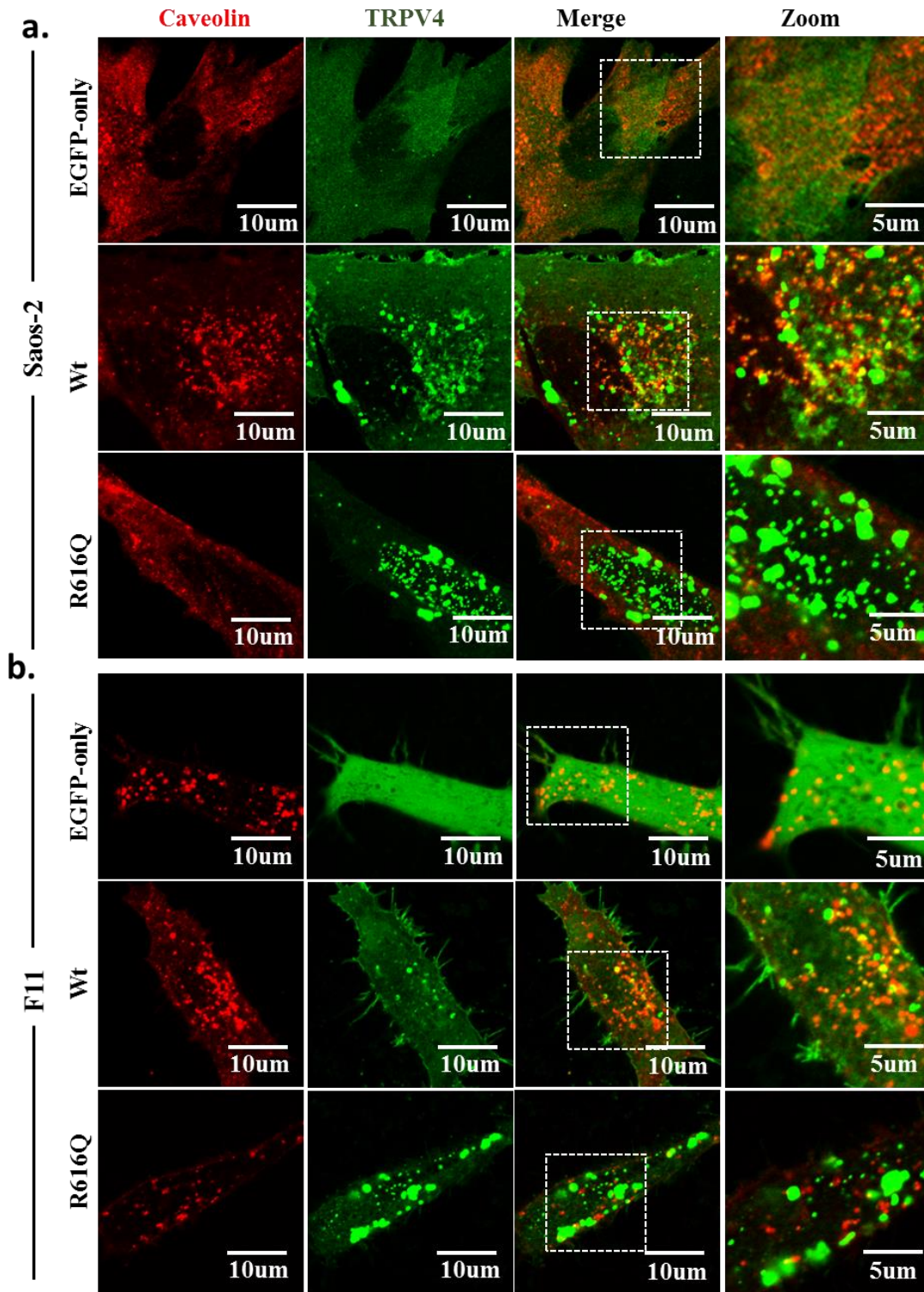
Figure 40. TRPV4-Wt but not TRPV4-R616Q localize in membrane micro domains in osteogenic and neuronal cell. Saos-2 (**a**) and F11 (**b**) cells co-expressing hTRPV4-GFP (green) or hTRPV4-R616Q-GFP (green) along with Caveolin-RFP (red) was fixed. Confocal images depicting TRPV4-Wt-GFP colocalizes with Caveolin-RFP. Notably, TRPV4-R616Q-GFP mutant does not colocalize with Caveolin-RFP even after over-expression. GFP-only localizes all over the cells.

2.3.4. TRPV4-R616Q mutant has less membrane mobility compared to TRPV4-Wt

To test the effect of cholesterol on the full-length TRPV4 in the functional context and especially *in vivo* condition, we expressed TRPV4-Wt-GFP or TRPV4-R616Q-GFP mutant in F11 cell and performed FRAP analysis (Figure 41a-b). In normal condition TRPV4-Wt-GFP has more mobility than TRPV4-R616Q-GFP. After cholesterol depletion (by β-MCD and pravastatin), the mobility of TRPV4-R616Q-GFP remain significantly low compared to the TRPV4-Wt-GFP.

2.3.5. Differential interaction of TRPV4-Wt and TRPV4-R6161Q to cholesterol

We expressedTRPV4-TM4-Loop4-TM5 sequence as GST-tagged protein and purified the same fragment. Purified protein representing GST-TRPV4-TM4-Loop4-TM5 fragment moves significantly slow (compared to its expected molecular weight 33kDa) in SDS-PAGE (Figure 41c). Notably, upon adding cholesterol in increasing concentration, intensity of the upper band (Up1) decreases and lower band (Lo2) increases, demonstrating a change in migration of GST-TRPV4-TM4-Loop4-TM5 fragment in cholesterol-dependent manner in gel (Figure 41d). High molecular weight complex also is formed by the GST-TRPV4-TM4-Loop4-TM5 in presence of cholesterol and is detected at the gel pockets (GeP). To confirm such changes are truly due to cholesterol interaction and is specific, we quantified the intensity of certain bands and plotted the values against each other. Such plots resulted in linear plot suggesting inverse relationship between Lo2 with Up1 and between GeP with Up1 and therefore suggests the importance of cholesterol in such relationship (Figure 41e). Ratio of Up1 vs. Lo2 as well as ratio of Up1 vs. GeP follow a linear slope when plotted against cholesterol concentration (Figure 41f).
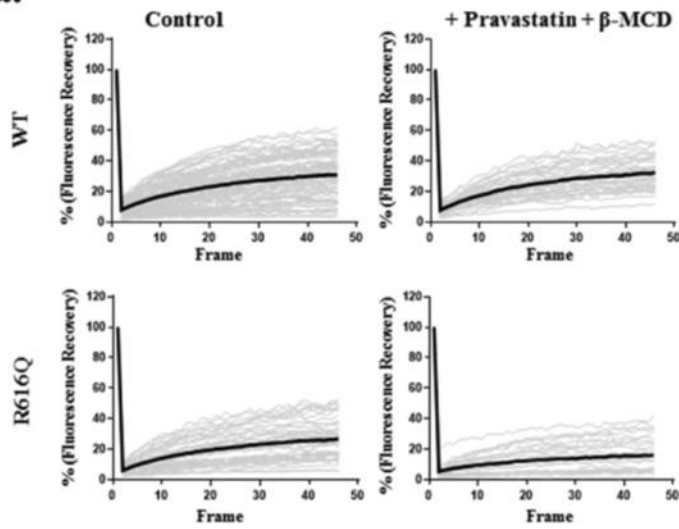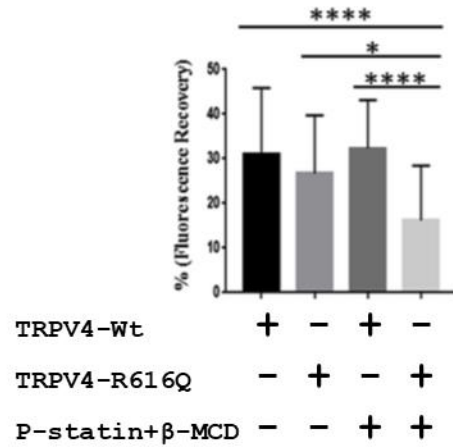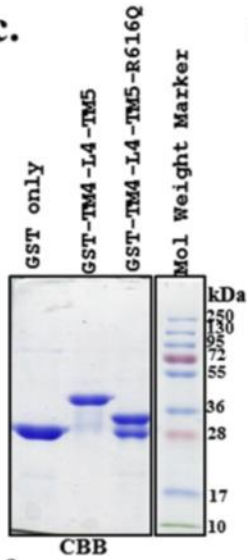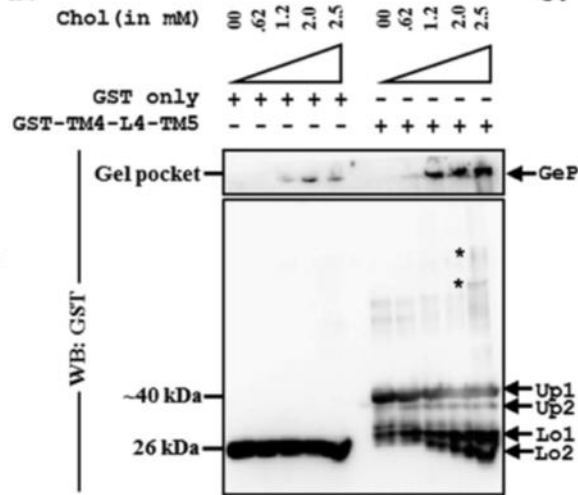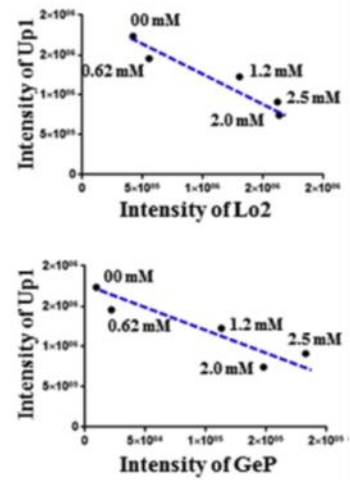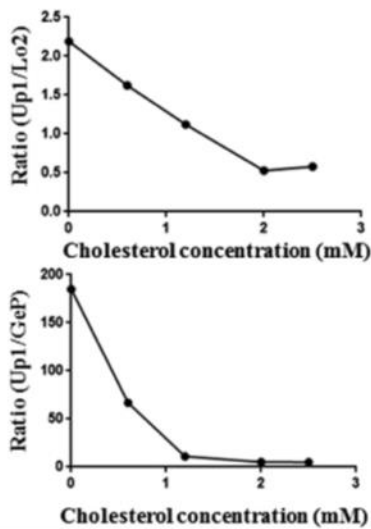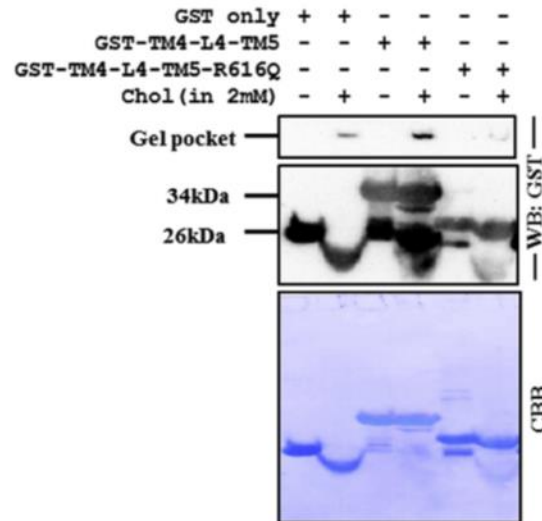
Figure 41. TRPV4-Wt but not TRPV4-R616Q mutant interacts with cholesterol. a. Membrane mobility of TRPV4 depends on the level of cholesterol. FRAP pattern of cells expressing TRPV4-Wt-GFP (top panel) or TRPV4-R616Q-GFP in control (left), in cholesterol-depleted conditions (right) are shown. In each case at least 30 ROIs were analyzed (grey lines) and the average value is indicated (bold black line). The fluorescence intensity (in % of the initial conditions) is plotted in Y-axis and frame numbers are plotted in X-axis. Time difference between each frame is 1 sec. **b.** The recovery values (shown in fig a) at the end of the experimental point are compared. **c.** Electrophoretic mobility of GST-only, GST-TRPV4-TM4-Loop4-TM5, or GST-TRPV4(R616Q)-TM4-Loop4-TM5 in SDS-PAGE is shown. Majority of the GST-TRPV4-TM4-Loop4-TM5 moves slower than its expected molecular weight. **d.** Fragment representing GST-TRPV4-TM4-Loop4-TM5 forms multiple bands in SDS-PAGE at ~40 kDa or bit lower size (termed as Up1 and Up2) and lower bands at around 26 kDa (termed as Lo1 and Lo2). GST-TRPV4-TM4-Loop4-TM5interacts with cholesterol and forms a complex at the gel pocket (termed as GeP). With increasing concentration of cholesterol, the complex formation at the gel pocket intensifies. Some other minor bands (indicated by asterisk) are visible in presence of high-amount of cholesterol only. GST-only is used as negative control. Samples were mixed in Laemmli buffer followed by incubation with 2mM cholesterol for 1 hour in 40°C. Samples were separated in 12% SDS-PAGE and probed with anti-GST monoclonal antibody. **e.** Up1 negatively correlates with the formation of Lo2 as well as GeP. Intensity of Lo2 as well as GeP have been plotted against intensity of Up1. In both cases, a linear relationship is observed. **f.** Formation of GeP or Lo2 positively correlates with the concentration of cholesterol, especially in the dynamic range (till 2mM). Ratio of Up1/Lo2 or Up1/GeP are plotted against different cholesterol concentration. **g.** While GST-TRPV4-TM4-Loop4-TM5 forms complex at the gel pocket, the mutant GST-TRPV4(R616Q)-TM4-Loop4-TM5 doesn't form such complex. Protein samples were mixed in Laemmli buffer followed by incubation with 2mM cholesterol for 1 hour in 40°C. Samples were run in12% SDS-PAGE thereafter and probed with anti-GST monoclonal antibody.

2.3.6   TRPV4-R616Q has reduced interaction with cholesterol

To test, if the CRAC- and CRAC-like motifs present in the TM4–Loop4–TM5 of TRPV4 indeed interact with cholesterol, we tested if the same fragment shows direct interaction with cholesterol. We performed cholesterol-mediated gel-shift assay with GST-TRPV4-TM4-Loop4-TM5 along with GST-only as a negative control. The same experiment was done with GST-TRPV4(R616Q)-TM4-Loop4-TM5 mutant also (Figure 41g). We noted that the wild-type fragment forms a complex at the gel pocket of SDS-PAGE which was confirmed by running a western blot and probing it with GST antibody. The same result was not seen in case of the hR616Q mutant. This result further validates that TRPV4-Wt interacts with cholesterol.

2.4. Steroidogenesis as a function of mitochondrial metabolism and the role of TRPV4 in it

As revealed from synteny analysis, TRPV4 gene share tight linkage with MVK and GLTP gene and this linkage is conserved for 450 MY suggesting the dependency and functional linkage between TRPV4 and cholesterol biosynthesis pathway (Buhaescu & Izzedine, 2007). Though the impact of various steroids on TRPV4 has not been completely described at this point, the crosstalk among TRPV4 and steroid hormones has been set up somewhat. For instance, progesterone can control TRPV4 expression (Jung et al., 2009). TRPV4 is an essential component for mechanosensitivity in the aldosterone-sensitive distal nephron (Mamenko et al., 2011). Steroid hormones additionally modify the mechanical hyperalgesia where TRPV4 is involved. Taken together, the outcomes uncover a solid reliance of TRPV4 on sterol compounds demonstrating that sterol biosynthesis pathway and TRPV4 function might have shared co-evolution.

To test these hypotheses, we have analyzed human adrenal cortex derived cell line H295R for functional TRPV4 expression and its role in steroidogenesis related functions. The endogenous expression of TRPV4 in H295R cell line was studied using immunofluorescence, western blot and FACS studies. To analyze the functional activity of the TRPV4 channel inside H295R, live cell imaging was performed for measuring cytosolic and mitochondrial Ca^{2+}. The significance of TRPV4 in the mitochondria was further studied by measuring the mitochondrial Cu^{2+} and Fe^{2+} levels, mitochondrial temperature, hormone production, steroidogenic enzyme expression, ER-mitochondria contact regulation, upon stimulation by specific agonist and antagonists.

2.4.1. "Adrenal Insufficiency" causes a change in the expression pattern of TRPV4 in the adrenal cortex

Etomidate and Ketamine are drugs that are known to induce Adrenal Insufficiency (Besnier et al., 2017). The effects of Etomidate and Ketamine on the level of TRPV4 expression on tissue sections of mice adrenal gland was determined and for those tissues were collected 12 hour's post-injection of Etomidate and Ketamine (Figure 42). Examination of sections of the adrenal cortex revealed loss of TRPV4 expression level when treated with drugs (Etomidate and Ketamine) that cause adrenal insufficiency. Especially in Ketamine-treated tissues, the expression of TRPV4 decreases significantly suggesting the possible role of TRPV4 in adrenal insufficiency.

2.4.2. TRPV4 channel is expressed endogenously in H295R cells

To investigate further the role of TRPV4 on adrenal steroidogenesis, we explored the endogenous expression levels of TRPV4 in H295R, the Adrenal cortex-derived cell line. We performed indirect immunofluorescence staining using the TRPV4 antibody (Alomone). Confocal microscopic analysis of H295R cells revealed the endogenous expression of TRPV4 in H295R (Figure 43a). The TRPV4 is detected throughout the cytoplasm as well as on the membrane of the cells. The specificity of the staining was confirmed by using specific blocking peptides which either reduced or abolished the staining pattern completely. The specificities of these antibodies were also verified by flow cytometry (Figure 43b), where the number of cells positive for the TRPV4 channel and the mean fluorescence intensity (MFI) was lowered when higher dilutions of antibodies were used (Figure 43c). Nearly 98.81%, 42.87%, and 19.19% of H295R cells are positive for TRPV4 when dilutions were made to 1:200, 1:400, 1:800 respectively (Figure 43b). Only 0.08% of cells were detected when an isotype control is used (Figure 43b).
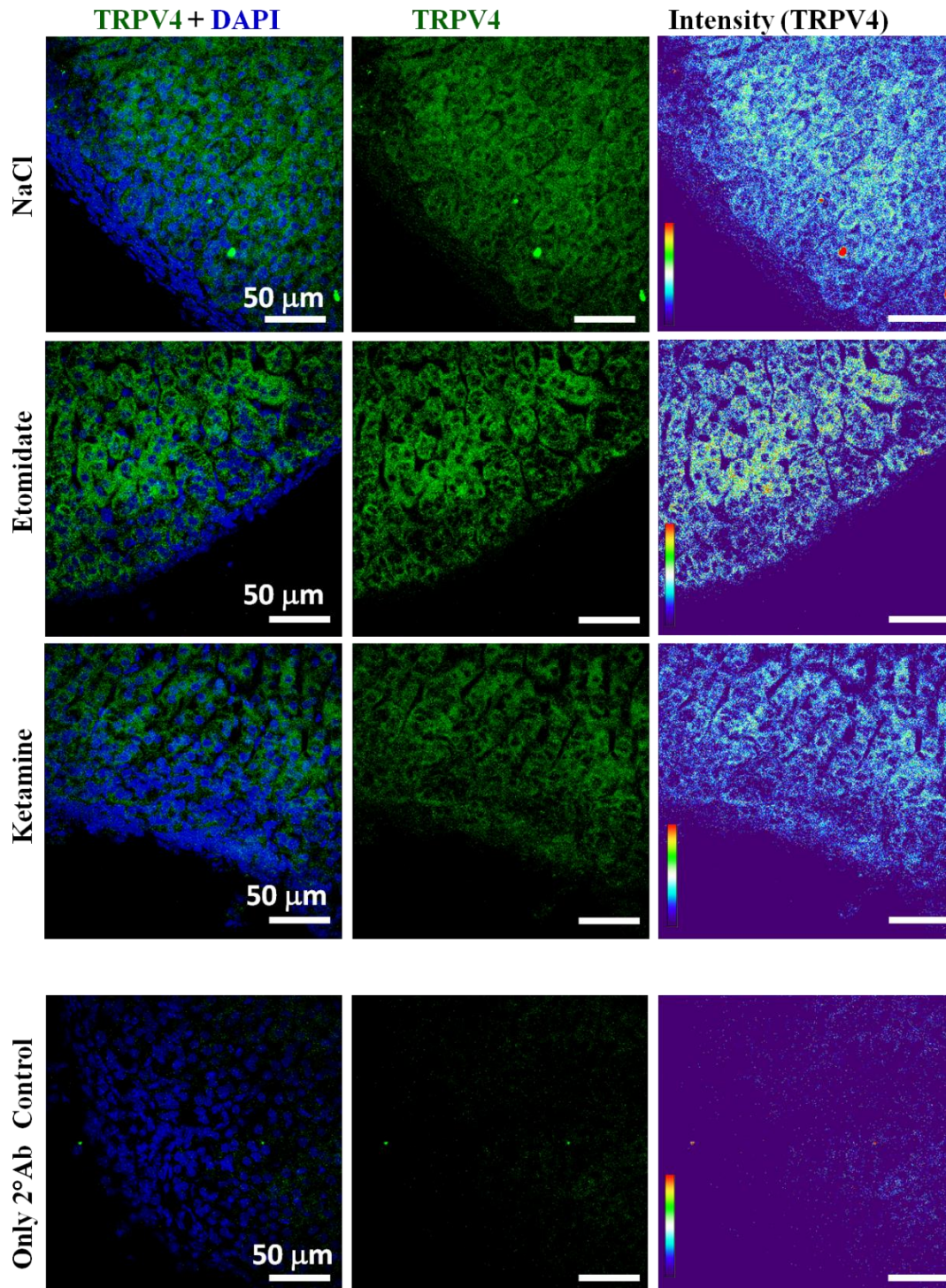
Figure 42: TRPV4 expression pattern in adrenal insufficiency model: Drug-treated mouse adrenal gland tissue sections are stained with anti-TRPV4 antibody (green) and DAPI (blue). Tissue-stained secondary antibody alone as negative control. Scale bar 50μm.Fluorescence intensity from TRPV4 in all cases is represented in pseudo rainbow colour (red and blue represents highest and lowest intensity respectively).
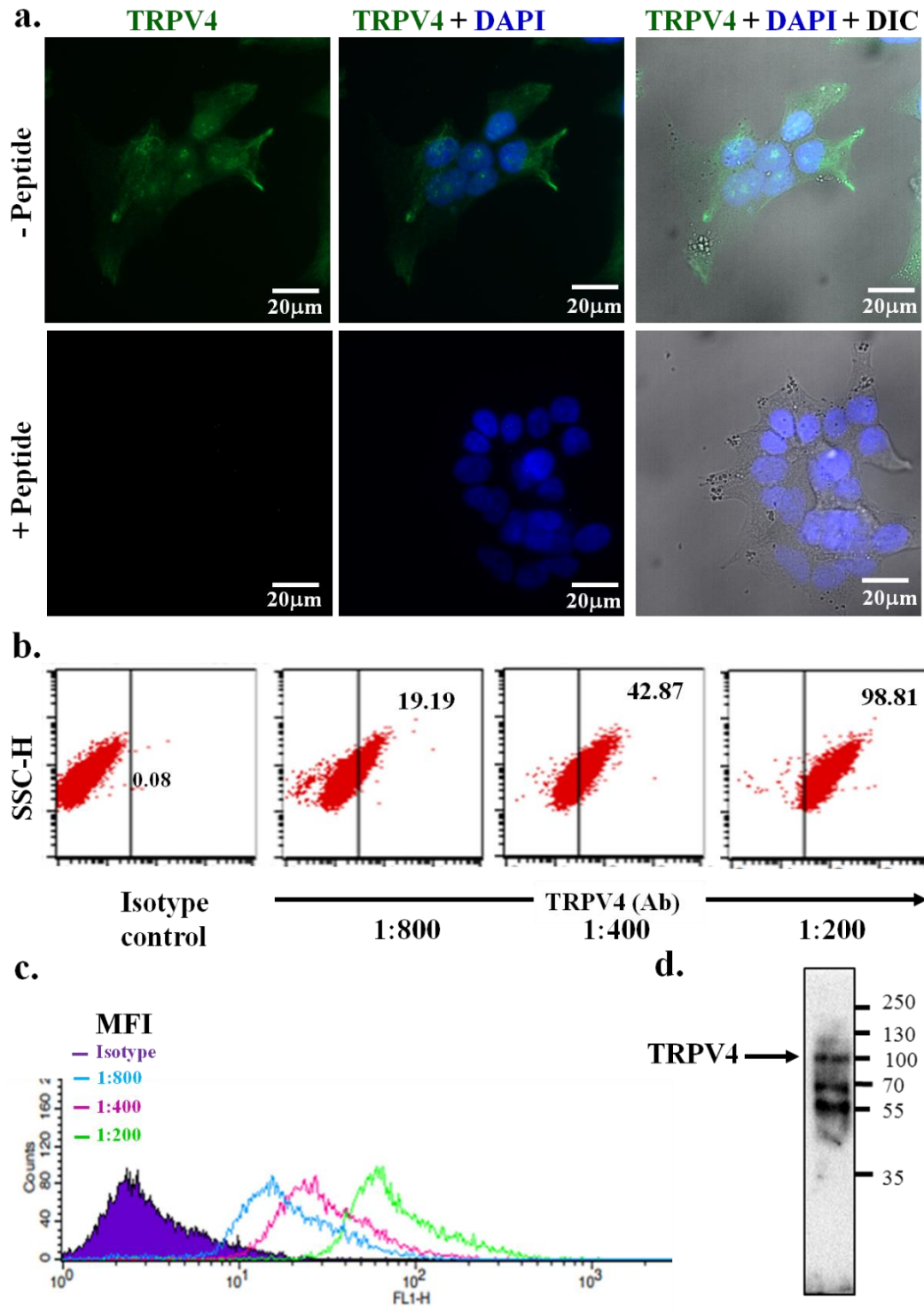
Figure 43: Endogenous TRPV4 expression in adrenal cortex-derived cell line H295R. a. Immunofluorescence image showing TRPV4 expression in H295R cells (green) stained by anti-TRPV4 antibody. Nucleus is stained with DAPI (blue). Peptide control is used as a negative control. **b.** FACS data showing endogenous staining of TRPV4 at various dilution. **c.** Mean Fluorescent Intensity histogram showing cells positive for TRPV4. **d.** Western blot data showing distinct band at ~100 kDa suggesting TRPV4 expression.

MFI histograms of cells positive for TRPV4 are also shown (Figure 43c). Western blot analysis using anti-TRPV4 antibody confirmed that a distinct band is present near 100 kDa which further suggests the endogenous expression of TRPV4 in H295R cells (Figure 43d).

2.4.3. Functional TRPV4 is expressed endogenously in H295R cells

To explore if endogenous TRPV4 is functional in H295R cells, we performed Ca^{2+}-imaging experiments in H295R cells using pGP-CMV-GCaMP6f vector. Live cell imaging revealed an increase in intensity upon stimulation by TRPV4 activator 4αPDD, intracellular Ca^{2+} levels increased in most of the cells (Figure 44). This suggests the functional expression of TRPV4 in H295R cells.

2.4.4. TRPV4 stimulation increases mitochondrial Ca^{2+}-fluctuations

To demonstrate the functional expression of TRPV4 in mitochondria of H295R cells, ratiometric-pericam transfected cells were stimulated with TRPV4 activator 4αPDD. The fluorescence ratio (fluorescence intensity at 488 nm /fluorescence intensity at 405 nm) calculated for the entire cell as ROI is represented (Figure 45a-b). In this way of calculation, the fluorescence intensity at 488 nm / 405 nm did not show any significant or visible change as the mitochondrion covers a less portion of the cell. We calculated intensity values before and after the addition of 4αPDD or DMSO (Figure 45c). The activation results an increased fluctuation in the fluorescence intensity. This analysis shows significant differences (Figure 45d) and therefore suggests that endogenous TRPV4 is important for regulating mitochondrial Ca^{2+} in the H295R cells. In this regard, further characterization, possibly a particle-based quantification may provide detail information.
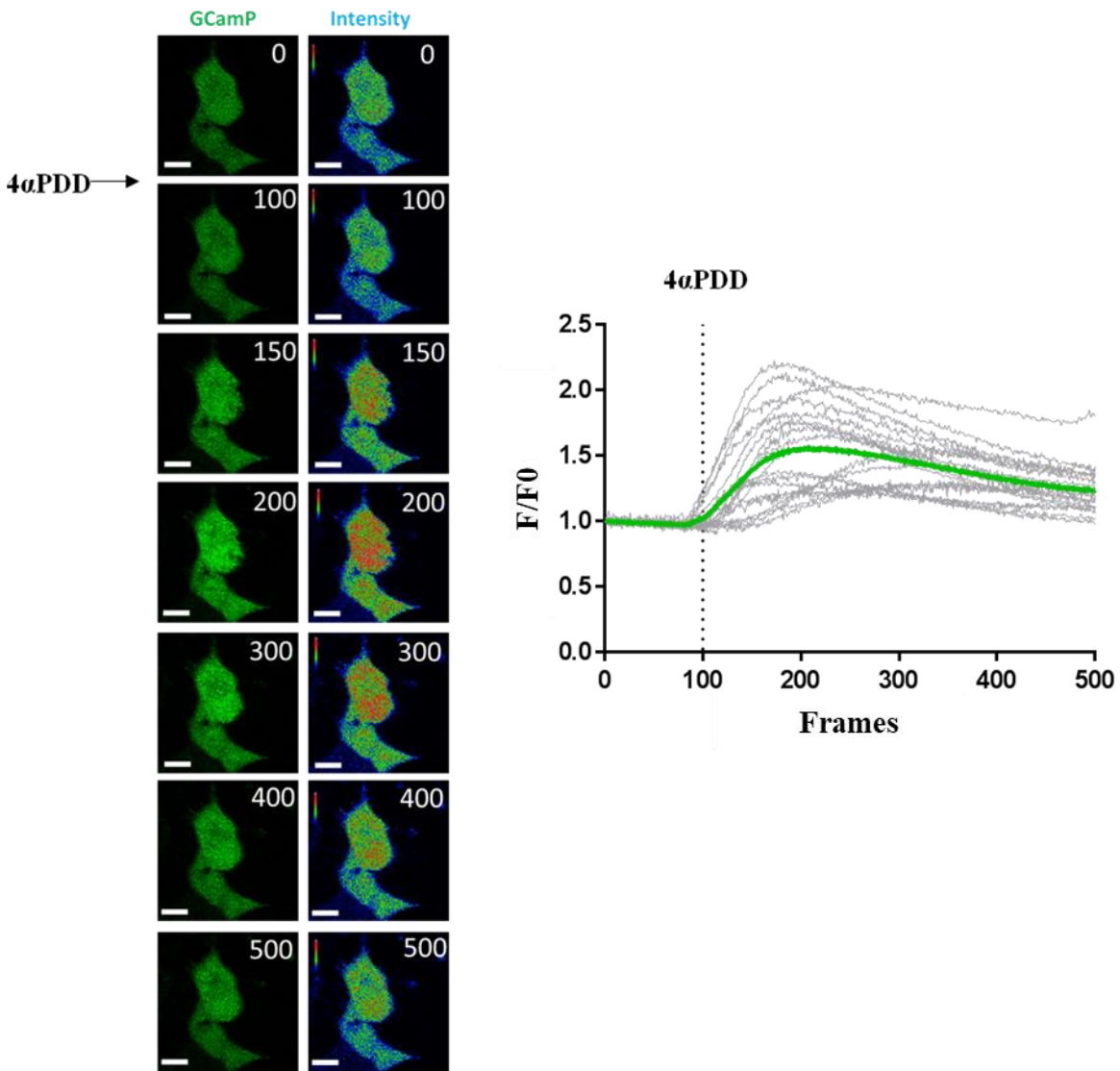
Figure 44: Ca^{2+}-imaging of H295R cells with TRPV4 agonist 4αPDD. H295R cells transfected with the Ca^{2+}-sensor pGP-CMV-GCaMP6f shows levels of Ca^{2+}-influx upon addition of TRPV4-specific agonist 4αPDD (5 μM) at 100th frame. The change in fluorescence intensity of pGP-CMV-GCaMP6f before and after agonist stimulation has been depicted in RGB mode. Quantification of pGP-CMV-GCaMP6f fluorescence intensity from cells shows change in intensities upon addition of 4αPDD at the 100th frame. For quantification, the initial value recorded at the 1st frame was considered as 1. The intensities for the remaining frames were subsequently calculated relative to the 1st frame.
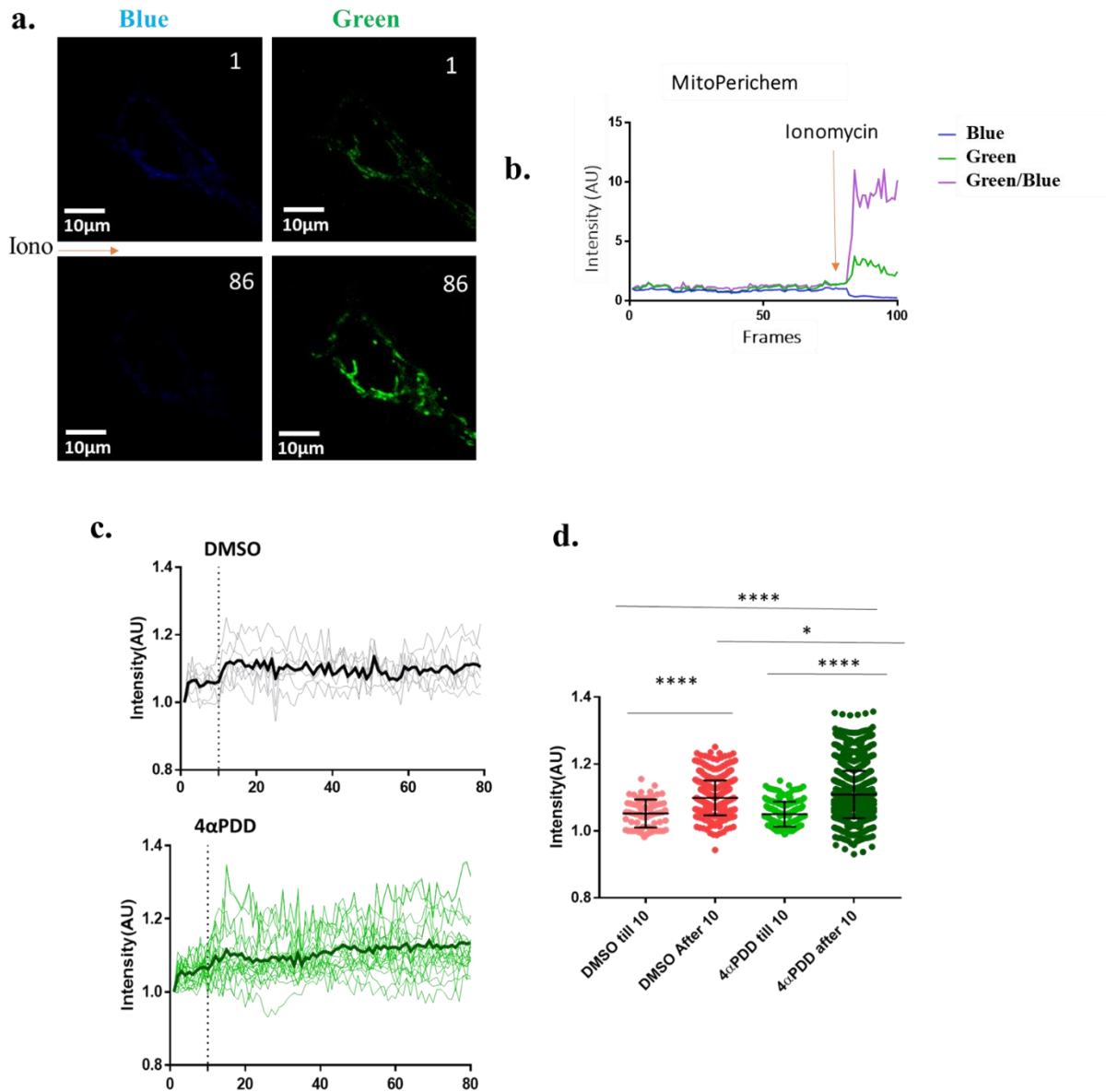
Figure 45: TRPV4 regulates mitochondrial Ca²⁺-influx. Mito-Pericam (Ca²⁺-sensing fluorescent protein targeted to mitochondria) was transiently expressed in H295R cells and live cell imaging was performed using confocal microscope. TRPV4 activator 4αPDD (5 μM) and solvent control DMSO was added after 10 frames of imaging to independent samples. Fluorescence ratio (fluorescence intensity at 488 nm /fluorescence intensity at 405 nm) was calculated for the entire cell. **a)** Qualitative image of green and blue intensity before and after addition of ionomycin is shown. Scale bar: 10 μm. **b)** Graph showing representative analysis that is done by dividing green/blue intensity to get the real mitochondrial calcium influx value. **c)** Ca²⁺-intensity graph of cells in 4αPDD (5 μM) and DMSO condition was quantified by Image J. Arrow indicates the time of addition of drug at 10th frame. **d)** Quantification of Mito-Pericam intensity fluctuation was performed by comparing the data points just before and after the addition of 4αPDD.

2.4.5. TRPV4 plays a role in the steroid production pathway

To access the role of TRPV4 in the steroidogenesis pathway, the levels of major pathway enzymes were analyzed using western blot. In the present study, we investigated the influence of TRPV4 modulators in human adrenocortical cell line (NCI-H295R) compared with forskolin stimulation. Forskolin is an agent that stimulates the intracellular production of cAMP. This action is actually exerted via adenylate-cyclase activation. Elevated cAMP levels can stimulate steroid production more than 100 fold, it is likely that cAMP is the principle second messenger regulator of steroid hormone production in the body. Stimulation of NCI-H295R cells with forskolin increases the expression of steroidogenic acute regulatory protein (StAR). The StAR protein is involved in cholesterol translocation from the cytosol into the mitochondria and serves as a rate-limiting step in steroid biosynthesis (Asif et al., 2006; Beavo et al., 2015).

In most cases, the basal level steroid production was not affected much but forskolin-activated condition gets affected when the H295R cells were treated with TRPV4 stimulators, i.e., 4αPDD (1μM) or RN1734 (5μM). In presence of 4αPDD (1μM) or RN1734 (5μM) in forskolin-activated conditions, the enzyme level alters, suggesting the requirement of the basal level TRPV4 function is appropriate and optimum for the functioning of this pathway (Figure 46). At least as a proof-of-concept, this subtle changes in the enzyme levels due to TRPV4 activation or inhibition suggest that TRPV4 may affect the steroidogenesis pathway.

2.4.6. TRPV4 may have regulatory role in the production of steroids

We evaluated the steroid-secreting capacities in the supernatants of H295R cells following 24 hour of treatment of TRPV4-specific drugs. Levels of the hormones secreted (cortisol, DHEA-S and Progesterone) were represented in fold change. However, upon TRPV4 modulation, there is not much changes in the levels of hormones in basal conditions (Figure 47). Forskolin increased the hormone levels significantly as expected. However, only a slight decrease in the hormone levels in the supernatants was seen. The combination of forskolin (10 µM) along with TRPV4-specific drugs exhibit a potentiation effect in inhibiting steroidogenesis. Though there are some trends of altered production of steroids due to TRPV4 modulation, it is important to note that with this n number, and with this detection level, this data set remain inconclusive and further experimentation is needed in future.

2.4.7. TRPV4 affects mitochondrial temperature regulation

Like in any metabolic pathway, steroid production is also a multi-step, multi enzyme-driven process that is highly regulated by temperature. In fact, in most species, steroid production is highly sensitive to slight changes in temperature. Mitochondria is the essential site for steroid hormone biosynthesis too. We, therefore, analyzed the changes in mitochondrial temperature in H295R cells due to TRPV4 activation or inhibition. TRPV4 modulatory drug-treated cells were incubated in mitochondrial thermal sensor "MTY" dye (Arai et al., 2015) and cells were imaged and fluorescence intensities are quantified (Figure 48). Our data suggest that TRPV4 modulating drugs induce changes in mitochondrial temperature independent of forskolin-mediated steroidogenesis. Both TRPV4 activation, as well as inhibition, resulting in a reduction in mitochondrial temperature which is independent of the state of steroid production.
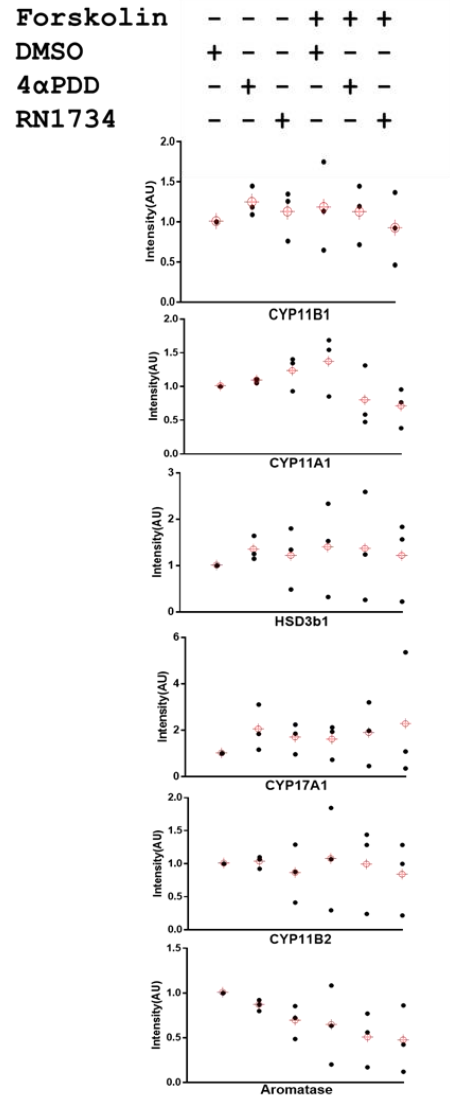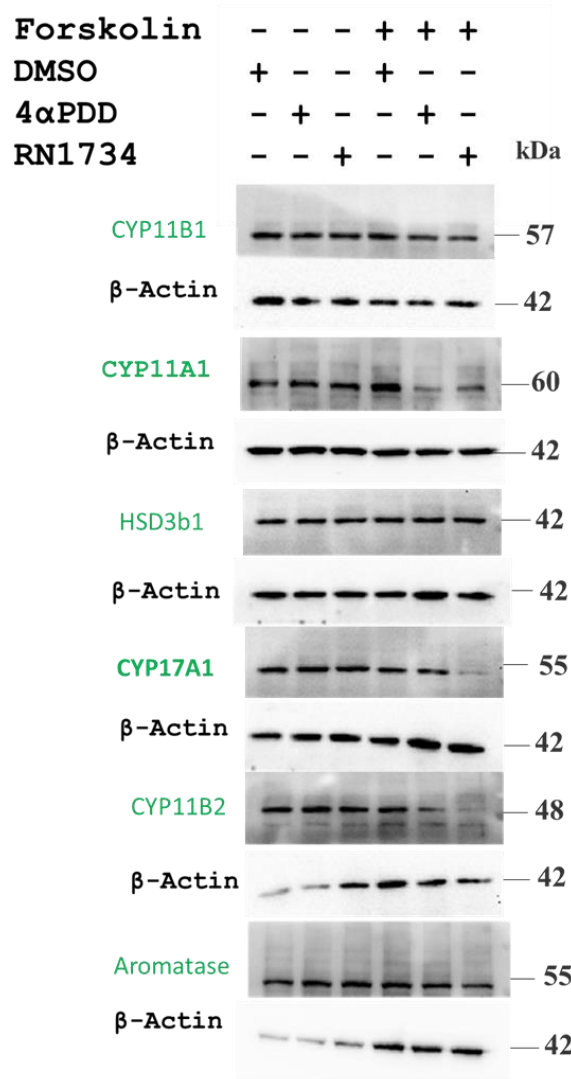
Figure 46: Steroidogenic enzyme levels in TRPV4 drug treated H295R cells. Western blot analysis of basal or forskolin activated H295R cell treated with 4αPDD or RN1734. Blots were probed with steroidogenic enzymes namely CYP11B1, CYP11A1, HSD 3β1, CYP17A1, CYP11B2 or Aromatase. β-actin was used as loading control. Corresponding densitometry plot suggest a decreasing trend of enzyme levels in most cases in forskolin activated TRPV4 drug treated condition, although statistically non-significant. All western blots were repeated at least three times.
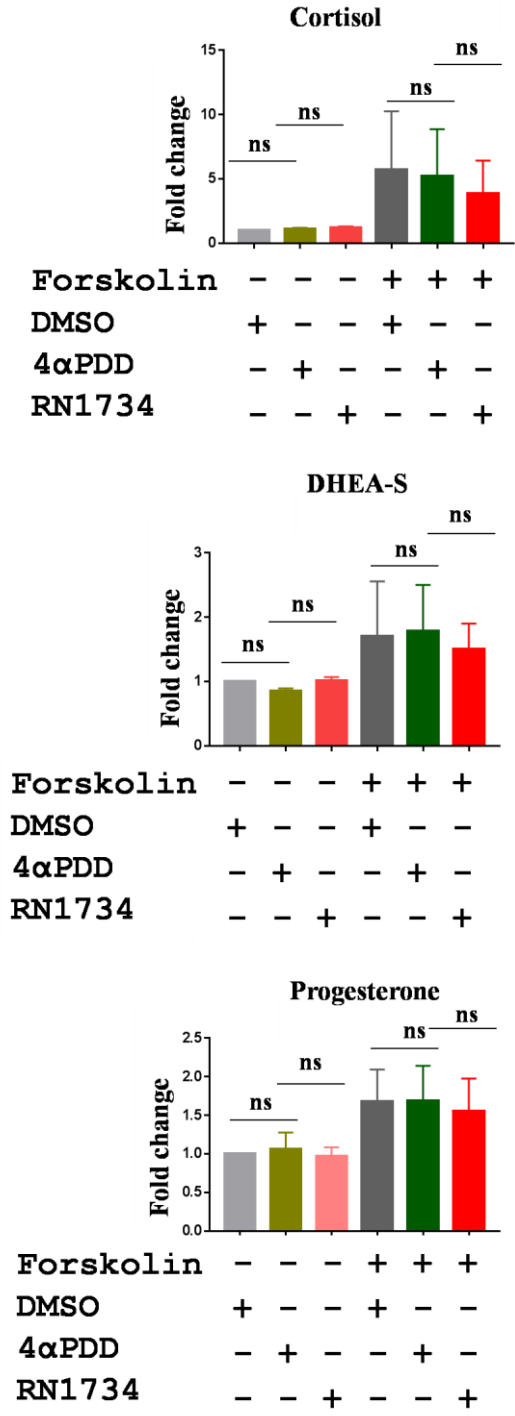
Figure 47: Steroid level quantification in H295R cells using TRPV4 drugs. Cell culture media from H295R cells treated with TRPV4 modulatory drugs were subjected to steroid level quantification using ELISA. Three steroids namely Cortisol, DHEA-S and Progesterone were quantified. As expected, forskolin activated condition gives a sharp rise in steroid level. In spite of certain trends, at this n number, no significant differences were observed in case of 4αPDD (1μM) or RN1734 (5μM) treatments.

In other words, disruption of TRPV4 function results in lowering the mitochondrial temperature which cannot be rescued by forskolin, suggesting that TRPV4 has a key role/dominant role in the regulation of mitochondrial temperature and thus overall steroid metabolism.

2.4.8. Role of TRPV4 in the regulation of ER-Mito contact points

Mitochondria forms functional contacts with ER for the regulation of several important functions. One of the relevant functions of ER-Mito contact is regulation of steroidogenesis as certain steps in steroid production needs shuttling of the metabolites from mitochondria to ER and *vice versa* (Midzak & Papadopoulos, 2016).
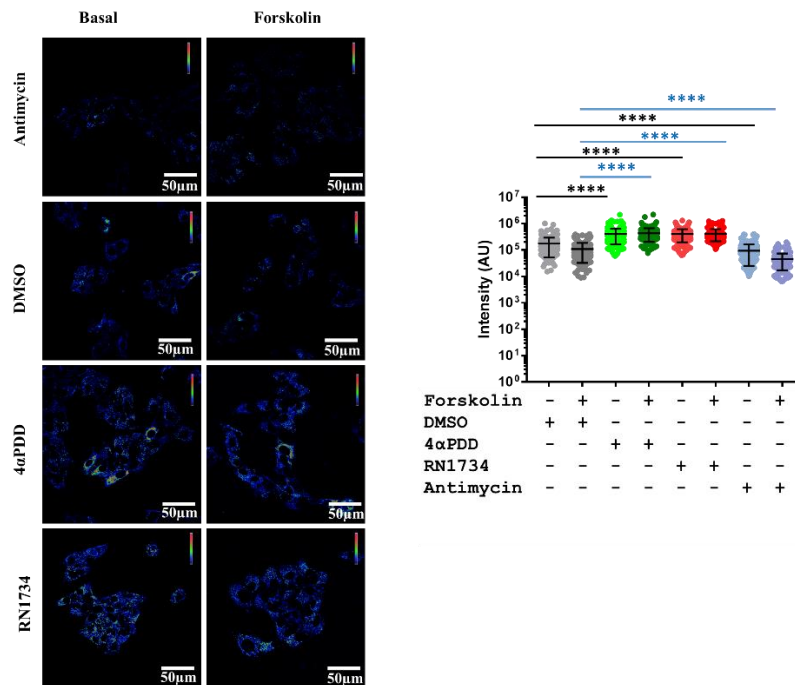
Figure 48: TRPV4 modulation interferes with temperature regulation inside mitochondria of the cell: H295R cells in basal or forskolin activated condition treated with antimycin, DMSO, 4αPDD or RN1734 show altered mitochondrial temperature that can be seen by either increase in fluorescence intensity (temperature decrease) or decrease in fluorescence intensity (temperature increase) of the mitochondrial temperature sensor MTY. The changes in fluorescence intensity of the sensor have been depicted in RGB pseudo colour. Scale bar is 50 µm. Quantitative analysis of the fluorescence from individual cells as depicted in dot plot analysis shows significant decrease in temperature in case of TRPV4 activation or inhibition in both basal or forskolin activated case.

a

	Mito perimeter	Mito Perimeter+ Mito-ER coloc	Mito+ER+ (Mito-ER coloc)	Mito perimeter+ (MitoP-ERP coloc)
Basal DMSO				
Basal 4αPDD				
Basal RN1734				
FSK DMSO				
FSK 4αPDD				
FSK RN1734				

110
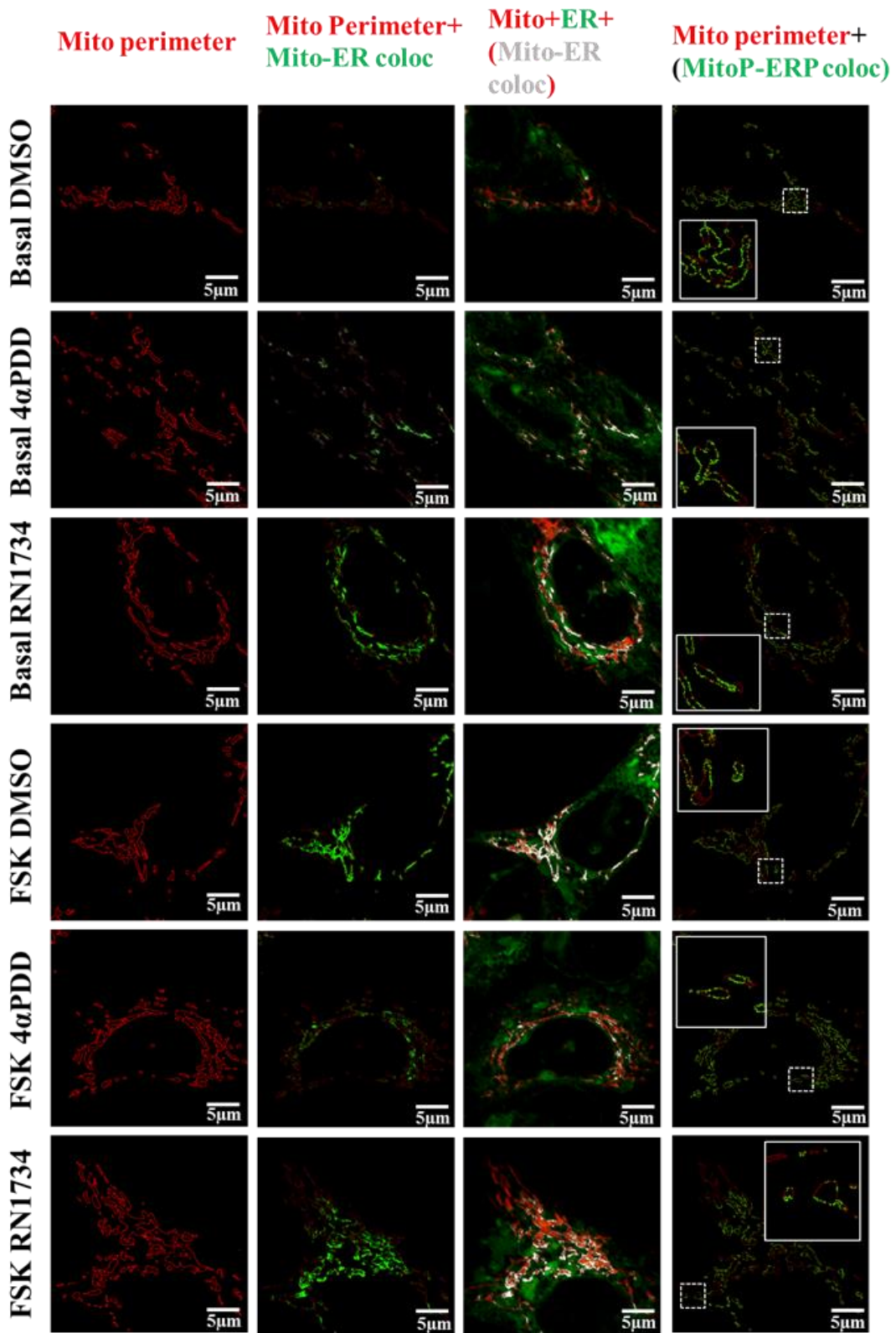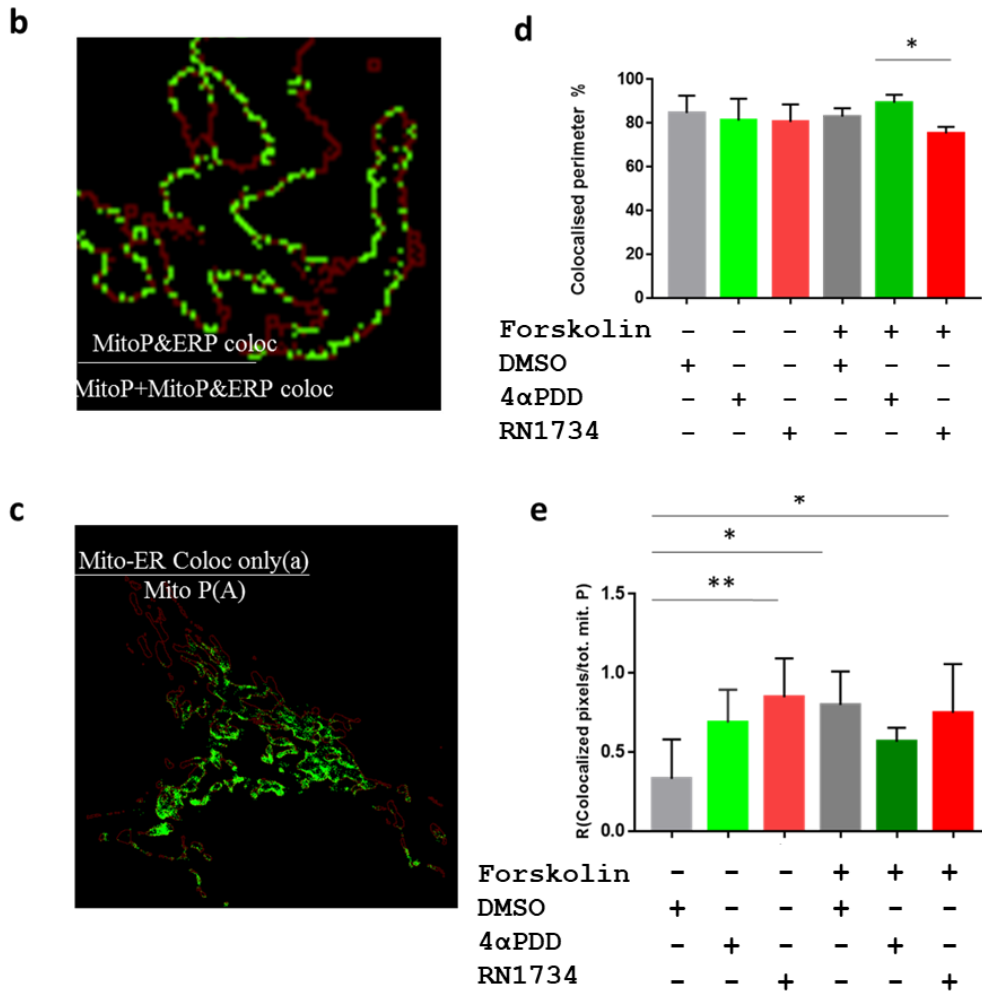
Figure 49: TRPV4 drug modulation impacts close contacts between ER and mitochondria. ER–mitochondria colocalization analysis in basal and forskolin activated condition treated with DMSO, 4αPDD or RN1734. Representative mitochondrial perimeter profile of the cell(red), Mitochondrial perimeter (red) + mitochondria-ER colocalization (green) overlap images, Mitochondria (red) + ER (green) + mitochondria-ER colocalization (white), mitochondrial perimeter + mitochondria perimeter –ER perimeter colocalization images are shown in (**a**). All the images were analyzed with the perimeter plugin (Materials and Methods). Red pixels correspond to the whole mitochondrial perimeter profiles; green pixels represent the points in which the mitochondrial perimeter is in contact with the ER (**b**). ER–mitochondria signal colocalization indexes, calculated as the ratio (R) between mitochondrial perimeter pixels colocalized with the ER and total mitochondrial perimeter pixels is shown in (**c**). The colocalised perimeter percentage and R (colocalised pixels/total mitochondrial perimeter) values are shown in (**d**) & (**e**) respectively.

Several reports suggest that Mitochondria-associated membranes (MAM) are the ER regions

which is in contact with mitochondria and are relevant in the synthesis of steroid hormones

111

(Doghman-Bouguerra & Lalli, 2019). Therefore, we evaluated the extent of formation of those contact points following the method as described previously (Filadi et al., 2015). We evaluated the changes in these contact points as a result of TRPV4 modulatory drugs to further explore the role of TRPV4 in steroidogenesis (Figure 49). Data suggests that TRPV4 activation or inhibition increases the colocalization of ER and mitochondria.

2.5. Characterization of TRPV4 interaction with mitochondrial protein cytochrome c

Cytochrome c (Cyt C) has a major role in the mitochondrial respiratory chain and its release from mitochondria triggers the initial steps towards apoptosis (Garrido et al., 2006). Cyt C resides in the inner mitochondrial membrane where it binds to cardiolipin (Elmer-Dixon et al., 2020; Ott et al., 2007). During apoptosis, cardiolipin migrates to the outer mitochondrial membrane where the levels of cholesterol are relatively high (In the cholesterol enriched condition of rat liver mitochondria, the outer mitochondrial membrane stores 80 times more cholesterol than the inner mitochondrial membrane) (Echegoyen et al., 1993). This transition may create a pore for Cyt C release. Studies suggest that Cholesterol plays a supporting role in the pore formation required for Cyt C leakage during apoptosis and therefore may have a regulatory effect on Cyt C release from mitochondria (Bergstrom et al., 2013). Our previous study advocates TRPV4 as a mitochondrial protein (Kumar et al., 2018.) and also reported the physical interaction of TRPV4 with different mitochondrial proteins, namely Mfn1, Mfn2, Hsp60, and Cyt C. The biochemical pull-down study performed in this work also confirmed that a short sequence of TRPV4 (MTS, 40 amino acids long) can interact with Cyt C directly in a Ca^{2+}-sensitive manner. We also have shown biochemical interaction of TRPV4 with cholesterol (Kumari et al., 2015). All these results suggest a possible TRPV4 and Cyt C interaction during apoptosis. Work described in this chapter characterizes the TRPV4 interaction with Cyt C. Bioinformatics analysis and biochemical pulldown experiments were performed to confirm the interaction of Cyt C with TRPV4. The conservation analysis of interacting residues was performed throughout the vertebrate evolution. To access the sensitivity of this interaction, pulldown was performed in the presence of different metals like Cu^{2+}, Mn^{2+}, Ni^{2+}, Zn^{2+} and Fe^{3+}. As the interacting region of TRPV4, i.e., MTS is a

hotspot to many mutations; the TRPV4- Cyt C interaction analysis was performed with four such TRPV4 mutants, namely R616Q, F617L, L618P and V620I.

2.5.1. Cyt C and TRPV4 co-localizes within mitochondria

As TRPV4 is detected within a sub-set of mitochondria, we explored the co-localization of TRPV4 with Cyt C by immunofluorescence analysis. For that purpose, we used HaCaT cell line and transfected the cells with TRPV4-RFP. We have stained the cells with Cyt C –specific primary antibody and Alexa Fluor 488-labelled secondary antibody. We observed the Cyt C status in control and TRPV4-activated conditions. We have noticed co-localization in both cases, though greater colocalization was seen in the TRPV4-activated (4αPDD, 1 µM) condition (Figure 50).
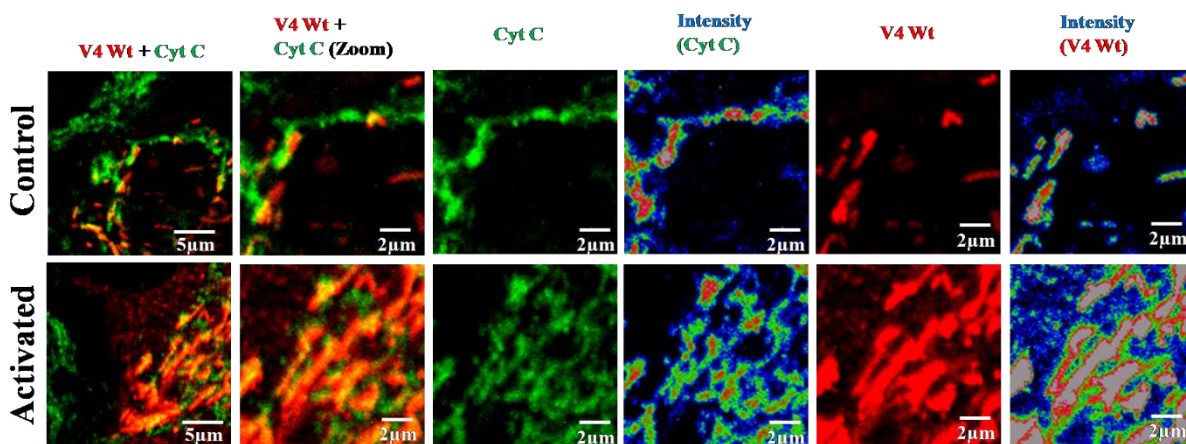
Figure 50: TRPV4 co-localizes with Cyt C. Confocal images demonstrating the co-localization of TRPV4 with Cyt C. The images depict TRPV4 (red) signals overlapping with Cyt C (green) in control and 4αPDD activated conditions. Fluorescence intensity from Cyt C and TRPV4 in all cases is represented in pseudo rainbow colour (red and blue represents highest and lowest intensity respectively).

2.5.2. Cyt C interacts with TRPV4 *in silico*

To analyze the specific interacting residues of TRPV4 involved in Cyt C interaction, we performed *in silico* global and local docking analysis using HADDOCK2.2 Web Server (Van Zundert et al., 2016). We performed global docking using TRPV4 tetramer protein and selected amino acid 470-

670 from chain A as active site (200 being the highest possible active site selection feasible in HADDOCK) and Cyt C monomer protein. HADDOCK webserver returned 118 structures in 16 cluster(s). The best structure from the top cluster was taken which is the most reliable according to HADDOCK, with the lowest Z-score of -1.4. The protein-protein docking had a total of 11 hydrogen bonds formed between amino acid Ser 667-Lys 25, Asp 662-Lys 22, Thr 665-Glu 21, Ser-663-Gly 23, Ser 663-Lys 22, Arg 661-Lys 22, Ala-565-Thr 28, Lys 530-Lys 87, Phe 533-Lys 87, Gly 627-Lys 7 and Ser 630-Lys 7 of TRPV4 and Cyt C respectively along with some other hydrophobic interactions. For simplifying purpose, only two H-bonds images are shown in detail that lie near the TM4-Loop4-TM5 region of TRPV4 using PyMol visualization interface (Figure 51). Another schematic representation of all possible bonds are depicted using LigPlot (Figure 52) (Laskowski & Swindells, 2011).

Subsequently, local docking was performed using TRPV4 monomer and selecting MTS (i.e., fragment 592-630) as the active sites, and docked it with Cyt C monomer protein. HADDOCK webserver returned 73 structures in 11 cluster(s). The best structure from the top cluster was taken which is the most reliable according to HADDOCK, with the lowest Z-score of -1.5. The protein-protein docking had a total of 7 hydrogen bonds formed with amino acid Phe 592, Thr-593, Arg-594, Ser-603, Gln-607, Leu 618, and Tyr 621 of TRPV4 MTS with Met-12, Lys-86, Phe-82, Gly-77, Lys-79, Lys-25, and Lys-22 of Cyt C respectively along with some hydrophobic interactions (Figure 53 & 54).

Next, we performed docking analysis of TRPV4 tetramer with Cyt C dimer. For this purpose, we have taken side-by-side Cyt C monomers and docked them with active site amino acid residues 470-670 of TRPV4 tetramer (Figure 55 & 56).
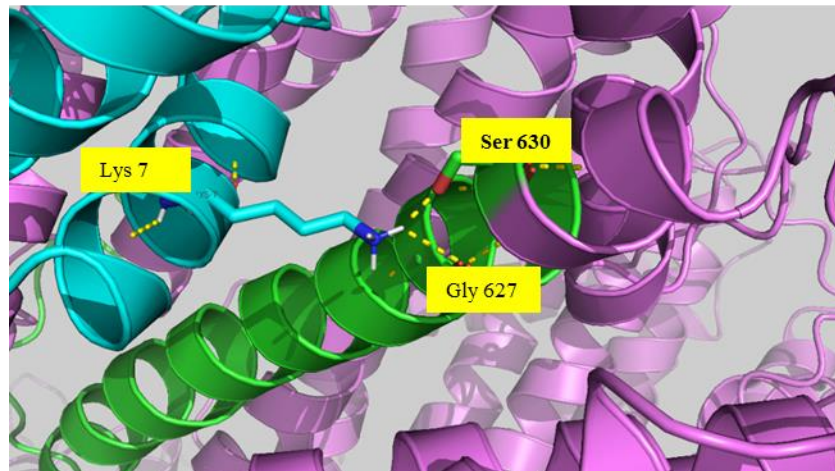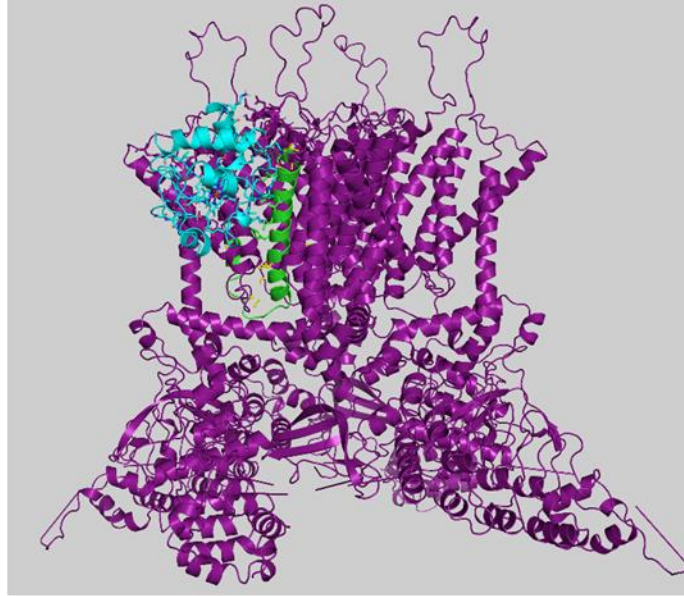
Figure 51: TRPV4 interacts with Cyt C monomer *in silico*. Docking analysis using PyMol illustrates TRPV4 tetramer (purple) interacts with Cyt C monomer (cyan) near the TM5-loop 4-TM5 region (green) of TRPV4 protein. A zoomed image is shown showing H-bonds in yellow dotted lines and residues forming the bonds are highlighted. In this image Lysine 7 from Cyt C forms two hydrogen bonds with Serine 630 and Glycine 627 of TRPV4 protein.

Figure 52: TRPV4 interacts with Cyt C *in silico*. Analysis using LigPlot provides 2D schematic diagrams of protein-protein interactions from the 3D co-ordinate files. Image suggests presence of several H-bonds and hydrophobic interactions between TRPV4 (A: blue) and Cyt C (B: green). Different bonds are depicted in different colour. Green dotted line: H-bond and its length, Red spiked semicircles: Non ligand residues involved in hydrophobic contacts.
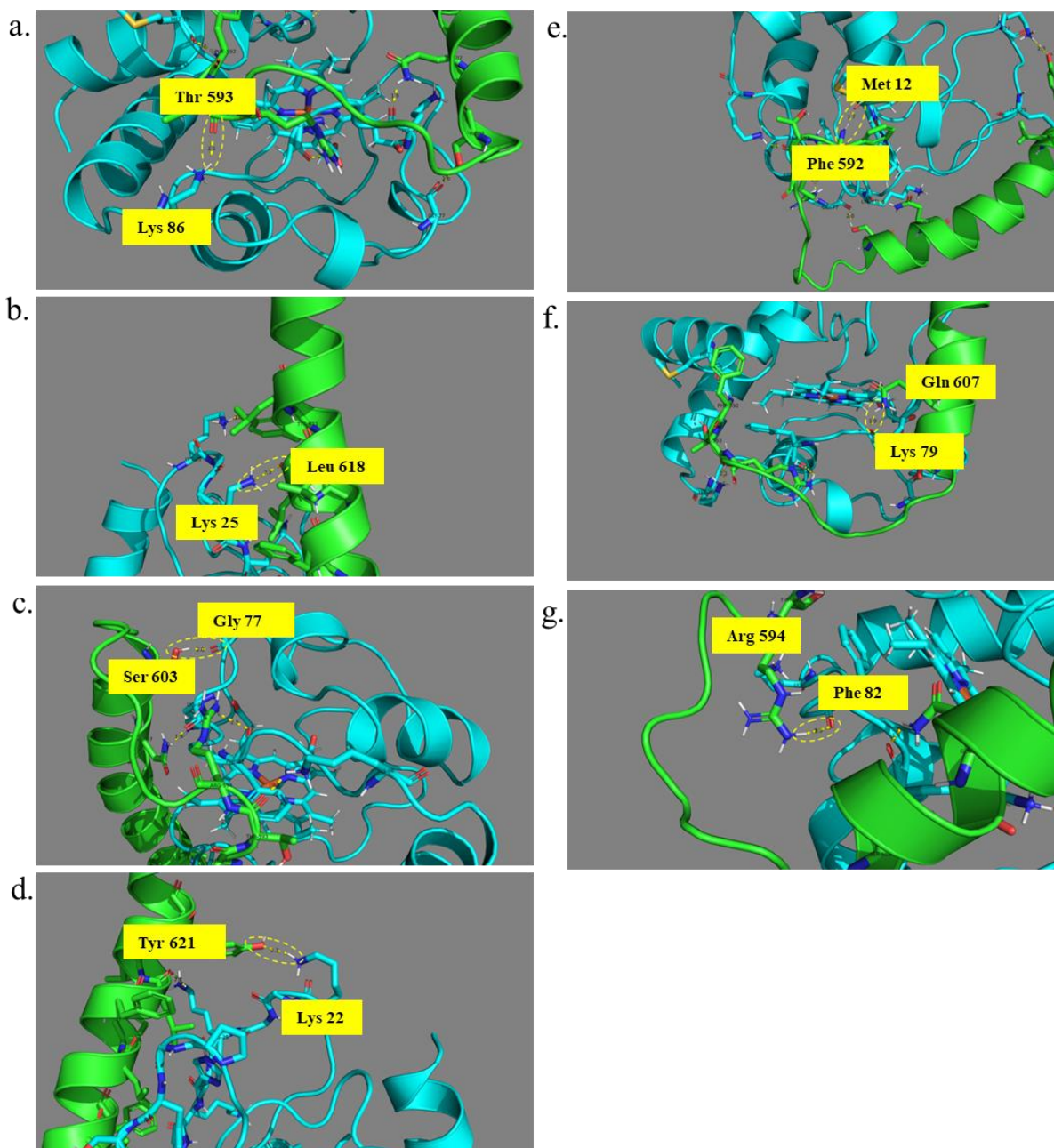
Figure 53: TRPV4 MTS fragment interacts with Cyt C monomer *in silico*. Docking analysis by PyMol suggests presence of several H-bonds (yellow dotted lines) between TRPV4 MTS region (green) and Cyt C monomer (cyan). Total seven H-bonds (Figure **a-g**) were found and the residues forming the bonds are highlighted in yellow.
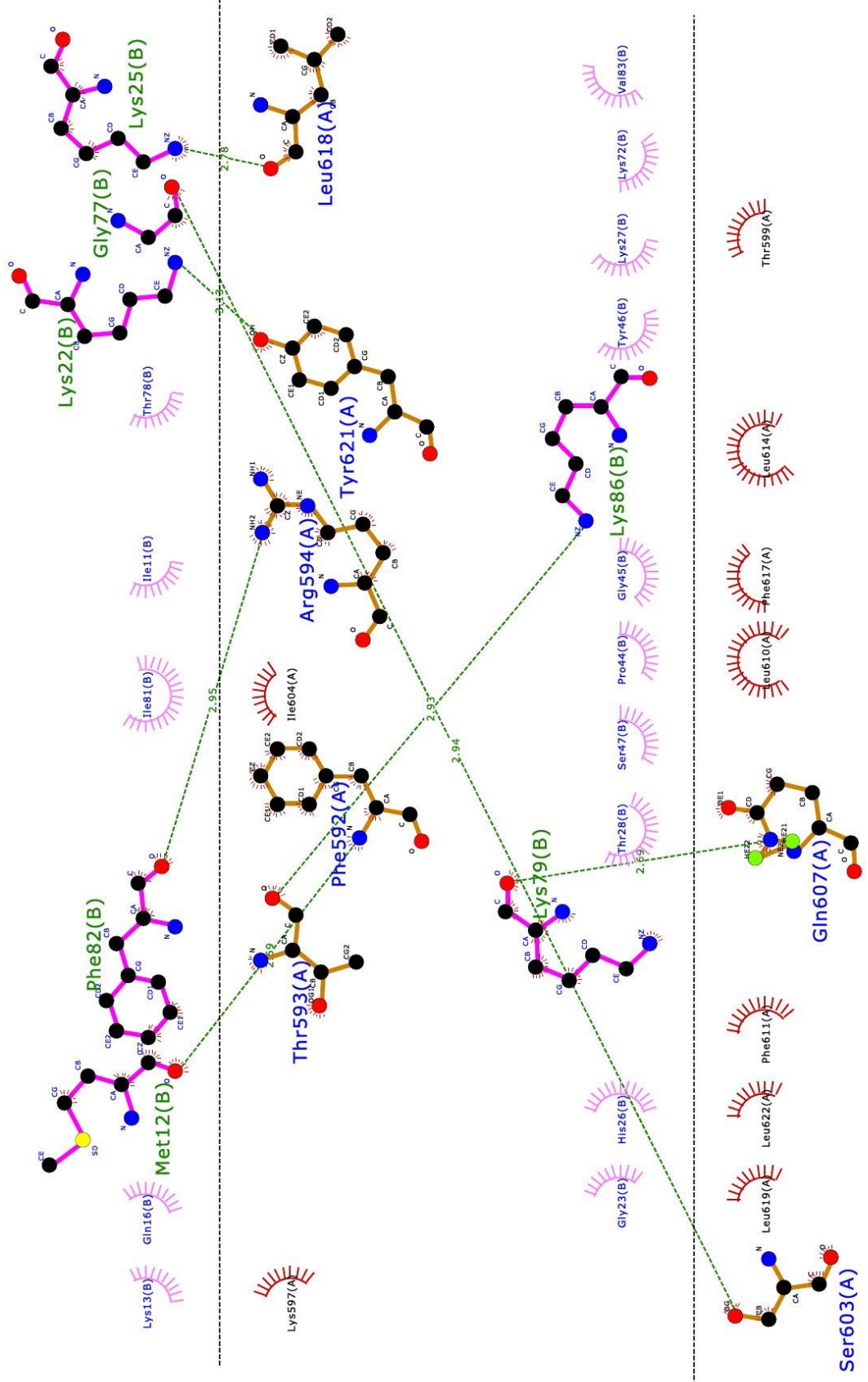
Figure 54: TRPV4 MTS fragment interacts with Cyt C *in silico*. Analysis using LigPlot provides 2D schematic diagrams of protein-protein interactions from the 3D co-ordinate files. Image suggests presence of several H-bonds and hydrophobic interactions between TRPV4 MTS fragment (A: blue) and Cyt C (B: green). The meaning of the colourful bonds on the plot is described in the image. Green dotted line: H-bond and its length, Red spiked semicircles: Non ligand residues involved in hydrophobic contacts.
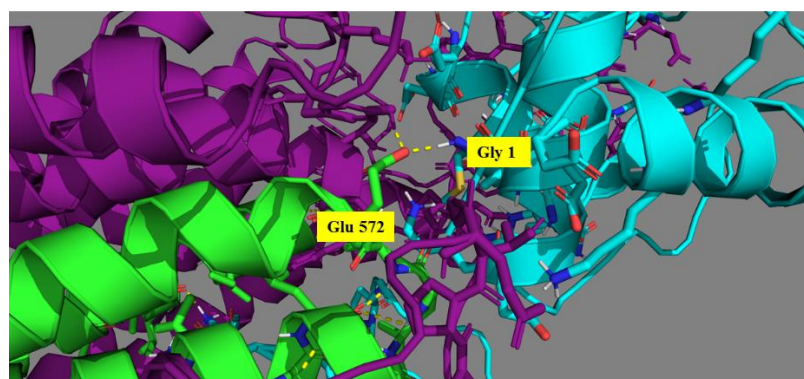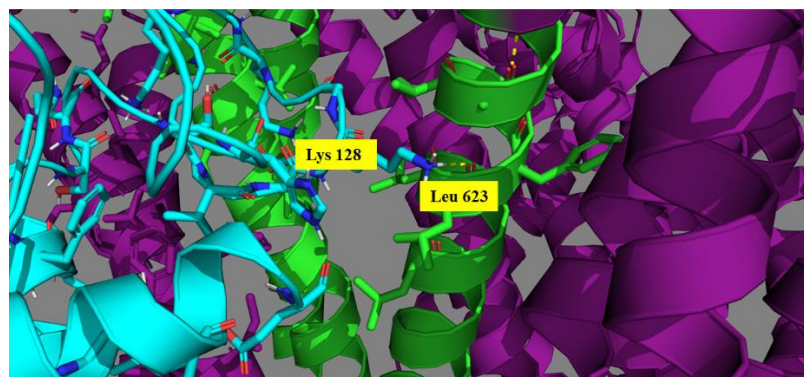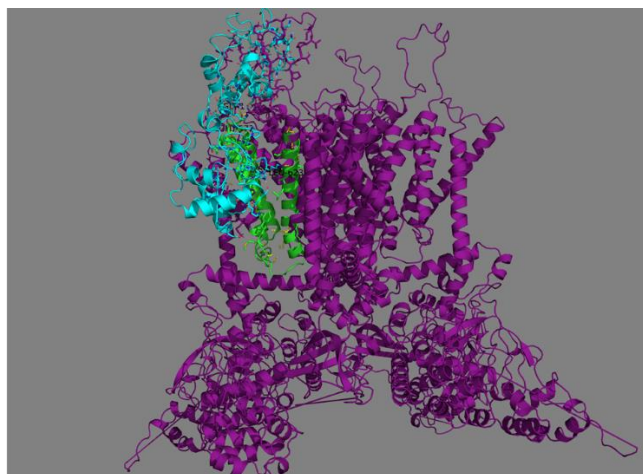
Figure 55: TRPV4 interacts with Cyt C dimer *in silico*. Docking analysis by PyMol suggests presence of several H-bonds (yellow dotted lines) between TRPV4 (green) and Cyt C dimer (cyan). Total 15 H-bonds were found and some selected residues forming the bonds are highlighted in yellow.
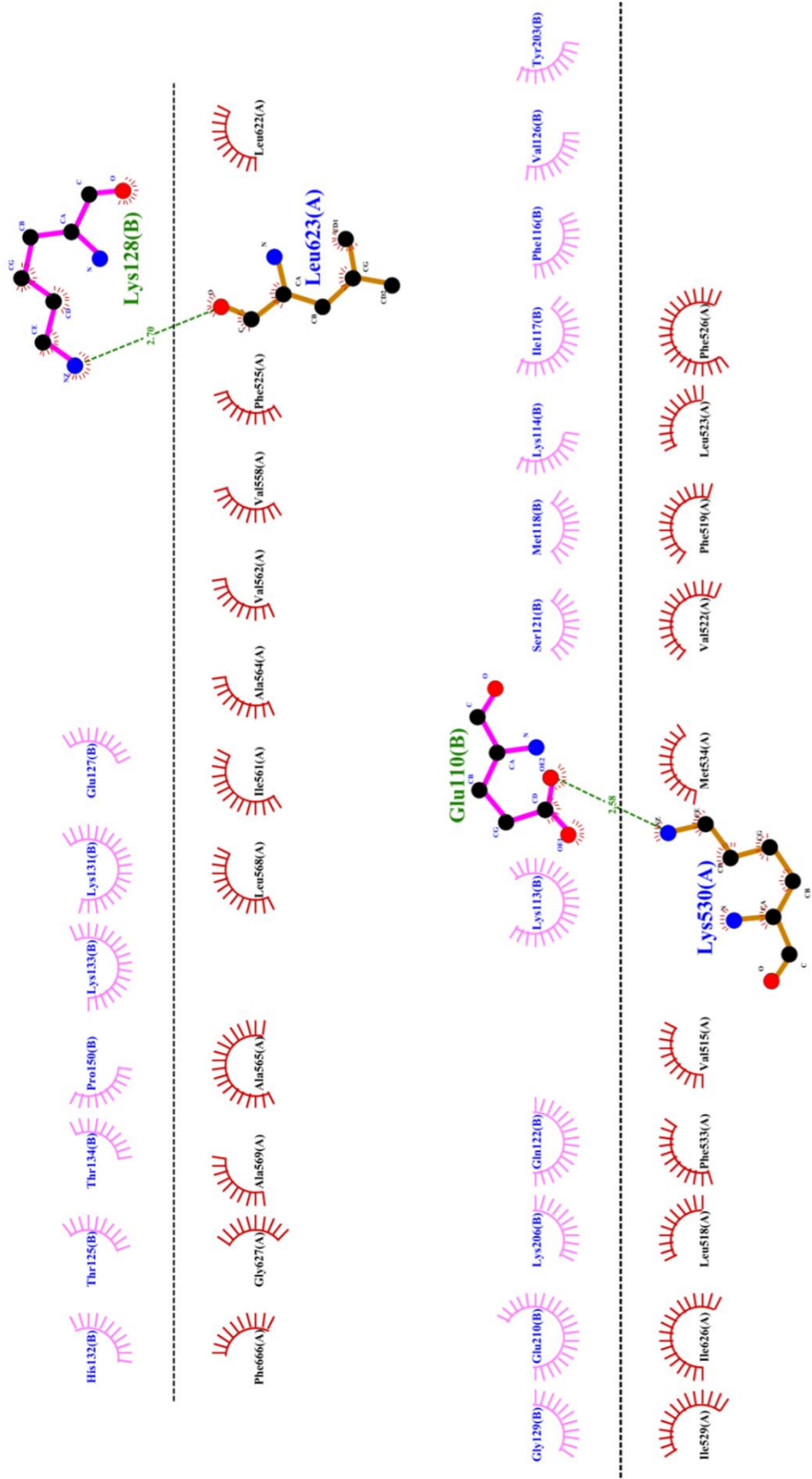
Figure 56: TRPV4 protein interacts with Cyt C dimer *in silico*. Analysis using LigPlot provides 2D schematic diagrams of protein-protein interactions from the 3D co-ordinate files. Image suggests presence of several H-bonds and hydrophobic interactions between TRPV4 tetrameric protein (A and C shown here: blue) and Cyt C (B: green). Green dotted line: H-bond and its length, Red spiked semicircles: Non ligand residues involved in hydrophobic contacts.

2.5.3. TRPV4 and Cyt C interacting sites are conserved throughout the vertebrate evolution

The interacting residues which were derived from *in silico* investigation were further analyzed for their evolutionary history. Protein sequences of Cyt C and TRPV4 were collected from several vertebrate species. The MTS of hTRPV4 was aligned with the full-length TRPV4 sequences from other species using the default parameters of MUSCLE in Mega 5 software. Similarly, the human Cyt C sequence from AA 12-86 was aligned with Cyt C of other species. The alignments were further visualized using JalView. The high similarity of these sequence suggests that these regions are highly conserved in vertebrates. The amino acids crucial for interaction are rarely substituted by any other residues suggesting their important role throughout vertebrate evolution (Figure 57 & 58).
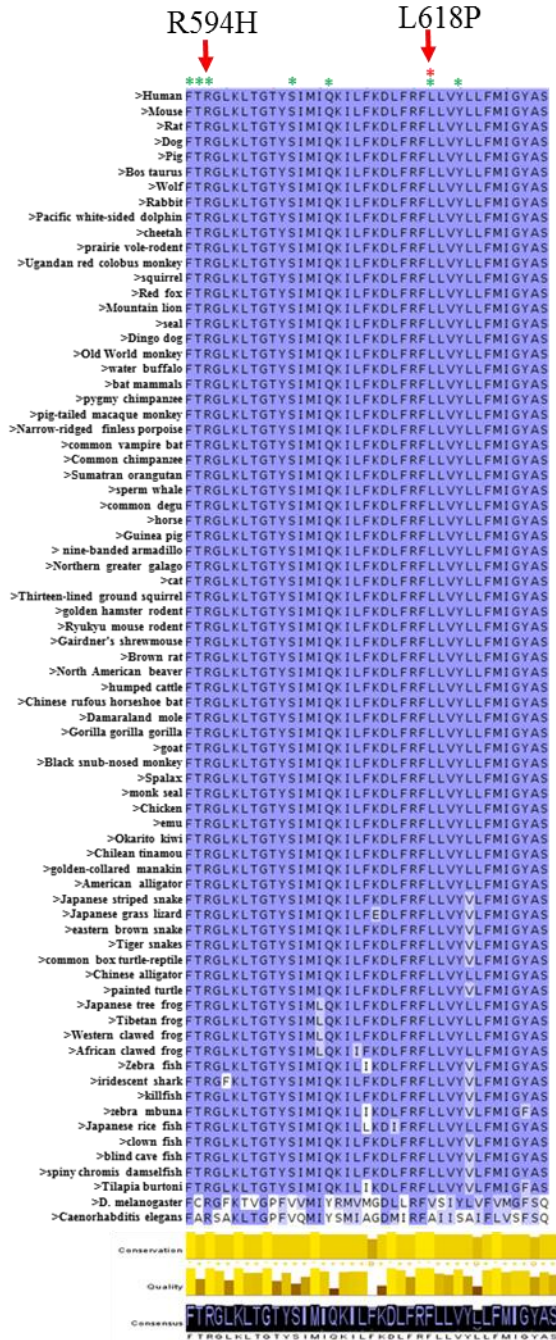
Figure 57: Conservation of Cyt C interacting residues of TRPV4. Conservation analysis of TRPV4-MTS amino acid sequence 592-630 is shown. The amino acids present in this region are mostly conserved in all vertebrates. The crucial amino acids that interact with Cyt C are indicated with green asterisk (*). Two human mutations occurring positions R594 & L618 are marked in red arrow.
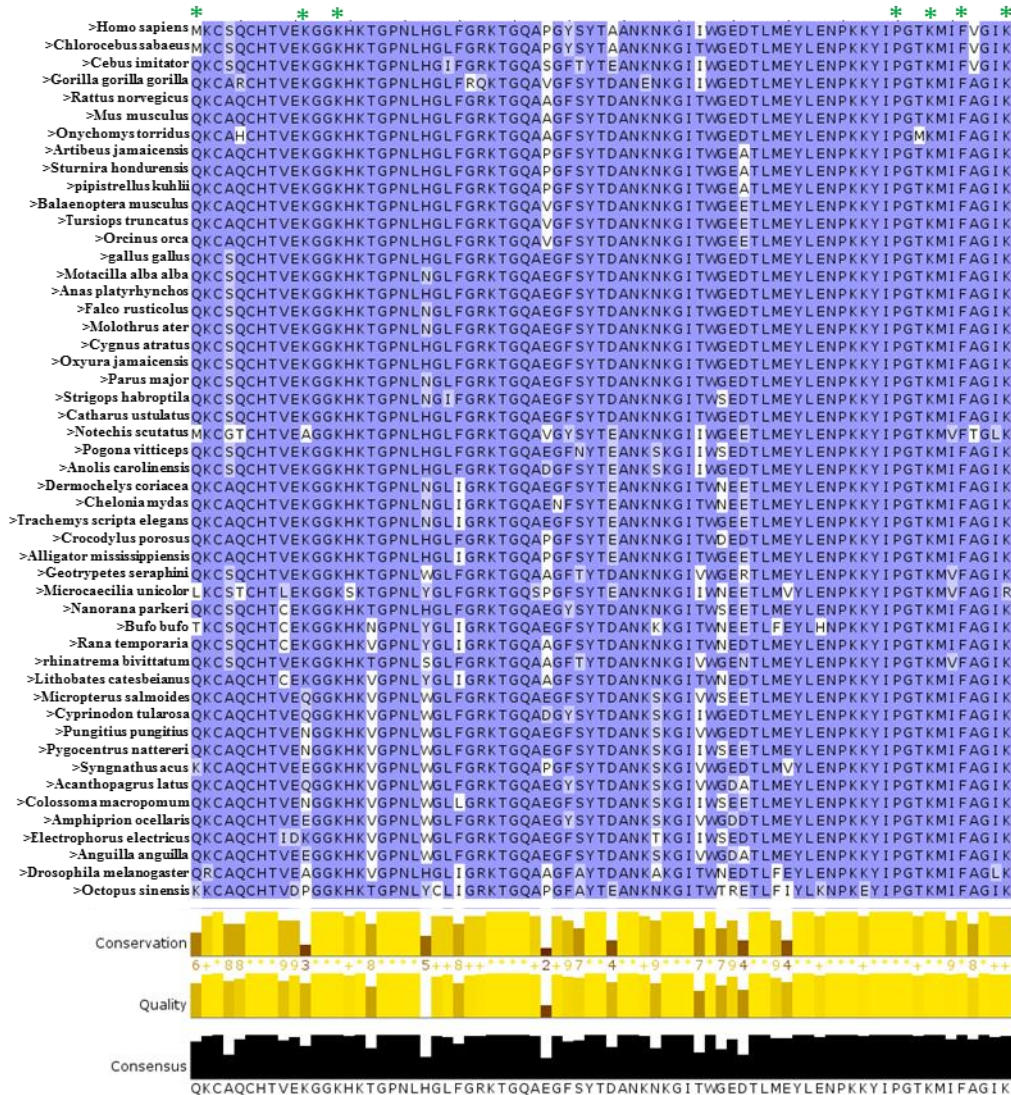
Figure 58: Conservation of TRPV4 interacting residues of Cyt C. Conservation analysis of Cyt C sequence from amino acid 12-86 is shown. The amino acids present in this region are mostly conserved in all vertebrates. The crucial amino acids that interact with TRPV4 are indicated with green asterisk (*).

2.5.4. Cyt C interacts with the MTS region of TRPV4

Bioinformatic prediction results suggest that amino acid 592-630 of TRPV4 has the maximum likelihood for mitochondrial localization. This is as per the comparative score obtained in contrast to the other fragments of TRPV4. To confirm that the predicted sequence can indeed interact with mitochondria, we cloned these 39 amino acids long sequence (AA number 592-630)

into pGEX6P1 vector [named as MTS-GST-TRPV4]. The protein was expressed, purified and then pull-down experiments with Cyt C (purified protein) ware performed. Only GST protein was also over expressed and used as a negative control. The samples were analyzed by Western Blotting after being probed with Cyt C antibody. The antibody detects a monomeric band at 14 kDa and often a dimeric band at ~35 kDa, only in the sample that was pulled down using MTS, but not in the pulldown sample that used only GST (Figure 59). This suggests direct interaction of Cyt C with TRPV4-MTS region.
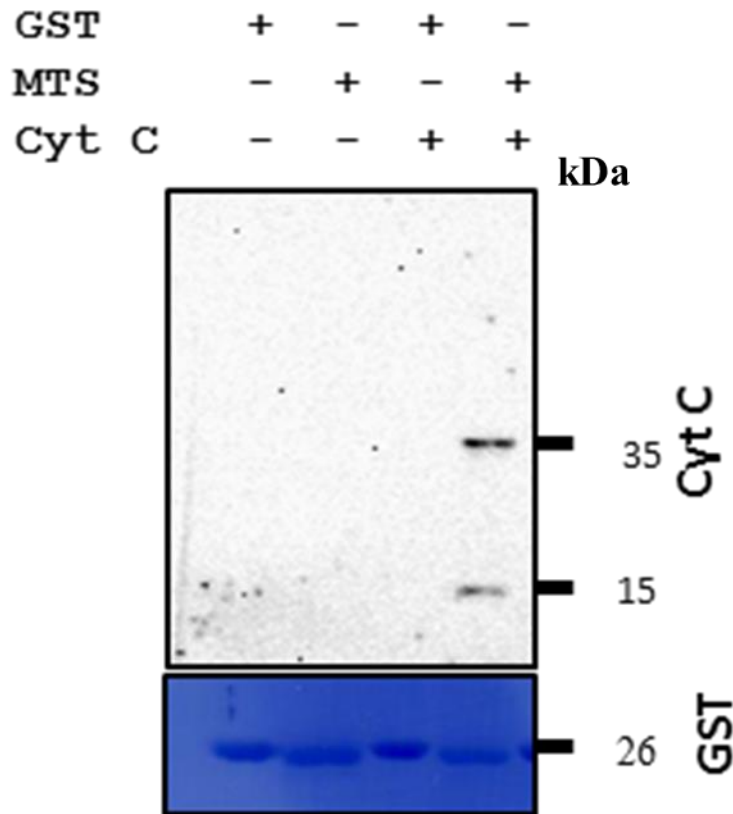
Figure 59: Cyt C interacts biochemically with TRPV4 MTS fragment. Image depicts the result from (Cyt C) pulldown experiment using GST-TRPV4-MTS fragment or only GST. Only GST is used as negative control. All the samples were probed for western blot analysis using anti- Cyt C antibody. A monomeric Cyt C band is observed at 15 kDa and another dimeric Cyt C band is observed near 35 kDa. Corresponding loading control is shown by Coomassie Brilliant Blue-stained (CBB) gel.

2.5.5. Metal-dependent interaction of Cyt C with TRPV4

TRPV4-MTS pull down results with Cyt C suggest that they interact in control conditions, i.e., even in absence of any added metals. Further experiments were done in presence of different divalent metals like Cu^{2+}, Zn^{2+}, Mn^{2+}, Ni^{2+} and trivalent ion like Fe^{3+}. Results indicate that Cyt C interacts with MTS differently in those metal conditions. Such type of interactions was not observed with GST protein (used as negative control). This result implies that Cyt C interaction with TRPV4-MTS is very specific and this interaction is sensitive to the presence of different metals (Figure 60).

2.5.6. Differential interaction of TRPV4-Wt-MTS and different mutants with Cyt C

As the MTS region of TRPV4 is a hotspot to many naturally occurring mutations, we explored if the interaction pattern of Cyt C with TRPV4 MTS with Wt or mutant sequences are different. It is to note that, on pulldown with Cyt C, not only a single Cyt C (monomeric) band but also oligomeric Cyt C bands were visible. Concluding a noteworthy stoichiometric interaction of TRPV4 with Cyt C. Both in the presence and absence of Ca^{2+}, the MTS-GST fragment does not show any significant changes in the interaction pattern with Cyt C, both in monomeric and oligomeric forms. While some mutations like R616Q-MTS and F617L-MTS show drastic changes in Ca^{2+}-bound and unbound state interaction with Cyt C, some other mutations like L618P-MTS and V620I-MTS seems to be less affected by Ca^{2+} and also bind less intensely with Cyt C (Figure 61). Along with biochemical evidences, immunofluorescence studies done by transfecting SaOS cells with TRPV4-Wt and mutants and staining them with anti-Cyt C antibody also suggests differential expression pattern of the wild type TRPV4 and its mutants with Cyt C (Figure 62).
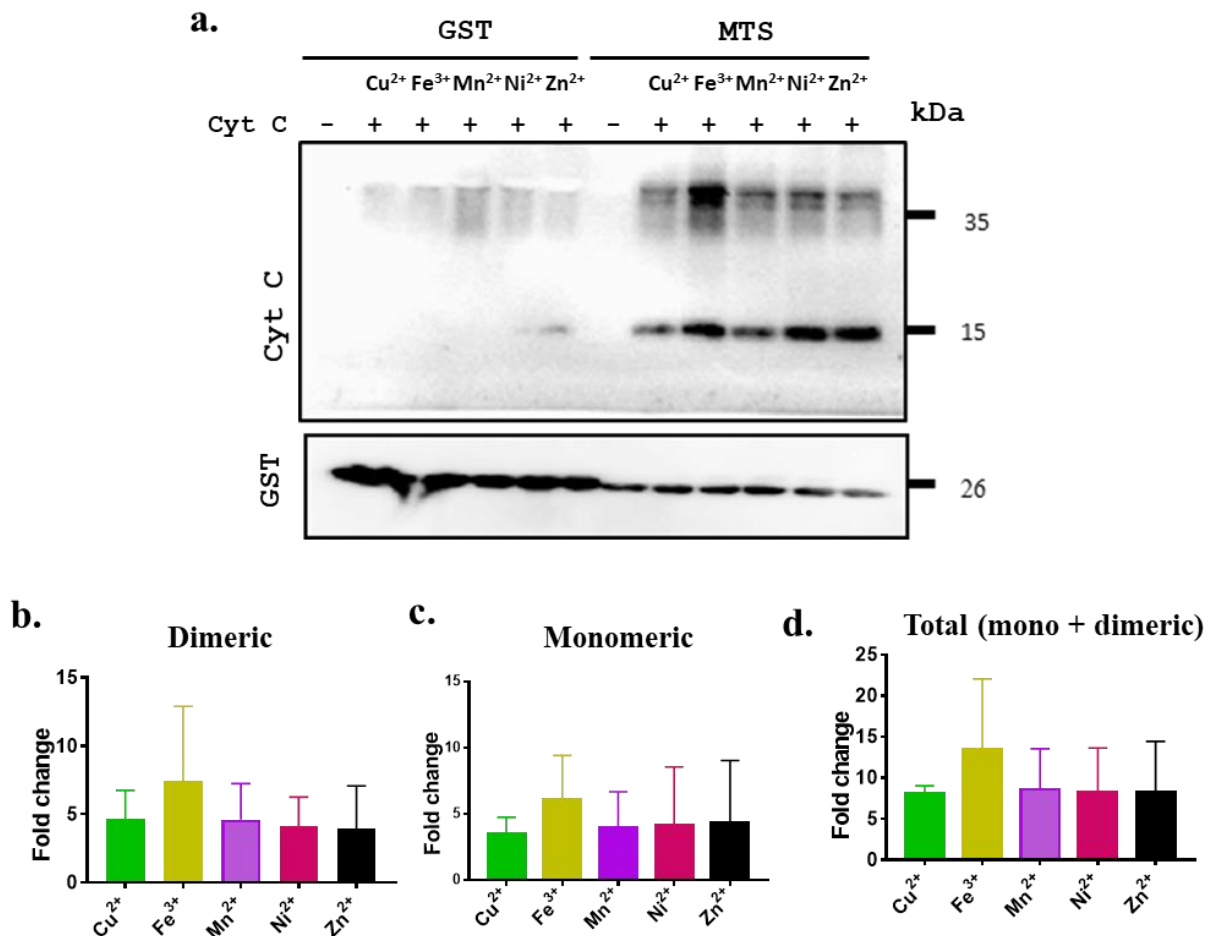
Figure 60: TRPV4-MTS interacts with Cyt C differently in presence of different metals. Pull down experiment was performed with purified Cyt C. GST-TRPV4-MTS or GST-only was expressed and subsequently purified Cyt C was added for binding with GST-TRPV4-MTS or with GST-only in presence of Cu^{2+}, Fe^{3+}, Mn^{2+}, Ni^{2+} or Zn^{2+} independently. Western blot was performed with Cyt C -specific antibody. Results indicate that GST-TRPV4-MTS but not GST-only interacts with Cyt C and differential interaction pattern is observed for different metals used. Only GST is used as negative control and the quantitative data was derived taking the value of GST only as 1. A band specific for monomeric Cyt C is observed at 15kDa and another band specific for dimeric Cyt C band is observed near 35kDa (**a**). Quantification of monomeric (**b**), dimeric (**c**) and their ratio (**d**) suggests that TRPV4 and Cyt C is sensitive to the presence of different metal ions. Equal amounts in loading are demonstrated by Western Blot analysis with GST antibody.
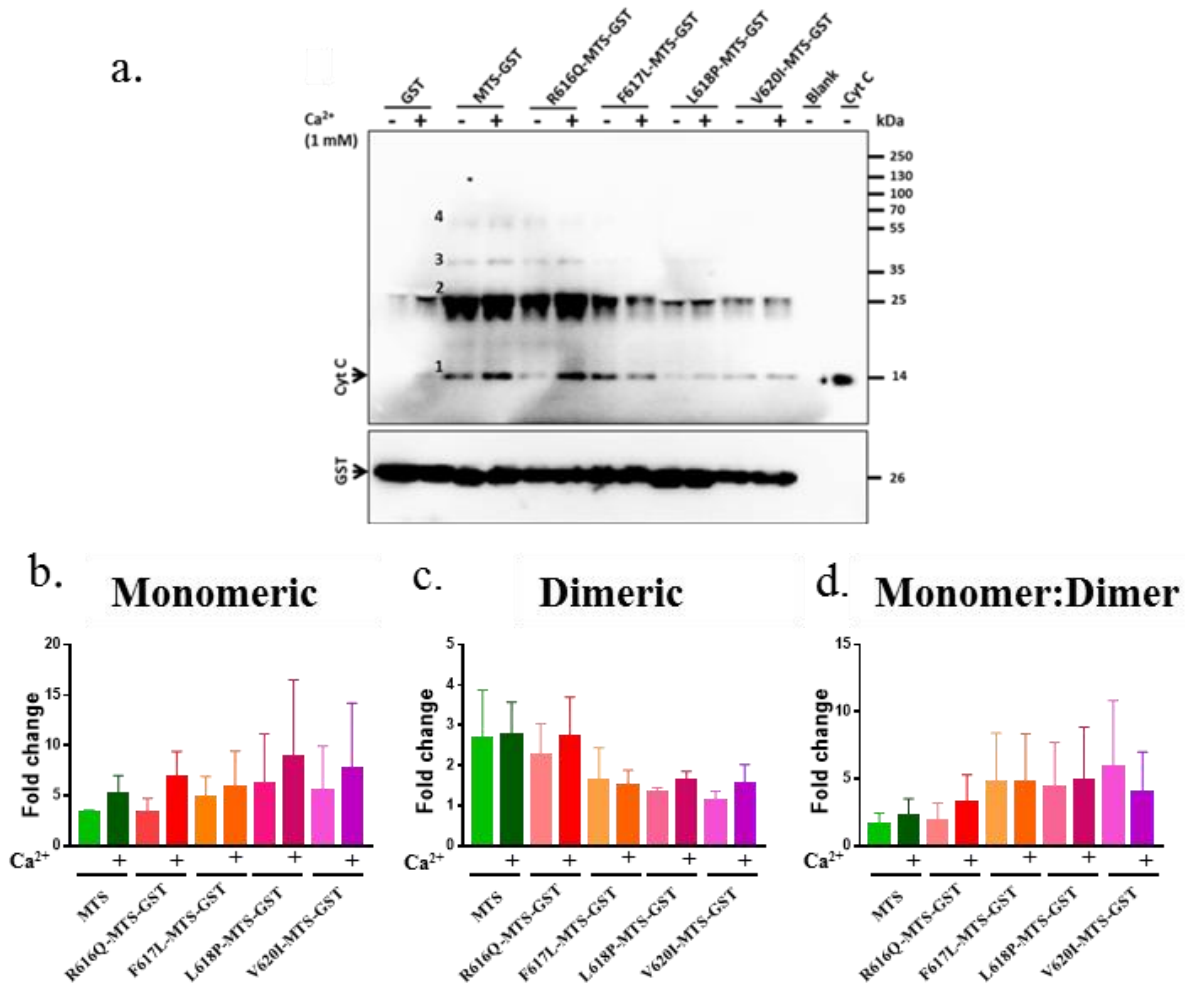
Figure 61: TRPV4 MTS mutants interacts directly with Cyt C in presence and absence of Ca^{2+}. Purified GST-TRPV4-MTS, GST-TRPV4-R616Q-MTS, GST-TRPV4-F617L-MTS, GST-TRPV4-L618P-MTS, GST-TRPV4-V620I-MTS and GST-only were incubated separately on glutathione sepharose beads alone or in presence of Ca^{2+}. Purified Cyt C was added and incubated. Western blot analysis using anti- Cyt C antibody identified bands at monomeric fraction as well as dimeric, trimeric and tetrameric fraction (**a**) (shown as 1, 2, 3 & 4). Quantification of monomeric (**b**), dimeric (**c**), and monomeric: dimeric (**d**) band intensity of Cyt C suggests differential interaction pattern of TRPV4 and its mutants with Cyt C. Equal amounts in loading is demonstrated by western blot staining by GST antibody.

	GFP+Cyt C+ DAPI	GFP+Cyt C	GFP	Cyt C	Intensity (Cyt C)
pEGFPN3	20μm	10μm	10μm	10μm	10μm
V4 Wt	20μm	10μm	10μm	10μm	10μm
R616Q	20μm	10μm	10μm	10μm	10μm
F617L	20μm	10μm	10μm	10μm	10μm
L618P	20μm	10μm	10μm	10μm	10μm
V620I	20μm	10μm	10μm	10μm	10μm
MTS	20μm	10μm	10μm	10μm	10μm

130
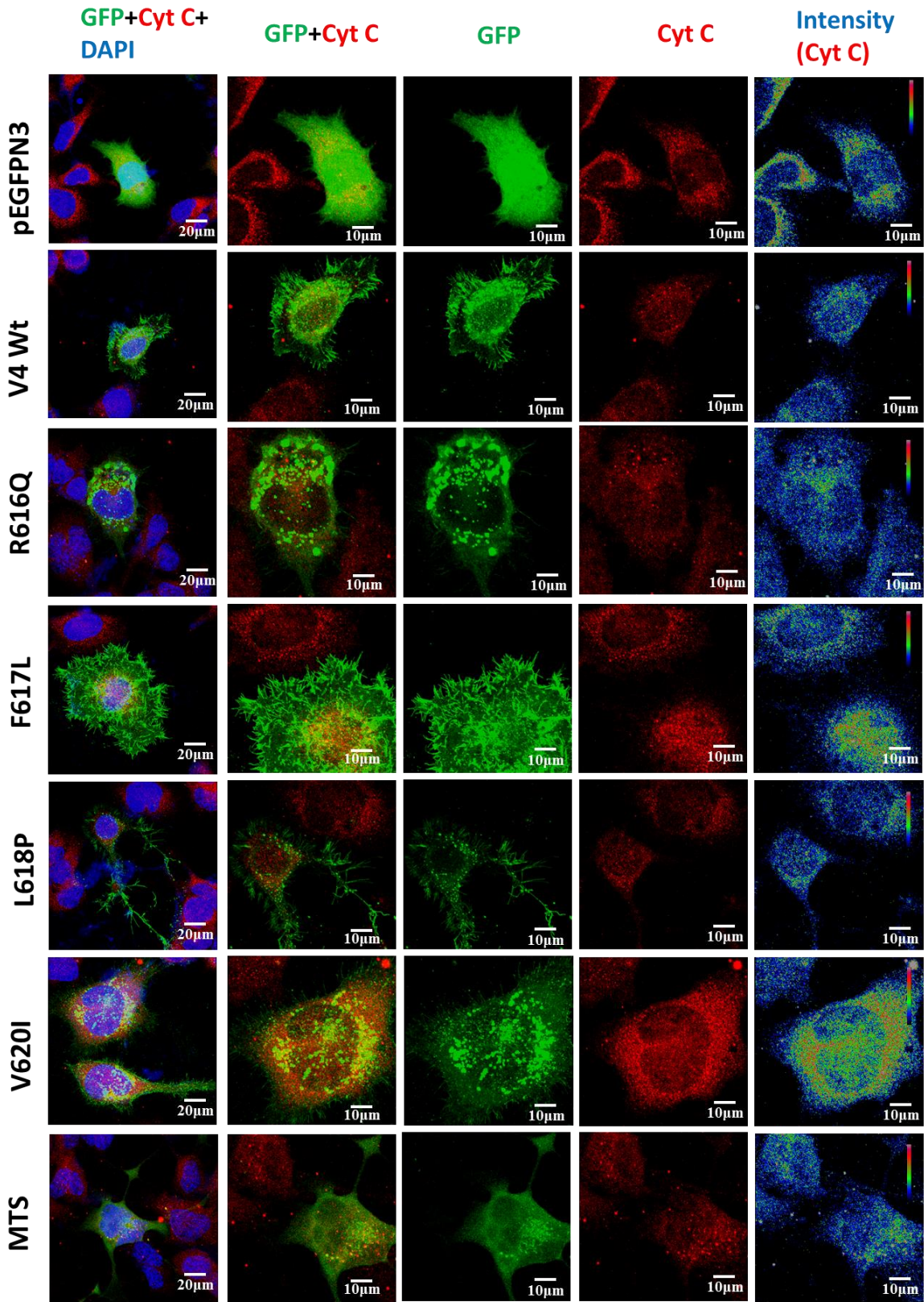
Figure 62: Cells expressing TRPV4 mutants have different levels and staining pattern of Cyt C. Shown are the confocal images of Saos-2 cells expressing TRPV4-Wt-GFP, TRPV4-R616Q-GFP, TRPV4-F617L-GFP, TRPV4-L618P-GFP, TRPV4-V620I-GFP, TRPV4-MTS-GFP or pEGFPN3-only (green). 36 hours post transfection, the cells were fixed and later stained with anti-Cyt C antibody (red). Nucleus is stained with DAPI (blue). Fluorescence intensity from Cyt C in all cases is represented in pseudo rainbow colour (red and blue represents highest and lowest intensity respectively).

2.5.7. Cyt C status in MSC alters due to TRPV4 modulation

The release of the heme protein Cyt C from mitochondria to the cytosol is a key event in initiation of apoptosis. In the cytosol, it binds to Apaf-1, which then activates caspase-9 that, in turn, activates caspase-3 (Di Matola et al., 2000; Hanske et al., 2012). We examined whether TRPV4 modulating drugs alter the expression of Cyt C. For this purpose, Mesenchymal Stem Cells (MSC) were grown on coverslips and different concentrations of drugs were applied. The cells were fixed after 24 hours by 4% PFA. The presence of Cyt C in the cytosol was detected by immunofluorescence analysis using an anti-Cyt C monoclonal antibody. Cyt C was detected at varying levels in the cytosol after 24 h of treatment with TRPV4 modulatory drugs (Figure 63).
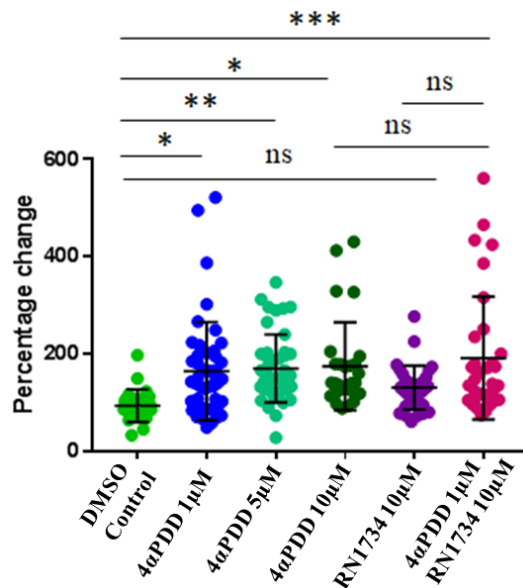
Figure 63: TRPV4 modulation affect Cyt C level in the total cell. Quantitative analysis of Cytosolic Cyt C level in the whole cell was analyzed by measuring the fluorescence intensity of Cyt C levels in the total cell. Notably in 1μM 4αPDD and 1μM 4αPDD + 10μM RN1734 concentration, higher levels of Cyt C were detected.

Chapter 3

Discussion

3.1. Molecular evolution of TRPV4

3.1.1. Factors that might have played a role in molecular evolution and importance of systematic sequence analysis

It is notable that the main essence of evolution in any population are mutation in genetic material, reshuffling of genes through sexual reproduction, natural selection, and gene flow (Saeb & Al-Naqeb, 2016). In addition to the above factors, few additional forces play various roles that are needed for the evolutionary precision to occur. Such as,

* epistasis and post-translational modifications, which are required for long term protein evolution.

* specific proteins, that are linked to the thermal tolerance of organisms and sex determination.

* for membrane and transmembrane proteins, lipid-mediated regulation drives the function/s of these proteins for perfection.

In the later context, cholesterol plays an important role. It's role is also significant in membrane sub compartmentalization and handling membrane oxidation which is essential for eukaryotic existence and hence in evolution (Breen et al., 2012; Brown & Galea, 2010).

Cholesterol synthesis is believed to coincide with the rise in oxygen levels during evolution. The evolution of oxygenic photosynthesis occurred ~2.45 billion years ago which significantly affected life on the planet. Although the proof for the presence of sterols in the geological record is a subject of thorough debate, molecular fossils of sterols (steranes) have been reported in shales that are 2.7 billion years of old, that is, originating before the Great Oxidation Event (~2.45–2.3 billion years ago) (Brown & Galea, 2010). As cholesterol synthesis is an incredibly oxygen-concentrated cycle, with 11 atoms of oxygen being expected to make one molecule of cholesterol, consequently, cholesterol could have only evolved as atmospheric oxygen levels rose. This is also evident from the example of lungfish, an earliest air breather, that have

cholesterol in their lung sulfactant. First biochemical synthesis of cholesterol might have overcome a bottleneck in evolution, permitting the formation of multicellular life forms because of cholesterol's role in processes required for correspondence between cells like endocytosis and exocytosis (Brown & Galea, 2010).

Proteins like TRP's were also evolved during early eukaryotic evolution. Considering how old these TRP family proteins are, investigation of TRP channels likewise stands to uncover much information regarding their role in evolution. TRP channels themselves and perhaps their sensory capacity pre-date the nervous system, which is so frequently credited as the basis for behavior. It is therefore conceivable that TRP channels might be considered among the "almost essential" and vital components which facilitated the evolution of complex behaviors and physiology; the components which made the nervous system, and other complex signaling mechanisms (Himmel & Cox, 2020). A recent study based on tuatara (*Sphenodon punctatus*, that diverged from snakes and lizards around 250 million years ago and is the only living member of the reptilian order Rhynchocephalia) has identified 7 known subfamilies of TRP genes suggesting role of TRP genes in thermal tolerance of the tuatara. It appears to be plausible that the genomic changes in TRP qualities are related with the evolution of thermoregulation in tuatara (Gemmell et al., 2020).

The improved innovations in DNA sequencing are quickly extending our insight into the genomes and proteomes of surviving species. These DNA and protein sequences provide detailed information about molecular evolution. These molecular evolution data can reveal insight into the relationship between protein sequence and function. Patterns of protein sequence conservation and divergence analyzed in several species can be utilized to propose amino acids that are significant for protein function. Amino acids that are conserved in related proteins in spite of adequate opportunity to diverge during evolution are most-likely remain critical for the protein function/s.

135

Different additional profiles might emerge from conservation of positive or negative charge, hydrophobicity, hydrophilicity or various other physico-chemical properties of amino acids (Thomas et al., 2006).

3.1.2. Importance of cholesterol as a regulator of channel function

TRPs operate in lipid membranes rich in cholesterol, and thus affecting the functions of a number of TRPs. Although no crystallographic or cryogenic electron microscopy (cryo-EM) constructions of TRPs show bound cholesterol, some TRP channels like TRPC4. TRPC5, TRPM2, TRPM4 show bound cholesterol hemisuccinate (CHS) molecules that are used for stabilizing membrane proteins. As CHS is a water-soluble derivative of cholesterol and have similar effects on the physical properties of lipid bilayers and on membrane protein function, their binding sites can therefore be considered as the regions where cholesterol could bind. Cryo-EM structure of TRPV2 and TRPV3 show density in certain pockets, which is suggested could be due to cholesterol (Zubcevic et al., 2016; Dang et al., 2019). Several TRP channels are found to be sensitive to cholesterol content of the plasma membrane like TRPM3, TRPM7, TRPM8, TRPV1, TRPV4 and TRPV3 (Levitan et al., 2014; Picazo-Juárez et al., 2011; Morales-Lázaro & Rosenbaum, 2017). The observed effects of cholesterol on TRP channel could follow from changes in the mechanical properties of the lipid bilayer and/or because of direct binding of cholesterol to the channel protein (Lee, AG., 2019; Kumari et al., 2015).

So far, involvement of TRPV4 in different physiological functions have been reported in great details. Accordingly, abnormality in the TRPV4 expression or function have been linked with the development of different pathophysiologies, commonly termed as channelopathies. Notably, most of these channelopathies are due to the different point mutations in TRPV4 and are

unique in nature. In human population also, TRPV4 has large spectrum of missense variations and other types of variations (Ghosh et al., 2016). While TRPV4 knock-out animals are viable and without much significant differences in most of the critical physiological functions, TRPV4 mutants have a wide-spectrum of physiological disorders. Such disorders range from embryonic lethality to more tolerable and heritable genetic disorders (Nilius & Voets, 2013). Such wide-spectrum phenotypes and large number of variations may suggest that TRPV4 has multiple modes of regulations and functions. TRPV4 gene mutations have been reported to cause more than 60 different types of heritable diseases in human among which mild to fatal forms of skeletal dysplasia are of significant importance (Bonafe et al., 2015). Interestingly, many of these reported cases of malformation syndromes are also caused by disorders of cholesterol synthesis, such as certain forms of skeletal dysplasia (Porter & Herman, 2010).

Physical interaction of TM4-Loop4-TM5 and Loop4 fragment with cholesterol and dependence of mobility of TRPV4-GFP on membrane cholesterol level further suggests strong influence of cholesterol on TRPV4 function (Kumari et al., 2015). Studies by Lakk et al in 2021 also describes TRPV4 function regulation by membrane cholesterol where they have established that the physiological levels of mechanical strain regulate the phospholipid/cholesterol ratio in human trabecular meshwork membrane via TRPV4 activation. Membrane cholesterol also negatively regulates TRPV4 activation by agonists and mechanical stimuli like swelling and stretch (Lakk et al., 2021). Such correlation strongly suggests that cholesterol may indeed act as regulator of TRPV4 at the molecular levels.

3.1.3. Lipid water interface and the specific micro environment at the LWI

The "Lipid Water Interface", i.e., ~15 Å thickness layer present at either side of the membrane which is composed of lipid head groups and water molecules is an important site for protein. This is mainly due to the fact that transmembrane regions are stably inserted in a bilayer, which requires a favourable interactions between the interfacial protein segments with membrane as a prime prerequisite (Domene et al., 2003; Wimley & White, 1996). The hydrophobic core of the surrounding lipid bilayer matches with the hydrophobic, transmembrane domain of a membrane protein. Mismatching in hydrophobicity between lipid and protein may lead to distortion of the lipid bilayer microdomain or distortion of the protein conformation, or distortion of both (Lee, AG., 2003). Frequency and conservation analysis of amino acids present in lipid-water interface regions shed light upon their physico-chemical behaviour at membrane microenvironment. Such analysis opens up the importance of maintenance of hydrophobic/hydrophilic and acidic/basic ratio in the LWI as well.

3.1.4. Behavior of TRPV4 amino acids at LWI

This work unravels that there is a specific signature of amino acids that are evident in the lipid-water interface of TRPV4. During the vertebrate evolution, there are certain amino acids that have been completely excluded from the LWI regions. In the same context, there are residues that are either positively selected or negatively selected or remain at a constant frequency.

The frequency of positively selected amino acids increased steadily, for example, Glu in the outer LWI and Gly in the inner LWI finally stabilized at higher frequencies in higher vertebrates while frequency of negatively selected amino acids decreased gradually during the course of evolution for example, Asp in outer LWI, Ala in inner LWI, Ser in total and outer LWI.

138

Certain amino acids are excluded in a certain region/s of TRPV4 throughout the vertebrate evolution and indicate their minimum importance and/or misfit in such microenvironments for example, Trp in all of the LWI's, Asn, His, Thr and Tyr in inner LWI's, Phe in outer LWI. There is a subgroup of amino acids whose frequency of occurrence remains constant throughout the vertebrate evolution. For example, Cys and Tyr residues in the outer LWI region, Asp, Gln, Lys, Pro, Arg, Met, Cys residues in the inner LWI region. Lys, Cys, Tyr residues in total LWI regions. No change, for example neither increase nor decline in frequency of these amino acids were endured in the LWI regions of TRPV4 during vertebrate advancement. All in all, such amino acids are illustration of critical amino acids present in LWI areas and are fundamental for TRPV4 functions. In some cases, these frequencies are also comparable to frequency of amino acids present in all proteins as standard natural frequency.

3.1.5. Importance of maintenance of ratio of positive-negative and hydrophobic-hydrophilic amino acids at the LWI of TRPV4

Most notably, the total frequency of positively charged residues and negatively charged residues and their respective ratio in the LWI regions remain constant, especially in the inner LWI region throughout the vertebrate evolution. Our observation fits well with the "positive inside" as well as "negative inside depletion/outside enrichment" theories proposed before (Baker et al., 2017; VonHeijne, 1989).

Similarly, the total frequency of hydrophobic as well as hydrophilic residues and their respective ratio in the LWI regions remain constant, especially in the inner LWI regions throughout the vertebrate evolution. Interestingly, our data suggest that the frequency of total hydrophobic or hydrophilic residues correlate well with the absolute hydrophobicity or hydrophilicity throughout

the vertebrate evolution. Notably, these hydrophobic and hydrophilic residues are not changed significantly during the transition of cold-blooded animals to warm-blooded animals, suggesting that the total frequency of hydrophobic and hydrophilic residues in the LWI region as well as their ratio may not be involved in the regulation of thermo-gating as such. In contrast, the changes in the total positive and negative residues might play important role in the regulation of the thermo-gating. This analysis points a "specific pattern" that remain conserved in the LWI regions of TRPV4 during vertebrate evolution. As this pattern remains conserved throughout the vertebrate evolution suggesting that the pattern is fundamentally involved in the TRPV4 channel function and its fine regulation by temperature and membrane microenvironments. Accordingly, different point-mutations located in the LWI regions may or may not alter this specific pattern and therefore may cause changes in the cell behaviour leading to certain pathophysiologies. Notably, we have reported a similar presence of "specific pattern of amino acids" in the LWI region of TRPV1 (Saha et al., 2020).

3.2. TRPV4 as a hot candidate for multiple channelopathies with different penetration

3.2.1. Mutations as a means of species adaptability during evolution

Various reports suggested that during vertebrate evolution, certain mutations in TRP channels have provided better adaptation ability to those species, especially in harsh environmental conditions, such as resistance from specific toxins, acidic conditions, or insensitivity towards specific stimulus. These mutations, (though act as loss-of-function mutants) have therefore helped the species to survive and have supported reproduction in extreme conditions. Diseases occurring due to mutation in ion channels causing channel dysfunction are termed as "Channelopathy". Out of approx. 300 ion channels predicted in human genome so far, only few are associated with human diseases and TRP's are among the selected few (Nilius B., 2007). Again, not all mutations in TRP channels found in nature give rise to channelopathies, very few mutations can cause diseases in human. The penetration of those diseases is also variable, simpler diseases like skin irritation to serious diseases like prenatal death occur due to different mutations (Table 8).

Table 8

Channel	Functional effect	Disease
TRPC6	Gain-of-function	Focal Segmental Glomerulosclerosis
TRPV3	Gain-of-function	Olmsted Syndrome (skin disorder)
TRPV4	Gain-of-function	Brachyolmia type 3
TRPV4	Gain-of-function	Spondylometaphyseal dysplasia, metatropic dysplasia
TRPV4	Gain-of-function	Congenital distal spinal muscular atrophy
TRPV4	Gain-of-function	Scapuloperoneal hereditary motor neuropathy
TRPV4	Loss-of-function	Hyponatremia
TRPV5	Loss-of-function	Kidney stones
TRPV6	Loss-of-function	Transient neonatal hyperparathyroidism (TNHP)
TRPV6	Loss-of-function	Early-Onset Chronic Pancreatitis

TRPV6	Gain-of-function	Kidney stones
TRPM1	Loss-of-function	Congenital Stationary Night Blindness
TRPM2	Loss-of-function	Western Pacific Amyotrophic Lateral Sclerosis (ALS) and Parkinsonism Dementia (PD)
TRPM3	Gain-of-function	Intellectual disability and epilepsy
TRPM4	Gain-of-function	Progressive familial heart block type I (PFHBI)
TRPM4	Gain-of-function	Progressive Symmetric Erythrokeratodermia
TRPM6	Loss-of-function	Hypomagnesemia with secondary hypocalcemia
TRPM7	Loss-of-function	Western Pacific Amyotrophic Lateral Sclerosis (ALS) and Parkinsonism Dementia (PD)
TRPA1	Gain-of-function	Familial Episodic Pain Syndrome
TRPML1	Loss-of-function	Mucolipidosis type IV
TRPP2	Loss-of-function	Autosomal dominant polycystic kidney disease (ADPKD)

Table 8: **Channelopathy caused by TRP channel mutations** (Zhao & Rohacs, 2021).

With the availability of abundant human genome data now-a-days, many variations in the human genome are anticipated to be identified based on ethnicity, gender, class, food habits etc. Surely all these variations would not lead to the occurrence of diseases. Recently a human genome data (2504 genomes) study could identify many mis-sense variations in the human population (Ghosh et al., 2016). It is thrilling to envision the genome sequencing of entire population on earth that would provide innumerable variations in the genome. It is highly possible that many channelopathies which are already present in nature are yet to be discovered through genome sequencing. Many pre-natal or neo-natal deaths which are not documented, could have mutations in TRP genes that are probably intolerable in nature. Without a doubt, these investigations, connecting TRP channels to illness, will turn into a significant priority in biomedical sciences.

With regards to all TRP-induced channelopathies, TRPV4 is significant. With approx. 60 mutations identified so far, this probably is one of the most disease-causing protein in the human body. In spite of the fact that TRPV4 mutations results in a variety of hereditary bone disorders, only irregular osmotic regulation in case of TRPV4 knock out mouse has been stated (Suzuki et al., 2003). It is right now indistinct why the behaviour of TRPV4 knock out⁻ mice is so vastly dissimilar than that of mice having only point mutations in TRPV4. While TRPV4 mutations result in a series of musculoskeletal disorders ranging from mild to very severe phenotypes, the TRPV4 knockout mouse doesn't completely demonstrate any such phenotypes seen in human population but only hearing loss and bladder dysfunction has been studied so far (Gevaert et al., 2007; Tabuchi et al., 2005). Only recently a report by Nishimura et al. showed that TRPV1 and TRPV4 double knockout mice (DKO) has higher bone mass than WT mice and DKO mice had less multinucleated osteoclasts and had lower bone resorption (Nishimura et al., 2020).

Dissecting the pathomechanisms linked to disease progression due to this gene is worth looking after. Never-the-less, it seems that each mutation affects cells and tissues differently and cause different phenotypic penetrations. Obviously, we have recently entered an interesting and fast progressing field of TRP channel research.

3.2.2. Mutations in TRP channels are locus specific

A study based on 2504 human genome data suggests the mutations in TRPV are clustered in specific regions suggesting the evolutionary stability of TRPV's in human population (Ghosh et al., 2016). They have used SIFT, PolyPhen and Grantham Deviation scores to evaluate amino acid substitutions that are deleterious in human population (Figure 64). According to the findings, TRPV4 among the thermosensitive ion channel of the TRPV subfamily is predicted to have the
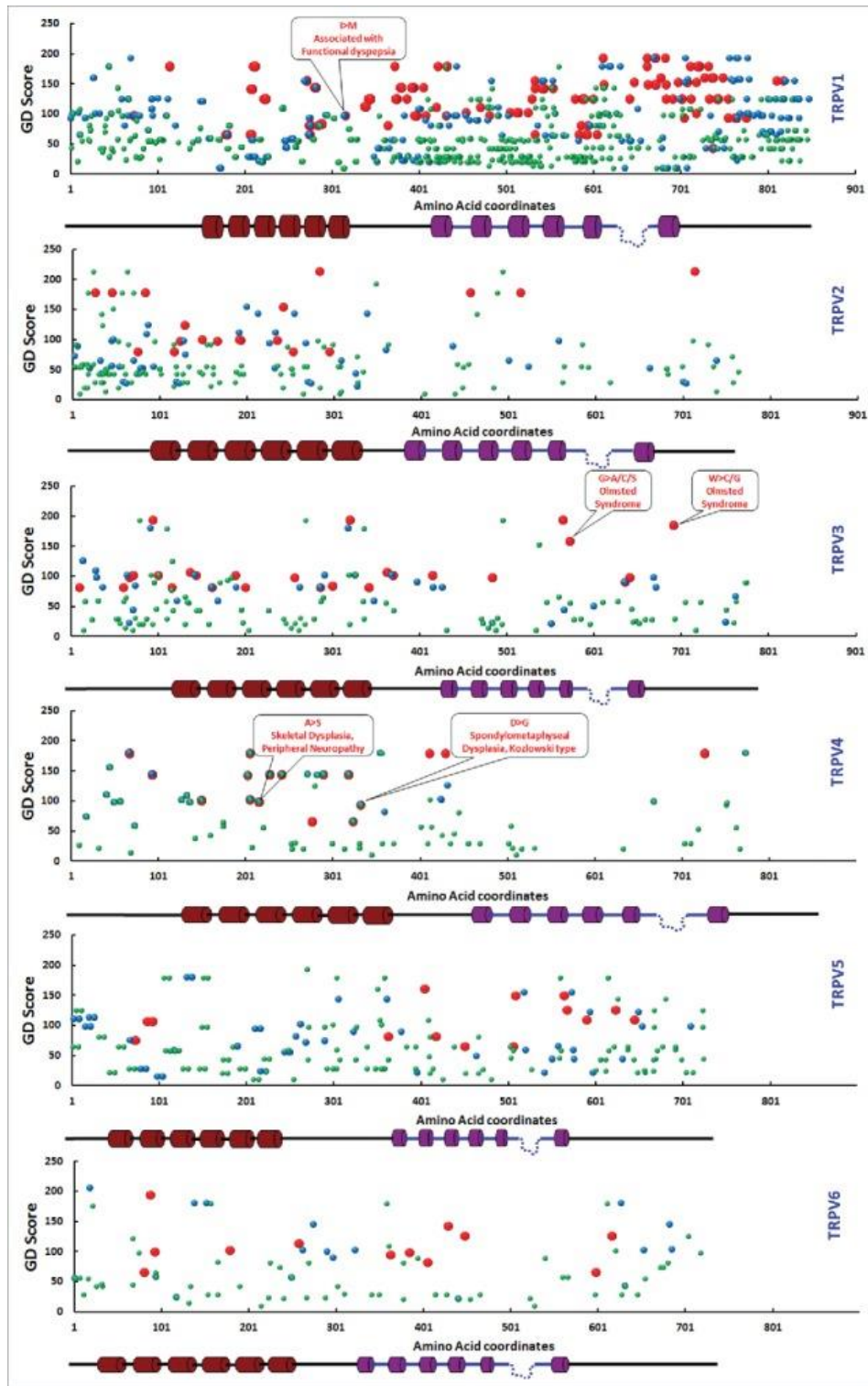
Figure 64: Analysis of missense variants of hTRPVs based on SIFT, PolyPhen and Grantham Deviation. Figure depicting amino acid substitutions in X-axis and GD scores in Y-axis. The mutations which were predicted by all three scoring systems were marked red, two scoring systems marked blue and only one scoring system is marked green (Ghosh et al., 2016).

144

least number of deleterious mutations suggesting the mutations in TRPV4 may not be tolerable. The prediction is in agreement with approx. 60 pathogenic mutations that are identified in TRPV4 termed as "channelopathies".

The distribution of several mutations in specific clusters suggests that the regions can tolerate the mutations and that the regions are effectively going through changes in the human population which may in future lead to channels which are steadier in architecture and functionally useful. One such mutation prone region in TRPV4 is the Tm4-Loop4-Tm5 region which has almost 14 mutations that give rise to several pathophysiological conditions. Two mutations namely L596P and R616Q which lie in the said fragment of TRPV4 were analyzed in detail in the thesis. These two cause SMDK and Brachyolmia respectively. While the former lies in the LWI region, the later mutation lies in the transmembrane region of the channel. The surrounding cholesterol molecules are believed to impact the channel function. Therefore, biochemical and microscopic analysis were performed in relation to presence and absence of cholesterol in the wild type and these two mutant proteins. Analysis of L596P mutation was found to have altered the pattern in the LWI which is believed to be conserved in specific areas of TRPV4. R616Q mutation was found to reduce the binding of cholesterol to the TRPV4 protein that possibly is the reason why the mutant behaves differently.

3.2.3. L596P-mutant alters the conserved amino acid pattern at the Lipid-Water-Interface of TRPV4 and changes cellular functions

In this work we demonstrate that point mutation, namely TRPV4-L596P cause significant shift in the correlation of absolute hydrophobicity to the frequency while another mutation (R594H) which is located in the inner LWI region does not cause that shift. Notably, TRPV4-

145

L596P mutation cause Spondylometaphyseal Dysplasia, Kozlowski (SMDK), a defect that typically affects bone cells. In this work, we show that the TRPV4-L596P has altered behaviour. For example, cells expressing TRPV4-L596P mutation induce more filopodia-like structures in Saos-2 cells. TRPV4-L596P-GFP also predominately localizes in such structures. Considering that TRPV4 forms a complex with Caveolin1, and other ion channels (Li et al., 2018), the impact on the Ca^{2+}-dynamics at the tip of the filopodia-like structures can be significant to the cells behaviour and ability to perform certain tasks such as cell adhesion and endocytosis. Accordingly, we could not detect phospho-Tyrosine, Vinculin and FAK in the cells expressing L596P mutant suggesting these signaling events might be different in cells expressing Wt and L596P mutant. In this context, the involvement of TRPV4 in filopodia-like structure formation and filopodial function has been well established (Goswami et al., 2010). This also matches with the fact that TRPV1 (a close homologue of TRPV4) or even its fragment is known to induce filopodia (Goswami et al., 2007; Goswami & Hucho, 2007). This is also in accordance with the involvement of TRP channels in the regulation of non-conventional myosin motors in different systems (Majhi et al., 2011).

However, when both TRPV4-Wt and TRPV4-L596P are co-expressed, cells do not induce filopodia-like structures. The exact reason for this is not clear, but it might be possible that the presence of both TRPV4-Wt and TRPV4-L596P in the same cell alter the Ca^{2+}-dynamics/Ca^{2+}-oscillations that is typically required for filopodia-like structure formation. This is also supported by the fact that we could demonstrate that the Ca^{2+}-levels as well as Ca^{2+}-dynamics at the tips of these filopodial-like structures are different for cells expressing TRPV4-Wt or TRPV4-L596P, especially after activating cells with 4αPDD. Notably the filopodial tips of L596P expressing cells have much higher levels of Ca^{2+} than the cells expressing TRPV4-Wt. Such differences can be crucial for bone cells to adhere on a surface and further survival and differentiation *in vivo*. Indeed,

importance of TRPV4 in the cell adhesion and mechanical-stiffness dependent differentiation of hematopoietic cell-lineages has been shown (Vellino et al., 2020). Generally, the cell edges (such as in Lamellipodia and in filopoidial tips) have higher level of Ca^{2+}-levels and TRPV4 is also know to interact with other channels and alter ionic homeostasis. Considering that TRPV4 is stimulated by a spectrum of physical and chemical stimuli such as heat, mechanical pressure, cytochrome P450-derived metabolites, arachidonic acid, endocannabinoids, the differences in the Ca^{2+}-dynamics as observed in the filopodial tips in cells expressing L596P mutant in experimental cell culture condition could be significant determining factor for bone cell functions *in vivo*.

3.2.4. Membrane mobility of TRPV4-Wt and L596P mutant differs in response to caveolin-1 interaction and cholesterol reduction

TRPV4 seem to have a profound role in the regulation of caveolae function also. This is mainly due to the fact that TRPV4 has been detected in the caveolae using different cell systems (Li et al., 2018 ; Shamsaldeen et al., 2020 ; Daneva et al., 2020). This is in full accordance with the mechanosensitivity response observed in caveolae (Echarri & Del Pozo, 2015). Our results accord well with the previous reports demonstrating that TRPV4 forms a complex with Caveolin1 (Li et al., 2018). It seems that both TRPV4-Wt and TRPV4-L596P are able to form this complex with Caveolin1. This is supported by the fact that both TRPV4-Wt as well as TRPV4-L596P are able to reduce the mobility of Caveolin1 significantly in different cellular conditions. Never-the-less, it seems that L596P mutation is less sequestered (as compared to the TRPV4-Wt) in presence of over expressed Caveolin1. This is matching with the observation that the filopodia-like structures induced by TRPV4-L596P seem to have less or no Caveolin1. Therefore, subtle change/s in membrane microdomain as induced by TRPV4-L596P mutation is evident. In

147

agreement with this, mobility of TRPV4-Wt and TRPV4-L596P differs in cholesterol-reduced condition, suggesting that Cholesterol indeed play a role in the fine-tuning of TRPV4 function and redistribution of Caveolin1, yet contains TRPV4-L596P-GFP. This is in accordance with the previous reports suggesting that cholesterol-reduction results in accumulation of Caveolin1 in Golgi from ER and plasmamembrane (Cohen et al., 2004). Notably, animals lacking Caveolin1 ($Cav1^{-/-}$) have increased bone size and bone stiffness (Rubin et al., 2007). This is also matching with the fact that defects in Cholesterol biosynthesis results in bone defects (Suzuki et al., 2020 ; Waterham, HR., 2006). It is noteworthy to mention here that TRPV4 interacts with cholesterol, forms a complex (Kumari et al., 2015). Different mutations, such as TRPV4-R616Q also shares altered interaction and functional relationship with cholesterol (Das & Goswami, 2019). Considering the results reported here, the differential function and regulation of Wt and L596P in the caveole, especially in the cholesterol-reduced condition can be critical for several clinical aspects also.

3.2.5. TRPV4-L596P may have more spontaneous opening in physiological conditions and thus cause altered cellular behaviour

Our results are also supported by the fact that TRPV4-L596P expressing cells have properties that suggest that this mutation may have more open probabilities, especially in optimum or sub-optimum level of agonists. Our results accord well with the hypothesis proposed before (Teng et al., 2015). It seems that L596 forms a "latch" by interacting with W733 located in the TRP-domain. Thus, mutation in L596 position possibly affect the latch formation and thus may affect the lower gate of the actual channel pore (Teng et al., 2015). Therefore, it is most-likely thatTRPV4-L596P has more spontaneous opening in physiological conditions and thus cause

altered cellular behaviour. TRPV4 is known to interact with actin cytoskeleton, localize in filopodial tips and regulate filopodial functions (Goswami et al., 2010). We propose that altered Ca^{2+}-dynamics in the tips of the filopodia-like structures are one of the major causes of TRPV4-L596P mutation which might be involved in the loss-of-bone cells and thus results in the formation of Spondylometaphyseal Dysplasia, Kozlowski. Our findings may have border significance in understanding the molecular and cellular mechanism behind channelopathy and thus may have implication in the bio-medical research. However, further and detailed characterization of these filopodia-like structures developed due to L596P mutant are needed.

3.2.6. Critical involvement of R616Q in cholesterol-binding of TRPV4

In this work we demonstrate that TRPV4 fragment containing a cholesterol-binding motif sequence actually interacts with cholesterol and forms a high-molecular weight complex. Such complex is fairly stable as such complex is visible in the gel pockets as well as in different positions in SDS-PAGE. Gel-shift assay also indicates that the TM4-Loop4-TM5 fragment of TRPV4 adapts "fast-moving complex" in SDS-PAGE in presence of cholesterol. Notably this "fast-moving complex" actually moves at the size of GST-only, and therefore mostly matching with the expected molecular weight of the fragment. This phenomenon, possibly suggest for a stabilization of TM4-Loop-TM5 fragment by cholesterol and/or other specific lipid components.

Our data suggest that Cholesterol-binding may trigger conformational changes in the protein structure and forms a confirmation that has different migration properties in SDS-PAGE. Generally, SDS-resistant oligomeric aggregates cannot enter a conventional polyacrylamide gel and get accumulated in the gel pocket.

The fragment TM4-Loop4-TM5 used in our study is small in size and contains an

unstructured loop that might be undergoing robust conformational changes upon binding to Cholesterol/Salt/detergent/bulk water and the complex becomes differentially resistant to SDS. These possibilities have been depicted by a schematic diagram (**Figure 65**).
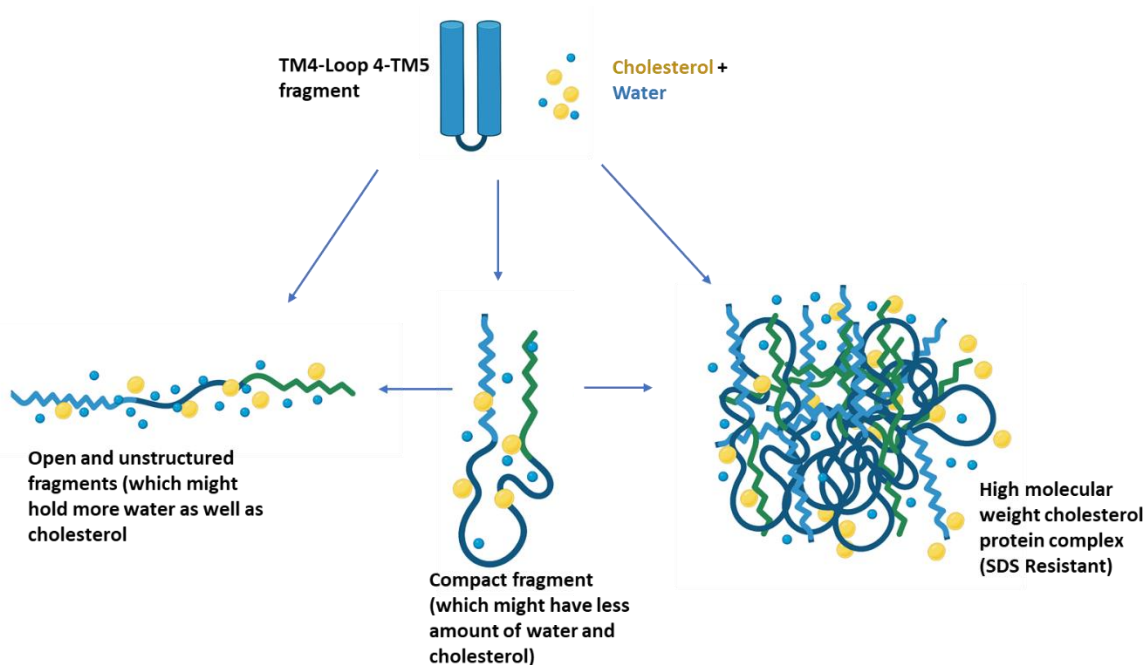
Figure 65: Model depicting various plausible conformations of TM4-Loop4-TM5 upon interaction with cholesterol. Cholesterol can induce different conformations in membrane proteins. Also, there are cases, where such differences in conformation can be distinguished in SDS-PAGE. The unstructured loop containing fragment TM4-Loop4-TM5 could acquire several forms including an open, compact, or high molecular weight complex consisting of varying quantities of cholesterol and water molecules.

Such findings are also in accordance with the localization of endogenous TRPV4 in lipid rafts observed in several cases (Carreño et al., 2008). The high-molecular weight complex formed by TRPV4 fragment with cholesterol matches well with what has been observed in case of TRPV2. Notably, cholesterol remain associated with TRPV2 even after purification and crystallization as observed in high-resolution TRPV2 structure (Huynh et al., 2016).

Using different approaches, we demonstrate that cholesterol interaction is reduced/ abolished

in case of TRPV4-R616Q mutant. This is supported by the fact that in, R616Q mutant reveals no interaction with cholesterol (in docking experiments); at least in the TM4-Loop4-TM5 region. Biochemical data suggests that R616Q do not interact with cholesterol. In accordance, R616Q mutant also preferably localized in non-lipid raft regions, i.e., regions that are not enriched with cholesterol. Membrane mobility of TRPV4-R616Q is lower than TRPV4-Wt, especially in cholesterol-depleted condition. All these factors strongly suggest different aspects of cholesterol-mediated regulation of TRPV4. First, cholesterol is needed for proper membrane mobility of TRPV4. Second, R616Q mutant has much less interaction with cholesterol. Considering that R616Q mutant remain "constitutively open, thus its "gain-of-function" property correlates with "loss-of-interaction" of cholesterol. Such relationship is of relevance and is suggestive for the regulatory role of cholesterol in TRPV4 function. It also suggests that cholesterol presence in lipid bilayer may actually help TRPV4 to stabilize in closed conformation, at least in physiological temperature. Our results fit well with the cases observed in other TRPs also. For example, cholesterol bonds with certain "Arginine" residues of TRPV1 only in closed- but not in open-conformation (Saha et al., 2017). TRPA1 is also interacts with cholesterol directly (Startek et al., 2019). In the three dimensional structure of TRPV2, cholesterol molecule densities were identified to occupy the crevice formed because of the S1–S4 segments (Huynh et al., 2016).Taken together, data suggest that TRPV4 interacts with cholesterol, and such interaction is strong enough and have evolutionary origin. We propose that TRPV4-R616Q mutant behave as a "loss-of-interaction" with cholesterol and thereby act as a "gain-of-function" mutant. Nevertheless, further work is expected to assess this perspective in greater details.

3.2.7. Somatic mutations in TRPV4 are also detected in several cases of cancer

Not only the heritable genetic mutations but also somatic mutations in TRPV4 can cause several diseases like various types of cancers (Figure 66).
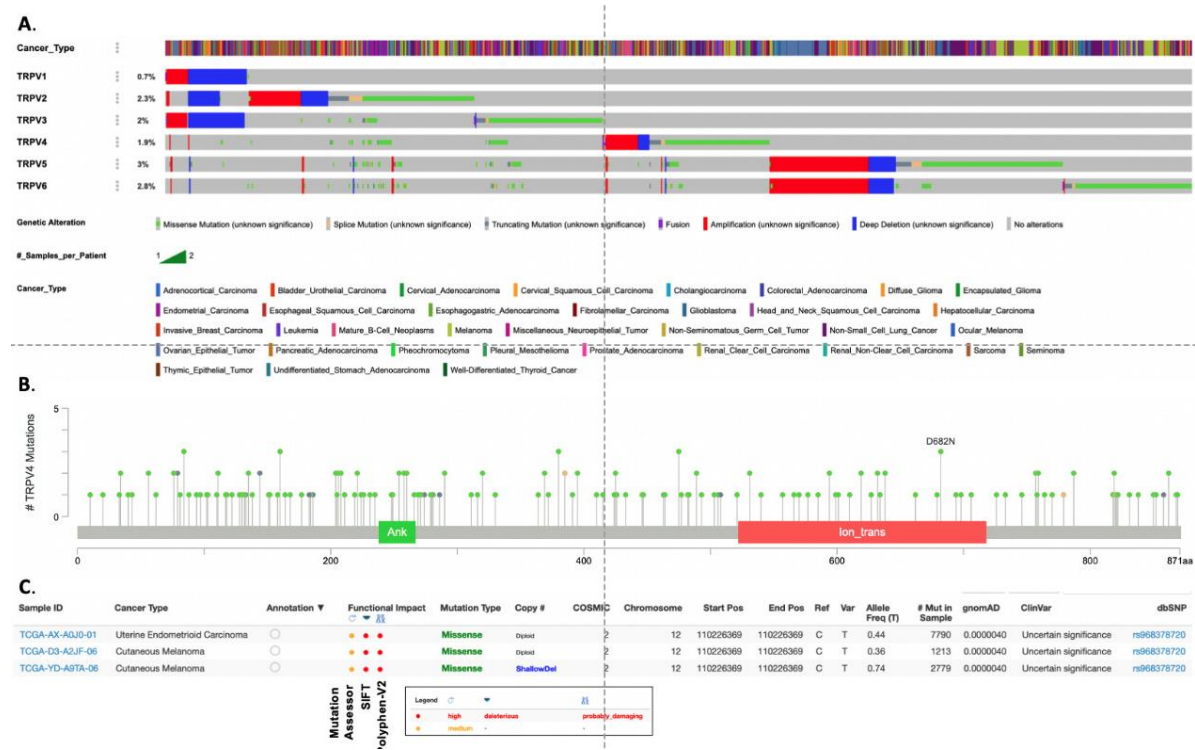
Figure 66: Somatic mutations profile of TRPV4 derived from cosmic data base. Data from more than 10000 cancer samples are summarized here. **A.** Percentage of mutations in individual TRPVs as seen in the cosmic data are shown here. **B.** Mutational hot-spots of TRPV4 as observed in cosmic data set is shown. Notably, D682N mutation (located in the TM and pore region) seem to be frequent and is observed in 3 different samples. **C.** The details of the D682N mutation containing samples are represented. (Data kindly provided by Dr. Abhishek Kumar. Data unpublished).

3.3. TRPV4 as a possible regulator of mitochondrial metabolism

3.3.1. TRPV4 localization in mitochondria and the regulation of mitochondrial structure and function

In the last few years, the intracellular localization of TRP channels was investigated in some extent (Table 3). Intracellular localization has successfully been demonstrated for many but the research is still in its infancy.

Mitochondria are frequently alluded to as the powerhouse of the cell, nevertheless, their physiological job goes positively past that. Ion channels are closely associated with mitochondrial function regulation as several ions like hydrogen (H^+), potassium (K^+), sodium (Na^+), and calcium (Ca^{2+}) are required to be transported across the mitochondrial membrane for various cellular functions. The primary route for mitochondrial ion transport is the voltage-dependent anion channel (VDAC) present in the outer membrane (OMM) (Strickland et al., 2019). Mitochondrial calcium uniport (MCU) complex, present in the inner mitochondrial membrane (IMM) is the primary ion channel for Ca^{2+} and Mn^{2+}-influx (Urbani et al., 2021).

Even though MCU is by all accounts the principle calcium entry pathway, other channels like leucine zipper-EF-hand–containing transmembrane protein 1 (LETM1) and Na/Ca/Li exchanger (NCLX) have likewise been proposed as Ca^{2+}-efflux channels (Csordás et al., 2012) (Figure 67).
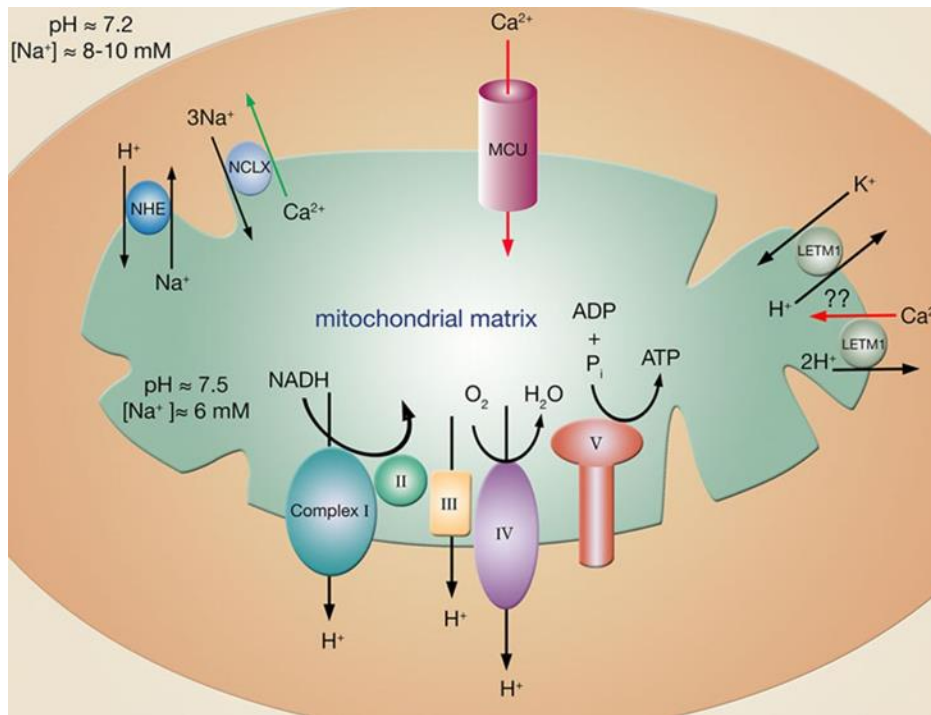
Figure 67: Channels involved in mitochondrial calcium influx and efflux (Csordás et al., 2012)**.**

Several other proteins like ryanodine receptors (RyRs) and TRPC3 are reported to be present in the IMM and play a role in Ca^{2+}-homeostasis. Mitochondrial penetrability progress pore (MPTP or PTP) addresses one more component for Ca^{2+}-discharge from mitochondria. Many proteins are thought to form the PTP and open the pore by Ca^{2+} or ROS challenge (Shoshan-Barmatz et al., 2017). A recent study observed in brain mitochondria using knock-out MCU resulted in the incomplete loss of mitochondrial Ca^{2+}, suggesting an optional mitochondrial Ca^{2+} uptake pathway (Hamilton et al., 2018). Similarly, in photoreceptor cells, proof for MCU-independent mitochondrial Ca^{2+} was observed (Bisbach et al., 2020).

A point mutation in TRPV4 protein leads to CMT2C disease, a neuropathic disorder. Pathophysiological symptoms similar to CMT2C are also caused by a mutation in Mfn2 protein, suggesting a possible connection between TRPV4 and the mitochondrial protein Mfn2 (Feely et al., 2011; Landouré et al., 2009). Evidence additionally suggests a potential link between TRPV4

and mitochondria. Activation of TRPV4 disrupted the mitochondrial function as suggested by increased mitochondrial ROS levels in pulmonary arterial endothelial cells (Lu et al., 2021). Another study reported R269C mutation of TRPV4 inhibiting mitochondrial axon transport (Woolums et al., 2020).

By-and-large, these new studies called out for a new and conceivable controller of mitochondrial Ca^{2+}-channel and thus possible location and function of TRPV4 in mitochondria was investigated in detail (Kumar et al., 2018). Using various biochemical and microscopic studies, it was confirmed that TRPV4 is indeed present in mitochondria.

In such a manner, the outcomes portrayed in their research like mitochondrial calcium, Copper and Iron dynamics by TRPV4 modulation, concurs well with these past reports as well as give trial proof showing that TRPV4 isn't just present into the cell membrane, yet additionally restricts in the mitochondria and controls its structure and function/s.

3.3.2. Interaction of TRPV4 with mitochondrial protein Cytochrome c

Cytochromes are a major class of heme-containing electron transport proteins first described in 1884 as respiratory pigments. These colored substances were later named "Cytochromes", or cellular pigments. More than 70000 cytochromes have been discovered as of today (Liu et al., 2014). These are proteins to which one to two tetrapyrrole rings are bound. These tetrapyrroles are very similar to the chromophores of chlorophylls, however, chlorophylls contain Mg^{2+} as the central atom in the tetrapyrrole, whereas the cytochromes have an Fe^{2+} atom. The tetrapyrrole ring of the cytochromes with iron as the central atom is called the heme. The bound iron atom can change between the oxidation states Fe^{3+} and Fe^{2+} so that cytochromes function only as a one-electron carrier, in contrast to quinones, $NAD(P)^+$ and FAD, which transfer two electrons

together with protons. Cytochromes are classified based on the electronic absorption maxima of the heme macrocycle, such as *a*, *b*, *c*, *d*, *f*, and *o* types of heme where these letter names represent characteristic absorbance maxima in the UV–vis electronic absorption spectrum (Heldt & Piechulla, 2021; Suman & Joseph, 2014).

This heme protein cytochrome c (Cyt C) transfers electrons in the mitochondrial respiratory chain from cytochrome bc1 complex to cytochrome c oxidase. The heme moiety of cytochrome c exists in interconvertible reduced (Fe^{2+}) or oxidized (Fe^{3+}) forms that shuttle electrons from Cyt C reductase to Cyt C oxidase. It is bound to the inner membrane in the mitochondrial intermembrane space especially with cardiolipin (CL) by electrostatic and hydrophobic interactions. In addition to its role in electron transport, it has a prominent role during the early stage of apoptosis. It is released into the cytoplasm where it forms "apoptosome" complex with Apaf-1 and caspase 9 , which leads to activation of the cascade of proteases executing apoptosis in cells. (Brown & Borutaite, 2008; Saleh et al., 1999; Tuominen et al., 2002; Zalk et al., 2005). Cyt C structure contains three long α-helices. The heme of Cyt C forms covalent bonds with two cysteine residues through their sulfur atoms and is coordinated in the native form by His18 and Met80 (Hirota et al., 2010). This water-soluble low-molecular-weight (13 000 Da; 104 amino acids) protein can exist in an aqueous solution as the native monomer as well as a dimer, trimer, and tetramer (Margoliash & Lustgarten, 1962).

Many aspects of mitochondrial physiology require transition metal ions. Copper, iron, manganese, and zinc are some known cofactors in metalloenzymes and metalloproteins present within the organelles. Upon perturbation in metal pools inside mitochondria, mis-metallation reactions may occur (Pierrel et al., 2007). The interaction of metal ions with proteins is important as many endogenous proteins utilize metals for stabilization or activity. Interfacial metal ions

stabilize permanent or transient protein-protein interactions, enable protein complexes involved in cellular signaling to adopt distinct conformations in response to environmental stimuli, and catalyze challenging chemical reactions that are uniquely performed by multiunit protein complexes (Finkelstein, J., 2009; Song et al., 2014). Ions are known to be transported across the mitochondrial membranes either by channels or translocases. Research has been done on the ion-binding properties of cytochrome c and also suggests a role for cytochrome c in mitochondrial ion transport. At least eight ion-binding sites on cytochrome c have been identified (Arean et al., 1988). There are four classes of substances involved in mitochondrial transport. Some are transported independently without any assistance such as ammonia. Some like chloride, maleate, and fumarate are incapable to penetrate the inner mitochondrial membrane. The third type is cations like K^+, Na^+, $Ca^{2+,}$ and Mg^{2+} which are accumulated in the mitochondrial matrix against a concentration gradient. The last class is the variety of anionic substances, which flow in and out of the mitochondrial matrix following a concentration gradient. The cytochrome c binds to chloride, maleate, fumarate, K^+, Na^+, $Ca^{2+,}$ and Mg^{2+} and some of the representatives from the last class like succinate, ATP, and ADP (Margoliash et al., 1970). The ion-binding properties of cytochrome c is of great interest as ion-binding to cytochrome c profoundly affects its reactivity with proteins.

As TRPV4 is a non-specific cation channel whose prevalence has been accessed in mitochondria and also its role has been recognized in the transport of metal ions, there exists a possibility of cross-talk between TRPV4 and cytochrome c because of their common functionality inside mitochondria. It could be highly possible that they may work in coordination and they are interdependent. TRPV4 and Cyt C interaction in presence and absence of several metals suggest the essential role of TRPV4 in mitochondrial mediated metal entry and the vital functions inside

the cells. Several TRPV4 mutations may disturb this interaction and probably may affect the metal

entry inside the cells.

3.4. TRPV4 as a candidate for steroid biology

3.4.1. TRPV4 as a means of metal entry inside the cells and the role of metals as cofactors in steroidogenesis pathway

Certain trace metals like Zinc (Zn^{2+}), iron (Fe^{2+}/Fe^{3+}), or copper (Cu^{+}/Cu^{2+}) are involved in a wide variety of biological progressions. Metal ions like cadmium (Cd^{2+}) or lead (Pb^{2+}) have only toxic properties as observed in vertebrate cells. Exposure to different heavy metals is significantly related to some genotoxicity and endocrine parameters. For example, a study done on the cleaners of "prestige" oil tanker spill in the coastal areas of Spain suggested the exposure to several metals like aluminum, cadmium, nickel, lead and zinc significantly altered the values of hormones like cortisol and prolactin (Pérez-Cadahía et al., 2008). Another study on children working/living near brick klin sites who are exposed to heavy metals like cadmium, chromium, nickel and zinc emitted from them suggested an increase level of cortisol and decreased level of growth hormone (David et al., 2020). A toxicity study on ovarian follicles of *Rana catesbeiana* suggested significantly inhibition of frog Pitutary Hormone-induced pregnenolone (P_5) by Hg^{2+}, Cd^{2+} and Zn^{2+} and suppression of conversion of testosterone (T) to estradiol 17β (E_2) as well as suppression of C_{17-20} lyase and 17β-HSD enzymes (Choi et al., 2010). Study on copper exposure in rainbow trout suggested the abolition of an acute cortisol response post-stress whereas Zinc was found to acutely and temporarily inhibit adrenal cortisol secretion in humans (Tellis et al., 2012 ; Brandão-Neto et al., 1990).

The molecular mechanisms by which these cations enter inside cells are still not completely perceived. Among the various factors contributing in the uptake of trace metal ions, ion channels signify an important class of proteins as they permit the import/ export of ions according to their electrochemical gradients (Bouron et al., 2014). TRPV4 along with its other subfamily members

are recognized for their metal entry properties. The pore diameter of TRPV4 at the lower gate increases considerably from 5.4 Å in the closed state to 10.6 Å in the open state (Botte et al., 2020). This pore diameter is bigger than the corresponding pore diameters in open and activated forms of TRPV1 channel (7.6 Å) and is sufficiently big where metal ions whose effective diameter falls within 10Å can enter (Deng et al., 2018).

The critical involvement of metal ions in the endocrine framework turned out to be much evident and relevant for health. Accordingly, new interdisciplinary field of endocrinology and inorganic chemistry has emerged that is termed as "metalloendocrinology" (Stevenson et al., 2019). Earlier, metals like zinc, selenium, and copper were tagged as toxic metals (Iavicoli et al., 2009), however recent advances have elucidated the essential role of metal micronutrients like copper, iron, zinc, and calcium in normal hormone activity. Copper and iron inadequacies have been investigated for associations with thyroid hormone imbalance and temperature regulation associated with it (Beard et al., 1990; Lukaski et al., 1995). Zinc deficiency is also linked to abnormal growth and retardation of development in children.

Influences of metals on steroids have been reported as early as 1972 when corticosteroids were observed to form complexes with Co(II). Several steroid hormones have since been reported to be impacted by metals, including the neurosteroid pregnenolone, the sex steroids estrogen, progesterone, and androgen, as well as the corticosteroid glucocorticoid. Certain metals have also been theorized to impact steroidogenesis (Alexander Jackson et al., 2001; Eger et al., 1972; Schmidt et al., 1982). For example, Ca^{2+}-entry inside adrenal mitochondria can stimulate the formation of pregnenolone (a neuro-steroid, and various steroid hormones precursor), mainly by increasing the interaction of mitochondrial cytochrome P-450 with its endogenous substrate (Simpson & Williams-Smith, 1975).

Steroid function can also be linked with Zn^{2+} altered levels. A relationship between Zn^{2+} and androgen production was observed in the testes of rats with testicular feminization where significantly lower Zn^{2+} was found. The exact factors that direct these metal–hormone cross-talks remain an open question (Stevenson et al., 2019).

3.4.1.1. TRPV4 possibly interferes with mitochondrial Cu^{2+}-uptake

Mitochondria has several Cu^{2+}-binding proteins and also certain levels of Cu^{2+} as it is involved in the electron transport chain. We noted that exposing the cells to only Cu^{2+} in the resting condition, the Cu^{2+}-uptake in the mitochondria is enhanced to almost 2-fold (1→1.89) than the control condition (Figure 68a). Notably, in Cu^{2+}-exposed condition, TRPV4 activation by 4αPDD (1 µM) brings down the mitochondrial Cu^{2+} -level almost to the control level. This suggests that TRPV4 function may be beneficial for proper Cu^{2+} homeostasis within mitochondria, especially in the high Cu^{2+}-exposed conditions or conditions when mitochondrial Cu^{2+}-level is high (Figure 68a). This preliminary results also suggests that TRPV4 activation may lead to the exit of Cu^{2+}-ions from mitochondria, especially upon conditions where mitochondria accumulate a high level of Cu^{2+} (as cells are exposed to a high level of Cu^{2+}). To explore that TRPV4 can indeed act as Cu^{2+}-exit route in mitochondria, we treated cells with higher doses of 4αPDD (5 µM), both in the absence and presence of Cu^{2+}. In case of stimulation by a higher dose of 4αPDD (5 µM, in Cu^{2+}-free condition), the mitochondria lose ~10% (1→0.76) Cu^{2+} than the control condition, but still retains some Cu^{2+} as expected (Figure 68b). Under high stimulation conditions, the same level of Cu^{2+} exposure increases the copper level, but the fold change is ~ 50% (1→1.41), which is much less as compared to the Cu^{2+} exposed condition in resting condition only. This also suggests that TRPV4 activation lowers the copper level in mitochondria. Notably, in presence of TRPV4

activator (4αPDD, 5 µM) and Cu^{2+}-exposed condition, the Cu^{2+}-level is reduced by the presence of RN1734, an inhibitor that specifically blocks TRPV4 (Figure 68c). Considering the fact that bi-directional movement of ions are possible in open condition, these preliminary results suggest that TRPV4 may act as a Cu^{2+}-exit point in mitochondria. However, this aspect needs further experiments.
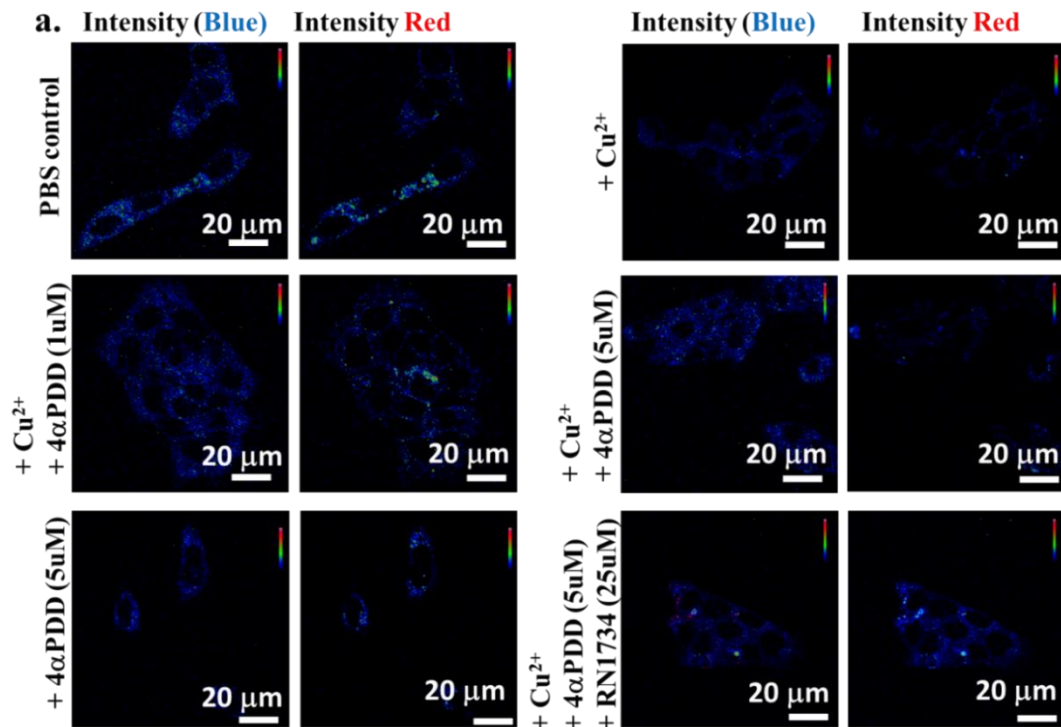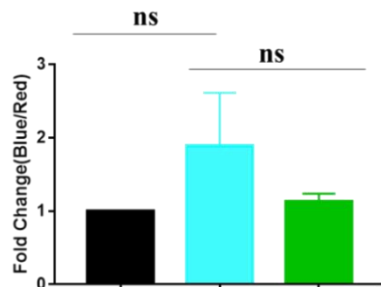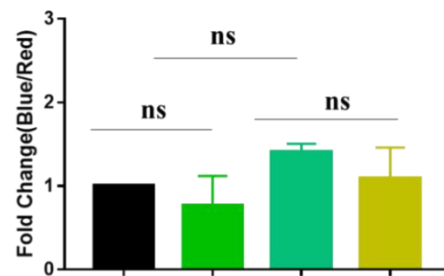
Figure 68: TRPV4 possibly interferes with mitochondrial Cu^{2+}-influx. Mitochondrial copper specific sensor InCCu1 was used for detection of copper levels in H295R cells by imaging. H295R cells pre-treated with varying concentrations of 4αPDD and RN1734 for 24 hours were treated with media containing either PBS or copper sulphate (100 μM) for 2 hours and then washed 3 times with PBS. Cells were incubated in 1 mL solution of the 0.1μM concentration of InCCu1 in H295R media. After 15 minutes of incubation, cells were washed 3 times with PBS and imaged in complete media immediately. InCCu1 consists of two fluorophores (material & method). Dividing the blue intensity by red gives the final copper entry status. Increased ratio suggests increase copper entry and *vice versa*. The changes in fluorescence intensity of both blue and red emission have been depicted in RGB pseudo colour. Scale bar is 20 μm.

3.4.1.2. TRPV4 inhibition limits iron uptake by mitochondria

Mitochondria have several Fe^{2+}-binding proteins. To investigate further the role of TRPV4 in mitochondrial Fe^{2+} accumulation in H295R cells, we used a mitochondrial Fe^{2+}-specific fluorescent sensor, RDA. The fluorescence of the sensor is strongly quenched by Fe^{2+} ions inside mitochondria. We have found that in TRPV4 activation by 4αPDD results in lowering the fluorescence, also in a dose-dependent manner to some extent (1μM and 5 μM), suggesting that TRPV4 may help as an entry route for Fe^{2+} (Figure 69). To confirm that, we applied a higher level of 4αPDD (5 μM) in presence of TRPV4 inhibitor, i.e., RN1734 (25 μM). In this condition, a very higher level of RDA signal is observed from mitochondria and this is almost 5 times more than the activation condition (10.88 vs 50.95) and 2.5 times more than the resting condition (20.0 vs 50.95) (Figure 69). This data strongly suggests that TRPV4 activation results in the entry of Fe^{2+} to mitochondria whereas TRPV4 inhibition results in increased fluorescence of RDA, suggesting lowering the Fe^{2+}-level within mitochondria; which means less entry of Fe^{2+} to the mitochondria which is also equivalent to the exit of Fe^{2+} from the mitochondria.
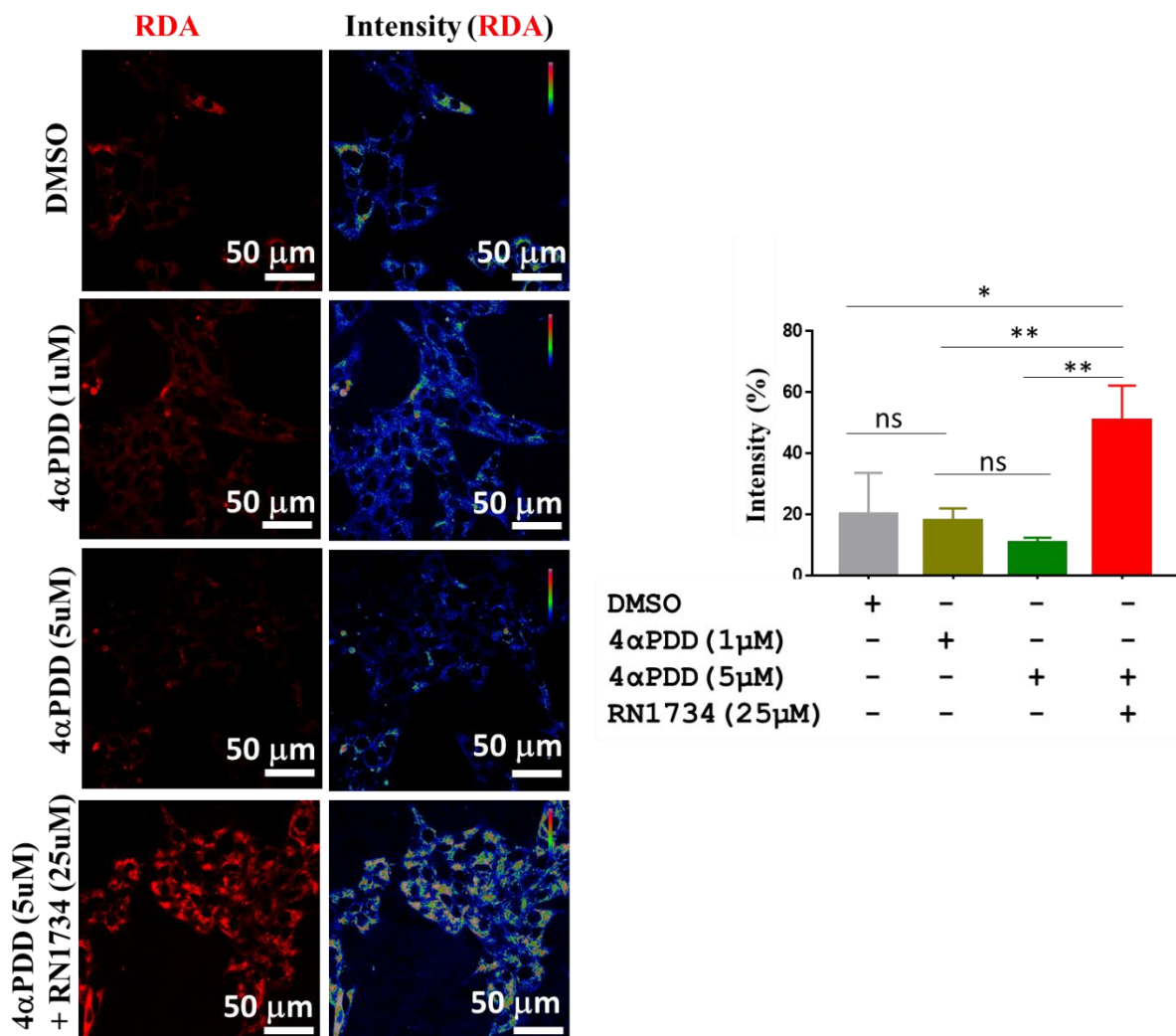
Figure 69: TRPV4 interferes with mitochondrial Fe^{2+} influx. Mitochondrial iron specific sensor RDA was used for detection of iron levels in H295R cells by imaging. H295R cells pre-treated with varying concentrations of 4αPDD and RN1734 for 24 hours were incubated with RDA (0.5 μM, prepared from stock solutions of 1mM in DMSO) for 15 min at 37°C. Cells were washed subsequently three times and incubated for another 15 minutes at 37°C. Images were taken thereafter. A decrease in RDA intensity suggests Fe^{2+} entry and *vice versa*. The changes in fluorescence intensity of RDA have been depicted in RGB pseudo colour. Scale bar is 50 μm.

3.4.2. Clues from role of TRPV4 in bone development and cross talk with steroids

Steroids are frequently associated with various skeletal complications. Skeletal dysplasias are one such a large heterogeneous group of disorders described by anomalies of bone or cartilage development (Nishimura et al., 2012). These disorders happen because of hereditary

164

transformations and their phenotype keeps on evolving all through life. Growth factors, as well as hormones, can impact bone development. It is normally considered that sex hormones are associated with the regulation of skeletal development and in its support. For example, 17β-estradiol (E2), during sexual development, adds to the extending of the bone. Though sex hormones are mainly produced by gonads, these can also be synthesized in growth plates with the help of enzymes produced by the chondrocytes. Similarly, androgens like testosterone stimulate bone formation (Emons et al., 2011). *In vitro* studies have identified the contribution of androgens in osteoblast progenitors proliferation, mature osteoblast differentiation, and osteoblasts apoptosis inhibition (Vanderschueren et al., 2004). Glucocorticoids are also involved in bone growth regulation by inhibiting chondrocyte proliferation, slowing growth plate senescence, or through their negative effect on muscle, influencing the normal modeling process (Lui & Baron, 2011; von Scheven et al., 2014).

Diseases in TRPV4 also result in the development of various types of bone related disorders like skeletal dysplasias, arthropathies, osteoarthritis or decreased osteoclast function, etc. (Clark et al., 2010; McNulty et al., 2015; Nilius & Voets, 2013; Verma et al., 2010). This common involvement of TRPV4 and sterols in the same functions are additionally noticeable from hereditary interaction studies. For example, in a patient with symptoms of Glucocorticoid Deficiency and Skeletal Dysplasia, analysis of steroid hormones led to a diagnosis of 17a-hydroxylase/17,20-lyase deficiency (170HD). They speculated that the association of partially combined 170HD with the Shprintzen-Goldberg phenotype in the patient could be a result of an aberration of an *unknown gene* that controls both steroid hormone synthesis and skeletal development (Adachi et al., 1999). Similarly, mutations in the lamin B receptor (LBR) gene that is the primary 3β-hydroxysterol Δ^{14}-reductase (acts on the conversion of lanosterol to cholesterol

in mammalian cells) were found in Greenberg skeletal dysplasia (Bennati et al., 2006). Deficiency of 3β-hydroxysterol Δ^{14}-reductase causing an error in cholesterol biosynthesis results in the development of stillborn infant with skeletal dysplasia and other birth defects (Bennati et al., 2006). Proper sulfation of endogenous molecules inside a cell is another essential element for growth and development. Notably, Skeletal Dysplasias are linked to proteins involved in sulfate metabolism and Sulfation also has a significant role in the biotransformation of cholesterol, bile acids, and steroids (Paganini et al., 2020). This linkage of skeletal dysplasia with steroid hormone synthesis additionally calls on for a missing link that could be TRPV4, for it has sufficiently proven its role regulation of both the functions individually.

Steroids are often linked with thermogenesis. Progesterone is well recognized for its involvement in the elevation of body temperature following ovulation. This thermogenic activity of progesterone is particularly evident in human (women), rats, and cattle. This activity is reported to be dependent on thyroid gland activity (Buxton & Atkinson, 1948; Davis & Fugo, 1948; Forman et al., 1987; Freeman et al., 1970). One of the 17-oxo-steroids, 3α-hydroxy5β-androstan-17-one, causes etiocholonanolone fever. Several other 5β-reduced C19 steroids cause fever when administered to humans by releasing interleukin-1 and other pro-inflammatory cytokines (Hampl et al., 2006). In contrast, Glucocorticoids as endogenous antipyretics act oppositely. Corticosterone which is a major glucocorticoid, decreases uncoupling proteins (UCP) expression involved in heat production, administration of glucocorticoid induce hypothermia, hyperglycemia, and activation of innate immunity (Kainuma et al., 2009). Similarly, testosterone caused a dose-dependent inhibition of UCP1 mRNA induced by adrenergic stimulation with noradrenaline (Kainuma et al., 2009). Another most abundant circulating steroid in humans is dehydroepiandrosterone (DHEA)

in its sulfate form (DHEAS) which increases UCP1 expression in brown adipose tissue (BAT) by acting at multiple steps (Ryu et al., 2003).

The role of TRPV4 as a warm temperature-sensitive ion channel is well defined in literature and thus provides a reasonable clue for temperature mediated regulation of steroid function.

Recent studies have identified that the non-genomic fast response of steroids is actually due to intracellular mobilization of Ca^{2+} and other ions suggesting that Ca^{2+} channels are involved in such effects (Kumar et al., 2015). Pregnenolone, which is synthesized from cholesterol, is considered a prohormone as it is the precursor of all other steroids. A recent study has shown that the sulfonated form, i.e. pregnenolone sulfate directly activates TRPM3 and evokes Ca^{2+}-influx, and promotes insulin release (Wagner et al., 2008). Similarly, steroids (and pirfenidone) activate TRPA1 and suppress collagen synthesis in InMyoFibs. They induce Ca^{2+}-influx that negatively regulates TGF-β1–Smad signaling and down-regulate anti-fibrotic factors collagen type I and α-SMA (Kurahara et al., 2018). Current proof also indicates that estrogen affects the expression and function of TRPV1, TRPV5/6, TRPM6, and TRPA1 (Greaves et al., 2014; Payrits et al., 2017; Cho & Chaban, 2012; Lee & Jeung, 2007; Méndez-Reséndiz et al., 2020; Öz et al., 2007). Androgens like testosterone/DHT modulate TRPV1, TRPV5, TRPM8, and TRPM3 (Hsu et al., 2010; Bidaux et al., 2005; Wagner et al., 2008). DHEA negatively affects TRPV1 and Androstenedione affects TRPA1 and TRPV1 both (Chen et al., 2004; Logu et al., 2016). Progesterone modulates the activity of several TRP channels including TRPV1, TRPV4, and TRPM3 (Jung et al., 2009; Majeed et al., 2012; Ortíz-Rentería et al., 2018). Pregnenolone sulfate (PregS) affects TRPM3 and TRPV1 (Nilius & Voets, 2008; Naylor et al., 2010; Harteneck, C., 2013). TRPM6 and TRPM7 channel associates to form functional heterotetramers and the actions

of aldosterone on TRPM6/7 heterotetramers are evident from several studies (Li et al., 2006; Yogi et al., 2013).

As TRPV4 is a multifunctional non-selective calcium permeant cation channel involved in osmotic sensitivity and mechanosensitivity, it is highly possible that TRPV4 mediated Ca^{2+} entry could be a key regulator for steroid function and steroid mediated Ca^{2+} entry might also have a link to TRPV4. Not only TRPV4 is indirectly linked with steroid metabolism but also it has some direct relations. TRPV4 shows physical association with cholesterol, its precursor, and its derivatives (Kumari et al., 2015). Loop4 alone or in combination with TM4 and/or TM5 of TRPV4 is sufficient to interact with cholesterol, its precursor mevalonate, and other cholesterol derivatives like stigmasterol, and steroid hormone aldosterone (Das & Goswami, 2019; Kumari et al., 2015). Further, the specific location of the TRPV4 gene in chromosome 12q 24.1 flanking two other genes namely MVK and GLTP (genes involved in cholesterol biosynthesis pathway) derived from synteny analysis hints at the reliance and fine regulation of TRPV4 by metabolites of the cholesterol biosynthesis pathway. Notably, this syntenic linkage remains conserved for 450 MY and indicates sterol biosynthesis pathway and TRPV4 function might have shared co-evolution during the radiation of vertebrates.

Taken together, this common involvement of steroid and TRPV4 in temperature regulation, metal entry, steroid-mediated TRP channel functions, and their common take on disease pathology, where mutations in TRPV4 results in phenotypes that are often caused by steroid insufficiency, imply testable crosstalk between TRPV4 and steroids which is worth looking at (Figure 70).
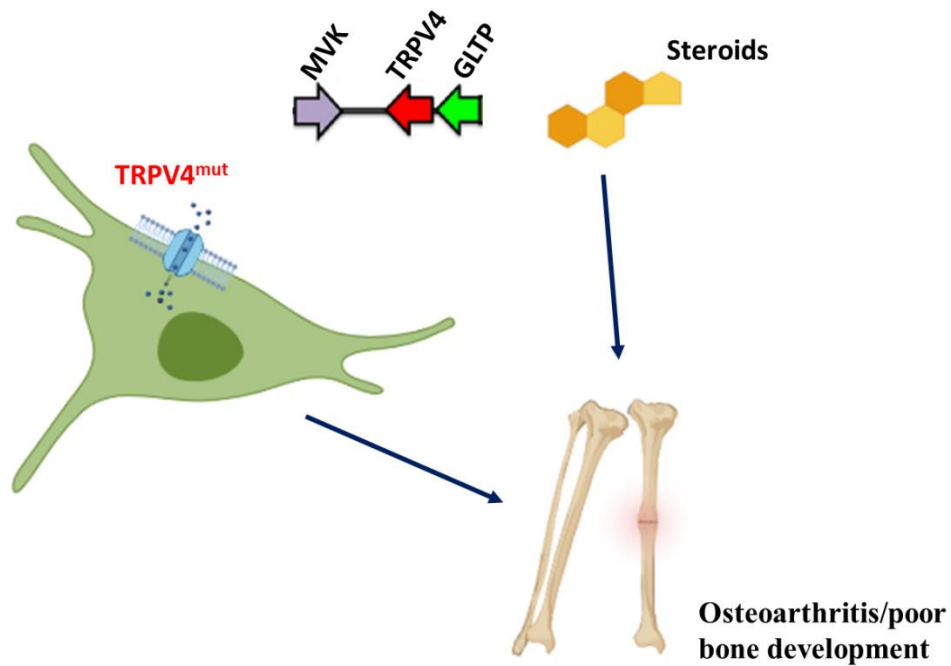
Figure 70: Crosstalk of TRPV4 and steroids. Synteny analysis showing gene location of TRPV4 (red) in between genes involved in the cholesterol biosynthesis pathway MVK (purple) and GLTP (green). Diagram depicting the common involvement of TRPV4 and steroids in bone development. Image Created with BioRender.com.

Importance of TRPV4 channels in steroid production and regulation is a major focus of this work. Work done so far indicate the endogenous localization of TRPV4 in adrenal gland-derived cell line H295R. The work also indicates that the steroid producing properties depends on TRPV4 modulation, at least in part. The metal entry to the cell as well as in the mitochondria may also affect the steroid production.

3.4.3. Clues from role of TRPV4 in temperature regulation and sex determination

Thermosensation is a fundamental property for the survival of living life forms and is basic even at the organism to tissue to cellular level. All creatures need to detect temperature to endure

169

and adjust. In any case, how they distinguish and perceive temperature remains inadequately comprehended. Among the 28 distinctive mammalian TRP channels, 11 individuals display temperature affectability, and each has a different temperature range for activation. Previously depicted as a hypo-osmolarity-activated ion channel, TRPV4 was later found to facilitate large inward currents in *Xenopus oocytes* and human kidney cells (Güler et al., 2002). TRPV4 ion channel is constitutively activated by physiological temperature of the body and also can recognize change in dynamic local temperature of the brain (Shibasaki, K., 2020). This constitutive activation of TRPV4 ion channel by physiological brain temperature is fundamental for typical brain activity. TRPV4 is also expressed in skin keratinocytes where it is activated by internal heat level that cause Ca^{2+} entry inside cells. Throughout the colder time of year, skin drying out is a typical event, and the constitutively active TRPV4 channel is repressed by cold winter temperatures (Shibasaki, K., 2020; Kida et al., 2012). TRPV4 is also reported to be the temperature-sensitive ion channel found in sperm (Mundt et al., 2018; Kumar et al., 2016a). In another report using *TRPV4$^{-/-}$* mice it was noticed that in response to a warm temperature the number and activity level of neurons decreased suggesting the role of TRPV4 in determining the sensitivity rather than the threshold of painful heat detection and assuming a fundamental part in warm hyperalgesia (Todaka et al., 2004). A recent report also suggests temperature reliance of microglia development basically depends on TRPV4 channel movement (Nishimoto et al., 2021).

Different methods of sex determination are detected in vertebrates. Most often, it is genotype-based and in some cases, incubation temperature play a role in it, also known as temperature-dependent sex determination (TSD) (Lang & Andrews, 1994). The sex of most turtles and a wide range of crocodilians is controlled by the climate post fertilization. Eggs hatched at different temperature frequently produce different sex. Apparently, the chemical aromatase (which

can change over testosterone into estrogen) also plays a significant role in temperature-dependent sex determination (Gilbert, SF., 2000).

Mammalian TRPV4 activates at 27–35 °C and thus is an ideal candidate as a potential thermosensor inside the TSD component. Indeed, a recent report suggests the involvement of TRPV4 ortholog (AmTRPV4) in temperature-dependent sex determination of *Alligator mississippiensis*.
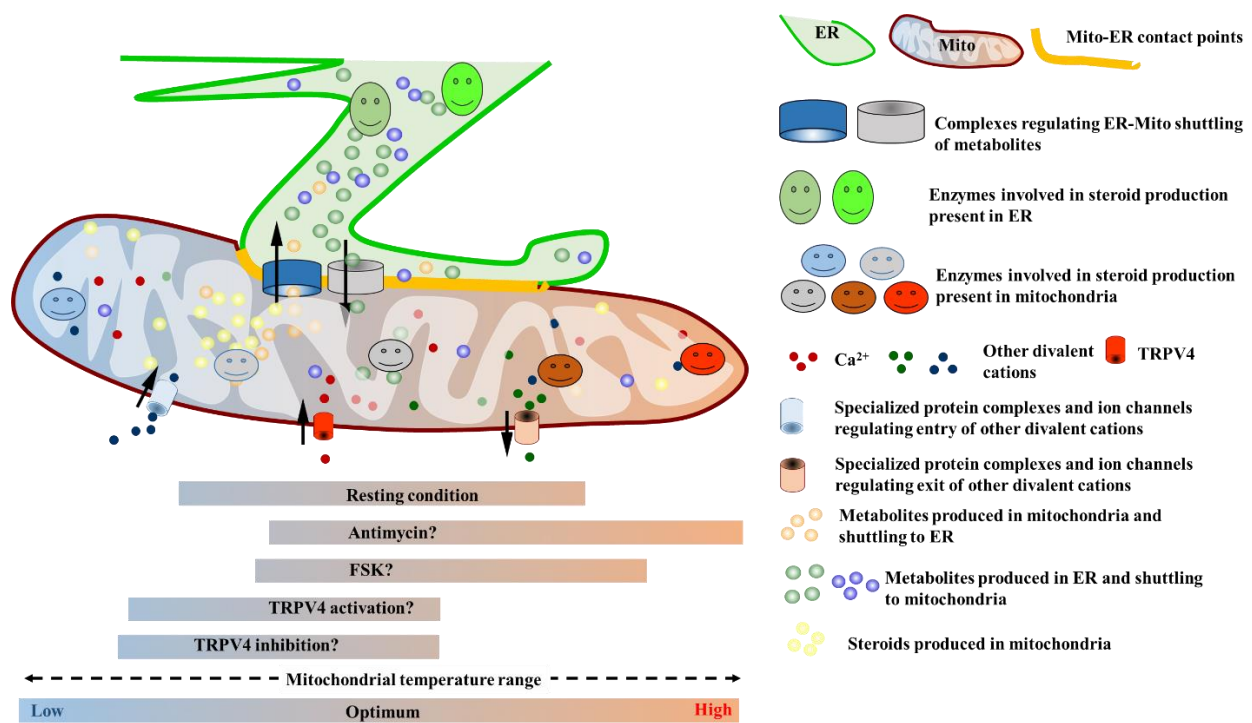
Figure 71: Plausible model for molecular signaling functions at ER-Mito contact sites. ER and mitochondria forms inter-organellar networks known as mitochondria-associated ER membranes (MAMs) that serve as a functional hub for the functions like transfer of Ca^{2+} between ER and mitochondria, regulation of mitochondrial fission, apoptosis, phospholipid synthesis and exchange. Studies revealed that MAMs are also the site for steroidogenesis. While lipid synthesis principally occurs in the ER, it needs the assistance of other organelles like mitochondria since several key enzymes are located on its membrane. An optimum level of mitochondrial temperature is assumed to play a role in steroid production. Modulation of mitochondrial temperature via TRPV4 may lead to alteration of steroid production that may lead to several pathophysiological conditions.

By pharmacological manipulation of TRPV4 channel activity, it was observed that the sexual differentiation processes are affected despite incubation temperature during development suggesting that TRPV4 directly interfere the temperature dependent sex determination, a process which is typically regulated by sex steroids (Yatsu et al., 2015). Results from this study demonstrated the role of TRPV4 in temperature regulation specifically inside mitochondria. TRPV4 modulation could alter mitochondrial temperature that is necessary for complex regulation of cellular functions inside the cells including steroid production. It could also alter the ER-mito contact whose fundamental properties include cell signaling, mitochondrial dynamics, lipid transfer etc. A probable model has been depicted that shows the mitochondrial temperature range by several modulators and likely role of TRPV4 in steroid biology (Figure 71).

Chapter 4

Conclusion

Conclusion and future prospects

The research output from this thesis work suggests the essential role of TRPV4 in various aspects of cellular functions. First, it addresses the significant role of critical amino acids present in the Lipid Water Interface of TRPV4. The percentage of occurrence for most of the amino acids found to be either highly conserved or conserved with minor variations throughout the vertebrate evolution. At least one naturally occurring mutation causing channelopathy, namely L596P alters this pattern significantly. Accordingly, we characterized this mutation and demonstrate subtle differences that are induced by this mutation leading to altered cellular functions. A second mutation study on R616Q variant suggested that cholesterol is a significant controller of TRPV4 and the "gain-of-function" of the mutant channel is caused because of "loss-of-interaction" with cholesterol. TRPV4 channel was found to regulate several factors needed for steroidogenesis like mitochondrial metal entry, temperature, steroidogenic protein expression and ER-mitochondria contact establishment. A possible involvement of TRPV4 in the steroid production has been explored in this thesis work, but more experiment are needed in this area to pinpoint and conclude its specific role. The interaction of TRPV4 with Cyt C has been established.

However, the analysis done in this thesis has been generally confined to a particular activator and inhibitor for TRPV4 and mostly were performed in confocal imaging set up. Calcium imaging experiments indicate a trend of possible types of changes in the "channel gating", that need to be evaluated by techniques that are suitable to detect such really fast events. Therefore, in future, the cellular and channel behaviour need to be accurately accessed in some better instruments, such as by electrophysiology of whole cell or even by single channel recording. Also, TRPV4-mediated modulation of mitochondrial Cu^{2+} and Fe^{2+} needs further detail investigation.

Never-the-less, these findings may have broader significance in understanding the molecular and cellular mechanism behind channelopathy and thus may have implication in the bio-medical research. In several steroid related disorders, the function of TRPV4 can be accessed in future, also through the individual genome sequencing.

Chapter 5

Material and methods

5.1: Materials

5.1.1. Reagents used

Chemical used	Source
4αpdd	Sigma - Aldrich
β-Mercaptoethanol	Biocore Lifesciences
Acetic Acid	MP Biomedicals
Acrylamide	Sigma-Aldrich
Agar agar, Type I	Himedia
Agarose	Lonza
Ampicillin	Sigma-Aldrich
Ammonium Persulphate (APS)	Sigma-Aldrich
Bis-acrylamide	Sigma-Aldrich
Bromophenol Blue	Sigma-Aldrich
Bovine Serum Albumin	MP Biomedicals
Coomassie Brilliant Blue G250	MP Biomedicals
Coverslips	Fisher Scientific
Complete Protease Inhibitor Cocktail	Sigma-Aldrich
Calcium Cholride Dihydrate	Sigma-Aldrich
Cytochrome C (Purified)	Sigma-Aldrich
DAPI	Invitrogen
DMEM	Sigma-Aldrich
DMEM:F12	Sigma-Aldrich
Dimethyl Sulfoxide (DMSO)	Invitrogen and MP biomedicals
dNTP's	NEB
EDTA	Sigma-Aldrich
EGTA	Sigma-Aldrich
Ethanol (Molecular Grade)	Merck Millipore
Ethidium bromide	Sigma-Aldrich
F12 media	Himedia
Fluoromount-G	Southern Biotech
Forskolin	Sigma-Aldrich
Glutathione sepharose	GE healthcare
Glycerol	Sigma-Aldrich
Glycine	MP Biomedicals
Hydrochloric Acid	Rankem
InCCu1	Dr. Elizabeth J. New The University of Sydney, Australia
Ionomycin	Sigma-Aldrich
IPTG	MP biomedical

ITS + Premix	Corning
Kanamycin	Sigma-Aldrich
L-Glutamine	Himedia
Lipofectamine	Invitrogen
Lysozyme	Amresco
Macoy's media	Himedia
Magnesium Chloride	MP Biomedicals
Manganese Chloride	BiocoreLifeSciences
Methanol	MP Biomedicals
Methyl β-Cyclodextrin	Sigma-Aldrich
Mito Thermo Yellow	Dr. Young-Tae Chang Department of Chemistry, POSTECH, Korea
MitoTracker Red	Invitrogen
NuSerum	Corning
Phenylmethylsulfonyl fluoride	Sigma-Aldrich
Phosphate Buffer Saline (10X)	Himedia
Potassium Chloride	MP Biomedicals
Potassium Hydroxide	MP Biomedicals
Pyridoxine·HCl	Sigma-Aldrich
PVDF membrane	Millipore
RDA	Squarix biotechnology
RN1734	Sigma - Aldrich
Rubidium Chloride	MP Biomedicals
Skimmed Milk Powder	Himedia
Sodium Bicarbonate	Sigma-Aldrich
Sodium Chloride	MP Biomedicals
Sodium Dodecyl Sulphate	MP Biomedicals
Sodium Hydroxide	MP Biomedicals
TEMED (Tetramethylethylenediamine)	Sigma-Aldrich
Tris	MP Biomedicals
Triton X-100	Sigma-Aldrich
Trpytone	Himedia
Tween-20	Sigma-Aldrich
Yeast Extract	Himedia

5.1.2. Kits, markers, and enzymes

Kit name	Source
Lipofectamine Cell transfection kit	Invitrogen
QIAprep Spin Miniprep Kit	Qiagen
QIAquick Gel Extraction Kit	Qiagen
Gel Extraction Kit	Qiagen
QuikChange Site-Directed Mutagenesis Kit	Agilent Technologies
PageRuler™ Plus Prestained Protein Ladder	Thermo Scientific
1 kb DNA ladder	Biosphere Corp.
100 bp DNA ladder	Biosphere Corp.
Q5 DNA Polymerase	NEB
EcoRI-HF	NEB
HindIII-HF	NEB
SalI-HF	NEB
T4-DNA Ligase	NEB
Cortisol competitive ELISA Kit	Invitrogen
DHEA-S competitive ELISA Kit	Invitrogen
Progesterone competitive ELISA Kit	Invitrogen

5.1.3. Bacterial strains

DH5α	CG lab, NISER
DE3	CG lab, NISER

5.1.4. Primary antibodies

Antibody	Host	Source	Application	Dilution used
cytochrome c	Mouse	Abcam	WB,IF	1:500
TRPV4	Rabbit	Almone lab	IF, WB	1: 500
β-actin	Mouse	Sigma	WB	1:500
HSD3b1	Rabbit	Abcam	WB	1:500
CYP17A1	Rabbit	Abcam	WB	1:500
CYP11B1	Rabbit	Abcam	WB	1:500

CYP11B2	Rabbit	Abcam	WB	1:500
Aromatase	Rabbit	Abcam	WB	1:500
CYP11A1	Rabbit	Abcam	WB	1:500
Caveolin-1	Mouse	Sigma-Aldrich	IF	1:500
GST antibody	Mouse	GE Healthcare	WB	1:500
Phospho tyrosine	Mouse	Abcam	IF	1:200
Vinculin	Mouse	Merck	IF	1:200
FAK	Mouse	Merck	IF	1:200
Cholera Toxin B-594	Mouse	Invitrogen	IF	1:200

WB: Western blot, IF: Immunofluorescence

5.1.5. Secondary antibodies

Antibody	Host	Source	Use	Dilution
Alexa-488-labelled anti-rabbit	Chicken	Molecular Probes	IF	1:1000
Alexa-594-labelled anti-rat	Chicken	Molecular Probes	IF	1:1000
Alexa-594-labelled anti-mouse	Chicken	Molecular Probes	IF	1:1000
HRP-labelled anti-mouse	Donkey	GE Healthcare	WB	1:10,000
HRP-labelled anti-rabbit	Donkey	GE Healthcare	WB	1:10,000

5.1.6. Constructs used

Vector	Expression system	Source
pGP-CMV-GCaMP6f	Mammalian	Addgene
Caveolin-1-RFP	Mammalian	Addgene
Mito Pericam EYFP	Mammalian	(Nagai et al., 2001)
MitoDsRed	Mammalian	Clontech
pGEX6P1	Bacterial	Dr. P V Alone (NISER)
GST-TRPV4-TM4-Loop4-TM5 pGEX6P-1	Bacterial	Prepared in CG lab
GST-TRPV4-R616Q-TM4-Loop4-TM5 pGEX6P-1	Bacterial	Prepared in CG lab
GST-TRPV4-MTS pGEX6P-1	Bacterial	Prepared in CG lab

GST-TRPV4-MTS-L596P pGEX6P-1	Bacterial	Prepared in CG lab
GST-TRPV4-MTS-R616Q pGEX6P-1	Bacterial	Prepared in CG lab
GST-TRPV4-MTS-F617L pGEX6P-1	Bacterial	Prepared in CG lab
GST-TRPV4-MTS-L618P pGEX6P-1	Bacterial	Prepared in CG lab
GST-TRPV4-MTS-V620I pGEX6P-1	Bacterial	Prepared in CG lab
pEGFPN3	Mammalian	Prof. J. Berreiter-Hahn (Frankfurt, Germany)
TRPV4-GFP pEGFPN3	Mammalian	(Becker et al., 2009)
TRPV4-L596P-GFP pEGFPN3	Mammalian	Prepared in CG lab
TRPV4-R616Q-GFP pEGFPN3	Mammalian	Prepared in CG lab
TRPV4-L618P-GFP pEGFPN3	Mammalian	Prepared in CG lab
TRPV4-V620I-GFP pEGFPN3	Mammalian	Prepared in CG lab
TRPV4-MTS-GFP pEGFPN3	Mammalian	Prepared in CG lab
TRPV4-MTS-L596P-GFP pEGFPN3	Mammalian	Prepared in CG lab
TRPV4-MTS-R616Q-GFP pEGFPN3	Mammalian	Prepared in CG lab
TRPV4-MTS-F617L-GFP pEGFPN3	Mammalian	Prepared in CG lab
TRPV4-MTS-L618P-GFP pEGFPN3	Mammalian	Prepared in CG lab
TRPV4-MTS-V620I-GFP pEGFPN3	Mammalian	Prepared in CG lab
pmCherry-C1	Mammalian	Takara
TRPV4-FL-WT-pmCherryC1	Mammalian	Prepared in CG lab
TRPV4-FL-L596P-pmCherryC1	Mammalian	Prepared in CG lab

5.1.7. Cell lines, primary cells, and tissue

F11	Prof. F. Hucho (FU, Berlin)
HaCaT	Prof. F. Hucho (FU, Berlin)
Saos-2	Prof. F. Hucho (FU, Berlin)
H295R	ATCC
Mouse adrenal gland	NISER, Bhubaneswar, India
Mesenchymal stem cells (Mouse)	NISER, Bhubaneswar, India

5.2. Methods

5.2.1. Methods related to molecular biology

5.2.1.1. Overview of construct preparation

Using a specific set of forward and reverse primers, desired DNA fragments were amplified by PCR amplification. The PCR amplified product, as well as the vector, were then digested with restriction enzymes to obtain cohesive overhanging ends. Using a gel extraction kit, the restriction enzyme digested PCR product and the vector was extracted from agarose gel. They were ligated and transformed into competent *E. coli* DH5α strain. In the antibiotic containing LB plates, the transformed *E. coli* were allowed to grow. The positive colonies were then picked and grown in LB media with antibiotics. Using a DNA miniprep kit, plasmid DNA was isolated. The isolated DNA was again restriction digested to confirm the presence of the desired fragment and later on sequence-verified using specific primers.

5.2.1.2. Polymerase Chain Reaction (PCR)

To incorporate specific regions of a gene into the desired expression vector, a polymerase chain reaction was conducted. For the sub-cloning of a specific region or entire gene into another vector, forward and reverse primers were designed to acquire specific restriction sites. The basic components of a PCR master mix are DNA template, forward primer, reverse primer, 10 X polymerase buffer, DNA polymerase enzyme, dNTP mix, and MilliQ water. The required conditions for PCR reactions have been tabulated below. All PCR-amplified DNA was further confirmed by agarose gel electrophoresis.

PCR reaction for Cloning:

Autoclaved MilliQ water	16.5 µl
10X buffer	2.5 µl
10 mM Dntp	2.5 µl
Forward Primer (25 µM)	1 µl
Reverse Primer (25 µM)	1 µl
DNA template (100 ng/µl)	0.5 µl
DNA Polymerase	1 µl
Total	25 µl

PCR cycle for cloning into pmCherry-C1 vector:

Step	Cycles	Temperature	Time
1	1	98°C	5 minutes
2	35	98°C	30 seconds
		55°C	30 seconds
		72°C	1 minute
3	1	72°C	5 minutes
4	1	4°C	∞

PCR cycle for cloning into pGEX-6P1 vector:

Step	Cycles	Temperature	Time
1	1	98°C	2 minutes
2	30	94°C	30 seconds
		58°C	1 minute
		72°C	30 seconds
3	1	72°C	10 minutes
4	1	4°C	∞

List of primers used for cloning into pmCherryC1 and pGEX-6P1vector

Construct	Primer sequence (5'-3')
TRPV4-FL WT/L596P **Forward primer RE** HindIII **Reverse primer RE** SalI	Forward Primer: CTCGAAGCTTATATGGCGGATTCCAGCGAAG Reverse Primer: GATAGTCGACCTAGAGCGGGGCGTCATC
GST-TRPV4-WT-MTS, GST-TRPV4-R616Q-MTS, GST-TRPV4-F617L-MTS, GST-TRPV4-L618P-MTS, and GST-TRPV4-V620I-MTS **Forward primer RE** BamHI **Reverse primer RE** SalI	Forward Primer: GTAGGATCCATGTTCACCCGTGGGCTGAAG Reverse Primer : GTTGTCGACTGAAGCGTAGCCGATCATGAA

5.2.1.3. Agarose gel electrophoresis

For electrophoretic separation of dsDNA, a horizontal agarose gel electrophoresis in 0.8-1.2% agarose gel (depending on the length of the dsDNA that needs to be separated) was used in 1X TAE buffer. Desired percentage of gel was prepared by mixing agarose powder with 1X TAE buffer and heated in a microwave till it becomes clear. For visualization of DNA in the gel, Ethidium Bromide (EtBr) at a concentration of 0.1-0.5μg/ml was added to the hot agarose solution. The final mixture was poured inside the casting tray containing a comb of desired thickness and allowed to solidify at room temperature. The comb was slowly removed after the solution became solidified and the gel along with the casting tray was carefully transferred into an electrophoresis chamber filled with electrophoretic buffer (1X TAE). DNA samples were mixed with DNA

loading dye and added to the wells. The device was associated with a steady power supply source. The tracking dyes present in the loading buffer enable visualization of DNA migration. Once there is sufficient DNA migration, electrophoresis was stopped and the gel was visualized under an ultraviolet trans-illuminator.

Solutions and buffer required:

(1 X) TAE buffer: 40 mM Tris/Acetic acid, pH7.8; 1 mM EDTA, pH 8.0

(5 X) DNA loading buffer: 40% (w/v) Sucrose, 240 mM Tris/Acetic acid, pH7.8, 5 mM EDTA, pH 0.8, 0.25% (w/v) Bromophenol blue, 0.25% (w/v) Xylene cyanol FF.

5.2.1.4. Restriction digestion

The PCR product (insert) of the desired gene was run on agarose gel electrophoresis and the correct size band was excised out using a clean scalpel. DNA from the cut gel was extracted using Qiagen Gel Extraction kit using the manufacturer's guidelines. Both the extracted PCR product and the vector were subjected to restriction digestion using specific restriction enzymes for 3 hours at 37°C.Two sets of restriction digestion reaction were set, one for insert DNA and another for vector DNA. The restriction digestion reaction requires DNA (Insert/vector), restriction enzymes, 1X CutSmart Buffer and Autoclaved MilliQ water. Approximately 1μg of dsDNA was used for the restriction digestion reaction and the reaction volume thus varies from 10-25 μl based on the concentration of DNA.

5.2.1.5. Ligation of insert and vector

The digested insert and the vector DNA were run on a 0.8% Agarose gel. The correct sized bands were excised out and gel extraction was done using Qiagen Gel Extraction Kit. Both insert

and vector DNA concentration was measured using Nanodrop (Thermo Scientific). A ligation mixture was prepared with the purified insert and vector in the ratio of 3:1, 1X T4 Ligation buffer (NEB), T4 DNA Ligase enzyme (NEB), and autoclaved MilliQ water. Depending upon the concentration of the insert and vector DNA, the reaction volume varied from 10-15 µl. The ligation mixture was incubated overnight at 16°C.

5.2.1.6. Transformation

E. coli competent cells (DH5α or DE3 strain) were taken out from -80°C and kept on ice for 5 minutes. 50µL of comp cells were taken in a 1.5mL tube and approximately 100 ng of purified plasmid DNA or 3.5-4 µl of the ligated product was added to the competent cells. After 10 minutes of incubation on ice, heat shock for 45 seconds was given by dipping the tube in a water bath set at 42°C. Immediately after heat shock, the tube was kept on ice for additional5 minutes. 900 µL LB media was added to the mix. The cells in the tube were allowed to grow for 1 hour at 37°C and 220 RPM in an incubator-shaker. After 1 hour, the transformed cells were centrifuged at 13,000 RPM for 1 minute. Around 800 µl of the supernatant was discarded and the bacterial pellet was re-suspended in the remaining media. Kanamycin (50mg/ml) or Ampicillin (100mg/ml) containing LB plates were pre-incubated at 37°C and the bacterial suspension was added to these plates. Using glass beads (MP Biomedicals) the bacterial culture was spread all over the antibiotic plate. The plates were incubated at 37°C for 12-14 hours and single colonies were obtained thereafter.

LB Media composition (for 1 liter)	
Yeast extract	5 gm
Tryptone	10 gm
Sodium Chloride	10 gm

5.2.1.7. Competent cell preparation by RbCl method

Competent *E. coli* cells were prepared using the Rubidium Chloride method. Two different bacterial strains were made: DH5α and DE3 using the below-mentioned protocol. A single colony *E. coli* bacterium (DH5α/ DE3) was picked from a freshly streaked LB plate and inoculated in 3 ml of LB broth. The culture was allowed to grow overnight at 37°C and 220 RPM. 1-2 ml of this grown culture was then added to a freshly prepared LB liquid medium and allowed to grow at 37°C and 220 RPM until the culture reached an OD between 0.4-0.6 at 600nm. Once the desired OD was reached, the culture was placed on ice for 15 minutes. The culture was then pelleted at 4500 RPM for 10 minutes at 4°C. The supernatant was discarded and the pellet was then re-suspended in 40ml TFBI buffer and incubated in ice for 15 minutes. The solution was again centrifuged at 4000 RPM for 5 minutes at 4°C. The supernatant was discarded and the pellet was re-suspended in 4 ml of TFBII buffer while keeping the tube in ice. This bacterial suspension was then aliquoted in small volumes of 50-100 µl in pre-chilled microcentrifuge tubes. These competent cells containing tubes were then snap-chilled in liquid nitrogen and stored at -80°C for further use.

Composition of TFBI buffer:

For 50 ml	
RbCl (100 mM)	0.725 gm
$MnCl_2$-$4H_2O$ (50 mM)	0.5 gm
Potassium acetate (30 mM)	0.147 gm
$CaCl_2$-$2H_2O$ (10mM)	0.075 gm
Glycerol (15% final)	7.5 ml
Autoclaved MilliQ water	42.5 ml
pH was adjusted to 5.8 with acetic acid, filter sterilized, and stored at 4°C away from light.	

Composition of TFBII buffer:

For 15 ml	
MOPS (10mM)	0.031 gm
RbCl (10mM)	0.018 gm
$CaCl_2, 2H_2O$ (75mM)	0.165 gm
Glycerol (15% final)	2.25 ml
Autoclaved MilliQ water	12 ml
pH was adjusted to 6.5 with KOH, filter sterilized, and stored at 4°C away from light.	

5.2.2. Methods related to protein and biochemistry

5.2.2.1. SDS-PAGE

SDS-PAGE separates proteins based on their molecular weight. Using Biorad mini-apparatus, SDS-PAGE was performed with 10-12% acrylamide gel. Protein samples were completely denatured by adding Laemmli buffer (final concentration 1X) and then heated at 95°C for 5 minutes. A pair of clean glass plates with 10 cm width and 7 cm height separated by a 1mm thickness spacer was set up in the cassette. Resolving gel was prepared according to the composition tabulated below and about 5 cm of the cassettes were filled up with the gel mixture that was allowed to polymerize. The top-most surface of the resolving gel was smoothened by the gradual addition of water to create a thin film coating over it. The water was decanted after polymerization and around 2 ml of stacking gel was added over the resolving gel. A 10 or 15 well comb was inserted into the gel for well formation. After polymerization of the stacking gel, the comb was removed carefully without disturbing the wells. Cassettes were then inserted vertically into the electrophoresis chamber filled with 1X SDS running buffer. Using a Hamilton syringe, denatured protein samples were loaded into the wells. The apparatus was then connected to a constant power supply of 10 mAmp. Protein migration within the gel was visualized by observing

the movement of bromophenol blue present in the Laemmli buffer. When the dye front approached the end of the gel, electrophoresis was stopped. The gel was taken out and the separated proteins in the gel were visualized by Coomassie blue staining. For Western blot analysis, the gel was transferred on a PVDF membrane and processed further.

12% SDS-PAGE gel composition			
Resolving		**Stacking**	
30% Acrylamide Solution	1.9 ml	30% Acrylamide Solution	500 µl
Autoclaved MilliQ water	1.7 ml	Autoclaved MilliQ water	2.1 ml
Tris (pH=8.8)	1.3 ml	Tris (pH=6.8)	380 µl
10% SDS	50 µl	10% SDS	30 µl
APS	50 µl	APS	30 µl
TEMED	8 µl	TEMED	4 µl

10X SDS running buffer (500 ml)	
Tris Base	15.1 gm
Glycine	94 gm
SDS	5 gm
The volume was made up to 500 ml by addition of double distilled water	

5X Laemmli buffer (for 10 ml)	
0.5 M TrisHCl (pH=6.8)	1.25 ml
β-Mercaptoethanol	0.5 ml
Glycerol	5 ml
20% SDS	1 ml
Bromophenol Blue	0.01 gm
Autoclaved Milli Q water	2.6 ml

5.2.2.2. Coomassie staining

The proteins in a gel separated by SDS-PAGE are commonly stained by 0.1% Coomassie blue dye, dissolved in 10% glacial acetic acid and 50% methanol. The gels are stained with staining solution by constant agitation on a rocker overnight. Excess dye gets washed out by agitating the gel in a destaining solution containing acetic acid/methanol for 2 hours. The dye binds to proteins primarily through basic amino acids (primarily arginine, lysine, and histidine). Protein-binding causes the dye to change from reddish-brown to bright blue colour, thus making the protein bands visible to the naked eye.

Staining Solution (for 500 ml)	
Coomassie Brilliant Blue G-250	0.5 gm
Methanol	250 ml
Glacial Acetic Acid	50 ml
Autoclaved milli Q water	200 ml

Destaining Solution (for 500 ml)	
Methanol	250 ml
Glacial Acetic Acid	50 ml
Autoclaved milli Q water	200 ml

5.2.2.3. Western blot analysis

After the proteins were separated by SDS-PAGE, they were transferred onto a PVDF membrane by the semi-dry method. Briefly, polyacrylamide gels were incubated in Western Transfer buffer for 5 minutes. Methanol pre-soaked PVDF membrane and Whatman paper were also soaked in the same transfer buffer. On the semi-dry transfer apparatus, the Whatman paper pad was positioned first and above it, the PVDF membrane was placed. The polyacrylamide gel was placed above the membrane and another Whatman paper pad was placed above this gel. At

every step, air bubbles were removed by rolling western blot roller above them. The semi-dry transfer unit was connected to a constant power supply and the electro-transfer was allowed to continue for 1 hour at a constant voltage of 17V. After the transfer, the PVDF membrane was blocked with 5% non-fat milk or BSA dissolved in 1X TBS-T buffer. The membrane was then incubated with primary antibody overnight at 4°C. After that, the membrane was washed thrice with 1X TBS-T and incubated in a secondary antibody for 1-2 hours at room temperature. The blot was then washed thrice with 1X TBST and developed by using SuperSignal™ West Femto reagent (ThermoScientific). The chemiluminescence signals were detected in ChemiDoc XRS+ (Bio-Rad, CA, USA). The relative abundances of protein levels were quantified using BioRad Quantity One 1D analysis software, normalized against housekeeping protein levels, and expressed as a percentage of the control value.

TBS (5X) for 500 ml	
Tris Base (20 mM)	6.05 gm
NaCl (150 mM)	21.915 gm
Volume adjusted by addition of autoclaved MilliQ water	

Western Transfer Buffer (for 1 liter)	
Tris	3.04 gm
Glycine	14.42 gm
Methanol	200 ml
SDS	0.373 gm
Volume adjusted by addition of autoclaved Milli Q water	

5.2.2.4. Protein expression and purification

Escherichia coli strain BL21DE3 was transformed by heat shock with a plasmid coding for TRPV4 MTS and its mutants fused with GST (GST-TRPV4-WT-MTS, GST-TRPV4-R616Q-

MTS, GST-TRPV4-F617L-MTS, GST-TRPV4-L618P-MTS, and GST-TRPV4-V620I-MTS). All these constructs were cloned in pGEX-6P1, which is a protein expression vector. Their cultures were made into glycerol stocks and kept at -80°C for long-term use. The glycerol stocks were revived as and when required by adding a small volume of the culture into 50ml LB liquid medium supplemented with 100 mg/ml Ampicillin and allowed to grow overnight at 37°C/220 RPM. The starter culture was then transferred to another flask containing 250 ml of sterile LB liquid supplemented with 100 mg/ml Ampicillin and was allowed to grow at 37°C/220 RPM until it reached an OD of 0.6-0.8 at 600 nm. *E. coli* cells were then induced to express the proteins by isopropyl thio galactoside (IPTG) (0.25 milliM) for 2 hours. The bacteria from the culture were then pelleted down by centrifuging at 10,000 RPM for 10 minutes in a centrifuge using 250ml Oak Ridge tubes. Thereafter, the cells were lysed by incubating in lysis buffer (1X PBS pH 7.4, lysozyme, protease inhibitor, PMSF) followed by freeze-thaw cycles in liquid nitrogen. The lysed extracts were cleared by spinning at 35000 RPM at 4°C for 2 hours. For protein purification, the cleared lysate containing the desired expressed proteins were incubated with Glutathione sepharose beads for 12 hours at 4°C with constant rotation after which the beads were washed with GST wash buffer followed by elution of bound proteins from the beads using elution buffer (20mM Glutathione reduced, 50mM Tris-Cl pH 8.0). Protein estimation was performed by using the Bradford estimation method immediately after protein purification.

Composition of Lysis buffer (50 ml)	
1X PBS	50 ml
Protease Inhibitor (2X)	2 ml
Lysozyme	500 μl
PMSF	500 μl

Composition of GST wash buffer(100ml)	
1M Tris-Cl (pH 7.5)	5ml
NaCl	1.5g
0.5M EDTA	200 µl
EGTA	38mg
H_2O	95ml

5.2.2.5. Protein quantification by bradford estimation

The "Bradford Reagent" is an acidic stain that becomes blue when it interacts with the protein. The subsequent absorbance is observed at 595 nm in a microplate reader. 1mg/ml BSA solution was prepared to make a standard curve by putting BSA solution from 0 to 16 µl in a 96 well plate in replicate. MiliQ water was added to make a final solution of 20µl in all wells. 2 µl unknown protein samples were added in other wells in replicate and MiliQ water was added to make the final volume 20µl in all wells. 180 microliters of Bradford reagent were added to each well and the wells were checked for bubbles. The 96 well plate was then kept inside the microplate reader and was allowed to be mixed inside. The absorbance was read at 595 nm and a standard curve was derived. The final protein concentrations were calculated considering the respective dilution factor.

5.2.2.6. GST pull-down assay for identifying TRPV4-MTS interaction with Cyt C

To explore if TRPV4-MTS interacts with Cyt C, pull-down experiments were performed using purified Cyt C (Sigma). TRPV4-MTS and its mutants were cloned into pGEX-6P1-GST vector and these fusion proteins were expressed in *E. coli*. Only GST was used as a negative control. After expression and purification, GST-tagged proteins were immobilized on Glutathione Sepharose beads for 12 hours at 4°C. Subsequently washed with GST wash buffer and 30 µL of

Cyt C (50μM protein) were added onto the sepharose beads bound with GST-TRPV4-MTS or mutant proteins and incubated for 4 hours at 4°C. This experiment was also done in the presence or absence of Cu^{2+}, Fe^{3+}, Mn^{2+}, Ni^{2+} and Zn^{2+} (100μM each). Thereafter, the beads were washed 3 times with GST wash buffer, and all protein/s bound to the beads were eluted in 100 μL of elution buffer (20 mM Glutathione reduced 50 mM Tris-Cl pH 8.0). Eluted samples were further analyzed by 12% sodium dodecyl sulfate-polyacrylamide gel electrophoresis (SDS–PAGE) and Western blot analysis with anti-Cyt C antibodies (Abcam).

5.2.2.7. Gel-shift assay

hTRPV4 fragment TM4-Loop4-TM5 and its mutant R616QTM4-Loop4-TM5 cloned into the pGEX-6P1 vector, expressed in *Escherichia coli* by IPTG-induction and purified further as described before. The purified proteins were normalized for molar concentrations and used for gel-shift experiments in the absence and presence of cholesterol (Sigma-Aldrich). After purification, 5 mg of each protein were taken and incubated with cholesterol in different concentrations for 1 hour at 40°C. Thereafter, the solution was taken in Laemmli buffer, separated in 12% SDS-PAGE followed by Western blot analysis using mouse monoclonal anti-GST antibody (1:500).

5.2.2.8. Measurement of hormones

Supernatants from the cell culture experiments were collected from each well and stored at -80°C. Hormones in culture medium were measured by competitive ELISA using the manufacturer's recommendations (Invitrogen, Cortisol [Cat # EIAHCOR], DHEA-S [Cat # EIADHEA], and Progesterone [Cat # EIAP4C21]). The readings were taken using a microplate reader (Bio-Rad iMARK) at 450 nm.

5.2.3. Methods related to cell biology and imaging

5.2.3.1. Cell culture and transfection

Saos-2 cells were grown in Macoy's media supplemented with 10% FBS (PAN), 100 mg/ml Penicillin-Streptomycin and Amphotericin-B. Cells were cultured in a humidified incubator maintained at 5% CO_2 and 37°C. Saos-2 cells were transiently transfected with TRPV4-Wt-GFP, TRPV4-L596P-GFP, TRPV4-R616Q-GFP pEGFPN3, or Caveolin 1-RFP (for co-localization studies) using Lipofectamine-3000 (Invitrogen). For calcium imaging studies, Saos-2 cells were transfected with TRPV4-WT-pmCherryC1 and TRPV4-L596P-pmCherryC1 plasmids. Each of these was co-transfected with ultrasensitive protein Ca^{2+}-sensor pGP-CMV-GCaMP6f. Approximately 24 hours after transfection, doubly transfected cells were imaged.

HaCaT cells were grown in RPMI media supplemented with 10% FBS (PAN), 100 mg/ml Penicillin-Streptomycin and Amphotericin-B. Cells were cultured in a humidified incubator maintained at 5% CO_2 and at 37°C. HaCaT cells were transiently transfected with TRPV4-Wt-RFP (for co-localization studies with Cyt C) using Lipofectamine-3000 (Invitrogen). Cells were fixed with 4% PFA 36-hour post-transfection.

H295R human adrenocortical carcinoma cell line was obtained from the American Type Culture Collection (ATCC, catalog no. CRL-2128). The cells were cultured in 75-mL flasks in DMEM/F-12supplemented with 1.2 g/L $NaHCO_3$, 2.5% NuSerum, 2 mg/L pyridoxine-HCl, and 1% ITS + Premix at 37°C with 5% CO_2 atmosphere. All experiments were performed using cells between passages 7 and 15.

Mouse mesenchymal stem cells isolated from bone marrow were cultured in Dulbecco's modified Eagle's medium (DMEM) supplemented with 10% fetal bovine serum and Amphotericin-Bat37°C with 5% CO_2 atmosphere.

5.2.3.2. Cholesterol reduction/depletion

For cholesterol reduction/depletion of Saos-2 or F11 cells, either pravastatin or methyl β-cyclodextrin (β-MCD) or both were used. Pravastatin reduce cholesterol biosynthesis by inhibiting HMG CoA reductase which is the rate-limiting enzyme in cholesterol synthesis (Valentovic, M., 2007) and βMCD sequesters cholesterol in its hydrophobic core into soluble inclusion complexes (Mangoura et al., 2016). After 24 hours of transfection, Pravastatin (1μM) was added to the cells in FBS-free media and allowed to act for 12 hours before the cells were fixed by 4% PFA or proceeded for live-cell imaging. βMCD(5mM) was added 15 minutes before live-cell imaging or fixation.

5.2.3.3. Immunocytochemistry

For immuno-cytochemical analysis, cells grown on coverslips were fixed with 4% PFA. The cells were permeabilized (wherever applicable) with 0.1% Triton X-100 in PBS (5 min). Subsequently, the cells were blocked with 5% BSA for 1 h. After incubation with primary antibodies at 4°C in PBST buffer (PBS supplemented with 0.1% Tween-20), excess antibodies were washed off with three times PBST wash. Coverslips were then treated with AlexaFluor labelled secondary antibodies. Blocking peptides (Peptide to antibody 1:1, by volume) were used to confirm the specificity of the immunoreactivity. Cells were then washed twice with 1X PBS (Himedia), treated with DAPI (Invitrogen, 1:1000 dilution), and mounted by using Flouromount-G (Southern Biotech). Cells were observed using Olympus FV3000 Confocal Microscope.

5.2.3.4. Cytoplasmic Ca^{2+}-imaging and quantification

Saos-2 cells were transfected with TRPV4-WT-pmCherryC1 and TRPV4-L596P-pmCherryC1 plasmids. Each of these was co-transfected with ultrasensitive protein Ca^{2+}-sensor

pGP-CMV-GCaMP6f. Approximately 24 hours after transfection, doubly transfected cells were imaged for 400 frames whereby cells were activated by adding 4αPDD (1 µM, if not mentioned specifically) at the 10th frame. Snaps of doubly transfected cells were acquired using 488 nm and 561 nm laser. Time series of live cells were acquired using 488 nm laser (0.4%) and images were acquired at a rate of 1 frame/4.97 second (for total of 1988 seconds). Change in intensity of the ultrasensitive protein Ca^{2+}-sensor pGP-CMV-GCaMP6f in each frame was quantified. Each cell was considered to be a single ROI and subsequently, the changes in intensity were quantified using Fiji software. The initial value was considered to be 1 and accordingly, the changes were calculated and the graphs were plotted using GraphPad Prism 7 software. Time taken to reach the maximum response after stimulation is considered as the relative responsiveness. The total area under the curve has been considered as the relative representation of the total amount of Ca^{2+}-influx each cell undergoes. Similarly, the time taken to reach half the maximum value from the maximum value is considered as the relative estimation of channel closures. The fluorescence intensity at the end of the experiment is also considered as the relative estimation of channel closures.

H295R cells were transiently transfected with pGP-CMV-GCaMP6f using Lipofectamine (Invitrogen). Approximately 24 hours after transfection, transfected cells were imaged for 500 frames whereby cells were activated by adding 5µM 4αPDD at the 100th frame. Time series of live cells were conducted using 488 nm laser and images were acquired for total of 217 seconds at the rate of 1 frame/1.085 second. Each cell was considered to be a single ROI and then the change in intensity was quantified using Fiji software. The initial value was considered to be 1 and accordingly, the changes were calculated and the graphs were plotted using GraphPad Prism 7 software. All images were acquired by using Olympus FV3000 Confocal Microscope.

5.2.3.5. Mitochondrial Ca^{2+}-imaging

Mitochondrial Ca^{2+}-fluctuations were recorded using mitochondrial ratiometric pericam probes. H295R cells were transiently transfected with ratiometric-pericam using Lipofectamine (Invitrogen). Approximately 24 hours after transfection, images were acquired sequentially by alternatively exciting with 405 nm and 488 nm laser with the use of a Coherent Solid-state monochromatic laser source. Emission was collected with continuously variable band path filter (spectral detector) through Dual-band dichroic mirror 405/488 with emission bandwidth set between the range 500-550nm. Ca^{2+}-binding to ratiometric pericam increases absorbance at 495 nm, thus the fluorescence ratio (fluorescence intensity at 488 nm /fluorescence intensity at 405 nm) was calculated for the entire cell. Changes in fluorescence ratio (reflecting variation in mitochondrial Ca^{2+}-levels) were then expressed as a function of time. All images were acquired as a time series by using Olympus FV3000 Confocal Microscope.

5.2.3.6. FRAP

Saos-2 cells were grown on a glass coverslip and Caveolin1-RFP along with hTRPV4-Wt-GFP or hTRPV4-L596P-GFP were co-expressed by transient transfection using lipofectamine 3000 (Invitrogen). In some experiments, only Caveolin-1-RFP, only hTRPV4-Wt-GFP, and only hTRPV4-L596P-GFP were expressed. Around 36 hours after transfection, the cells were used for FRAP experiments. In each case, at least 15 or more region-of-interest (ROI) values were measured. For cholesterol reduction, cells were maintained in serum-free media and in presence of β-MCD (5 mM, Sigma-Aldrich) to reduce membrane cholesterol 15 min before performing the FRAP experiments.

The cells were subjected to time series for total 30 frames (approximately 2.58 min in total duration, time interval between each frame is 5.96 sec) and photobleaching was performed at the 3rd frame (using 100% laser at 488/561λ nm).

The mobile fraction was calculated as "the fraction (%) of the recovered molecules at the end of experiment (typically in 2.58 min). While cell to cell variation can be observed by individual cell traces, the average value is considered as the final value. Based on these average values, the mobile and immobile fraction was calculated.

In all cases, the ROI size and shape was maintained as constant. Original Fluorescence value in the ROI at T1 was considered as 100% for each ROI. All the values were normalized to this T1 values and then plotted using GraphPad Prism.

For F11 cells-based FRAP work, cells were grown on a glass coverslip and hTRPV4-Wt-GFP or hTRPV4-R616Q-GFP were expressed by transient transfection. Around 36 h after transfection, the cells were used for FRAP experiments. In each case, at least 30 or more region-of-interest (ROI) values were measured.

5.2.3.7. Flow cytometry

H295R cells were harvested by scraping and immediately fixed with 4% paraformaldehyde (PFA) for 10 min at RT. Next, the cells were suspended in FACS buffer and stored at 4°C. These cells were stained with TRPV4 antibody for 30 minutes on ice. After incubation, excess unbound antibody was removed by washing with FACS buffer (1X PBS, 1% BSA, 0.01% NaN_3). Then, secondary fluorochrome-conjugated AF488 was added and incubated for 30 minutes, followed by washing with FACS buffer. Rabbit IgG was used as an isotype control. Finally, the cells were acquired using a BD FACS CaliburTM flow cytometer (BD Biosciences) and analyzed using CellQuest Pro software (BD Biosciences). Approximately ten thousand cells were acquired per

sample. The percentages of cells expressing the markers were represented in dot-plots while the MFI values represent the expression levels of the markers per cell.

5.2.3.8. Mitochondrial Cu^{2+}-imaging

InCCu1, a ratiometric fluorescent sensor selective to mitochondrial Cu(I) was used for H295R mitochondrial copper entry analysis (Shen et al., 2016). H295R cells were treated with media containing vehicle control (phosphate-buffered saline, PBS) or copper sulfate (100 μM) and then washed 3 times with PBS. After 15min incubation, cells were washed 3 times with PBS and incubated in 1 mL solution of the desired concentration of InCCu1 (0.1 or 0.2 μM) in H295R media. After 15 minutes, cells were washed 3 times with PBS and imaged in complete media immediately after treatment. Emission was collected in the blue channel (450/50 nm) and red channel (585/15 nm) upon excitation at 405 nm. With increasing amounts of copper, the fluorescence at 480 nm keeps unchanged, while fluorescence at 600 nm decreases. The ratio was determined by I425-520/I570-670(Blue/Red). All images were acquired by using Olympus FV3000 Confocal Microscope.

5.2.3.9. Mitochondrial Fe^{2+}-imaging

RDA is a mitochondria-specific fluorescence sensor for Fe^{2+}used for the assessment of alterations of the mitochondrial chelatable iron pool. This especially labels mitochondria of viable cells, RDA fluorescence (λ max 598 nm) is strongly and stoichiometrically (3:1) quenched by Fe^{2+} ions.H295R cells, grown on 25mm coverslips were incubated with RDA (0.5 μM, prepared from stock solutions of 1mM in DMSO) for 15 min at 37°C. Cells were washed subsequently three times and incubated for another 15 minutes at 37°C. The red fluorescence of RDA is excited at

λexc. =561 nm and emissions were collected with continuously variable band path filter between the ranges 570nm to 620nm. All images were acquired by using Olympus FV3000 Confocal Microscope.

5.2.3.10. Monitoring the change in mitochondrial temperature

We have used Mito Thermo Yellow (MTY), a small molecule with temperature-dependent fluorescence property that specifically localizes to the mitochondria. The fluorescence intensity of Mito Thermo Yellow declines with an increase in the temperature. The fluorescence excitation and emission range of MTY are used at 530 nm/570 nm λab = 542 nm, λem = 564 nm. For live-cell experiments, cells were grown in 25 mm glass coverslip and were treated with TRPV4 activator 4αPDD (1μM), inhibitor RN1734 (5μM), Forskolin (10μM) for 24 hours or left untreated. Antimycin (25 μM) treatment for 6 hours was given in some conditions. 0.25 μM of Mito Thermo Yellow DMSO stock solution (1 mM) was added into 1 mL of pre-warmed culture medium and then incubated at 37 °C, 5% CO_2 for 15 minutes. Subsequently, cells were washed with media and taken for live-cell imaging. 561 nm laser was used for excitation and emission wavelength were collected in the range 570nm-620nm. All images were acquired by using Olympus FV3000 Confocal Microscope.

5.2.3.11. Endoplasmic reticulum and mitochondria fluorescence labelling

For Endoplasmic Reticulum-Mitochondria contact point analysis, H295R cells were grown on 25mm coverslips and incubated for 24 hours before drug treatment. Cells were treated with TRPV4 activator 4αPDD (1 μM), inhibitor RN1734 (5 μM) or Forskolin (10μM) for 24 hours or left untreated. Later the cells were incubated with 0.25μM ER-Tracker Blue-White DPX dye (Cat

no. E12353) and 0.3 μM MitoTracker® Red CM-H2XRos (Cat. no. M7513). Cells were later washed to remove any unbound dye and kept in H295R media. ER-Tracker Blue-White DPX dye was excited with 405nm laser and emission was collected between 455 and 545 nm. MitoTracker® Red CM-H2XRos was excited with 561 nm laser and emission was collected between 570 and 620 nm. To trace the profile of the mitochondrial perimeter, single-plane confocal images of cells stained with MitoTracker® Red CM-H2XRoswere transformed into binary images, and then the ImageJ plugin isophotcontour2 was applied. To estimate the amount of mitochondrial perimeter in contact with the ER, images of the whole mitochondrial perimeter were merged with the eight-bit image of the ER-mitochondria colocalization pixels obtained with the ImageJ plugin colocalization. The ratio (R) of the number of pixels in the resulting image to the number of pixels in the whole mitochondrial profile was determined. To calculate the colocalization perimeter percentage, both Mitochondria and ER perimeter were obtained and the colocalization plugin was used to get the common pixels. It was then merged with the mitochondria perimeter and the percentage of MitoPerimeter and ER Perimeter colocalized pixels to MitoPerimeter + MitoPerimeter and ER Perimeter colocalized pixel was calculated.

5.2.3.12. Animal handling and tissue section preparation

For mesenchymal stem cell-based work, bone marrow was collected from adult BALB/c mice (4-6weeks old) (NISER/SBS/AH/IAEC-55) that were euthanized in a CO_2 chamber. The bones from hind limbs were taken and cleared from muscles and chopped at ends to open up. In a 2 mL syringe, 1.5mL α-MEM supplemented with 10% heat-inactivated FBS and 100 mg/ ml penicillin/streptomycin was drawn and bone marrow was harvested. The cell suspension was centrifuged at 400xg for 6 min and the supernatant was discarded. The cell pellet was dislodged

and treated with 1X RBC Lysis buffer for 2 min at 25 °C, and subsequently, media was added to neutralize the RBC Lysis buffer. Cells were centrifuged and the supernatant was discarded, the pellet was dissolved in α-MEM and plated in a culture dish. After 12 h, the non-adherent cells were removed by 2-3 washes with 1XPBS, and adherent cells were further cultured in a complete medium for 4 days. Cells were scarped and plated in well plates for further experiments.

For adrenal cortex-based work, healthy Balb/c mice (6–8 weeks old) were used for the current work. All the animal experiments were carried out as per IAEC approval (NISER/SBS/AH-68) as per CPCSEA guidelines. Mice were randomized to receive an intraperitoneal injection of etomidate (30 mg/kg), ketamine (100 mg/kg), or NaCl. The mice were sacrificed 12 hour post-administration of anesthetics or NaCl. Animal sacrifice was achieved by cervical dislocation. The adrenal glands were removed, fixed in 4% paraformaldehyde for 24 hours, soaked in 25% sucrose solution for 2 days, quickly frozen in dry ice, and then made into 10 μm thick slices using a cryostat (CM3050 S, Leica Biosystems, Nussloch, Germany). The slices were placed on poly-l-lysine coated glass slides. After washing thrice with PBS to remove the embedding medium, the tissues were permeabilized using 0.5% Triton X100. After blocking with 5% BSA, the tissues were incubated with primary antibodies at 1:500 dilution overnight and stained with Alexa-dye labelled secondary antibodies. The confocal imaging was performed using 63X oil immersion objective (Olympus FV3000)

5.2.4. Methods related to *in-silico* analysis

5.2.4.1. Retrieval of sequences and analysis of human TRPV4 protein sequence

The protein sequence for TRPV4 from humans was retrieved from Uniprot (accession no-Q9HBA0). All other protein sequences of TRPV4 from different species used in this study were

retrieved from either NCBI or Uniprot database (Annexure 7). All the sequences were stored in FASTA format and MUSCLE alignment tool in MEGA 5.1 software suite was used for the alignment of the proteins. ENSEMBL database was used for Histone H4 sequence retrieval.

5.2.4.2. Identification of cholesterol and sphingolipid-binding motifs

Proteins that interact with cholesterol often possess certain amino acid consensus sequences termed CRAC (cholesterol recognition/ interaction amino acid consensus), CARC (Inverted CRAC) or CCM (cholesterol-consensus-motif). The full-length TRPV4 sequence was scanned for any such motif with [L/V]-(X)(1-5)-Y-(X)(1-5)-[R/K], [R/K]-[X](1-5)-[Y]-[X](1-5)-[L/V] or [R/K]-X(2-6)-[I/V/L]-X3-(W/Y) for CRAC, CARC and CCM respectively (Fantini & Barrantes, 2013). Similarly, the sphingolipid-binding motif represents the signature sequence (VXXTLXXIY) where either (I/T/V) or Leu is allowed in any of the first four positions, and at the last position, any aromatic residue (F/W/Y) is allowed (Contreras et al., 2012). JalView Software was used to generate the conservation data. In all cases, hTRPV4 sequence was taken as a reference template. For alignment purposes, MUSCLE software was used and the respective regions present in other species were found out.

5.2.4.3. Construction of the phylogenetic tree for TRPV4

For phylogenetic analysis, MUSCLE alignment program was used to align the amino acid sequences. The evolutionary history was inferred by using the Maximum Likelihood method based on the JTT matrix-based model. The analysis involved 74 species sequences. All positions containing gaps and missing data were eliminated. Evolutionary analyses were performed by using by MEGA5.

5.2.4.4. Membrane representation and SeqLogo generation for TRPV4 LWI regions

Graphical representation of hTRPV4 and its regions are based on Uniprot derived topology and plotted in Protter (Omasits et al., 2014). LWI residues are identified as a stretch of 5 residues before and after each transmembrane region of the protein sequence. Total 60 amino acids constituting 12 LWI stretches were considered. The sequence logos were generated using WebLogo webserver (http://weblogo.berkeley.edu/).

5.2.4.5. Homology modeling and docking of cholesterol on TRPV4

A homology model of the hTRPV4 protein was built using the *Xenopus tropicalis* TRPV4 as a template (PDB: 6BBJ). Yasara's homology modeling suite was used that includes building alignment, loop modeling, rotamer selection, optimization, and validation of the model. Both the wild-type and TRPV4-R616Q mutant protein were modeled using this template. The parameters used for the homology modeling are described in annexure (Annexure 1).

A flexible docking with cholesterol as ligand and TRPV4 WT or TRPV4-R616Q protein as receptor was performed using VINA with default parameters. The best hit (25 runs) was manually chosen. Active site amino acids were identified based on the description in previous literatures. Interactions that are with thermodynamically unfavourable orientations or binding in areas not previously mentioned in the literature were not considered.

5.2.4.6. Docking of Cyt C with TRPV4

Structure of recombinant human Cyt C protein, PDB ID-3ZCF was downloaded from PDB and TRPV4 3D structure was made by homology modeling with *Xenopus tropicalis* as the target structure using YASARA homology modeling module. The protein-protein docking was performed using HADDOCK Web Server keeping the default parameters as standard settings.

5.2.4.7. Frequency calculation of all amino acid residues in the Lipid-Water-interface

Different mammals, birds, reptiles, amphibians, and fish sequences were retrieved from online databases. The percentage content of each type of amino acid in the LWI was calculated. Combined frequencies of Positive, negative, hydrophobic, and hydrophilic residues were also plotted for total LWI, outer LWI, and inner LWI in Graphpad Prism 6 (www.graphpad.com/).

5.2.4.8. Calculation of absolute hydrophobicity and hydrophilicity at Lipid-Water-Interface

The total hydrophobicity or hydrophilicity of individual residues in the lipid-water interface and the corresponding frequency of the specific residues were calculated as described before(Saha et al., 2020)(Wimley & White, 1996). Briefly, the whole residue interfacial hydrophobicity scale was used for obtaining transfer free energies of each amino acid where contributions of the peptide bonds as well as side chains were taken into consideration. Whole residue scales for POPC bilayer interfaces and for n-octanol using two families of peptides: host-guest pentapeptides of the form AcWL-X-LL, for determining sidechain hydrophobicities, and the homologous series AcWLm (m = 1 to 6), for determining peptide bond hydrophobicities was used as described before (Wimley & White, 1996). The values used for calculating the hydrophobicity and hydrophilicity were derived from free energies of transfer of AcWL-X-LL peptides from bilayer interface to water (Wimley & White, 1996). The decision level for selection of hydrophobic

amino acid (tryptophan, phenylalanine, tyrosine, leucine, isoleucine, cysteine & methionine) was taken as $\Delta G > 0$ and Hydrophilic (alanine, arginine, aspergine, aspartic acid, glutamine, glutamic acid, histidine, proline, serine, threonine, lysine, glycine & valine) as $\Delta G < 0$. In this analysis, the impact of side chain only was considered.

5.2.4.9. Conservation analysis and boxplot of the LWI stretch, cholesterol-binding motifs, domains and nearby protein sequences of TRPV4

hTRPV4 sequence was taken as a template for Conservation and Boxplot analysis of LWI stretch, cholesterol-binding motifs, and for different domains present in TRPV4. For TRPV4 nearby protein sequence conservation, human proteins were taken as a template. For alignment purposes, MUSCLE software was used and the respective regions present in other species were found out. Regions from all vertebrate species were aligned in MEGA 5.1 and pairwise matrices were generated to measure the distance between two different amino acid sequences in a group of aligned sequences. In the distance estimation analysis method, for variance estimation, Bootstrap method was chosen (Bootstrap value = 1000), amino acid substitution method was set to p-distance model, pairwise deletion model was chosen to treat the gaps or missing data. The distance matrices thus generated showed the respective pairwise distance of all sequences in a group. This distance data was used for generating the boxplot for conservation analysis using "R" software.

5.2.4.10. Statistical tests

The pairwise distance values from the matrices were calculated and boxplots were generated in "R" software package for different regions and motifs of TRPV4 to evaluate the evolutionary relationship and differential selection pressure between these regions. Kruskal-Wallis

test of variance was performed in "R" to check the reliability and significance of the data generated. "R" was also used to calculate the median values of each group and a box plot was generated. The box plots depict divergence of a particular domain or motif and the Y-axis represents the extent of divergence of those regions. The lower the values in the Y-axis, the higher is the level of conservation of the proteins. For other statistical significance tests, non-parametric student's T test or one-way ANNOVA (wherever applicable) were performed using GraphPad Prism 7.0 software (GraphPad Software Inc., San Diego, CA, USA). Data are presented as the mean $\pm$ SD. The data presented are representative of at least three independent experiments. Statistical significance is represented by asterisks (*) for p-value(s) and is marked correspondingly in the figures (*, $p < 0.05$; **, $p < 0.01$; ***, $p < 0.001$). The values that are non-significantly different are marked as "ns".

Chapter 6

Bibliography

Abel M van, et al. Regulation of the epithelial Ca^{2+} channels in small intestine as studied by quantitative mRNA detection. Am J Physiol Gastrointest Liver Physiol. 2003; 285: 78–85.

Adachi M, et al. A Male Patient Presenting with Major Clinical Symptoms of Glucocorticoid Deficiency and Skeletal Dysplasia, showing a Steroid Pattern Compatible with 17α-Hydroxylase/ 17, 20-Lyase Deficiency, but without Obvious CYP17 Gene Mutations. Endocrine Journal. 1999;46:, 285–292.

Akazawa Y, et al. Activation of TRPV4 Strengthens the Tight-Junction Barrier in Human Epidermal Keratinocytes. Skin Pharmacol Physiol. 2013; 26:15–21.

Alberts B, et al. Principles of Membrane Transport. Molecular Biology of the Cell. 2002. ISBN-10: 0-8153-3218-1

Alexander Jackson, et al. Estrogen-Derived Steroidal Metal Complexes: Agents for Cellular Delivery of Metal Centers to Estrogen Receptor-Positive Cells. Inorganic Chemistry. 2001; 40, 3964–3973.

Andreucci E, et al. TRPV4 related skeletal dysplasias: a phenotypic spectrum highlighted byclinical, radiographic, and molecular studies in 21 new families. Orphanet J Rare Dis. 2011; 6:1–8.

Arai S, et al. Mitochondria-targeted fluorescent thermometer monitors intracellular temperature gradient. Chem Commun. 2015; 51:8044–8047.

Arean, C.O., et al. Ion binding to cytochrome c. European Journal of Biochemistry. 1988; 173, 607–615.

Asif, A.R., et al. Regulation of steroid hormone biosynthesis enzymes and organic anion transporters by forskolin and DHEA-S treatment in adrenocortical cells. Am. J. Physiol. - Endocrinol. Metab. 2006; 291: 1351–1359.

Astrea G, et al. Muscle MRI in TRPV4-related congenital distal SMA. Neurology 2012; 78:364–365.

Auer-Grumbach M, et al. Alterations in the ankyrin domain of TRPV4 cause congenital distal SMA, scapuloperoneal SMA and HMSN2C. Nat Genet. 2010; 42:160–164.

Baker, J. A., et al. Charged residues next to transmembrane regions revisited : " Positive-inside rule " is complemented by the " negative inside depletion / outside enrichment rule ." BMC Biology. 2017; 15: 1–29.

Baratchi S, et al. Shear Stress Regulates TRPV4 Channel Clustering and Translocation from Adherens Junctions to the Basal Membrane. Sci Reports.2017;7:1–9.

Beard, J. L., et al.. Impaired thermoregulation and thyroid function in iron-deficiency anemia. The American Journal of Clinical Nutrition. 1990; 52, 813–819.

Beavo, J. et al.,. Regulation of steroid production by cAMP and cAMP-phosphodiesterases. Endocrinol. Metab. Syndr. 2015; Polycystic Ovarian Syndrome Conference. November 16-18, 2015 Seattle, USA.

Becker D, et al. Functional interaction of the cation channel transient receptor potential vanilloid 4 (TRPV4) and actin in volume regulation. Eur J Cell Biol. 2009; 88:141–152.

Bennati, A. M., et al. Sterol dependent regulation of human TM7SF2 gene expression: Role of the encoded 3β-hydroxysterol Δ14-reductase in human cholesterol biosynthesis. Biochimica et Biophysica Acta (BBA) - Molecular and Cell Biology of Lipids. 2006; 1761, 677–685.

Bergstrom CL, et al. Cytochrome c causes pore formation in cardiolipin-containing membranes. Proc Natl Acad Sci. 2013; 110:6269–6274.

Besnier, E.,et al. Ketamine and Etomidate Down-regulate the Hypothalamic–Pituitary–Adrenal Axis in an Endotoxemic Mouse Model. Anesthesiology. 2017; 127: 347–354.

Bezzerides VJ, et al. Rapid vesicular translocation and insertion of TRP channels. Nat Cell Biol 2004; 6:709–720.

Bidaux G, et al. Evidence for specific TRPM8 expression in human prostate secretory epithelial cells: functional androgen receptor requirement. Endocr Relat Cancer. 2005; 12:367–382.

Bisbach, C. M., et al. Mitochondrial Calcium Uniporter (MCU) deficiency reveals an alternate path for Ca2+ uptake in photoreceptor mitochondria. Scientific Reports. 2020; 10: 1–19.

Bonafe, L.,et al. Nosology and classification of genetic skeletal disorders: 2015 revision. American Journal of Medical Genetics, Part A. 2015; 167: 2869–2892.

Botte, M., et al. Cryo-EM structural studies of the agonist complexed human TRPV4 ion-channel reveals novel structural rearrangements resulting in an open-conformation. BioRxiv. 2020.

Bouron A, et al. Permeation, regulation and control of expression of TRP channels by trace metal ions. Pflügers Arch - Eur J Physiol. 2014; 467:1143–1164.

Bowen C V., et el. *In Vivo* Detection of Human TRPV6-Rich Tumors with Anti-Cancer Peptides Derived from Soricidin. PLoS One. 2013; 8:1-11.

Brandão-Neto, J., et al. Zinc acutely and temporarily inhibits adrenal cortisol secretion in humans. A preliminary report. Biological Trace Element Research. 1990; 24: 83–89.

Brauchi S, et al. TRPM7 facilitates cholinergic vesicle fusion with the plasma membrane. Proc Natl Acad. 2008; 105:8304–8308.

Breen, M. S., et al. Epistasis as the primary factor in molecular evolution. Nature. 2012; 490: 535–538.

Brown, A. J., & Galea, A. M. Cholesterol as an evolutionary response to living with oxygen. Evolution. 2010; 64: 2179–2183.

Brown, G. C., & Borutaite, V. Regulation of apoptosis by the redox state of cytochrome c. Biochimica et Biophysica Acta - Bioenergetics. 2008; 1777: 877–881.

Brown KA, Nguyen TP. A rare case of scapular winging due to a novel trpv4 mutation. J of Genet Disord and Genet Med. 2017;1: 2-3.

Buxton, C. L., & Atkinson, W. B. Hormonal factors involved in the regulation of basal body temperature during the menstrual cycle and pregnancy. the journal of clinical endocrinology & metabolism. 1948; 8: 544–549.

Buhaescu I, Izzedine H . Mevalonate pathway: a review of clinical and therapeutical implications. Clin Biochem 2007; 40:575–584.

Caires R, et al. Omega-3 Fatty Acids Modulate TRPV4 Function through Plasma Membrane Remodeling. Cell Rep. 2017; 21:246–258.

Camacho N, et al. Dominant TRPV4 mutations in nonlethal and lethal metatropic dysplasia. Am J Med Genet. 2010; 152:1169–1177.

Cao E, et al. TRPV1 channels are intrinsically heat sensitive and negatively regulated by phosphoinositide lipids. Neuron 2013; 77:667–679.

Cao E. Structural mechanisms of transient receptor potential ion channels. J Gen Physiol. 2020;152:1-18.

Carpenter EP, et al. Overcoming the challenges of membrane protein crystallography. Curr Opin Struct Biol. 2008;18:581–586.

Carreño, F. R., et al. Altered central TRPV4 expression and lipid raft association related to inappropriate vasopressin secretion in cirrhotic rats. American Journal of Physiology-Regulatory, Integrative and Comparative Physiology. 2008; 296: 454–466.

Che H, et al. Functional TRPV2 and TRPV4 channels in human cardiac c-kit+ progenitor cells. J Cell Mol Med. 2016; 20:1118–1127.

Chen DH, et al. CMT2C with vocal cord paresis associated with short stature and mutations in the TRPV4 gene. Neurology. 2010; 75:1968–1975.

Chen Q, et al. Structure of mammalian endolysosomal TRPML1 channel in nanodiscs. Nature. 2017; 550:415–418.

Chen, S.C., et al.. Competitive Inhibition of the Capsaicin Receptor-Mediated Current by Dehydroepiandrosterone in

Rat Dorsal Root Ganglion Neurons. Journal of Pharmacology and Experimental Therapeutics. 2004; 311: 529–536.

Cho, T., & Chaban, V. V. Expression of P2X3 and TRPV1 receptors in primary sensory neurons from estrogen receptors-α and estrogen receptor-β knock-out mice. Neuroreport. 2012; 23: 530-534.

Cho TJ, et al. TRPV4-pathy manifesting both skeletal dysplasia and peripheral neuropathy: A report of three patients. Am J Med Genet. 2012;158 A:795–802.

Choi, M. J., et al. Effects of heavy metals on the in vitro follicular steroidogenesis in amphibians. Integrative Biosciences. 2006; 10: 211-217.

Ciardo MG, Ferrer-Montiel A. Lipids as central modulators of sensory TRP channels. Biochim Biophys Acta – Biomembr. 2017; 1859:1615–1628.

Clark, A. L., et al. Chondroprotective role of the osmotically sensitive ion channel transient receptor potential vanilloid 4: Age- and sex-dependent progression of osteoarthritis in Trpv4-deficient mice. Arthritis & Rheumatism. 2010; 62: 2973–2983.

Cohen, A. W., et al. Role of caveolae and caveolins in health and disease. In Physiological Reviews. 2004; 84:1341–1379.

Cohen DM. TRPV4 and the mammalian kidney. Pflügers Arch. 2005; 451:168–175.

Contreras FX, et al. Molecular recognition of a single sphingolipid species by a protein's transmembrane domain. Nature. 2012; 481:525–529.

Cosens DJ, Manning A. Abnormal electroretinogram from a Drosophila mutant. Nature.1969; 224: 285–287.

Csordás, G., et al. Calcium transport across the inner mitochondrial membrane: Molecular mechanisms and pharmacology. Molecular and Cellular Endocrinology. 2012; 353: 109–113.

Dai J, et al. Novel and recurrent TRPV4 mutations and their association with distinct phenotypes within the TRPV4 dysplasia family. J Med Genet. 2010; 47:704–709.

Daneva Z, et al. Impaired Endothelial Caveolin-1-TRPV4 Channel Signaling Contributes to Endothelial Dysfunction in Pulmonary Hypertension. FASEB J. 2020; 34:1–1.

Dang, S., et al. Structural insight into TRPV5 channel function and modulation. Proceedings of the National Academy of Sciences of the United States of America. 2019; 116: 8869–8878.

Das R, Goswami C. TRPV4 expresses in bone cell lineages and TRPV4-R616Q mutant causing Brachyolmia in human reveals "loss-of-interaction " with cholesterol. Biochem Biophys Res Commun. 2019; 517.566-574.

David, M., et al. Evaluation of environmental effects of heavy metals on biochemical profile and oxidative stress among children at brick kiln sites. Arch Environ Occup Health. 2021;76: 441-449

Davis, M. E., & Fugo, N. W. The cause of physiologic basal temperature changes in women. The Journal of Clinical Endocrinology & Metabolism. 1948; 8: 550–563.

Delong R, Siddique T. A Large New England Kindred with Autosomal Dominant Neurogenic Scapuloperoneal Amyotrophy with Unique Features. Arch Neurol. 1992; 49:905–908.

Deng HX, et al. Scapuloperoneal spinal muscular atrophy and CMT2C are allelic disorders caused by alterations in TRPV4. Nat Genet. 2010; 42:165–169.

Deng Z, et al. Cryo-EM and X-ray structures of TRPV4 reveal insight into ion permeation and gating mechanisms. Nat Struct Mol Biol. 2018; 25:252–260.

Denis V, Cyert MS. Internal Ca^{2+} release in yeast is triggered by hypertonic shock and mediated by a TRP channel homologue. J Cell Biol. 2002; 156:29–34.

Di Matola T, et al. Amiodarone Induces Cytochrome c Release and Apoptosis through an Iodine-Independent Mechanism. J Clin Endocrinol Metab. 2000; 85:4323–4330.

Doghman-Bouguerra M, Lalli E. ER-mitochondria interactions: Both strength and weakness within cancer cells. Biochim Biophys Acta - Mol Cell Res. 2019; 1866:650–662.

Domene, et al. Lipid/Protein Interactions and the Membrane/Water Interfacial Region. Journal of the American Chemical Society. 2003;125:14966–14967.

Dong XP, et al. The type IV mucolipidosis-associated protein TRPML1 is an endolysosomal iron release channel. Nature. 2008; 455:992–996.

Dong XP, et al. Activating mutations of the TRPML1 channel revealed by proline-scanning mutagenesis. J Biol Chem. 2009; 284:32040–32052.

Dong XP, et al. TRP channels of intracellular membranes. J Neurochem. 2010; 113:313-28.

Dyer KF. The Quiet Revolution: A New Synthesis of Biological Knowledge. J Biol Educ. 1971; 5:15–24.

Earley S, et al. TRPV4-dependent dilation of peripheral resistance arteries influences arterial pressure. Am J Physiol Heart Circ Physiol. 2009; 297:1096–1102.

Echaniz-Laguna A, et al. Phenotypic spectrum and incidence of TRPV4 mutations in patients with inherited axonal neuropathy. Neurology. 2014; 82:1919–1926.

Echarri, A., & Del Pozo, M. A. Caveolae - mechanosensitive membrane invaginations linked to actin filaments. In Journal of Cell Science. 2015; 128: 2747–2758.

Echegoyen S, et al. Cholesterol increase in mitochondria: its effect on inner-membrane functions, submitochondrial localization and ultrastructural morphology. Biochem J. 1993; 289:703–708.

Eger, C. H., et al. Molecular interactions of hormonal steroids: The participation of the 17β side chain of corticosteroids in the formation of complexes with Co (II). Part I. Steroids. 1972; 20: 349–360.

Elmer-Dixon MM, et al. Curvature-Dependent Binding of Cytochrome c to Cardiolipin. J Am Chem Soc. 2020; 142:19532–19539.

Emons, J., et al. Mechanisms of Growth Plate Maturation and Epiphyseal Fusion. Hormone Research in Paediatrics. 2011; 75: 383–391.

Evangelista T, et al. Phenotypic variability of TRPV4 related neuropathies. Neuromuscul Disord. 2015; 25:516–521.

Everaerts W, et al. The vanilloid transient receptor potential channel TRPV4: From structure to disease. Prog Biophys Mol Biol. 2010; 103:2–17.

Falcón D, et al. TRP Channels: Current Perspectives in the Adverse Cardiac Remodeling. Front Physiol. 2019; 10:1-12.

Fantini J, Barrantes FJ. How cholesterol interacts with membrane proteins: an exploration of cholesterol-binding sites including CRAC , CARC , and tilted domains. 2013; 4:1–9.

Fawcett KA, et al. Comprehensive analysis of the TRPV4 gene in a large series of inherited neuropathies and controls. J Neurol Neurosurg Psychiatry. 2012; 83:1204–1209.

Fearnley CJ, et al. Calcium Signaling in Cardiac Myocytes. Cold Spring Harb Perspect Biol. 2011; 3:1-20.

Feely, S. M. E., et al. MFN2 mutations cause severe phenotypes in most patients with CMT2A. Neurology. 2011; 76: 1690–1696.

Feng Q. Temperature Sensing by Thermal TRP Channels: Thermodynamic Basis and Molecular Insights. Curr Top Membr 2014; 74:19–50.

Feng S, et al. Canonical transient receptor potential 3 channels regulate mitochondrial calcium uptake. Proc Natl Acad Sci.2013; 110:11011–11016.

Filadi R, et al. Mitofusin 2 ablation increases endoplasmic reticulum–mitochondria coupling. Proc Natl Acad Sci. 2015; 112:2174–2181.

Finkelstein, J. Metalloproteins. Nature. 2009; 460: 813–813.

Fiorillo C, et al. TRPV4 mutations in children with congenital distal spinal muscular atrophy. Neurogenetics. 2012; 13:195–203.

Forman, R. G., et al. The effect of endogenous progesterone on basal body temperature in stimulated ovarian cycles. Human Reproduction. 1987; 2: 631–634.

Freeman, M. E., et al. Thermogenic Action of Progesterone in the Rat. Endocrinology. 1970; 86: 717–720.

Freichel M, et al. TRP Channels in the Heart. In: Neurobiology of TRP Channels: CRC Press/Taylor & Francis; 2017. Chapter 9.

Gao F, et al. Salt Intake Augments Hypotensive Effects of Transient Receptor Potential Vanilloid 4. Hypertension. 2009; 53:228–235.

Garrido C, et al. Mechanisms of cytochrome c release from mitochondria. Cell Death Differ. 2006; 13:1423–1433.

Gemmell, N. J., et al. The tuatara genome reveals ancient features of amniote evolution. Nature. 2020; 584: 403–409.

Geng L, et al. Syntaxin 5 regulates the endoplasmic reticulum channel-release properties of polycystin-2. Proc Natl Acad Sci. 2008; 105:15920–15925.

Gevaert, T., et al. Deletion of the transient receptor potential cation channel TRPV4 impairs murine bladder voiding. The Journal of Clinical Investigation. 2007; 117: 3453–3462.

Ghosh, A., et al. Why individual thermo sensation and pain perception varies? Clue of disruptive mutations in TRPVs from 2504 human genome data. Channels. 2016; 10: 339–345.

Gilbert, S. F. Environmental Sex Determination. Gilbert SF. Developmental Biology. 2000; 6th edition.

Goldenberg NM, et al. TRPV4: physiological role and therapeutic potential in respiratory diseases. Naunyn-Schmiedeberg's Arch Pharmacol. 2014; 388:421–436.

Gomes CC, et al. TRPV4 and KRAS and FGFR1 gain-of-function mutations drive giant cell lesions of the jaw. Nat Commun. 2018; 9:1–8.

Goretzki B, et al. Unstructural Biology of TRP Ion Channels: The Role of Intrinsically Disordered Regions in Channel Function and Regulation. J Mol Biol. 2021;433:

Goswami, C., & Hucho, T. TRPV1 expression-dependent initiation and regulation of filopodia. Journal of Neurochemistry. 2007; 103: 1319–1333.

Goswami, C., et al. TRPV1 at nerve endings regulates growth cone morphology and movement through cytoskeleton reorganization. FEBS Journal. 2007; 274: 760–772.

Goswami, C et al. Importance of Non-Selective Cation Channel TRPV4 Interaction with Cytoskeleton and Their Reciprocal Regulations in Cultured Cells. PLoS ONE. 2010; 5: 1-16.

Greaves, E., et al. Elevated Peritoneal Expression and Estrogen Regulation of Nociceptive Ion Channels in Endometriosis. The Journal of Clinical Endocrinology & Metabolism. 2014; 99: 1738–1743.

Güler, A. D., et al. Heat-Evoked Activation of the Ion Channel, TRPV4. Journal of Neuroscience. 2002; 22: 6408–6414.

Gutorov R, et al. Modulation of Transient Receptor Potential C Channel Activity by Cholesterol. Front Pharmacol. 2019; 10:1-9.

Hamano K, et al. Involvement of Transient Receptor Potential Vanilloid (TRPV) 4 in mouse sperm thermotaxis. J Reprod Dev. 2016; 62:415–422.

Hamilton, J., et al. Deletion of mitochondrial calcium uniporter incompletely inhibits calcium uptake and induction of the permeability transition pore in brain mitochondria. Journal of Biological Chemistry. 2018; 293: 15652–15663.

Hampl, R., et al. Steroids and Thermogenesis. Physiol Res. 2006; 55:123-131.

Hanske J, et al. Conformational properties of cardiolipin-bound cytochrome c. Proc Natl Acad Sci. 2012;109:125–130.

Harteneck, C. Pregnenolone Sulfate: From Steroid Metabolite to TRP Channel Ligand. Molecules. 2013; 18: 12012-12028.

Hasan R, Zhang X. Ca^{2+} Regulation of TRP Ion Channels. Int J Mol Sci. 2018; 19:1-16.

Heldt, H.W., & Piechulla, B. Photosynthesis Is an Electron Transport Process. Plant Biochemistry. 2021; 63–105.

Heller S, O'Neil R. Molecular Mechanisms of TRPV4 Gating. CRC Press/Taylor & Francis. 2007;113–124.

Hellmich UA, Gaudet R. Structural Biology of TRP Channels. Handb Exp Pharmacol 2014; 223:963–990.

Himmel NJ, Cox DN. Transient receptor potential channels: current perspectives on evolution, structure, function and nomenclature. Proc R Soc B. 2020; 287:1-9.

Hirota, S., et al. Cytochrome c polymerization by successive domain swapping at the C-terminal helix. Proceedings of the National Academy of Sciences. 2010; 107:12854–12859.

Hsu WL, Yoshioka T. Role of TRP channels in the induction of heat shock proteins (Hsps) by heating skin. Biophysics (Oxf). 2015; 11:25–32.

Hsu, Y.J., et al. Testosterone increases urinary calcium excretion and inhibits expression of renal calcium transport proteins. Kidney International. 2010; 77: 601–608.

Huang Y, et al. Architecture of the TRPM2 channel and its activation mechanism by ADP-ribose and calcium. Nature. 2018; 562:145–149.

Hübner W, Blume A. Interactions at the lipid-water interface. Chem Phys Lipids. 1998; 96:99–123.

Hurt CM, et al. Transient Receptor Potential Vanilloid 1 Regulates Mitochondrial Membrane Potential and Myocardial Reperfusion Injury. J Am Heart Assoc. 2016; 5:1-13.

Huynh, K. W., et al. Structure of the full-length TRPV2 channel by cryo-EM. Nature Communications. 2016; 7, 1–8.

Iavicoli, I., et al. The Effects of Metals as Endocrine Disruptors. J Toxicol Environ Health B Crit Rev. 2009;12: 206–223.

Jordt SE, Julius D. Molecular Basis for Species-Specific Sensitivity to "Hot" Chili Peppers. Cell. 2002; 108:421–430.

Jung C, et al. The progesterone receptor regulates the expression of TRPV4 channel. Pflugers Arch Eur J Physiol. 2009; 459:105–113.

Ryu, J. W., et al. DHEA administration increases brown fat uncoupling protein 1 levels in obese OLETF rats. Biochemical and Biophysical Research Communications. 2003; 303:726–731.

Kainuma, E., et al. Association of glucocorticoid with stress-induced modulation of body temperature, blood glucose and innate immunity. Psychoneuroendocrinology. 2009; 34:1459–1468.

Kang SS, et al. Human skeletal dysplasia caused by a constitutive activated transient receptor potential vanilloid 4 (TRPV4) cation channel mutation. Exp Mol Med. 2012; 44:707–722.

Kida, N., et al. Importance of transient receptor potential vanilloid 4 (TRPV4) in epidermal barrier function in human skin keratinocytes. Pflugers Archiv European Journal of Physiology. 2012. 463:715–725.

Killian JA, Von Heijne G. How proteins adapt to a membrane-water interface. Trends Biochem Sci. 2000; 25:429-34.

King JL, Jukes TH. Non-Darwinian evolution. Science.1969;164:788–798.

Klein CJ, et al. TRPV4 mutations and cytotoxic hypercalcemia in axonal Charcot-Marie-Tooth neuropathies. Neurology. 2011; 76:887–894.

Koulen P, et al. Polycystin-2 is an intracellular calcium release channel. Nat Cell Biol. 2002; 4:191–197.

Krakow D, et al. Mutations in the Gene Encoding the Calcium-Permeable Ion Channel TRPV4 Produce Spondylometaphyseal Dysplasia, Kozlowski Type and Metatropic Dysplasia. Am J Hum Genet. 2009; 84:307–315.

Krapivinsky G, et al. The TRPM7 Ion Channel Functions in Cholinergic Synaptic Vesicles and Affects Transmitter Release. Neuron. 2006; 52:485–496.

Kumar A, et al. Regulation of TRP channels by steroids: Implications in physiology and diseases. Gen Comp Endocrinol. 2015; 220:23–32.

Kumar A, et al. TRPV4 is endogenously expressed in vertebrate spermatozoa and regulates intracellular calcium in human sperm. Biochem Biophys Res Commun. 2016a; 473:781–788.

Kumar A. Importance of TRPV4 channel in the mitochondrial structure-function relationship: Implication in pain and other pathophysiology. 2016b; Doctoral Thesis. http://www.hbni.ac.in/phdthesis/life/LIFE07201004001.pdf

Kumar A, et al. TRPV4 interacts with mitochondrial proteins and acts as a mitochondrial structure-function regulator. bioRxiv preprint. 2018. doi:10.1101/330993.

Kumari S, et al. Influence of membrane cholesterol in the molecular evolution and functional regulation of TRPV4. Biochem Biophys Res Commun. 2015; 456:312–319.

Kurahara, L. H., et al. Activation of Myofibroblast TRPA1 by Steroids and Pirfenidone Ameliorates Fibrosis in Experimental Crohn's Disease. Cellular and Molecular Gastroenterology and Hepatology. 2018; 5: 299–318.

Lakk, M., et al. Membrane cholesterol regulates TRPV4 function, cytoskeletal expression, and the cellular response to tension. Journal of Lipid Research. 2021; 62:

Lamandé SR, et al. Mutations in TRPV4 cause an inherited arthropathy of hands and feet. Nat Genet. 2011; 43:1142–1146.

Lamas JA, et al. Ion Channels and Thermosensitivity: TRP, TREK, or Both? Int J Mol Sci. 2019; 20:1-16.

Landouré G, et al. Exome sequencing identifies a novel TRPV4 mutation in a CMT2C family. Neurology 2012; 79:192-194.

Landouré, G., et al. Mutations in TRPV4 cause Charcot-Marie-Tooth disease type 2C. Nature Genetics. 2009; 42:170–174.

Lang, J. W., & Andrews, H. V. Temperature-dependent sex determination in crocodilians. Journal of Experimental Zoology. 1994; 270: 28–44.

Lange I, et al. TRPM2 functions as a lysosomal Ca^{2+}-release channel in β cells. Sci Signal. 2009; 2:1-11.

Lange M, et al. The Transient Receptor Potential (TRP) Channel Family in *Colletotrichum graminicola*: A Molecular and Physiological Analysis. PLoS One. 2016; 11:1-25.

Laskowski RA, Swindells MB. LigPlot+: Multiple LigandÀProtein Interaction Diagrams for Drug Discovery. J Chem Inf Model. 2011; 51:2778–2786.

Lavender V, et al. Increasing the expression of calcium-permeable TRPC3 and TRPC7 channels enhances constitutive secretion. Biochem J. 2008; 413:437–446.

Lawhorn BG, et al. Recent advances in TRPV4 agonists and antagonists. Bioorganic Med Chem Lett. 2020; 30:1-6.

Lee, A. G. Lipid-protein interactions in biological membranes: A structural perspective. In Biochimica et Biophysica Acta - Biomembranes. 2003; 1612: 1–40.

Lee, Anthony G. Interfacial Binding Sites for Cholesterol on TRP Ion Channels. Biophysical Journal. 2019; 117:2020–2033.

Lee, G.S., & Jeung, E.B. Uterine TRPV6 expression during the estrous cycle and pregnancy in a mouse model. Am J Physiol Endocrinol Metab. 2007; 293: 132–138.

Lee N, et al. Expression and Characterization of Human Transient Receptor Potential Melastatin 3 (hTRPM3). J Biol Chem. 2003; 278:20890–20897.

Levitan, I., et al. Cholesterol binding to ion channels. Frontiers in Physiology. 2014; 65: 1-14.

Li, M., et al. Functional Characterization of Homo- and Heteromeric Channel Kinases TRPM6 and TRPM7. Journal of General Physiology. 2006; 127:525–537.

Li Y, et al. Caveolae facilitate TRPV4-mediated Ca^{2+} signaling and the hierarchical activation of Ca^{2+}-activated K^+ channels in K^+-secreting renal collecting duct cells. Am J Physiol - Ren Physiol. 2018; 315:1626–1636.

Liedtke W, et al. Vanilloid Receptor–Related Osmotically Activated Channel (VR-OAC), a Candidate Vertebrate Osmoreceptor. Cell. 2000; 103:525–535.

Liu, J., et al. Metalloproteins Containing Cytochrome, Iron–Sulfur,or Copper Redox Centers. Chemical Reviews,

2014; 114: 4366-4469.

Liu L, et al. Role of Transient Receptor Potential Vanilloid 4 in Vascular Function. Front Mol Biosci. 2021; 8:1-11.

Liu M, et al. TRPV1, but not P2X, requires cholesterol for its function and membrane expression in rat nociceptors. Eur J Neurosci 2006; 24:1–6.

Liu Z, et al. Predator-secreted sulfolipids induce defensive responses in *C. elegans*. Nat Commun. 2018; 9:1–13.

Logu, F. De, et al. TRPA1 Mediates Aromatase Inhibitor–Evoked Pain by the Aromatase Substrate Androstenedione. Cancer Research. 2016; 76: 7024–7035.

Lu, Q., et al. Activation of the mechanosensitive Ca^{2+} channel TRPV4 induces endothelial barrier permeability via the disruption of mitochondrial bioenergetics. Redox Biology. 2021; 38: 1-12.

Lui, J. C., & Baron, J. Effects of Glucocorticoids on the Growth Plate. Endocrine Development. 2011; 20: 187–193.

Lukacs V, et al. Distinctive changes in plasma membrane phosphoinositides underlie differential regulation of TRPV1 in nociceptive neurons. J Neurosci. 2013; 33:11451-63.

Lukaski, H. C., et al. Body temperature and thyroid hormone metabolism of copper-deficient rats. The Journal of Nutritional Biochemistry. 1995; 6: 445–451.

Majeed, Y., et al. Pregnenolone sulphate-independent inhibition of TRPM3 channels by progesterone. Cell Calcium. 2012; 51: 1–11.

Majhi RK, et al. Functional expression of TRPV channels in T cells and their implications in immune regulation. FEBS J. 2015; 282:2661–2681.

Mamenko M, et al. Purinergic Activation of Ca^{2+}-Permeable TRPV4 Channels Is Essential for Mechano-Sensitivity in the Aldosterone-Sensitive Distal Nephron. PLoS One. 2011; 6:1-11.

Mangoura D, Asimaki O, Tsirimonaki E, Sakellaridis N. Role of Lipid Rafts and the Underlying Filamentous-Actin Cytoskeleton in Cannabinoid Receptor 1 Signaling. Neuropathol Drug Addict Subst Misuse. 2016; 1:689–701.

Margoliash, E., et al. Differential Binding Properties of Cytochrome c: Possible Relevance for Mitochondrial Ion Transport. Nature. 1970; 228: 723–726.

Margoliash, E., & Lustgarten, J. Interconversion of horse heart cytochrome C monomer and polymers. The Journal of Biological Chemistry. 1962; 237: 3397–3405.

Masuyama R, et al. TRPV4-Mediated Calcium Influx Regulates Terminal Differentiation of Osteoclasts. Cell Metab. 2008; 8:257–265.

McCray BA, et al. Autosomal dominant TRPV4 disorders. GeneReviews®. 2020;1–27.at (http://www.ncbi.nlm.nih.gov/pubmed/24830047).

McKemy DD, et al. Identification of a cold receptor reveals a general role for TRP channels in thermosensation. Nature. 2002; 416:52–58.

McNulty, A. L., et al. TRPV4 as a Therapeutic Target for Joint Diseases. Naunyn-Schmiedeberg's Archives of Pharmacology. 2015; 388: 437-50.

Méndez-Reséndiz KA, et al. Steroids and TRP Channels: A Close Relationship. Int J Mol Sci. 2020; 21:1-36.

Metatropic Dysplasia with a Novel Mutation in TRPV4. (n.d.). Retrieved October 10, 2021, from https://www.indianpediatrics.net/aug2016/aug-735-737.html

Michalick L, Kuebler WM. TRPV4—A Missing Link Between Mechanosensation and Immunity. Front Immunol. 2020; 11:1-9.

Midzak A, Papadopoulos V. Adrenal Mitochondria and Steroidogenesis: From Individual Proteins to Functional Protein Assemblies. Front Endocrinol (Lausanne) 2016; 7:1-14.

Minke B, et al. Induction of photoreceptor voltage noise in the dark in Drosophila mutant. Nature.1975;258:84–87.

Minke B. Drosophila mutant with a transducer defect. Biophys Struct Mech. 1977; 3:59–64.

Minke B. Light-induced reduction in excitation efficiency in the trp mutant of Drosophila. J Gen Physiol 1982; 79:361–385.

Minke B. The trp is a Drosophila mutant sensitive to developmental temperature. J Comp Physiol. 1983; 151:483–486.

Minke B, Parnas M. Insights on trp channels from *in vivo* studies in drosophila. annurev. physiol 2006; 68:649–684.

Minke B. The History of the Drosophila TRP Channel: The Birth of a New Channel Superfamily. J Neurogenet. 2010; 24:216–233.

Miyake T, et al. Activation of mitochondrial transient receptor potential vanilloid 1 channel contributes to microglial migration. Glia. 2015; 63:1870–1882.

Montell C, et al. A Unified Nomenclature for the Superfamily of TRP Cation Channels. Mol Cell. 2002; 9:229–231.

Montell C. The TRP superfamily of cation channels. Sci STKE 2005; 272:1-24.

Morales-Lázaro SL, Rosenbaum T. Multiple Mechanisms of Regulation of Transient Receptor Potential Ion Channels by Cholesterol. Curr Top Membr. 2017; 80:139–161.

Morenilla-Palao C, et al. Regulated exocytosis contributes to protein kinase C potentiation of vanilloid receptor activity. J Biol Chem. 2004; 279:25665–25672.

Morenilla-Palao C, et al. Lipid Raft Segregation Modulates TRPM8 Channel Activity. J Biol Chem. 2009; 284:9215-24.

Muller C, et al. Cannabinoid Ligands Targeting TRP Channels. Front Mol Neurosci. 2019;487: 1-15.

Mundt N, et al. TRPV4 is the temperature-sensitive ion channel of human sperm. Elife 2018; 7:1-20.

Muramatsu S, et al. Functional Gene Screening System Identified TRPV4 as a Regulator of Chondrogenic Differentiation. J Biol Chem. 2007; 282:32158–32167.

Nagai T, et al. Circularly permuted green fluorescent proteins engineered to sense Ca^{2+}. Proc Natl Acad Sci. 2001; 98:3197–3202.

Naylor, J., et al. Pregnenolone sulphate-and cholesterol-regulated TRPM3 channels coupled to vascular smooth muscle secretion and contraction. Circulation Research. 2010; 106:1507–1515.

Nilius, B. TRP channels in disease. In Biochimica et Biophysica Acta - Molecular Basis of Disease. 2007;1772: 805-12

Narayanan DL, et al. Metatropic Dysplasia with a Novel Mutation in TRPV4. Indian Pediatr. 2016; 53:735-737.

Nilius B, et al. Fast and Slow Inactivation Kinetics of the Ca^{2+} Channels ECaC1 and ECaC2 (TRPV5 and TRPV6): Role of the intracellular loop located between transmembrane segments 2 and 3. J Biol Chem. 2002; 277:30852–30858.

Nilius, B., & Voets, T. A TRP channel-steroid marriage. Nature Cell Biology. 2008; 10: 1383–1384.

Nilius B, Owsianik G. Transient receptor potential channelopathies. Pflügers Arch - Eur J Physiol. 2010; 460:437–450.

Nilius B, Owsianik G. The transient receptor potential family of ion channels. Genome Biol. 2011; 12:1–11.

Nilius B, Voets T. The puzzle of TRPV4 channelopathies. EMBO Rep. 2013; 14:152–163.

Nishimoto, R., et al. Thermosensitive TRPV4 channels mediate temperature-dependent microglia movement.

Proceedings of the National Academy of Sciences of the United States of America. 2021;118:

Nishimura G, et al. Spondylo-epiphyseal dysplasia, Maroteaux type (pseudo-Morquio syndrome type 2), and parastremmatic dysplasia are caused by TRPV4 mutations. Am J Med Genet. 2010; 152:1443–1449.

Nishimura, G., et al. TRPV4-associated skeletal dysplasias. American Journal of Medical Genetics Part C: Seminars in Medical Genetics. 2012; 160C:190–204.

Nishimura, H., et al. Transient receptor potential vanilloid 1 and 4 double knockout leads to increased bone mass in mice. Bone Reports. 2020; 12:1-10.

Nonaka K, et al. Novel gain-of-function mutation of TRPV4 associated with accelerated chondrogenic differentiation of dental pulp stem cells derived from a patient with metatropic dysplasia. Biochem Biophys Reports. 2019; 19:1-7.

Numata T, et al. Activation of TRP Channels in Mammalian Systems. In: TRP Channels. CRC Press/Taylor & Francis; 2011; 3:43–90.

Omasits U, et al. Interactive protein feature visualization and integration with experimental proteomic data. Bioinformatics. 2014; 30:884–886.

Ortíz-Rentería, M., et al. TRPV1 channels and the progesterone receptor Sig-1R interact to regulate pain. Proceedings of the National Academy of Sciences. 2018; 115: 1657–1666.

Ott M, et al. Role of cardiolipin in cytochrome c release from mitochondria. Cell Death Differ. 2007; 14:1243–1247.

Öz, O. K., et al. Aromatase Deficiency Causes Altered Expression of Molecules Critical for Calcium Reabsorption in the Kidneys of Female Mice. Journal of Bone and Mineral Research. 2007; 22:1893–1902.

Paganini, C., et al. Skeletal Dysplasias Caused by Sulfation Defects. International Journal of Molecular Sciences 2020; 21: 1-17.

Pairet N, et al. TRPV4 inhibition attenuates stretch-induced inflammatory cellular responses and lung barrier dysfunction during mechanical ventilation. PLoS One. 2018; 13:1-17.

Palmer CP, et al. A TRP homolog in Saccharomyces cerevisiae forms an intracellular Ca^{2+}-permeable channel in the yeast vacuolar membrane. Proc Natl Acad Sci. 2001; 98:7801–7805.

Palovcak E, et al. Comparative sequence analysis suggests a conserved gating mechanism for TRP channels. J Gen Physiol. 2015; 146:37–50.

Parenti A, et al. What is the evidence for the role of TRP channels in inflammatory and immune cells? Br J Pharmacol. 2016; 173:953–969.

Partida-Sanchez S, et al. Editorial: TRP Channels in Inflammation and Immunity. Front Immunol 2021; 12:1-176.

Patapoutian A, et al. ThermoTRP channels and beyond: mechanisms of temperature sensation. Nat Rev Neurosci. 2003; 4:529–539.

Payrits, M., et al. Estradiol Sensitizes the Transient Receptor Potential Vanilloid 1 Receptor in Pain Responses. Endocrinology. 2017; 158: 3249–3258.

Peng G, Shi X, Kadowaki T. Evolution of TRP channels inferred by their classification in diverse animal species. Mol Phylogenet Evol. 2015; 84:145–157.

Pérez-Cadahía, et al. Relationship between blood concentrations of heavy metals and cytogenetic and endocrine parameters among subjects involved in cleaning coastal areas affected by the "Prestige" tanker oil spill. Chemosphere. 2008; 71:447–455.

Picazo-Juárez, G., et al. Identification of a binding motif in the S5 helix that confers cholesterol sensitivity to the TRPV1 ion channel. Journal of Biological Chemistry. 2011; 286:24966–24976.

Pierrel, F., et al. Metal Ion availability in mitochondria. BioMetals. 2007; 20: 675-82.

Porter, F. D., & Herman, G. E.. Malformation syndromes caused by disorders of cholesterol synthesis. Journal of Lipid Research. 2010; 52: 6–34.

Prasad M, et al. Mitochondria-associated endoplasmic reticulum membrane (MAM) regulates steroidogenic activity via steroidogenic acute regulatory protein (StAR)-voltage-dependent anion channel 2 (VDAC2) interaction. J Biol Chem. 2015;290:2604–16.

Rajan S, et al. Ca^{2+} Signaling by TRPV4 Channels in Respiratory Function and Disease. Cells 2021; 10:3-14.

Randhawa PK, Jaggi AS. TRPV4 channels: physiological and pathological role in cardiovascular system. Basic Res Cardiol. 2015; 110:1–19.

Ridone P, et al. Piezo1 mechanosensitive channels: what are they and why are they important. Biophys Rev. 2019; 11:795–805.

Rock MJ, et al. Gain-of-function mutations in TRPV4 cause autosomal dominant brachyolmia. Nat Genet. 2008; 40:999–1003.

Rosenbaum T, et al. Ca^{2+}/Calmodulin Modulates TRPV1 Activation by Capsaicin. J Gen Physiol. 2004; 123:53–62.

Rubin, J., et al. Caveolin-1 Knockout Mice Have Increased Bone Size and Stiffness. Journal of Bone and Mineral Research. 2007; 22: 1408–1418.

Saeb, A. T. M., & Al-Naqeb, D. The Impact of Evolutionary Driving Forces on Human Complex Diseases: A Population Genetics Approach. Scientifica. 2016; 1-10.

Saha S, et al. Ratio of hydrophobic-hydrophilic and positive-negative residues at lipid-water-interface influences surface expression and channel-gating of TRPV1. bioRxiv. 2020. doi:10.1101/2020.09.04.272484.

Saha, S., et al. Preferential selection of Arginine at the lipid-water-interface of TRPV1 during vertebrate evolution correlates with its snorkeling behaviour and cholesterol interaction. Scientific Reports. 2017; 7: 1–21.

Saito M, et al. Luminal chloride-dependent activation of endosome calcium channels: Patch clamp study of enlarged endosomes. J Biol Chem. 2007; 282:27327–27333.

Sakai K, et al. Mouse model of imiquimod-induced psoriatic itch. Pain. 2016; 157:2536–2543.

Saleh, A., et al. Cytochrome c and dATP-mediated oligomerization of Apaf-1 is a prerequisite for procaspase-9 activation. Journal of Biological Chemistry. 1999; 274:17941–17945.

Scheraga RG, et al. The Role of Transient Receptor Potential Vanilloid 4 in Pulmonary Inflammatory Diseases. Front Immunol 2017; 8:1-7.

Schmidt, T. J., et al. Activation of the glucocorticoid–receptor complex. Journal of Cellular Biochemistry. 1982; 20: 15–27.

Shamsaldeen, Y. A., et al. Dysregulation of TRPV4, eNOS and caveolin-1 contribute to endothelial dysfunction in the streptozotocin rat model of diabetes. European Journal of Pharmacology. 2020; 888:

Shang S, et al. Intracellular TRPA1 mediates Ca^{2+} release from lysosomes in dorsal root ganglion neurons. 2016; 215:369–381.

Shen C, et al. A ratiometric fluorescent sensor for the mitochondrial copper pool. Metallomics. 2016; 8:915–919.

Shibasaki, K. TRPV4 activation by thermal and mechanical stimuli in disease progression. Laboratory Investigation. 2020; 100: 218–223.

Shoshan-Barmatz, V., De, S., & Meir, A. The Mitochondrial Voltage-Dependent Anion Channel 1, Ca2+ Transport, Apoptosis, and Their Regulation. Frontiers in Oncology. 2017; 7: 1-12.

Siemens J, Hanack C. Modulation of TRP Ion Channels by Venomous Toxins. Handb Exp Pharmacol. 2014; 223:1119–1142.

Simpson, E. R., & Williams-Smith, D. L. Effect of calcium(ion) uptake by rat adrenal mitochondrial on pregnenolone formation and spectral properties of cytochrome P-450. Biochimica et Biophysica Acta (BBA) - General Subjects. 1975; 404: 309–320.

Singh AK, et al. Structural bases of TRP channel TRPV6 allosteric modulation by 2-APB. Nat Commun. 2018; 9:1–11.

Singh BB, et al. VAMP2-dependent exocytosis regulates plasma membrane insertion of TRPC3 channels and contributes to agonist-stimulated Ca^{2+} influx. Mol Cell. 2004; 15:635–646.

Song, W. J., et al. Metals in Protein–Protein Interfaces. Annurev-Biophys. 2014; 43:409–431.

Spassova MA, et al. A common mechanism underlies stretch activation and receptor activation of TRPC6 channels. Proc Natl Acad Sci. 2006; 103:16586–16591.

Startek, J. B., et al. Mouse TRPA1 function and membrane localization is modulated by direct interactions with cholesterol. ELife. 2019; 8:1-24.

Stevenson, et al. Metal-dependent hormone function: the emerging interdisciplinary field of metalloendocrinology. Metallomics. 2019; 11: 85–110.

Strickland, M., et al. Relationships Between Ion Channels, Mitochondrial Functions and Inflammation in Human Aging. Frontiers in Physiology. 2019; 158: 1-22.

Strotmann R, et al. OTRPC4, a nonselective cation channel that confers sensitivity to extracellular osmolarity. Nat Cell Biol.2000; 2:695–702.

Suman, S. P., & Joseph, P. Chemical and physical characteristics of meat. Color and Pigment. Encyclopedia of Meat Sciences. 2014; 244–251.

Suzuki, A., et al. Disruption of Dhcr7 and Insig1/2 in cholesterol metabolism causes defects in bone formation and homeostasis through primary cilium formation. Bone Research. 2020; 8:1–14.

Suzuki, M., et al. Impaired Pressure Sensation in Mice Lacking TRPV4 . Journal of Biological Chemistry. 2003; 278: 22664–22668.

Suzuki M, et al. Localization of mechanosensitive channel TRPV4 in mouse skin. Neurosci Lett. 2003; 353:189–192.

Suzuki T, et al. Osteoblastic differentiation enhances expression of TRPV4 that is required for calcium oscillation induced by mechanical force. Bone 2013; 54:172–178.

Tabuchi, K., et al. Hearing impairment in TRPV4 knockout mice. Neuroscience Letters. 2005; 382:304–308.

Tellis, M. S., et al. Effects of copper on the acute cortisol response and associated physiology in rainbow trout. Comparative Biochemistry and Physiology. Toxicology & Pharmacology : CBP. 2012; 155: 281–289.

Teng, J., et al. L596-W733 bond between the start of the S4-S5 linker and the TRP box stabilizes the closed state of TRPV4 channel. PNAS. 2015; 112: 3386-3391.

Taberner FJ, et al. TRP channels interaction with lipids and its implications in disease. Biochim Biophys Acta. 2015; 1848:1818–1827.

Thebault S, et al. Novel role of cold/menthol-sensitive transient receptor potential melastatine family member 8 (TRPM8) in the activation of store-operated channels in LNCaP human prostate cancer epithelial cells. J Biol Chem. 2005; 280:39423–39435.

Thomas, P. D., et al. Applications for protein sequence–function evolution data: mRNA/protein expression analysis and coding SNP scoring tools. Nucleic Acids Research. 2006. 34:645–650.

Tian W, et al. A loss-of-function nonsynonymous polymorphism in the osmoregulatory TRPV4 gene is associated with human hyponatremia. Proc Natl Acad Sci. 2009; 106:14034–14039.

Tissue expression of TRPV4 - Summary - The Human Protein Atlas. (https://www.proteinatlas.org/ENSG00000111199-TRPV4/tissue).

Todaka, H., et al. Warm Temperature-sensitive Transient Receptor Potential Vanilloid 4 (TRPV4) Plays an Essential Role in Thermal Hyperalgesia . Journal of Biological Chemistry. 2004; 279: 35133–35138.

Toft-Bertelsen TL, Macaulay N. TRPing to the Point of Clarity: Understanding the Function of the Complex TRPV4 Ion Channel. Cells. 2021; 10:1-16.

Saha, S . et al. Ratio of hydrophobic-hydrophilic and positive-negative residues at lipid-water-interface influences surface expression and channel-gating of TRPV1. BioRxiv. https://doi.org/10.1101/2020.09.04.272484

Tuominen, E. K. J., et al. Phospholipid-cytochrome c interaction. Evidence for the extended lipid anchorage. Journal of Biological Chemistry. 2002; 277:8822–8826.

TRP Channel Family.png (https://en.wikipedia.org/wiki/File:TRP_Channel_Family.png).

TRP - The Human Protein Atlas. (https://www.proteinatlas.org/search/TRP).

Turner H, et al. Discrimination of intracellular calcium store subcompartments using TRPV1 (transient receptor potential channel, vanilloid subfamily member 1 release channel activity. Biochem J. 2003; 371:341–350.

Unger S, et al. Fetal akinesia in metatropic dysplasia: The combined phenotype of chondrodysplasia and neuropathy. Am J Med Genet. 2011; 155:2860–2864.

Urbani, A., et al. Mitochondrial Ion Channels of the Inner Membrane and Their Regulation in Cell Death Signaling. Frontiers in Cell and Developmental Biology. 2021; 1: 1-10.

Valentovic M. Pravastatin. xPharm Compr Pharmacol Ref. 2007;1–4.

Van de Graaf SFJ, et al. Direct Interaction with Rab11a Targets the Epithelial Ca^{2+} Channels TRPV5 and TRPV6 to the Plasma Membrane. Mol Cell Biol. 2006; 26:303–312.

Van Zundert GCP, et al. The HADDOCK2.2 Web Server: User-Friendly Integrative Modeling of Biomolecular Complexes. J Mol Biol. 2016; 428:720–725.

Vanderschueren, D., et al. Androgens and Bone. Endocrine Reviews. 2004; 25: 389–425.

Velilla J, et al. Homozygous TRPV4 mutation causes congenital distal spinal muscular atrophy and arthrogryposis. Neurol Genet. 2019; 5:1-9.

Vellino, S., et al. Cross-talk between the calcium channel TRPV4 and reactive oxygen species interlocks adhesive and degradative functions of invadosomes. Journal of Cell Biology. 2021; 220:1-19.

Venkatachalam K, Montell C. TRP Channels. Annu rev.biochem. 2007; 76:387–417.

Vennekens R, et al. Herbal Compounds and Toxins Modulating TRP Channels. Curr Neuropharmacol. 2008; 6:79–96.

Verma P, et al. TRPV4-mediated channelopathies. Channels (Austin). 2010;4: 319-28.

Voets T, et al. The principle of temperature-dependent gating in cold- and heat-sensitive TRP channels. Nature. 2004; 430:748–754.

Voets T, et al. TRPM8 voltage sensor mutants reveal a mechanism for integrating thermal and chemical stimuli. Nat Chem Biol. 2007; 3:174–182.

Vogt-Eisele AK, et al. Monoterpenoid agonists of TRPV3. Br J Pharmacol 2007; 151:530–540.

Von Scheven, E., et al. Glucocorticoid-Associated Osteoporosis in Chronic Inflammatory Diseases: Epidemiology, Mechanisms, Diagnosis, and Treatment. Current Osteoporosis Reports. 2014; 12: 289–299.

VonHeijne, G. Control of topology and mode of assembly of a polytopic membrane protein by positively charged residues. Nature. 1989; 341: 456–458.

Wada M, et al. Responses to transient receptor potential (TRP) channel agonists in *Chlamydomonas reinhardtii*. Biol Open. 2020; 9:1-7.

Wagner, T. F. J., et al. Transient receptor potential M3 channels are ionotropic steroid receptors in pancreatic β cells. Nature Cell Biology. 2008;10: 1421–1430.

Watanabe H, et al. Activation of TRPV4 channels (hVRL-2/mTRP12) by phorbol derivatives. J Biol Chem. 2002; 277:13569–13577.

Waterham, H. R. Defects of cholesterol biosynthesis. In FEBS Letters. 2006; 580: 5442–5449

White JPM, et al. Molecular Conductor of a Diverse Orchestra. Physiol Rev. 2016; 96:911–973.

Wimley WC, White SH. Experimentally determined hydrophobicity scale for proteins at membrane interfaces. Nat Struct Biol 1996; 3: 842–848.

Woolums, B. M.,et al. TRPV4 disrupts mitochondrial transport and causes axonal degeneration via a CaMKII-dependent elevation of intracellular Ca^{2+}. Nature Communications. 2020; 11: 1–17.

Wu L, et al. Dual role of the TRPV4 channel as a sensor of flow and osmolality in renal epithelial cells. Am J Physiol Renal Physiol. 2007; 293:1699-713.

Xiao R, et al. Calcium Plays a Central Role in the Sensitization of TRPV3 Channel to Repetitive Stimulations . J Biol Chem. 2008; 283:6162–6174.

Xu H, et al. Camphor Activates and Strongly Desensitizes the Transient Receptor Potential Vanilloid Subtype 1 Channel in a Vanilloid-Independent Mechanism. J Neurosci. 2005; 25:8924–8937.

Yadav M, Goswami C. TRPV3 mutants causing Olmsted Syndrome induce impaired cell adhesion and nonfunctional lysosomes. Channels. 2017; 11:196–208.

Yan J, et al. Cimifugin relieves pruritus in psoriasis by inhibiting TRPV4. Cell Calcium. 2021;97.

Yan T, et al. Estrogen amplifies pain responses to uterine cervical distension in rats by altering transient receptor potential-1 function. Anesth Analg. 2007; 104:1246–1250.

Yang S, et al. A pain-inducing centipede toxin targets the heat activation machinery of nociceptor TRPV1. Nat Commun. 2015; 6:1–11.

Yatsu, R., et al. TRPV4 associates environmental temperature and sex determination in the American alligator. Scientific Reports. 2015; 5: 1–10.

Yogi, A., Callera, et al. Aldosterone signaling through transient receptor potential melastatin 7 cation channel

(TRPM7) and its α-kinase domain. Cellular Signalling. 2013; 25: 2163–2175.

Yoo S, et al. Sensory TRP Channel Interactions with Endogenous Lipids and Their Biological Outcomes. Molecules. 2014; 19:4708–4744.

Zalk, R., et al. Oligomeric states of the voltage-dependent anion channel and cytochrome c release from mitochondria. Biochemical Journal. 2005; 386: 73–83.

Zhang, Q., et al. Emerging Role of Transient Receptor Potential Vanilloid 4 (TRPV4) Ion Channel in Acute and Chronic Itch. International Journal of Molecular Sciences.2021;22:1-9.

Zhang, X., et al. Organellar TRP channels. Nature Structural & Molecular Biology. 2018; 25: 1009–1018.

Zhao, S., & Rohacs, T. The newest TRP channelopathy: Gain of function TRPM3 mutations cause epilepsy and intellectual disability. Channels. 2021; 15: 386-397.

Zheng J. Molecular mechanism of TRP channels. Compr Physiol. 2013; 3:221–242.

Zhang Q, et al. Emerging Role of Transient Receptor Potential Vanilloid 4 (TRPV4) Ion Channel in Acute and Chronic Itch. Int J Mol Sci.2021; 22:1-9.

Zhang X, et al. Organellar TRP channels. Nat Struct Mol Biol. 2018; 25:1009–1018.

Zhou XL, et al. The transient receptor potential channel on the yeast vacuole is mechanosensitive. Proc Natl Acad Sci. 2003; 100:7105–7110.

Zhu MX. TRP Channels. CRC Press/Taylor & Francis; 2011.

Zimmermann K, et al. Transient receptor potential cation channel, subfamily C, member 5 (TRPC5) is a cold-transducer in the peripheral nervous system. Proc Natl Acad Sci. 2011; 108:18114–18119.

Zimoń M, et al. Dominant mutations in the cation channel gene transient receptor potential vanilloid 4 cause an unusual spectrum of neuropathies. Brain. 2010; 133:1798–1809.

Zubcevic, L., et al. Cryo-electron microscopy structure of the TRPV2 ion channel. Nature Structural & Molecular Biology. 2015; 23: 180–186.

Annexure

Annexure-1: Homology modeling parameter details & 3-Dimensional model of the hTRPV4 and TRPV4-R616Q using 6BBJ as a template

Both the wild type and the mutant protein were modeled using *Xenopus tropicalis* TRPV (PDB Id-6BBJ) as a template.

The following parameters were chosen for the target:

Modeling speed (slow = best):	Slow
Number of PSI-BLAST iterations in template search (PsiBLASTs):	3
Maximum allowed (PSI-)BLAST E-value to consider template (EValue Max):	0.5
Maximum number of templates to be used (Templates Total):	5
Maximum number of templates with same sequence (Templates SameSeq):	1
Maximum oligomerization state (OligoState):	4 (tetrameric)
Maximum number of alignment variations per template: (Alignments):	5
Maximum number of conformations tried per loop (LoopSamples):	50
Maximum number of residues added to the termini (TermExtension):	10

Overall quality Z-score, shown per residue for hTRPV4 protein

Overall quality Z-score, shown per residue for hTRPV4-R616Q protein

3-Dimensional model of the TRPV4-R616Q using 6BBJ as a template. a) side view b) Top view
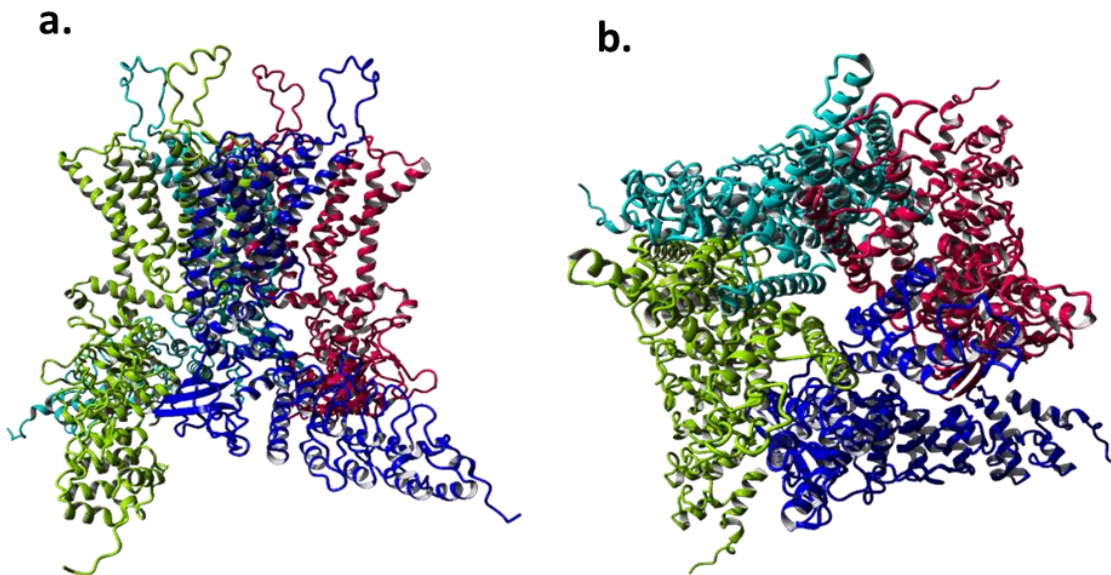
Superimposed structure of hTRPV4-WT (in yellow) and hTRPV4-R616Q (in blue) showing changes in amino acid residue at position 616 from Arginine to Glutamine.

Annexure 2: Critical amino acids that mark the signature of CRAC-motif in TM4-Loop-TM5 are highly conserved in the vertebrates, but not so much in invertebrates

|	
Mutation in human ↓	CRAC 596-608
Critical AA ★ ★	★ ★
Human	LKLTGTYSIMIQK
Mouse	LKLTGTYSIMIQK
Rat	LKLTGTYSIMIQK
Dog	LKLTGTYSIMIQK
Pig	LKLTGTYSIMIQK
Cattle	LKLTGTYSIMIQK
Wolf	LKLTGTYSIMIQK
Rabbit	LKLTGTYSIMIQK
Pacific white-sided dolphin	LKLTGTYSIMIQK
cheetah	LKLTGTYSIMIQK
Prairie vole	LKLTGTYSIMIQK
squirrel	LKLTGTYSIMIQK
red fox	LKLTGTYSIMIQK
mountain lion	LKLTGTYSIMIQK
seal mammal	LKLTGTYSIMIQK
Dingo Dog	LKLTGTYSIMIQK
Old World monkey	LKLTGTYSIMIQK
water buffalo	LKLTGTYSIMIQK
bat	LKLTGTYSIMIQK
pygmy chimpanzee	LKLTGTYSIMIQK
pig-tailed macaque monkey	LKLTGTYSIMIQK
common vampire bat	LKLTGTYSIMIQK
Common chimpanzee	LKLTGTYSIMIQK
Sumatran orangutan	LKLTGTYSIMIQK
sperm whale	LKLTGTYSIMIQK
common degu	LKLTGTYSIMIQK
Guinea pig	LKLTGTYSIMIQK
Nine-banded armadillo	LKLTGTYSIMIQK
Northern greater galago	LKLTGTYSIMIQK
Cat	LKLTGTYSIMIQK
Thirteen-lined ground squirrel	LKLTGTYSIMIQK
golden hamster	LKLTGTYSIMIQK
Ryukyu mouse	LKLTGTYSIMIQK
Gairdner's shrewmouse	LKLTGTYSIMIQK
Brown rat	LKLTGTYSIMIQK
North American beaver	LKLTGTYSIMIQK
humped cattle	LKLTGTYSIMIQK
Chinese rufous horseshoe bat	LKLTGTYSIMIQK
Damaraland mole	LKLTGTYSIMIQK
Gorilla	LKLTGTYSIMIQK
Goat	LKLTGTYSIMIQK
Black snub-nosed monkey	LKLTGTYSIMIQK
Spalax	LKLTGTYSIMIQK
monk seal	LKLTGTYSIMIQK
Chicken	LKLTGTYSIMIQK
Emu	LKLTGTYSIMIQK
Chilean tinamou	LKLTGTYSIMIQK
golden-collared manakin	LKLTGTYSIMIQK
American alligator	LKLTGTYSIMIQK
Japanese striped snake	LKLTGTYSIMIQK
Japanese grass lizard	LKLTGTYSIMIQK
eastern brown snake	LKLTGTYSIMIQK
Tiger snakes	LKLTGTYSIMIQK
common box turtle	LKLTGTYSIMIQK
Chinese alligator	LKLTGTYSIMIQK
painted turtle	LKLTGTYSIMIQK
Japanese tree frog	LKLTGTYSIMLQK
Tibetan frog	LKLTGTYSIMLQK
Western clawed frog	LKLTGTYSIMLQK
African clawed frog	LKLTGTYSIMLQK
Zebra fish	LKLTGTYSIMIQK
iridescent shark	FKLTGTYSIMIQK
killfish	LKLTGTYSIMIQK
zebra mbuna	LKLTGTYSIMIQK
Japanese rice fish	LKLTGTYSIMIQK
clown fish	LKLTGTYSIMIQK
blind cave fish	LKLTGTYSIMIQK
spiny chromis damselfish	LKLTGTYSIMIQK
Tilapia burtoni	LKLTGTYSIMIQK
Fruit fly	FKTVGPFVVMIYR
Round worm	AKLTGPFVQMIYS
Conservation	
Quality	
Consensus	LKLTGTYSIMIQK

Total LWI

Outer LWI

Inner LWI

Hydrophobicity

Hydrophillicity

Annexure 4: Localization of TRPV4-Wt and TRPV4-L596P mutant in osteogenic cells

Localization of TRPV4-Wt and TRPV4-L596P mutant in osteogenic cells. Shown are the confocal images of Saos-2 cells expressing either TRPV4-Wt-GFP or TRPV4-L596P-GFP. Expression of TRPV4-L596P-GFP often results in the development of enhanced filopodia-like structures.

Representative images showing normal and filopodia-like structures of the SaOS cells expressing TRPV4-L596P-GFP.

Annexure 5: Actins are not present in the periphery of cells expressing TRPV4-L596P mutant
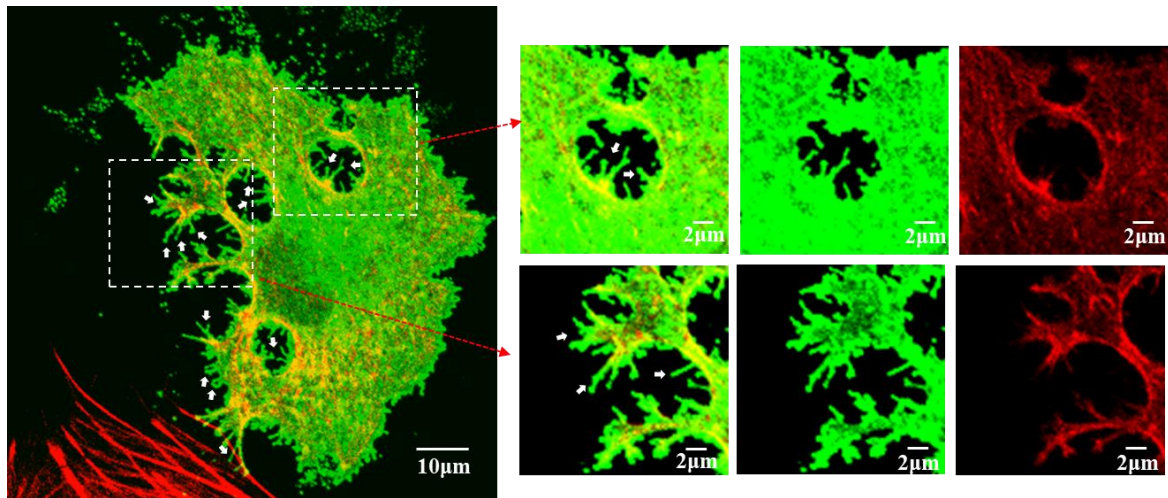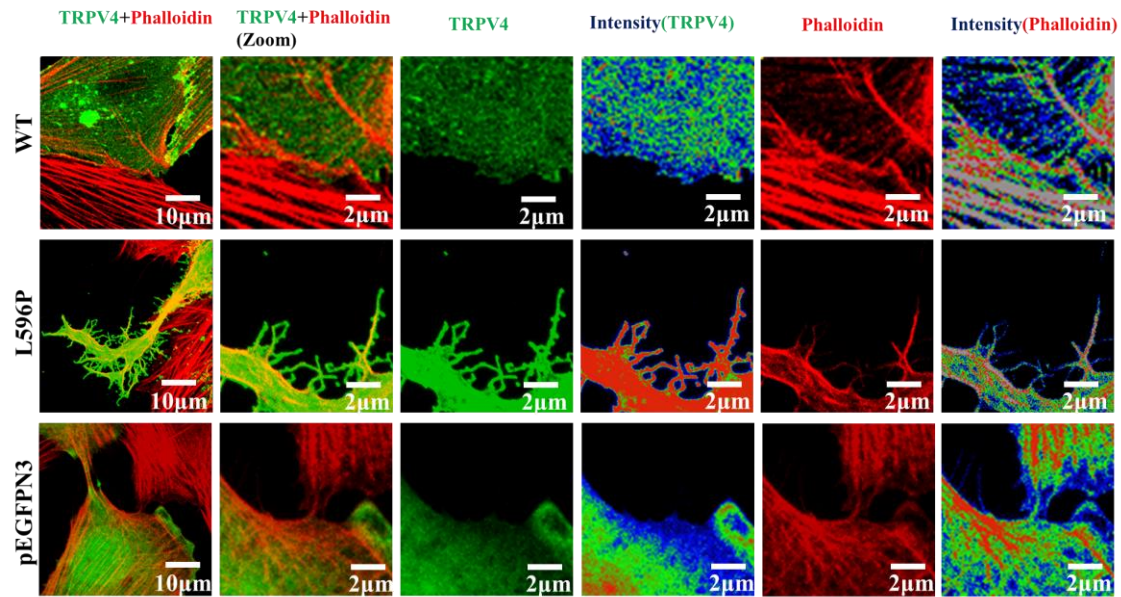
Filamentous actin is not present in the filopodia-like structures of cells expressing TRPV4-L596P mutant. Shown are the confocal images of Saos-2 cells expressing either TRPV4-Wt-GFP, TRPV4-L596P-GFP or only E-GFP (green) stained with Phalloidin (red). The fluorescence intensity of GFP or phalloidin is shown in intensity scale. The enlarged area of the peripheral region of cell with filopodia-like structure is shown in right side. Another L596P mutant expressing cell (Below, enlarged) is shown to have filopodia-like structures where this marker is not present.

Annexure 6: **No significant fluorescence differences were noticed between Wt or mutant expressing cells at basal level.**
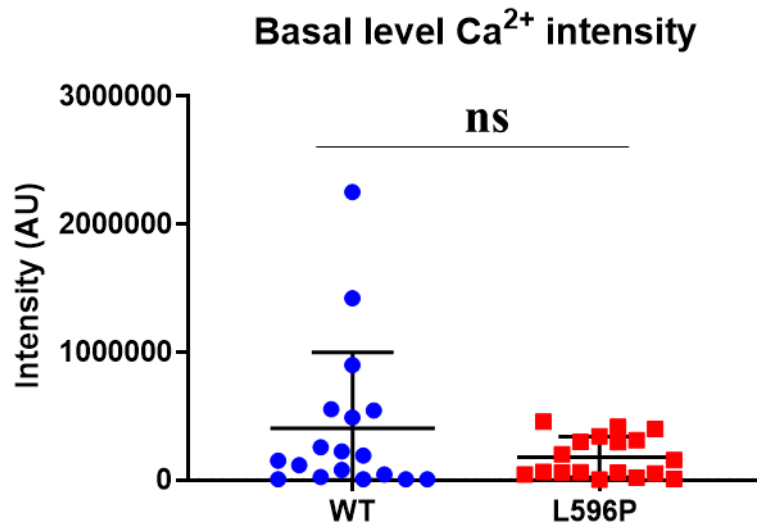
Basal levels fluorescence differences in TRPV4-Wt or TRPV4-L596P mutant expressing cell population.

Annexure-7: TRPV4-L596P mutant behaves same with TRPV4-Wt in response to higher concentration of stimulus
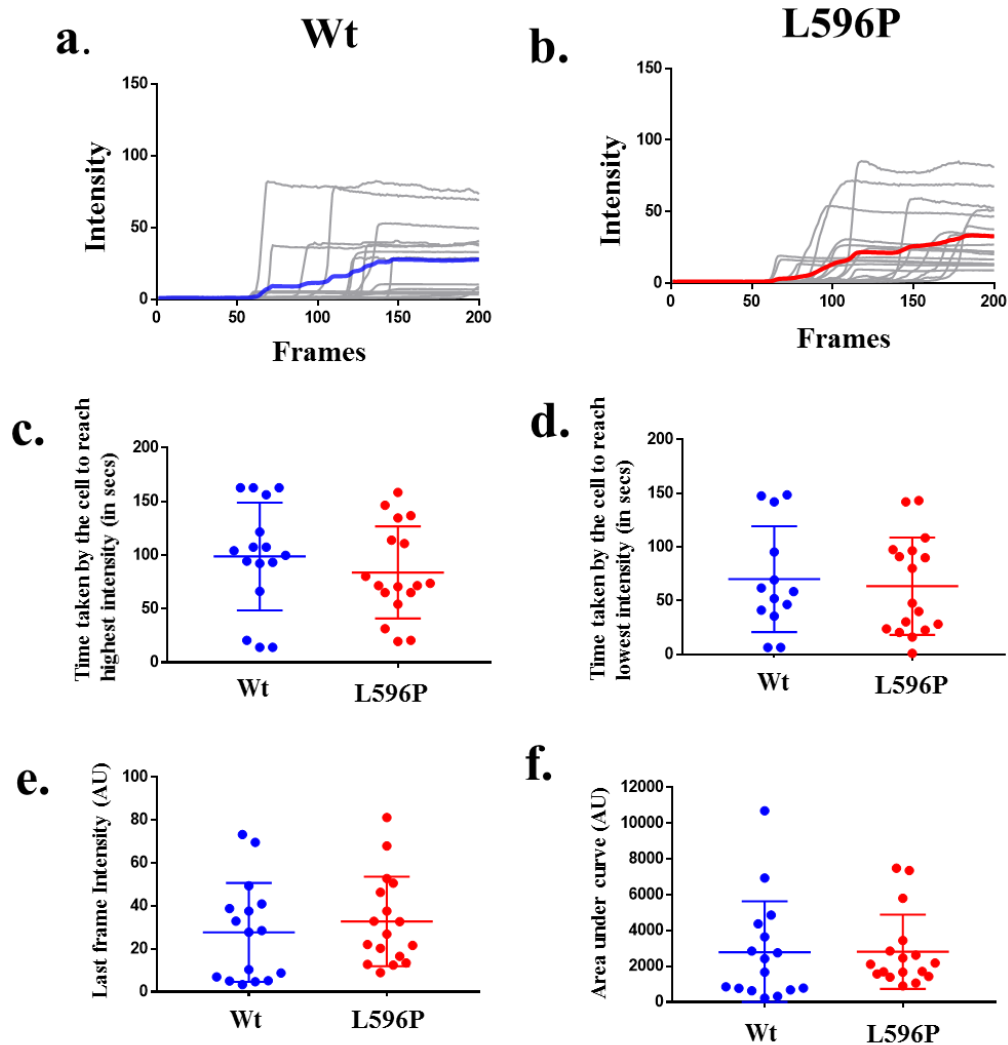
TRPV4-L596P mutant behaves same with TRPV4-Wt in response to higher concentration of stimulus. a-b. Shown are the time-series changes in the fluorescence of Ca^{2+}-sensor protein (GCaMP6f) expressed in the Saos-2 cells in response to TRPV4 activation. The Saos-2 cells were doubly transfected with plasmids coding for either TRPV4-Wt-mCherry, TRPV4-L596P-mCherry along with the Ca^{2+}-sensor GCaMP6f. In all cases, cells were stimulated with TRPV4-specific agonist 4αPDD (10 μM) added at 50th frame. In both TRPV4-Wt and TRPV4-L596P mutant expressing cells, Ca^{2+}-influx appears quickly and sustained for longer duration. The initial value recorded at the 1st-frame is considered as 1 and the intensities for all the frames were subsequently calculated relative to the 1st-frame. Values from individual cells and average value from all the cells are as thin and thick lines. **c-f.** There is no significant differences between the cells expressing TRPV4-Wt or TRPV4-L596P in terms of time taken to reach the point of highest fluorescence intensity after stimulation (c), and time taken to fall fluorescence intensity to lowest value (d) for each individual cells have been calculated. The relative fluorescence intensities at the end of the experiment (e), areas under the curve as a parameter for total Ca^{2+}-influx (f) were calculated. All these values show no significant differences between Wt and L596P mutant.

244

Annexure-8: Details of sequences used for analysis

Organisms	Scientific Name	Protein ID	Length (aa)
Human	Homo sapiens	UniProtKB - Q9HBA0	871
Mouse	Mus musculus	UniProtKB - Q9EPK8	871
Rat	Rattus norvegicus	UniProtKB - Q9ERZ8	871
Dog	Canis lupus familiaris	GenBank: ABU40239.1	871
Pig	Sus scrofa	NCBI NP_001124201.1	871
Cattle	Bos taurus	NCBI :NP_001179314.1	871
Wolf	Canis lupus familiaris	NCBI:NP_001120787.1	871
Rabbit	Oryctolagus cuniculus	GenBank: AOV86376.1	866
Pacific white-sided dolphin	Lagenorhynchus obliquidens	NCBI: XP_026980306.1	870
cheetah	Acinonyx jubatus	NCBI:XP_026899867.1	871
Prairie vole	Microtus ochrogaster	NCBI:XP_005344323.1	871
squirrel	Urocitellus parryii	NCBI: XP_026264981.1	871
red fox	Vulpes vulpes	NCBI : XP_025842436.1	868
mountain lion	Puma concolor	NCBI: XP_025789376.1	867
seal mammal	Callorhinus ursinus	NCBI : XP_025745161.1	871
Dingo Dog	Canis lupus dingo	NCBI : XP_025330048.1	871
Old World monkey	Theropithecus gelada	NCBI : XP_025257875.1	871
water buffalo	Bubalus bubalis	NCBI : XP_025123264.1	871
bat	Pteropus alecto	NCBI : XP_015452796.1	875
pygmy chimpanzee	Pan paniscus	NCBI : XP_008956168.1	871
pig-tailed macaque monkey	Macaca nemestrina	NCBI : XP_011759392.1	871
common vampire bat	Desmodus rotundus	NCBI : XP_024422550.1	870
Common chimpanzee	Pan troglodytes	NCBI : XP_016779641.1	871
Sumatran orangutan	Pongo abelii	NCBI : XP_024113283.1	871
sperm whale	Physeter catodon	NCBI : XP_007115658.2	871
common degu	Octodon degus	NCBI : XP_023576734.1	871
Guinea pig	Cavia porcellus	NCBI : XP_003477960.1	871
nine-banded armadillo	Dasypus novemcinctus	NCBI : XP_004478492.1	871
Northern greater galago	Otolemur garnettii	NCBI : XP_012660746.1	870
Cat	Felis catus	NCBI: XP_023097285.1	871
Thirteen-lined ground squirrel	Ictidomys tridecemlineatus	NCBI : XP_005340170.1	871
golden hamster	Mesocricetus auratus	NCBI : XP_012975259.1	870
Ryukyu mouse	Mus caroli	NCBI: XP_021017792.1	871
Gairdner's shrewmouse	Mus pahari	NCBI : XP_021078175.1	870
Brown rat	Rattus norvegicus	NCBI : XP_006249528.1	871
North American beaver	Castor canadensis	NCBI : XP_020021894.1	871

humped cattle	*Bos indicus*	NCBI : XP_019833659.1	871
Chinese rufous horseshoe bat	*Rhinolophus sinicus*	NCBI : XP_019613090.1	871
Damaraland mole	*Fukomys damarensis*	NCBI : XP_010602262.1	871
Gorilla	*Gorilla gorilla gorilla*	NCBI : XP_018894818.1	871
Goat	*Capra hircus*	NCBI : XP_017916595.1	871
Black snub-nosed monkey	*Rhinopithecus bieti*	NCBI: XP_017735181.1	871
Spalax	*Nannospalax galili*	NCBI : XP_017657653.1	871
monk seal	*Neomonachus schauinslandi*	NCBI : XP_021559167.1	871
Chicken	*Gallus gallus*	UniProtKB - A0A1D5PXA5	852
emu	*Dromaius novaehollandiae*	NCBI : XP_025970319.1	858
Chilean tinamou	*Nothoprocta perdicaria*	NCBI : XP_025892494.1	846
golden-collared manakin	*Manacus vitellinus*	NCBI : XP_017931657.1	894
American alligator	*Alligator mississippiensis*	NCBI : NP_001304074.1	857
Japanese striped snake	*Elaphe quadrivirgata*	GenBank: BAK64200.1	868
Japanese grass lizard	*Takydromus tachydromoides*	GenBank: BAK64199.1	868
eastern brown snake	*Pseudonaja textilis*	NCBI : XP_026575079.1	869
Tiger snakes	*Notechis scutatus*	NCBI : XP_026541264.1	868
common box turtle	*Terrapene mexicana triunguis*	NCBI : XP_026512671.1	869
Chinese alligator	*Alligator sinensis*	NCBI : XP_025055210.1	865
painted turtle	*Chrysemys picta bellii*	NCBI : XP_023957245.1	869
Japanese tree frog	*Dryophytes japonicus*	GenBank: BAN04747.1	871
Tibetan frog	*Nanorana parkeri*	NCBI : XP_018416484.1	870
Western clawed frog	*Xenopus tropicalis*	UniProtKB - F7BWY7	868
African clawed frog	*Xenopus laevis*	UniProtKB - A0A1L8HQ36	868
Zebra fish	*Danio rerio*	NCBI : NP_001036195.1	841
iridescent shark	*Pangasianodon hypophthalmus*	NCBI : XP_026767179.1	854
killfish	*Kryptolebias marmoratus*	NCBI : XP_017269494.1	873
zebra mbuna	*Maylandia zebra*	NCBI : XP_004544601.1	873
Japanese rice fish	*Oryzias latipes*	NCBI : XP_020561608.1	871
clown fish	*Amphiprion ocellaris*	NCBI : XP_023125651.1	873
blind cave fish	*Astyanax mexicanus*	NCBI : XP_022521975.1	866
spiny chromis damselfish	*Acanthochromis polyacanthus*	NCBI: XP_022054098.1	873
Tilapia burtoni	*Haplochromis burtoni*	NCBI : XP_014194860.1	873
Fruit fly	D. melanogaster	FBpp0088509 NAN protein	833
Round worm	Caenorhabditis elegans	OSM-9 B0212.5	937